Depinning and transport in disordered one-dimensional arrays of Josephson junctions

Zur Erlangung des akademischen Grades eines
DOKTORS DER NATURWISSENSCHAFTEN
von der Fakultät für Physik des
Karlsruher Instituts für Technologie

genehmigte
Dissertation
von
Dipl. Phys. Nicolas Franz Wolfgang Vogt
aus
Karlsruhe

Referent:	Professor Dr. Alexander Shnirman
Koreferent:	Professor Dr. Alexey V. Ustinov

Tag der mündlichen Prüfung: 19. Dezember 2014

Contents

1. Introduction

This thesis concerns the transport properties of the simplest one-dimensional configuration of Josephson junctions, a linear array of superconducting islands separated by tunnelling junctions with the Josephson coupling energy E_J. One can regard the one-dimensional arrays as a many-island extension of the superconducting single electron transistor (SSET) [1, 2]. The one-dimensional arrays show a great wealth of physical phenomena that warrants ongoing experimental studies [3, 4, 5, 6, 7, 8, 9] . Although the arrays contain only well known superconducting circuit elements, the Josephson junctions [10], providing a theoretical description of the experimentally observed phenomena has proven to be non-trivial. The development of theoretical model is ongoing [11, 12].

A theoretical model of a one-dimensional Josephson junction array has at least three free parameters, the Josephson coupling energy E_J, the capacitance C_J of the Josephson junctions in the array and the capacitance C_0 between the superconducting islands and the ground. Due to the large parameter space the Josephson junction array can show very different conductance behaviour. A reduction of the Josephson coupling energy E_J for example can lead to a superconductor-insulator phase transition in the array [13]. In the insulating regime Coulomb blockade prevents electrical currents through the array when small bias voltages are applied.

In this work we will focus on Josephson junction arrays in the Coulomb blockade regime. A Josephson junction array in the insulating regime shows a zero-current response to applied voltages V lower than the switching voltage V_{sw}. Applied voltages above V_{sw} drive the array into the conducting regime [3, 13]. In the conducting regime the current increases linearly with the applied voltage $I = G(V - V_0)$. At the transition point the current jumps from zero to the value $I = G(V_{sw} - V_0)$. Once in the conducting regime, the Josephson junction array is stable even for voltages lower than the original switching voltage. The array reverts back to the insulating behaviour once the applied voltage is decreased below the retrapping voltage $V_{re} < V_{sw}$. The IV-curve of a Josephson junction in the insulator phase shows a pronounced hysteresis [3, 13].

Early attempts at obtaining the switching voltage from an effective sine-Gordon model of the array failed to reproduce the experimentally observed linear dependence of the switching voltage on the array length N [3]. The origin of the hysteresis is still an open question. It has been proposed that it is brought about by large effective inductances in the array [4]. Another possibility is overheating, the raising of the effective quasi-particle temperature of the islands by the energy that is dissipated in the transport process. The

higher temperature could lower the activation threshold of the charge carriers that provide the electrical current. At the time of writing, such a model is under active theoretical investigation.

The switching voltage V_{sw} and the differential conductance in the conducting regime both depend on the Josephson coupling energy E_J. The differential conductance is proportional to E_J^2 which suggests, that Cooper pair tunnelling is essential for the electrical transport process [14]. The E_J^2-dependence was also found in kinetic Monte-Carlo simulations of the array [15]. These simulations neglect coherent tunnelling processes and obtain the incoherent tunnelling rates form P-of-E theory.

At large voltages the array enters a second transport regime where the differential conductance is independent of the Josephson coupling energy E_J and larger than in the first transport regime. The voltage drop per junction is large enough to break Cooper pairs into quasi-particles. The current is carried by incoherent quasi-particle tunnelling [14].

About this thesis

The aim of this thesis is to contribute to the theoretical understanding of Josephson junction arrays in the Coulomb blockade regime. Following the IV-curve in the direction of increasing voltage, we provide a description of the insulating array based on the well known depinning theory of elastic media [16], compare the switching voltage obtained from this description with numerical and experimental data and finally study the respective importance of coherent and incoherent Cooper pair tunnelling in the transport regime.

We also shortly discuss one-dimensional quantum phase slip ladders and show that they are described by a model that is mathematically equivalent to the Josephson junction array model.

We set $\hbar = 1$ throughout this thesis.

The thesis is devided into the following chapters:

Chapter 2:

Here we introduce the reader to the effective quasi-charge description of the Josephson junction arrays that has been widely used in the literature [3, 17, 12]. We go through the derivation introducing our notation and including charge disorder in the model. The quasi-charge model has the form of a sine-Gordon-like model, a discrete version of the sine-Gordon model with disorder and a periodic potential term that deviates from the exact cosine shape of the original sine-Gordon model.

We show the reader that a voltage biased Josephson junction coupled to a large inductance in the low frequency regime is approximately equivalent to a quantum phase slip element [18]. The discussion is based on the duality of superconducting elements under the exchange of charge and phase as well as capacitance and inductance [19]. The notion of approximate equivalence is used to discuss the relation of four types of one-dimensional superconducting arrays, Josephson junction arrays [3], Josephson junction ladders [20], quantum phase slip ladders and quantum phase slip chains. At the end of the chapter we discuss the zero-dimensional limit of a quantum phase slip ladder.

Chapter 3:

In this chapter we map the effective quasi-charge model of the Josephson junction array to the well known problem of the depinning of elastic media [16]. The connection between Josephson junction arrays in the insulating regime and pinned charge density waves was first pointed out in Ref.[17]. We develop this mapping further to obtain analytic expressions

for the switching voltage in the two regimes of long and short Josephson junction arrays. We compare the analytic results with numerical simulations of the arrays and use them to fit experimental data provided by R. Schäfer, H. Rotzinger, W. Cui, A. Fiebig and A.V. Ustinov (all Karlsruhe Institut of Technology, KIT, Germany).

Chapter 4:

When studying the influence of coherent Cooper pair tunnelling on the electrical transport in Josephson junction arrays we need to solve the equation of motion of the density matrix of very large open quantum systems. We extend the quantum jump approach, a numerical method that stochastically unravels the Lindblad master equation [21], to the stochastic Bloch-Redfield algorithm. The stochastic Bloch-Redfield algorithm can find a stochastic unravelling directly from a Bloch-Redfield type model of an open quantum system. Compared to a standard numerical solver for differential equations, it allows us to solve the master equation of much larger open quantum systems.

Chapter 5:

We test the stochastic Bloch-Redfield algorithm with the help of the well known example of a superconducting single electron transistor (SSET) [1]. We simulate two different modes of electrical transport through the SSET, transport by incoherent Cooper pair tunnelling and transport via the Josephson quasi-particle cycle [2].

Chapter 6:

We start by giving a short review of the incoherent transport model used in Ref.[15] to simulate the transport through Josephson junction arrays. In these simulations the incoherent tunnelling rates of the charge carriers were obtained from P-of-E theory. In this thesis we introduce a simplified model, a Josephson junction array segment whose charge states are restricted to a single excess Cooper pair that can be dressed by surrounding Cooper pair dipoles. We use the simplified model to determine in which parameter regimes it is sufficient to use incoherent tunneling rates obtained from P-of-E theory. In the simulations of the simplified model we make use of the stochastic Bloch-Redfield algorithm.

Chapter 7:

In the last chapter we summarize the key results of the thesis and conclude with an outlook on possible extensions of this work.

2. Array models and the zero-dimensional limit

In this chapter we present the fundamental model of the Josephson junction array that we use for most of this work. Other one-dimensional arrays containing quantum phase slip (QPS) elements and Josephson junctions are introduced and it is shown that they are closely related to Josephson junction arrays. We discuss the derivation of an effective sine-Gordon-like model as it has been used to study clean Josephson junction arrays in Refs.[22, 23, 3, 4, 24, 12]. At the end of the chapter we take a look at the limit of large interaction lengths Λ, where the arrays are effectively zero-dimensional systems.

2.1 Duality of array elements

Before introducing the full array models we want to discuss the building blocks of the arrays, Josephson junctions and quantum phase slip elements. We will show that in the low frequency regime a Josephson junction coupled to a large inductance is approximately equivalent to a quantum phase slip element. The same is true for a QPS-element parallel to a large capacitance in the low frequency regime. It is approximately equivalent to a Josephson junction.

In a Josephson junction (Fig.2.1) a current can flow without dissipation due to the coherent tunnelling of Cooper pairs [10]. The Hamiltonian of a single Josephson junction includes the charging energy of the charge q on the capacitance of the junction and the Josephson tunnelling term. The tunnelling term allows Cooper pairs to tunnel coherently from one side of the Josephson junction to the other. Its amplitude is known as the Josephson coupling energy E_J and it takes the form of the cosine of the phase difference ϕ over the junction. The Hamiltonian of a current-biased Josephson junction is given by,

$$H_{JJ} = \frac{1}{2C_J} q^2 - E_J \cos(\frac{2\pi}{\Phi_0}\phi) - I^{ext}\phi \ , \tag{2.1}$$

$$\Phi_0 = \frac{h}{2e} = \frac{\pi\hbar}{e} \ , \tag{2.2}$$

where Φ_0 is the magnetic flux quantum. In the special case of the external current being fixed to zero, $I^{ext} = 0$, the Hamiltonian simplifies to,

$$H_{JJ} = \frac{1}{2C_J} q^2 - E_J \cos(\frac{2\pi}{\Phi_0}\phi) \ . \tag{2.3}$$

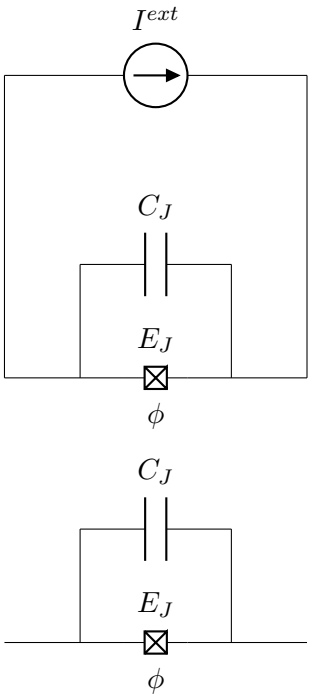

Figure 2.1: Upper circuit: sketch of a current-biased Josephson junction with capacitance C_J and Josephson coupling energy E_J.The phase-difference over the Josephson junction is given by ϕ, the charge on the Josephson junction capacitance by q. Lower circuit: The special case of $I^{ext} = 0$, an open Josephson junction element.

It is well known that the equation of motion of the phase-difference ϕ of the current-biased Josephson junction is given by [19, 25],

$$C_J \frac{d^2}{dt^2}\phi + I_c \sin\left(\frac{2\pi}{\Phi_0}\phi\right) = I^{ext} \ , \tag{2.4}$$

where I_c is the critical current of the Josephson junction,

$$I_c = E_J \frac{2\pi}{\Phi_0} \ . \tag{2.5}$$

The typical frequency scale of the Josephson junction is given by the plasma frequency,

$$\omega_p^{>} = \sqrt{2E_C E_J} \ , \tag{2.6}$$

$$E_C = \frac{(2e)^2}{2C_J} \ , \tag{2.7}$$

where E_C is the charging energy of the Josephson junction capacitance C_J with respect to one Cooper pair.

A quantum phase slip element is the dual superconducting circuit-element to a Josephson junction. In a quantum phase slip element it is the superconducting phase difference over the QPS-element that can change by 2π in a coherent tunnelling event. The Hamiltonian of a voltage-biased QPS-element (Fig.2.2) consists of an inductive term, the phase tunnelling term with the phase slip energy E_s and the voltage bias [18],

$$H_{ps} = \frac{1}{2L_{ps}}\phi^2 - E_s \cos\left(\frac{\pi}{e}Q\right) - V^{ext}Q \ , \tag{2.8}$$

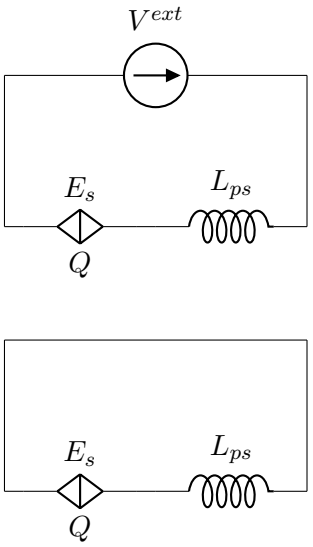

Figure 2.2: Upper circuit: sketch of a voltage-biased quantum phase slip element with inductance L_{ps} and a quantum phase slip energy E_s.The total charge that has flown through the QPS-element is given by Q, the phase-difference over the inductance L_{ps} by ϕ.
Lower circuit: The special case of $V^{ext} = 0$, a quantum phase slip element in a superconducting loop.

where ϕ is the phase difference over the inductance L_{ps} and Q is the total charge that has flown through the QPS-element. The special case of zero external voltage V^{ext} corresponds to the case of vanishing external current for Josephson junctions. The Hamiltonian simplifies to,

$$H_{ps} = \frac{1}{2L_{ps}}\phi^2 - E_s \cos\left(\frac{\pi}{e}Q\right) \ . \tag{2.9}$$

The equation of motion of the biased QPS-element is,

$$L_{ps}\frac{d^2}{dt^2}Q + V_c \sin\left(\frac{\pi}{e}Q\right) = V^{ext} \ , \tag{2.10}$$

where V_c is the critical voltage of the QPS-element,

$$V_c = E_s\frac{\pi}{e} \ . \tag{2.11}$$

The plasma frequency of the QPS-element in a closed superconducting ring is,

$$\omega_p^{QPS} = \sqrt{2E_L E_s} \ , \tag{2.12}$$

$$E_L = \frac{\Phi_0^2}{2L_{ps}} \ . \tag{2.13}$$

The inductive energy E_L plays the role of the charging energy E_C in the Josephson junction case.

The two Hamiltonians H_{ps} and H_{JJ} are dual under the exchange of charge and phase, if we identify capacitance with inductance and E_s with E_J. A detailed discussion of this duality between quantum phase slip elements and Josephson junctions can be found in Ref.[26] and Ref.[18].

In superconducting circuits the quantum phase slip elements are implemented as long thin wires of superconducting material, for example Molybdenum-Germanium compounds [27], Niobium [18] or Aluminum [28].

2.1.1 Josephson junction with enforced slow quasi-charge dynamics

We will now discuss the approximate equivalence of QPS-elements and Josephson junctions coupled to a large inductance in the low frequency regime. This problem has been studied in Ref.[19] for circuits that were coupled to a dissipative environment. Here we will discuss the approximate equivalence without considering complications due to a dissipative environment.

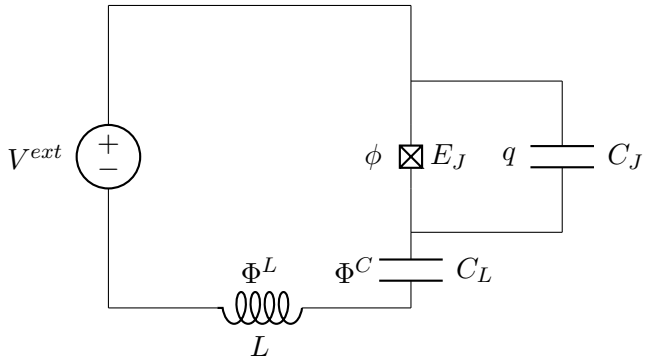

Figure 2.3: The schematics of a Josephson junction in series with a large inductance L in a voltage-biased circuit (CJL-model). The phase Φ^L is dropping over the inductance and the phase Φ^C is dropping over the measurement capacitance C_L. The charge on the capacitance of the Josephson junction is given by q. The phase ϕ dropping over the Josephson junction is conjugate to the number of Cooper pairs n that have tunnelled through the Josephson junction. The large measurement capacitance C_L decouples the degrees of freedom ϕ and Φ^L.

The approximate equivalence can be shown most conveniently when comparing the equation of motion of a voltage-biased linear circuit containing a Josephson junction and an inductance L (CJL-model) with the equation of motion of a voltage-biased quantum phase slip element. The CJL-model is shown in Fig.2.3 . The Lagrangian of the model is given by,

$$\mathcal{L}^{CJL} = \frac{1}{2}C_L\left(\dot{\Phi}^L + \dot{\phi} + V^{ext}\right)^2 - \frac{1}{2L}\left(\Phi^L\right)^2 + \frac{1}{2}C_J\left(\dot{\phi}\right)^2 + E_J\cos\left(\frac{2\pi}{\Phi_0}\phi\right) \ . \tag{2.14}$$

The phase Φ^L is the phase dropping over the inductance L, ϕ is the phase dropping over the Josephson junction and V^{ext} is the externally applied voltage. Defining the quasi-charge Q,

$$Q = \frac{\partial\mathcal{L}^{CJL}}{\partial\dot{\Phi}^L} \ , \tag{2.15}$$

one can find the Hamiltonian of the problem in terms of the quasi-charge and the number of tunnelled Cooper pairs n,

$$H_{CJL} = \frac{1}{2C_L}Q^2 + \frac{1}{2L}\left(\Phi^L\right)^2 + \frac{1}{2C_J}\left(Q - 2e\ \hat{n}\right)^2 - E_J\left(|n+1\rangle\langle n| + \text{h.c.}\right) - QV^{ext} \ . \tag{2.16}$$

The large inductance L prevents fast oscillations of the quasi-charge. Fast oscillations of Q imply a large current $\dot{Q}$ through the inductance, incurring a large energy cost $\frac{1}{2}L\dot{Q}^2$. The quasi-charge changes adiabatically compared to the rate of Cooper pair tunnelling when the inductive energy is much smaller than the Josephson coupling energy,

$$E_L \ll E_J \ . \tag{2.17}$$

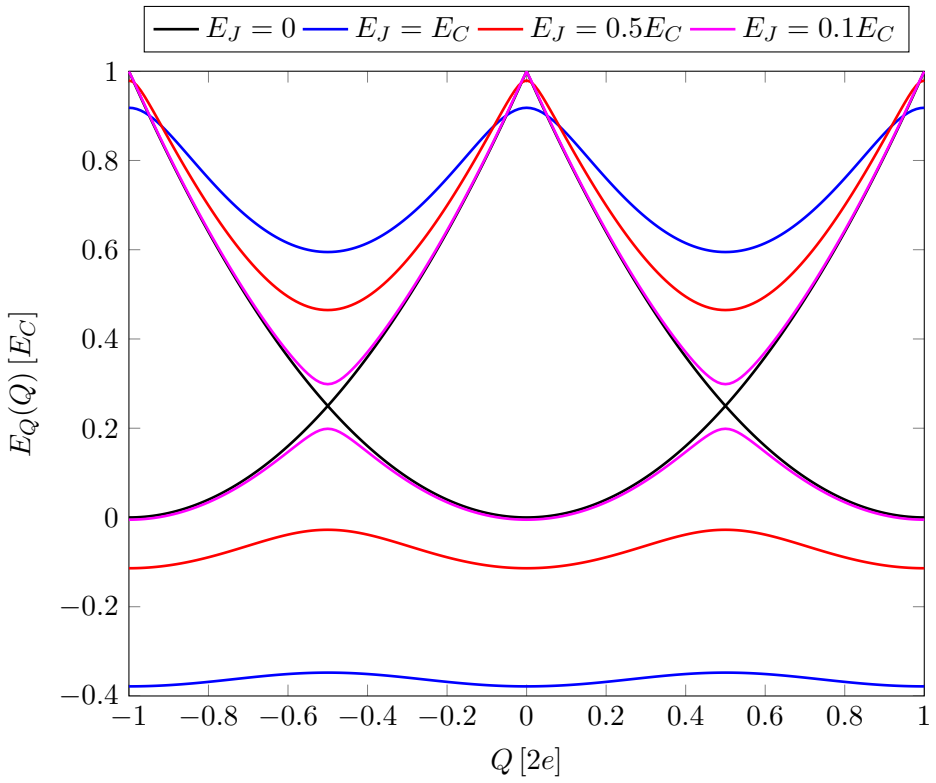

Figure 2.4: The charging energy of Hamiltonian Eq.2.18 is given by an infinite succession of parabolas, each corresponding to a different $|n\rangle$-state. The Josephson coupling energy E_J lifts the degeneracy between $|n\rangle$-states. For a large ratio of E_J and charging energy $E_J \gtrsim E_C$ the ground-state band is approximately cosine-shaped. With decreasing E_J the ground-state band approaches as succession of parabola segments with avoided crossings at the degeneracy points $Q = (e + 2e\ z) \quad z \in \mathbb{Z}$.

In the adiabatic limit, the CJL-model can be solved by applying the Born-Oppenheimer approximation. The quasi-charge is taken to be a classical parameter of the Josephson junction contribution, $H_{JJ}(Q)$, to the Hamiltonian H_{CJL},

$$H_{JJ}(Q) = \frac{1}{2C_J}\left(Q - 2e\ \hat{n}\right)^2 - E_J\left(|n+1\rangle\langle n| + \text{h.c.}\right)\ . \tag{2.18}$$

For each possible value of the quasi-charge Q, the Cooper pair Hamiltonian $H_{JJ}(Q)$ is diagonalised. The quasi-charge changes adiabatically and the change in Q does not lead to Landau-Zener transitions. The system can be approximated to be in the $|n\rangle$-ground-state. The ground state energy of $H_{JJ}\,(Q)$ provides an effective potential energy for every possible quasi-charge Q. Compared to the standard Born-Oppenheimer approximation used to model ionized atoms and conduction electrons in condensed matter systems [29], the quasi-charges take the role of the slowly varying positions of the ions. The Cooper pair number n takes the role of the position of the conduction electrons.

The charging energy as a function of the classical parameter Q is given by an infinite number of parabolas. Each parabola corresponds to one $|n\rangle$-state in the Cooper pair number basis and is shifted from the origin $Q = 0$ by $2en$. At the crossing points of the parabolas the degeneracy is lifted by the tunnelling term $E_J\left(|n+1\rangle\langle n| + \text{h.c.}\right)$, as shown in Fig.2.4.

We refer to the Q-dependent $|n\rangle$-ground-state of $H_{JJ}(Q)$ by $|\text{g.s.}\rangle$. The ground state

energy as a function of the quasi-charge is given by,

$$E_Q(Q) = \langle \text{g.s.}| \frac{(2e\hat{n} - Q)^2}{2C_J} - E_J \left(|n+1\rangle \langle n| + \text{h.c.}\right) |\text{g.s.}\rangle \ . \tag{2.19}$$

As the number of Cooper pairs n is unbounded, the Hamiltonian $H_{JJ}(Q)$ is invariant under a shift of the quasi-charge by integer multiples of two electron charges,

$$H_{JJ}(Q) = H_{JJ}(Q + 2e\ z) \quad z \in \mathbb{Z} \ . \tag{2.20}$$

As a consequence, the ground state energy and indeed any eigenenergy of $H_{JJ}(Q)$ is $2e$-periodic in Q,

$$E_Q(Q) = E_Q(Q + 2e) \ . \tag{2.21}$$

For Josephson coupling energies much larger than the charging energy, $E_J \gg E_C$, the ground state energy $E_Q(Q)$ approaches a cosine-shape. The amplitude E_Q^{max} of the periodic function $E_Q(Q)$ is exponentially suppressed with growing Josephson coupling energy [17],

$$E_Q^{max} = \max_{Q\in[-e,e]} \left(E_Q(Q)\right) - \min_{Q\in[-e,e]} \left(E_Q(Q)\right) \ , \tag{2.22}$$

$$E_Q^{max} = 16 E_J \left(\frac{E_C}{\pi^2 E_J}\right)^{\frac{1}{4}} \exp\left(-2\sqrt{\frac{E_J}{E_C}}\right) \quad \text{for} \quad \frac{E_J}{E_C} \to 0 \ . \tag{2.23}$$

In the opposite limit $E_J \ll E_C$ the degeneracy between $|n\rangle$-states is barely lifted and separation between lowest and second energy-band is approximately given by the Josephson coupling Energy E_J. The ground state band is a periodic succession of parabola segments, as shown in Fig.2.4. The amplitude of the periodic function is $\frac{e^2}{2C} = \frac{1}{4}E_C$.

For intermediate regimes it is easiest to calculate the ground state energy numerically by diagonalizing $H_{JJ}(Q)$ for a finite number of $|n\rangle$-states in the interval $-e < Q \leq e$. For values of Q outside this interval the function is continued periodically. As long as E_J is not much larger than E_C a relatively small number of $|n\rangle$-states is sufficient. In the numerical calculations used in the rest of this thesis we always use,

$$N_{|n\rangle\text{-state}} = 15 \ , \tag{2.24}$$

$|n\rangle$-states.

The ground-state energy E_Q obtained from the Born-Oppenheimer approximation provides an effective potential for the quasi-charge equation of motion [19],

$$L\frac{d^2}{dt^2}Q + \frac{1}{C_L}Q + \frac{d}{dQ}E_Q\left(Q\right) = V^{ext} \ . \tag{2.25}$$

We now assume that the measurement capacitance C_L is so large that the characteristic frequency of the L-C_L-circuit,

$$\omega_{LCL} = \frac{1}{LC_L} \ , \tag{2.26}$$

is much smaller than all relevant frequency scales at which the system is probed. In this case we can use the limit,

$$C_L \to \infty \ , \tag{2.27}$$

$$L\frac{d^2}{dt^2}Q + \frac{d}{dQ}E_Q\left(Q\right) = V^{ext} \ . \tag{2.28}$$

In this limit, the equations of motion of the CJL-model and of the voltage-biased quantum phase slip element are approximately equivalent. The equivalence is only approximate as the lowest Bloch-band energy $E_Q(Q)$ is not exactly cosine-shaped. It approaches a cosine with increasing Josephson coupling energy. The duality between the two models becomes exact in the limit $E_J^{CJL} \ll E_C^{CJL}$.

The Hamiltonian of the system in the large C_L limit is given by,

$$H = \frac{1}{2L}\left(\Phi^L\right)^2 + E_Q\left(Q\right) - V^{ext}Q \ . \tag{2.29}$$

The characteristic frequency of oscillations given by the equation of motion Eq.2.25 is the new lower plasma frequency,

$$\omega_p^< \approx \sqrt{E_L E_Q^{max}} \ , \tag{2.30}$$

$$E_L = \frac{1}{2L}\Phi_0^2 \ , \tag{2.31}$$

where E_L is the inductive energy of L. Due to the large inductance it is much smaller than the original plasma frequency of the Josephson junction,

$$E_L \ll E_J \ , \tag{2.32}$$

$$\omega_p^< \ll \omega_p^> \ . \tag{2.33}$$

Driving the CJL-circuit at large frequencies ω comparable to $\omega_p^>$ forces the quasi-charge to change on timescales of $1/E_J$. The quasi-charge does not change adiabatically compared to the Cooper pair tunnelling and the Born-Oppenheimer approximation is no longer valid.

The approximate equivalence is linked to the energy scale E_L introduced by the large inductance. It was shown in Ref.[31] that shunting a Josephson junction with a large inductance introduces new energy-levels in the spectrum of the Josephson junction. The scale of the level spacing of the eigenenergies of the bare Josephson junction is given by the large plasma frequency of the junction $\omega_p^>$. With the introduction of L, the energy levels of the bare Junction split into new levels with a level spacing of the order of the small plasma frequency $\omega_p^<$.

2.1.2 QPS-element with enforced slow quasi-phase dynamics

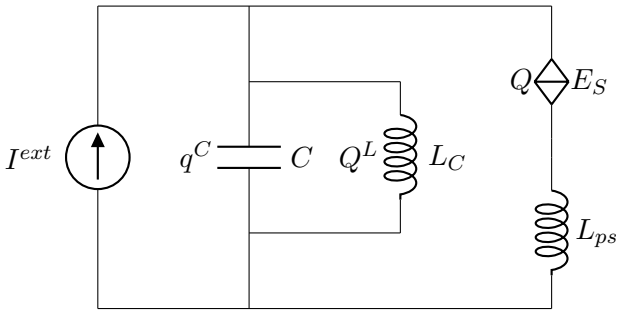

Figure 2.5: The schematics of a quantum phase slip element parallel to a large capacitance C in a current-biased circuit (PSC-model). The charge q^C is the charge on the large shunting capacitance C. The total charge that has flown through the QPS-element is given by Q. The large measurement inductance L_C decouples the degrees of freedom Q and q^C.

The same type of approximate equivalence can be found between a current-biased QPS-element and a current-biased Josephson junction. In this case the QPS-element is shunted by a large capacitance C and is considered in the low frequency regime (PSC-model as given in Fig.2.5),

$$\mathcal{L}^{PSC} = \frac{1}{2}L_C\left(\dot{Q} + \dot{q}^C + I^{ext}\right)^2 - \frac{1}{2C}\left(q^C\right)^2 + \frac{1}{2}L_{ps}\left(\dot{Q}\right)^2 + E_S\cos\left(\frac{\pi}{e}Q\right) \ , \tag{2.34}$$

where q^C is the charge on the shunting capacitance, Q is the charge that has flown through the QPS-element and I^{ext} is the bias current.

The derivation of an effective equation of motion of the PSC-model is mathematically identical to the derivation of the effective equation of motion of the CJL-model. The equation of motion is now an equation of the quasi-phase Φ,

$$\Phi = \frac{\partial\mathcal{L}^{PSC}}{\partial\dot{q}^C} \ . \tag{2.35}$$

The effective quasi-phase Hamiltonian of the shunted QPS-element is,

$$H_{PSC} = \frac{1}{2C}\left(q^C\right)^2 + \frac{1}{2L_C}\left(\Phi\right)^2 + E_\Phi\left(\Phi\right) - I^{ext}\Phi \ , \tag{2.36}$$

where $E_\Phi(\Phi)$ is the effective quasi-phase potential. We assume that the measurement inductance L_C is large compared to all other scales of the system, $L_C \to \infty$. The Hamiltonian is dual to the effective Hamiltonian of the CJL-model Eq.2.29,

$$H_{PSC} = \frac{1}{2C}\left(q^C\right)^2 + E_\Phi\left(\Phi\right) - I^{ext}\Phi \ , \tag{2.37}$$

and corresponds to the Hamiltonian of a current-biased Josephson junction Eq.2.1. The function of a Josephson junction in a superconducting circuit can also be fulfilled by a QPS-element in a high capacitance environment. In Refs.[32, 33] a Cooper pair box and a superconducting single electron transistor (SSET) where the Josephson junctions are replaced by quantum phase slip elements were proposed. The new devices were called the phase slip box and the QPS transistor.

2.2 The Josephson junction array

We now derive the Hamiltonian used to describe the Josephson junction array shown in Fig.2.6. The Josephson junction array consists of superconducting islands connected by Josephson junctions with capacitance C_J and Josephson coupling energy E_J. Capacitances C_0 couple the islands to the ground.

Considering two neighbouring islands inside the array the state of this array section in a Lagrangian description is given by the phase-differences ϕ_i^q of the Josephson junction and ψ_i^q and ψ_{i+1}^q of the capacitances C_0. An array segment is shown in Fig.2.7.

The Lagrangian of this section is,

$$\mathcal{L}_i = \frac{1}{2}C_J\left(\dot{\phi}_i^q\right)^2 + \frac{1}{2}C_0\left(\dot{\psi}_i^q\right)^2 + E_J\cos\left(\frac{2\pi}{\Phi_0}\phi_i^q\right) \ , \tag{2.38}$$

where the phase differences ϕ^q and ψ^q are given in units of the magnetic flux quantum,

$$\Phi_0 = \frac{h}{2e} = \frac{\pi\hbar}{e} \ . \tag{2.39}$$

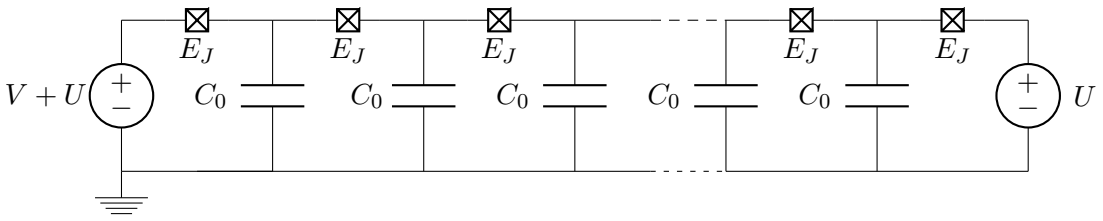

Figure 2.6: A sketch of the boundary-biased Josephson junction array. The chain of N superconducting islands is voltage-biased with an offset voltage U and a bias-voltage V. Each island is coupled to the two neighbouring islands by Josephson junctions and to the ground by the capacitance C_0. The Josephson junctions are characterized by the Josephson coupling energy E_J and the capacitance C_J.

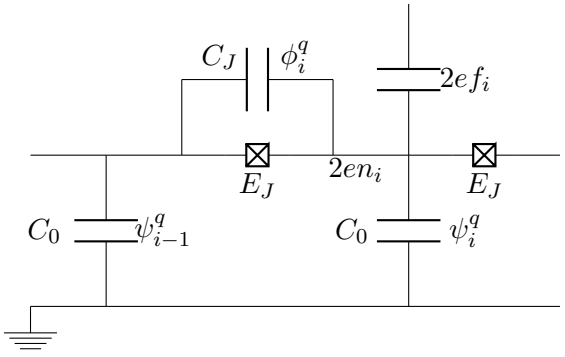

Figure 2.7: A segment from the bulk of the Josephson junction array. The state of the segment is defined by the phase differences over the Josephson junction ϕ_i^q and the capacitances to the ground ψ_{i-1}^q and ψ_i^q. The number of excess Cooper pairs on the i-th island is given by n_i. For each superconducting island we include constant background-charges $2e\ f_i$. In the disorder-free model without background-charges the frustration is zero $f_i = 0$. Kirchhoff's law and charge neutrality of each island connect the degrees of freedom ϕ_i^q, ψ_i^q and n_i.

The phase degrees of freedom are connected by the conservation of electrical charge on the island and Kirchhoff's circuit law. The charge neutrality of the island leads to the relation,

$$C_J\dot{\phi}_i^q + C_0\dot{\psi}_i^q - C_J\dot{\phi}_{i+1}^q = 2e\,(n_i + f_i)\ , \tag{2.40}$$

where n_i is the number of excess Cooper pairs on the island compared to the equilibrium number of Cooper pairs n_i^0 in the BCS condensate.

Additionally to the discrete number of Cooper pairs we include continuous disorder background charges $2e\ f_i$ in our model. The background charges are determined by the dimensionless frustration f_i. At this point we do not need to specify any particular disorder model. It is sufficient to note that charge disorder is present in every realistic superconducting circuit containing small superconducting islands [34]. Microscopic sources of disorder could include charge impurities or inhomogeneities in the substrate and the amorphous insulating layer of the Josephson junctions. We will present several specific models of the probability distribution $p(f_i)$ in Ch.3.

Kirchhoff's law connects the phase differences in a closed loop of the circuit to the enclosed magnetic flux. We assume that no magnetic field is applied parallel to the fabrication plane of the Josephson junction array. As the loop consisting of the Josephson junctions and the

two capacitances C_0 in the array segment is perpendicular to the fabrication plane, the sum over the phase differences is zero,

$$\phi_i^q + \psi_i^q - \psi_{i-1}^q = 0 \quad i \in \{2, \dots N\} \ . \tag{2.41}$$

Real world experiments are conducted with finite size arrays. We do not use the theoretical simplification of an infinite or semi-infinite array but consider a boundary biased finite-size array. The terminating circuit loops (Fig.2.8) consist of one Josephson junction, one capacitance C_0 and the voltage source biasing the array with an offset voltage U and a bias voltage V on the left and just the offset voltage U on the right.

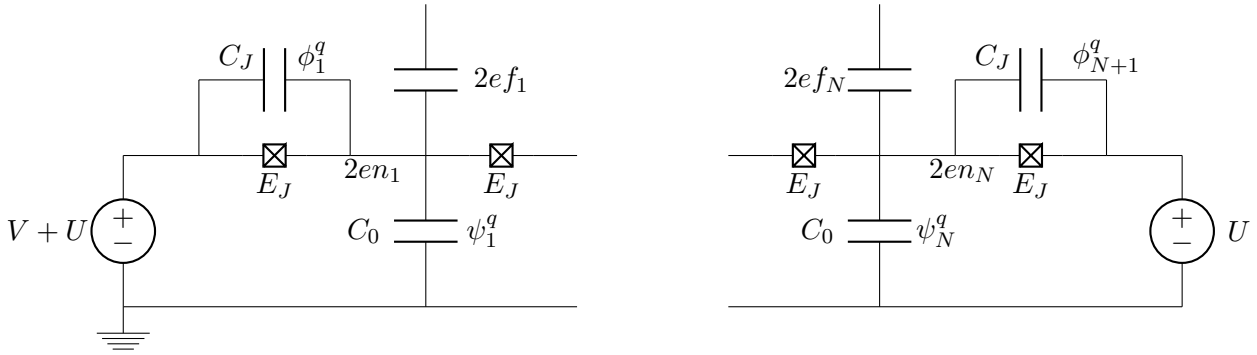

Figure 2.8: A sketch of the left and right terminating loops of the Josephson junction array. The array contains $N+1$ Josephson junctions but only N superconducting islands. The capacitive energy term of the capacity C_0 is missing from the Lagrangian of the rightmost loop $\mathcal{L}_{N+1}$.

The Lagrangian of the left terminating loop $\mathcal{L}_1$ is the same as the one given for the bulk of the array $\mathcal{L}_i$. The Lagrangian of the right loop,

$$\mathcal{L}_{N+1} = \frac{1}{2} C_J \left(\dot{\phi}_{N+1}^q\right)^2 + E_J \cos\left(\frac{2\pi}{\Phi_0}\phi_{N+1}^q\right) \ , \tag{2.42}$$

is missing the term corresponding to the charging energy of the capacitance to the ground. An array of $N+1$ junctions has only N superconducting islands and by convention each capacitor C_0 is counted together with the left Josephson junction of the island. The N equations of charge neutrality of the islands all have the same form, Eq.2.40. Kirchhoff's law is modified for both terminating loops,

$$\begin{aligned} \phi_1^q + \psi_1^q &= (V+U)\, t \ , \\ \phi_{N+1}^q - \psi_N^q &= -U\, t \ . \end{aligned} \tag{2.43}$$

The full Lagrangian description of the model is now given by summing over the Lagrangians of all single array segments,

$$\mathcal{L} = \sum_{i=1}^{N} \mathcal{L}_i + \mathcal{L}_{N+1} \ . \tag{2.44}$$

We introduce the canonical conjugate variables of the phases ϕ_i^q and ψ_i^q, the charge q_i on the capacitances of the Josephson junctions and the charge q_i^ψ on the capacitances to the ground,

$$q_i = \frac{\partial \mathcal{L}}{\partial \dot{\phi}_i^q} = C_J \dot{\phi}_i^q \ , \tag{2.45}$$

$$q_i^\psi = \frac{\partial \mathcal{L}}{\partial \dot{\psi}_i^q} = C_0 \dot{\psi}_i^q \ . \tag{2.46}$$

The energy of the system in terms of q_i and q_i^{ψ} is given by,

$$E = \sum_i \frac{1}{2C_J} q_i^2 + \frac{1}{2C_0}\left(q_i^{\psi}\right)^2 - E_J \cos\left(\frac{2\pi}{\Phi_0}\phi_i\right) + \frac{1}{2C} q_{N+1}^2 \ . \tag{2.47}$$

In this formulation of the problem the energy is not the Hamiltonian function as it contains $4N+2$ continuous variables that are not independent. Using charge neutrality (Eq.2.40) and Kirchhoff's law (Eq.2.41 and Eq.2.43), the energy can be expressed in terms of the discrete Cooper pair numbers n_i and the phase differences ϕ_i^q. The energy in terms of ϕ_i^q and n_i gives the Hamiltonian of the problem,

$$H = \sum_{i\ j} \frac{1}{2}\left(2\ e\right)^2 \left(\tilde{n}_i + f_i\right)\left(C_m^{-1}\right)_{ij}\left(\tilde{n}_j + f_j\right) - \sum_i E_J \cos\left(\phi_i^q\right) \ , \tag{2.48}$$

$$\cos\left(\phi_i^q\right) = \sum_i |n_{i+1}+1, n_i - 1\rangle\langle n_{i+1}, n_i| + |n_{i+1}-1, n_i+1\rangle\langle n_{i+1}, n_i| + \text{h.c.} \ , \tag{2.49}$$

$$\tilde{n}_i = n_i + (V+U)\,\delta_{i,1} - U\delta_{i,N} \ . \tag{2.50}$$

The inverse capacitance matrix $\left(C_m^{-1}\right)_{ij}$ determines the Coulomb-interaction between charges on sites i and j that is mediated by the capacitances C_J and C_0 [35, 12],

$$\left(C_m\right)_{ij} = (2C_J + C_0)\,\delta_{i,j} - C_J\delta_{i,j-1} - C_J\delta_{i,j+1} \ . \tag{2.51}$$

The modified number of Cooper pairs $\tilde{n}_i$ was introduced to take into account the charging energy due to the applied voltages V and U.

Here it is useful to introduce the Cooper pair charging energy,

$$E_C = \frac{\left(2\ e\right)^2}{2C_J} \ , \tag{2.52}$$

that sets the relevant energy scale associated with the capacitance matrix.

For large arrays the inverse of the capacitance matrix is approximately [15, 36],

$$\left(C_m^{-1}\right)_{ij} \approx \frac{1}{2\sinh(\lambda^{-1})}\left(\frac{1}{C_J} e^{-\frac{|i-j|}{\lambda}} - \delta_{ij}\frac{1}{2C_J}\right) \ . \tag{2.53}$$

The relevant length scale of the interaction between charges is given by λ [15],

$$\lambda = \cosh^{-1}\left(1 + \frac{C_0}{C_J}\right) \ . \tag{2.54}$$

We always assume $C_0 \ll C_J$ where λ can be approximated by,

$$\lambda \approx \sqrt{\frac{C_J}{C_0}} \equiv \Lambda \ . \tag{2.55}$$

The length Λ is given in the natural units of the array, the number of array sites between two points. In many condensed matter problems the model is defined on a discrete lattice but the number of array-sites is huge and not exactly known (take for example any tight binding model of a semiconductor sample of experimentally realistic size). In this case it is most convenient to use the lattice constant a_0 to define all lengths in terms of real spatial distance. The parameters of the problem are measured in the form of densities per unit length. In an Josephson junction array for example, the capacitance density would be $c_j = \frac{C_J}{a_0}$. Indeed this has also been used in parts of the literature on Josephson junction arrays [3, 4].

The Josephson junction arrays we consider are deliberately fabricated. The number of array sites is exactly known and the parameters like C_J can be directly measured without resorting to capacitance densities (for a discussion on the measurement of C_J see also Sec.3.4). It is more convenient to work in the dimensionless units of inter-array-site distances. We will do so for the rest of this work and all distances have to be understood to be in the dimensionless units. The results we obtain do not depend on the actual real-space size of the arrays. They are influenced by the physical size of the array only insofar, as the other parameters E_J, C_J and C_0 depend on the size of the Josephson junction or the superconducting islands.

Taking the Cooper pair number $\hat{n}_i$ to be a quantum operator the canonical conjugate operator is the exponential of the superconducting phase of the i-th island $\hat{\theta}_i$ [35, 37],

$$\left[\hat{n}_i, e^{\pm i\hat{\theta}_j}\right] = \pm\delta_{i,j} e^{i\hat{\theta}_j} \ . \tag{2.56}$$

We expressed the Hamiltonian in terms of the phase difference ϕ instead of the superconducting phase. With,

$$\hat{\phi}_i^q = \hat{\theta}_i - \hat{\theta}_{i-1} \ , \tag{2.57}$$

$$\left[\hat{\theta}_i, \hat{\theta}_j\right] = 0 \ , \tag{2.58}$$

we obtain,

$$\left[\hat{n}_i, e^{\pm i\frac{2\pi}{\Phi_0}\hat{\phi}_j^q}\right] = \pm\left(\delta_{i,j} e^{i\frac{2\pi}{\Phi_0}\hat{\phi}_j^q} + \delta_{i,j-1} e^{i\frac{2\pi}{\Phi_0}\hat{\phi}_j^q}\right) \ , \tag{2.59}$$

as the commutation relation between the operators in the Hamiltonian Eq.2.48.

Writing the Hamiltonian as a function of Cooper pair occupation and hopping operators is especially useful when considering transport processes in the arrays. Recently the model in the Cooper pair representation has been used in kinetic-Monte-Carlo simulations of the electrical transport in Josephson junction arrays [15].

2.2.1 The quasi-charge representation

A different well established (see for example Refs.[3, 4, 24, 35, 12]) representation of the Josephson junction arrays introduces a continuous degree of freedom, the quasi-charge Q_i. Using this representation an effective low-frequency model, similar to the sine-Gordon model can be obtained. The derivation of the sine-Gordon-like model will be discussed later in Sec.2.2.2.

The idea behind the quasi-charge model is to decouple the discrete degrees of freedom of different array-sites by introducing a new continuous degree of freedom. It was demonstrated in Ref.[12] and Ref.[39] that this operation is equivalent to the Hubbard-Stratonovich transformation in field theory.

The first step in the introduction of the quasi-charge is defining the fields m_i, the cumulative number of Cooper pairs, and the quasi-frustration F_i,

$$m_i = -\sum_{j=1}^{i-1} n_j \quad i > 1 \ , \tag{2.60}$$

$$n_i = m_i - m_{i+1} \ , \tag{2.61}$$

$$F_i = \sum_{j=1}^{i-1} f_j \quad i > 1 \ . \tag{2.62}$$

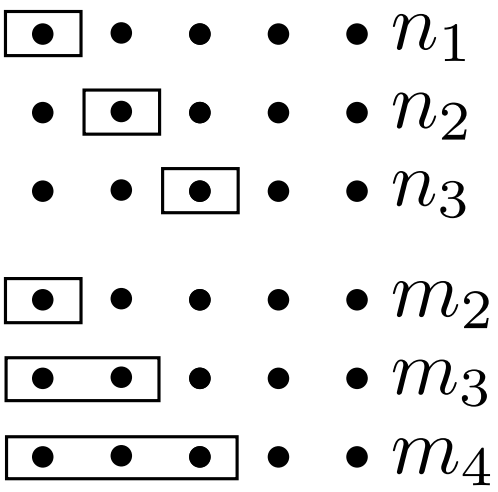

Figure 2.9: Schematic picture to illustrate the difference between the discrete degrees of freedom n_i and m_i. The first gives the number of Cooper pair on the i-th island of the array, the later gives the cumulative number of Cooper pairs on the first $(i-1)$-islands

Instead of writing the Hamiltonian purely in terms of m_i, the quasi-charge Q_i is introduced. In terms of the original degrees of freedom, Q_i is given by,

$$Q_i = \sum_{j=1}^{i-1}(q_j^{\psi}) + q_1 \ , \tag{2.63}$$

$$q_i = \sum_{j=1}^{i-1}(q_j^{\psi} + 2e\ f_j) + 2e\sum_{j=1}^{i-1} n_i + q_1 \tag{2.64}$$

$$= Q_i + 2e\ F_i + 2e - m_i \ , \tag{2.65}$$

$$q_i^{\psi} = Q_{i+1} - Q_i \ , \tag{2.66}$$

and the energy of the array is given by,

$$E(Q,m) = \sum_{i=1}^{N}\left[\frac{(2e\hat{m}_i - 2eF_i - Q_i)^2}{2C_J} + \frac{(Q_i - Q_{i+1})^2}{2C_0} - E_J\cos\left(\frac{2\pi}{\Phi_0}\phi_i\right)\right]$$
$$- (V+U)\,Q_1 + UQ_{N+1} \ , \tag{2.67}$$

$$Q \equiv \{Q_i\} \ , \tag{2.68}$$

$$m \equiv \{m_i\} \ . \tag{2.69}$$

By introducing m_i, F_i and the quasi-charge Q_i we change from a picture where the array is divided into N equal islands to a picture where the array is divided into islands of successively increasing size, as seen in Fig.2.9. Increasing the island-number i, the islands described by n_i move along the array, the islands given by m_i expand along the array. Both n_1 and m_2 give the Cooper pair occupation of the first superconducting island. The degree of freedom n_2 corresponds to the second island but m_3 gives the number of Cooper pairs of the first two islands of the array. The same is the case for the frustration f_i compared to the quasi-frustration F_i. The quasi-charge Q_{i+1} corresponds to the total charge on the capacitances to the ground C_0 of the first i islands. Assuming that at the time t_0 the quasi-charge is zero throughout the array, the quasicharge Q_i at a time t_1 also gives the amount of charge that has flown through the i-th junction between $t = t_0$ and $t = t + 1$.

Before we go on to discuss the nature of the quasi-charge we want to note that in the definition of m_i and F_i, Eq.2.60 and Eq.2.62, m_1 and F_1 are not well defined. The degrees

of freedom m_1 and F_1 are introduced in the transition to the Hamiltonian Eq.2.67. In the transition from the number of Cooper pairs n_i to the fields m_i we use the fact that the Josephson junction arrays are essentially open systems. The Hamiltonian Eq.2.48 describes a closed quantum system of finite size. Without adding additional terms to the Hamiltonian, Cooper pairs can not tunnel in and out of the system via the leads. This is not a problem in the infinite system limit and the question of the correct definition of boundary terms in Eq.2.60 and Eq.2.62 can be compensated by adding a constant offset at $i = -\infty$ [35].

As we explicitly deal with finite systems, we have to be more careful here. The m_i are essentially a measure of the number of Cooper pairs that have tunneled through the i-th Josephson junction. In a closed system, Cooper-pairs can not tunnel into the array and m_1 is zero. When going from Hamiltonian H Eq.2.48 to $E(Q, m)$ Eq.2.67, we use the Cooper pair tunnelling between array and leads, to implicitly introduce an new discrete degree of freedom, the number of Cooper pairs exchanged between the Josephson junction array and the leads. In this way we go from N discrete degrees of freedom n_i to the $N+1$ degrees of freedom m_i in Eq.2.67. The field m_1 is a normal degree of freedom in $E(Q, m)$. The quasi-disorder on the first site will be zero, $F_1 = 0$. The array has only N islands with N background charges f_i. The open system character does not change that. The superconducting leads do not carry a background-charge with respect to the ground of the superconducting circuit.

It is important to take the open-system character into account here. Failing to introduce m_1 as an additional degree of freedom would lead to a potential term in $E(Q, m)$ that grows infinitely with increasing Q_1. It would be impossible to describe any transport processes in the quasi-charge model. This has to be expected for a model in which the array is decoupled from the leads.

The quasi-charges we introduced in $E(Q, m)$ are strictly speaking not independent degrees of freedom. The Q_i can be expressed as functions of the fields m_i with the help of the charge neutrality condition (Eq.2.40) and Kirchhoff's law (Eq.2.41 and Eq. 2.43) . The set of equations that connect Q_i and m_i can also be directly obtained from $E(Q, m)$ by minimising $E(Q, m)$ with respect to the Q_i. The solutions of the set of equations,

$$\frac{\partial}{\partial Q_i} E(Q, m) = 0 \ , \tag{2.70}$$

determines the quasi-charge configuration $\{Q_i\}$ that minimizes the energy $E(Q, m)$ for a given set of $\{m_i\}$ [35, 39]. In the same way the relation between q_i, q_i^{ψ} and n_i can be obtained from the Lagrangian Eq.2.44 via the Euler-Lagrange equations.

The introduction of the quasi-charge corresponds to a Hubbard-Stratonovich transformation in field theory [35, 39]. In the Hubbard-Stratonovich transformation an additional field is introduced into the path-integral that determines the partition function [40, 41],

$$\begin{aligned} Z &= \int \prod_i Dm_i D\phi_i^q \, e^{i\int dt \left[\sum_i m_i \dot{\phi}_i^q - \sum_{i,j} (2e)^2 (m_i - F_i) D_{ij} (m_j - F_j) + \sum_i E_J \cos\left(\frac{2\pi}{\Phi_0}\phi_i^q\right)\right]} \\ &= \mathcal{N} \int \prod_i DQ_i Dm_i D\phi_i^q \, e^{i\int dt \left[\sum_i m_i \dot{\phi}_i^q - E(Q,m)\right]} \ , \end{aligned} \tag{2.71}$$

$$D_{ij} = \left(C_m^{-1}\right)_{i+1,j+1} + \left(C_m^{-1}\right)_{i,j} - \left(C_m^{-1}\right)_{i+1,j} - \left(C_m^{-1}\right)_{i,j+1} \ , \tag{2.72}$$

where $\mathcal{N}$ is a normalization factor that compensates the introduction of the additional functional field integration over Q_i. The additional fields Q_i decouple the fields m_i and m_j for different sites $i \neq j$. Originally they are coupled by the matrix D_{ij}, the inverse capacitance matrix in the m_i-basis.

2.2.2 The sine-Gordon-like model

In this section we discuss the derivation of the effective sine-Gordon-like model that has often been used in Literature [3, 4, 24] to describe the behaviour of Josephson junction arrays. In most papers that use the sine-Gordon-like model it was derived under the assumption that large inductances are present in the array. We will discuss this case in the next section Sec.2.2.3. It has been recently conjectured in Refs.[12, 39] that a sine-Gordon-like model also gives a valid description of Josephson junction arrays that do not a priori contain large inductances L. We follow the logic of the derivation given in Ref.[39] for the inductance-free case.

Starting from the energy $E(Q, m)$, one arrives at the effective model for the quasi-charge Q_i by tracing out the discrete degrees of freedom of the fields m_i. For the general case this is a non-trivial problem. We make the assumption that the quasi-charges Q_i change very slowly in time compared to the Cooper pair hopping. The Q_i can be regarded as classical constant parameter in a Hamiltonian of the form,

$$H^m\left(\{Q\}\right) = \sum_{i=1}^{N} \frac{\left(2e\hat{m}_i - 2eF_i - Q_i\right)^2}{2C_J} - E_J\left(|m_i+1\rangle\langle m_i| + \text{h.c.}\right) \ , \tag{2.73}$$

that operates on the Hilbert-space of the occupation numbers m_i. With this assumption we can use the Born-Oppenheimer approximation [24, 12].

At this point a word of caution is in order. We must not violate the Born-Oppenheimer approximation by applying an external driving force at frequencies ω_{ext} that would drive Landau-Zener transitions in the system. Save driving frequencies meet the condition,

$$\omega_{ext} \ll \frac{E_J^2}{E_C} \ . \tag{2.74}$$

If the system is externally driven at higher frequencies, the driving can lead to transitions from the m_i-ground-state to higher states that are excluded in the Born-Oppenheimer approximation. Practically this is not too much of a problem. Most experiments we are interested in [3, 4, 9, 39] are conducted in the DC regime with $\omega_{ext} = 0$.

When diagonalising the Cooper pair Hamiltonian we see that for a fixed quasi-charge configuration $\{\langle Q\rangle\}$ the Hamiltonian $H\left(\{\langle Q\rangle\}\right)$ separates into $N+1$ identical single particle Hamiltonians [24, 12] of the fields m_i of each island,

$$H_i(Q_i) = \frac{\left(2e\hat{m}_i - 2eF_i - Q_i\right)^2}{2C_J} - E_J\left(|m_i+1\rangle\langle m_i| + \text{h.c.}\right) \ . \tag{2.75}$$

The single particle is to be understood as a fictitious single particle that can move on a discrete lattice in a potential where the lattice position is determined by the operator $\hat{m}_i$. The Hamiltonians for each site differ only by the value of the quasi-charge Q_i and frustration F_i on the sites. The problem simplifies significantly as only the ground-state of a single particle Hamiltonian $H_i(Q)$ has to be found for all relevant values of Q. This was exactly the reason behind the introduction of the quasi-charge Q_i and the fields m_i in Sec.2.2.

The Hamiltonian $H_i(Q)$ can be diagonalised in the same way as the Josephson junction contribution to the Hamiltonian of the CJL-model in Sec.2.1. From the diagonalization in the Born-Oppenheimer approximation we obtain the Hamiltonian of the effective quasi-charge model where the ground state energy of $H_i(Q)$ provides an effective potential term,

$$H_Q = \sum_i \frac{\left(Q_i - Q_{i+1}\right)^2}{2C_0} + E_Q(Q_i) \ . \tag{2.76}$$

Coming back to the remark on introducing the additional degree of freedom m_1, we can now see what would happen if we do not take into account the fact that Josephson junction arrays are open quantum systems. In that case the field m_1 of the first island is not an independent degree of freedom. The Hamiltonian $H^m(\{Q\})$ does not contain m_1-tunnelling terms and the single particle Hamiltonian of the first site is simply a quasi-charge dependent energy term with constant m_1,

$$H_1(Q_1) = E_Q^1(Q_1) = \frac{(2em_1 - Q_1)^2}{2C_J} \ . \tag{2.77}$$

The parabolic potential $E_Q^1(Q_1)$ in H_Q diverges as the absolute quasi-charge on the first site goes to infinity $|Q_1| \to \infty$. It prevents DC charge transport through the array.The effective quasi-charge model of a closed Josephson junction array correctly predicts that no long term current can flow through an array without Cooper-pairs tunnelling between the array and the leads. Currents can only flow in the array to redistribute charge internally to compensate external perturbations.

The Born-Oppenheimer approximation is exact in the full adiabatic limit of a vanishing quasi-charge velocity,

$$v_i^Q = \frac{\partial}{\partial t} Q_i \to 0 \ . \tag{2.78}$$

Whenever v_i^Q is finite one can consider corrections to the adiabatic assumption. In the Josephson junction arrays these corrections give an inductive term in the effective quasi-charge model [35, 12],

$$\mathcal{L}_Q = \sum_i \frac{1}{2} L_B(Q_i + F_i) \left(\partial_t Q_i\right)^2 - \frac{(Q_i - Q_{i+1})^2}{2C_0} - E_Q\left(Q_i + 2e\ F_i\right) + (V+U)\, Q_1 - U Q_{N+1} \ , \tag{2.79}$$

$$H_Q = \sum_i \frac{1}{2L_B(Q_i + F_i)} \left(\Phi_i^L\right)^2 + \frac{(Q_i - Q_{i+1})^2}{2C_0} + E_Q\left(Q_i + 2e\ F_i\right) - (V+U)\, Q_1 + U Q_{N+1} \ , \tag{2.80}$$

where $L_B(Q)$ is the quasi-charge dependent Bloch inductance [34]. The detailed derivation of the Bloch inductance from time dependent perturbation theory and a discussion of the valid parameter space can be found in Refs.[35, 12].

To give a short summary of the mechanism behind the appearance of the Bloch inductance let us consider the degeneracy point of two parabolas $m = 0$ and $m = 1$ in Fig.2.10. Neglecting the other $|m\rangle$-states, scanning through the degeneracy point with a constant v^Q is equivalent to the Landau-Zener problem [42, 43, 44, 45]. We assume the system is in the lower band at infinite negative times $t_0 = -\infty$ and $Q = -\infty$ and Q grows with the constant velocity v^Q until, at $t_1 = 0$, the point of minimal level splitting between lower and upper band is reached. The velocity v^Q is kept constant so that the system moves away from the degeneracy point. The probability that the finite velocity leads to a transition from lower to upper band in the infinite time limit $t \to \infty$ is given by [12, 42],

$$P \approx e^{-\frac{\pi}{2\hbar} E_J^2 \frac{2e}{E_C} \frac{1}{|v^Q|}} \ . \tag{2.81}$$

If the velocity is small enough the system will still be in the ground-state in the infinite time limit and no transition occurs.

During the time-evolution of the system state,

$$|\psi(t)\rangle = \alpha(t)\,|m=0\rangle + \beta(t)\,|m=1\rangle \ , \tag{2.82}$$

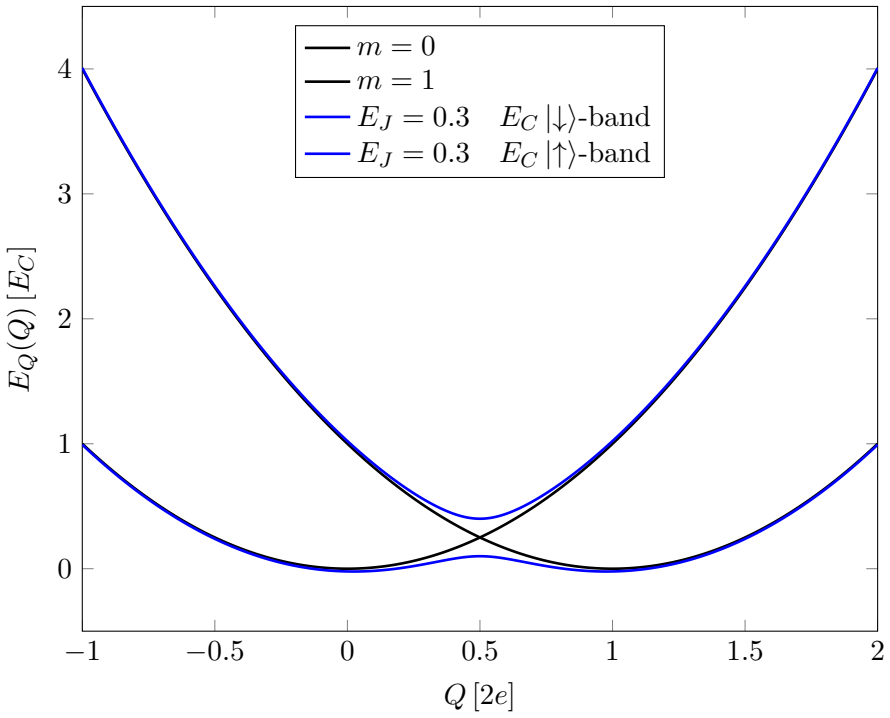

Figure 2.10: The degeneracy between the charging energies of the states $|m = 0\rangle$ and $|m = 1\rangle$ (plotted in black) at $Q = e$ is lifted by the Josephson coupling energy E_J. Here we only plot two of the m-bands for simplicity. Moving the quasi-charge through the degeneracy point with a finite velocity v^Q leads to a mixing between the upper $|\uparrow\rangle$ and lower band $|\downarrow\rangle$ in the vicinity of $Q = e$. Even when no transition to the upper band occurs in the infinite time limit at $Q \to \infty$, the mixing around the degeneracy point incurs an energy cost.

the finite velocity of the classical parameter $Q(t)$ leads nonetheless to a mixing p_{mix} with the upper band state,

$$p_{mix} = \langle \psi(t) \mid \uparrow \rangle \neq 0 \; . \tag{2.83}$$

The mixing with the upper band state increases with increasing velocity and decreasing energy difference between the bands. As the energy difference depends on the value of the quasi-charge Q so does the mixing p_{mix}.

The mixing with the higher energy eigenstates of $H_i(Q)$ carries an energy cost and leads to an additional inductive term in the Hamiltonian of the effective quasi-charge model Eq.2.80 [35, 12]. The Bloch inductance is peaked around the avoided level crossings, $Q_i = e + n\ 2e$, where the level splitting is minimal. The peak Bloch inductance is large enough to slow down the time evolution of the quasi-charge sufficiently to justify the Born-Oppenheimer approximation [35, 12]. One can argue that the large value of $L_B(Q)$ makes the adiabatic assumption self-consistent.

The self-consistency arguments presented here are more qualitative arguments than exact quantitative mathematical statements. With the help of depinning-theory we will give an estimated range of validity for the self-consistency argument in the following chapter, Ch.3.

Equations of motion

The physical behaviour of the Josephson junction arrays is often directly obtained from the equations of motion of the quasi-charge [3, 12]. The equations of motion following

from the Lagrangian $\mathcal{L}_Q$ (Eq.2.79) are given by,

$$V_i^{dyn} + \frac{2Q_i - Q_{i-1} - Q_{i+1}}{C_0} + V_Q(Q_i + 2e\ F_i) = 0, \tag{2.84}$$

for the bulk,

$$V_1^{dyn} + \frac{Q_1 - Q_2}{C_0} + V_Q\left(Q_1\right) = V + U\ , \tag{2.85}$$

for the leftmost island and,

$$V_{N+1}^{dyn} + \frac{Q_N - Q_{N+1}}{C_0} + V_Q\left(Q_{N+1} + 2e\ F_{N+1}\right) = -U\ , \tag{2.86}$$

for the rightmost island. We used the shorthand notation,

$$V_i^{dyn} = L_B(Q_i + 2e\ F_i)\,\ddot{Q}_i + \frac{\partial}{\partial Q_i} L_B(Q_i + 2e\ F_i)\,\dot{Q}_i^2\ . \tag{2.87}$$

The function $V_Q(Q)$ is the quasi-charge derivative of the effective potential $E_Q(Q)$,

$$V_Q\left(Q + 2e\ F\right) = \frac{\partial}{\partial Q} E_Q(Q + 2e\ F)\ . \tag{2.88}$$

From our previous discussion of the form of $E_Q(Q)$ (Fig.2.4) we know that, in the $E_J \geq E_C$ limit, $V_Q(Q)$ is sinusoidal. In the opposite limit, $E_J \ll E_C$, it approaches the shape of a saw function. As the potential $E_Q(Q)$, the voltage function $V_Q(Q)$ is $2e$-periodic in the quasi-charge. The limits of the amplitude V_Q^{max} of $V_Q(Q)$ are given by,

$$V_Q^{max} = \max_{Q\in[-e,e]}\left(V_Q(Q)\right) - \min_{Q\in[-e,e]}\left(V_Q(Q)\right)\ , \tag{2.89}$$

$$V_Q^{max} \to \begin{cases} \frac{\pi}{e}\frac{1}{4}E_C & \text{for} \quad \frac{E_J}{E_C} \to 0 \\ 0 & \text{for} \quad \frac{E_J}{E_C} \to \infty \end{cases}\ . \tag{2.90}$$

A sample of $V_Q(Q)$ for different ratios of E_J/E_C is plotted in Fig.2.11.

The equations of motion Eq.2.84, Eq.2.85 and Eq.2.86 can be simplified by replacing the Q-dependent Bloch inductance with a constant inductance, $L_B(Q) \to L$, when modelling of the onset of transport. In the insulating regime the quasi-charge velocity is zero and the inductive term in the Hamiltonian gives no energy-contribution. Once the transport threshold set by the potential $E_Q(Q)$ is overcome, the inductance determines the time-scale of the acceleration of the charge transport. To find the value of the threshold the exact value of $L_B(Q)$ is not important and we can use the simplified version of the equations of motion,

$$L\ddot{Q}_i + \frac{2Q_i - Q_{i-1} - Q_{i+1}}{C_0} + V_Q\left(Q_i + 2e\ F_i\right) = 0\ , \tag{2.91}$$

$$L\ddot{Q}_1 + \frac{Q_1 - Q_2}{C_0} + V_Q\left(Q_1\right) = V + U\ , \tag{2.92}$$

$$L\ddot{Q}_{N+1} + \frac{Q_N - Q_{N+1}}{C_0} + V_Q\left(Q_{N+1} + 2e\ F_{N+1}\right) = -U\ , \tag{2.93}$$

and the simplified Hamiltonian,

$$H_Q = \sum_i \frac{1}{2L}\left(\Phi_i^L\right)^2 + \frac{\left(Q_i - Q_{i+1}\right)^2}{2C_0} + E_Q(Q_i) - \left(V + U\right)Q_1 + UQ_{N+1}\ . \tag{2.94}$$

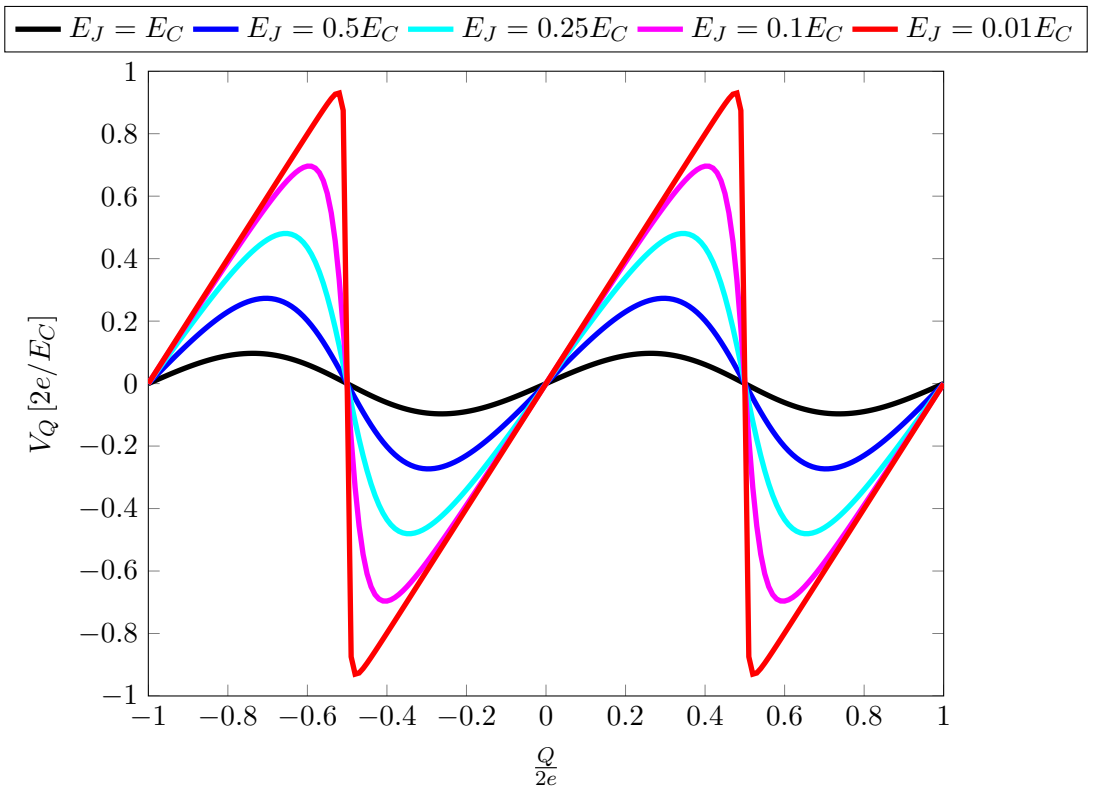

Figure 2.11: A sample of quasi-charge dependent voltage functions $V_Q(Q)$ obtained from the diagonalisation of the Q-dependent Hamiltonian Eq.2.75. Decreasing the ratio between Josephson coupling energy and charging energy $\frac{E_J}{E_C}$ changes the form of the function from a sine to a saw-shape and increases the amplitude of the periodic function.

We will use these simplified equations of motion in the next chapter Ch.3 to study the switching voltage in the IV-curve of Josephson junction arrays.

We finally see why the effective quasi-charge model can also be referred to as the sine-Gordon-like model. When taking the continuum limit of the equation of motion Eq.2.91 the coupling term between the quasi-charges on neighbouring sites takes the form of a second spatial derivative [3],

$$L\ddot{Q}\,(x,t) + \frac{1}{C_0}\frac{\partial^2}{\partial x^2}Q\,(x,t) + V_Q\,(Q(x,t) + 2e\ F(x)) = 0\ , \tag{2.95}$$

and the equations of motion for the terminating islands Eq.2.92 and Eq.2.93 take the form of boundary conditions [3],

$$\begin{aligned} \frac{1}{C_0}\frac{\partial}{\partial x}Q\,(x,t)\Big|_{x=0} &= V + U\ , \\ \frac{1}{C_0}\frac{\partial}{\partial x}Q\,(x,t)\Big|_{x=N} &= -U\ . \end{aligned} \tag{2.96}$$

The continuum limit is justified when the typical length scale of the problem is large $\Lambda \gg 1$ and the quasi-charge can be expected to be a smooth function over many array sites.

For $E_J \gg E_C$, the continuum limit can be approximated by,

$$L\ddot{Q}\,(x,t) + \frac{1}{C_0}\frac{\partial^2}{\partial x^2}Q\,(x,t) + \frac{\pi}{e}E_Q^{max}\sin\left(\frac{\pi}{e}Q\,(x,t) + 2\pi\ F\,(x)\right) = 0\ , \tag{2.97}$$

the sine-Gordon-equation with disorder in the potential term. In the same limit, $E_J \gg E_C$, the simplified equation of motion Eq.2.91 is the discrete version of the sine-Gordon-equation also known as Frenkel-Kontorova equation [46]. In the general case the voltage $V_Q(Q)$ is not sinusoidal but still $2e$-periodic and bears a certain resemblance to a sine. To introduce a short hand notation and to keep in mind that the resulting physics is strongly connected to the exact sine-Gordon-model we call Eq.2.91, Eq.2.92 and Eq.2.93 the sine-Gordon-like model.

2.2.3 The Josephson junction array with additional inductances

Many works on Josephson junction arrays in the past have used a different circuit model of the array than it was used in the previous sections. It was assumed that in each array segment a large inductance L follows each Josephson junction [22, 23, 3, 4, 24], see also Fig2.12 for an array segment with an additional inductance. With inductances present in the array, the Lagrangian of a bulk array segment takes the form,

$$\mathcal{L}_i = \frac{1}{2}C_J\left(\dot{\phi}_i^q\right)^2 + \frac{1}{2}C_0\left(\dot{\psi}_i^q\right)^2 - \frac{1}{2L}\left(\Phi_i^L\right)^2 + E_J\cos\left(\frac{2\pi}{\Phi_0}\phi_i^q\right) \ , \tag{2.98}$$

where Φ_i^L is the phase dropping over the inductance in units of Φ_0.

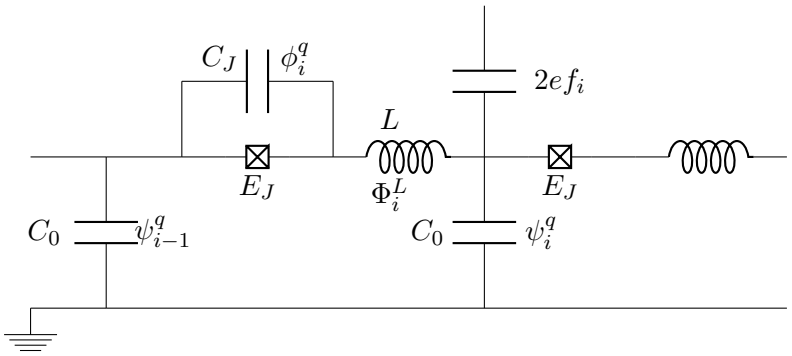

Figure 2.12: In the literature [22, 23, 3, 4, 24] Josephson junction arrays with large inductances L after each Josephson junction are often considered. The large inductance introduces an additional degree of freedom, the phase-difference Φ_i^L over the inductance.

In the presence of inductances L the phase-drop over the inductance has to be considered in Kirchhoff's law Eq.2.41 and one obtains,

$$\phi_i^q + \Phi_i^L + \psi_i^q - \psi_{i-1}^q = 0 \quad i \in \{2, \dots N\} \ , \tag{2.99}$$

as a sum rule for the phase differences in the bulk of the array. The boundary Lagrangians are modified in the same way as for the array without inductances. The left Lagrangian $\mathcal{L}_1$ is given by the bulk $\mathcal{L}_i$ and the right loop Lagrangian,

$$\mathcal{L}_{N+1} = \frac{1}{2}C_J\left(\dot{\phi}_{N+1}^q\right)^2 - \frac{1}{2L}\left(\Phi_{N+1}^L\right)^2 + E_J\cos\left(\frac{2\pi}{\Phi_0}\phi_{N+1}^q\right) \ , \tag{2.100}$$

is missing the $\frac{1}{C_0}$-term. Kirchhoff's law for the terminating loops is given by,

$$\begin{aligned} \phi_1^q + \Phi_1^L + \psi_1^q &= (V+U)\,t \ , \\ \phi_{N+1}^q + \Phi_{N+1}^L - \psi_N^q &= -U \ . \end{aligned} \tag{2.101}$$

As before we can define the fields m_i, the quasi-frustration F_i and the quasi-charge Q_i,

$$m_i = -\sum_{j=1}^{i-1} n_j \ , \tag{2.102}$$

$$F_i = \sum_{j=1}^{i-1} f_j \ , \tag{2.103}$$

$$Q_i = \sum_{j=1}^{i-1} (q_j^{\psi}) + q_1 \ . \tag{2.104}$$

The quasi-charge Q_i is the canonical conjugate to the phase Φ_i^L dropping over the inductances,

$$\left[\Phi_k^L, Q_l\right] = i\delta_{k,l} \ . \tag{2.105}$$

Due to the additional independent degrees of freedom Φ_i^L, the quasi-charge is not introduced by a Hubbard-Stratonovich transformation. In the presence of inductances the introduction of the quasi-charge is essentially equivalent to a linear transformation [3, 24].

This does not only hold for large inductances L as we assume in this section but also for arbitrarily small inductances. From the start the system has $N+1$ more degrees of freedom than the array without inductances. The equations of charge neutrality and Kirchhoff's law eliminate $2N+1$ independent degrees of freedom from the problem by expressing them as functions of other variables. Without the Φ_i^L introduced by the inductances L this is sufficient to express all original continuous degrees q_i, q_i^{psi} as functions of the Cooper pair number n_i. With the inductances two sets of independent variables remain, the discrete n_i and the continuous q_i^{ψ}. The quasi-charges Q_i and the m_i are therefore independent degrees of freedom.

Naturally the quasi-charge can be introduced in this way for the models that assume large inductances as in Eq.2.98 and Fig.2.12. The argument is even valid for infinitesimal inductances, $L = L_{inf}$, as long as the Φ_i^L are not exactly zero. A model without any inductances in the Hamiltonian H Eq.2.47 relies on the assumption that the charge distribution on each superconducting island is in equilibrium at all times. A change in the phase difference over the capacitances connecting the island to its neighbours leads to an instantaneous redistribution of charge between the capacitances C_J and C_0. This is of course not exactly correct in the microscopic model of an array island. A shift in the density distribution of the superconducting condensate takes a small but finite amount of time.

The delay in the response of the charge distribution to the applied voltage corresponds to a non-vanishing inductance L_{inf} of the island. However the inductance L_{inf} can be infinitesimal compared to all other parameters of the model. We also want to note that the microscopic argument for the presence of an infinitesimal L_{inf} is only relevant as far as one can write down the Hamiltonian $H\left(\{Q\}\right)$ Eq.2.67 without invoking a Hubbard-Stratonovich transformation. The number of required assumptions in the derivation of the effective sine-Gordon model is only reduced in the presence of large inductances L.

Writing down the Hamiltonian in the quasi-charge representation,

$$H\left(\{\hat{Q}\}\right) = \sum_{i=1}^{N} \frac{1}{2L}\left(\Phi_i^L\right)^2 + \frac{\left(2e\hat{m}_i - 2eF_i - \hat{Q}_i\right)^2}{2C_J} + \frac{\left(\hat{Q}_i - \hat{Q}_{i+1}\right)^2}{2C_0} - E_J\left(|m_i+1\rangle\langle m_i| + \text{h.c.}\right) \ , \tag{2.106}$$

we see why the derivation of the effective quasi-charge model is more robust in the presence of large inductances L. So far the slow rate of change of the quasi-charges has only been postulated. The inductive energy term in the Hamiltonian has the form of a pseudo mass term. Fast changes in the quasi-charge carry an additional energy cost that grows linearly with L. A large inductance forces Q_i to change adiabatically, so that the Born-Oppenheimer approximation is valid without resorting to the Bloch-inductance and self-consistency arguments. The equations of motion of the quasi-charge can be obtained in the same way as the equations of motion in the inductance-less case. In the equations of motion, the pure Bloch inductance $L_B(Q)$ has to be replaced by a combination $L_{comb}(Q)$ of the microscopic inductance L and the emergent inductance $L_B(Q)$,

$$L_B(Q) \to L_{comb}(Q) = L + L_B(Q) \ . \tag{2.107}$$

We assume that the inductances L are large, $L \gg L_B(Q)$, and obtain the simplified model,

$$L_{comb}(Q) = L \ , \tag{2.108}$$

with,

$$L\ddot{Q}_i + \frac{2Q_i - Q_{i-1} - Q_{i+1}}{C_0} + V_Q\left(Q_i + 2e\ F_i\right) = 0 \ , \tag{2.109}$$

$$L\ddot{Q}_1 + \frac{Q_1 - Q_2}{C_0} + V_Q\left(Q_1\right) = V + U \ , \tag{2.110}$$

$$L\ddot{Q}_{N+1} + \frac{Q_N - Q_{N+1}}{C_0} + V_Q\left(Q_{N+1} + 2e\ F_{N+1}\right) = -U \ , \tag{2.111}$$

and the effective quasi-charge Hamiltonian,

$$H_Q = \sum_i \frac{1}{2L}\left(\Phi_i^L\right)^2 \frac{\left(Q_i - Q_{i+1}\right)^2}{2C_0} + E_Q\left(Q_i + 2e\ F_i\right) - \left(V + U\right)Q_1 + UQ_{N+1} \ . \tag{2.112}$$

2.3 The quantum phase slip array

Although the Josephson junction array is the main topic of this work, we also want to discuss the dual model to the Josephson junction array, the quantum phase slip array (QPS-array). The QPS-array is in large parts governed by the same mathematical equations as the Josephson junction array, except that the role of charge is exchanged with the role of phase and the role of voltage is exchanged with the role of current.

A circuit of $N+1$ quantum phase slip elements that is arranged in a ladder geometry (Fig.2.13) is dual to the Josephson junction array of N superconducting islands. The vertical connections in the array are the QPS-elements. They are characterized by the inductance L_{ps} and the phase slip energy E_s. The phase difference over the $i-th$ QPS-element is ϕ_i. The horizontal elements are superconducting connections. In the upper rail the connection has a kinetic inductance L_0 and a vanishing quantum phase slip amplitude. The upper rail corresponds to the capacitance to the ground in the Josephson junction array. The phase differences over the inductances L_0 in the upper rail is given by ψ_i. The lower rail has a vanishingly small inductance. Again all phase-differences are given in units of Φ_0. A sketch of two loops of the ladder with all relevant phases is shown in Fig.2.14.

The QPS-array is dual to our model of the Josephson junction array.

In the quantum phase slip ladder Kirchhoff's law takes the form,

$$\phi_i + \psi_i - \phi_{i+1} = \Phi_0\left(n_i + f_i\right) \ , \tag{2.113}$$

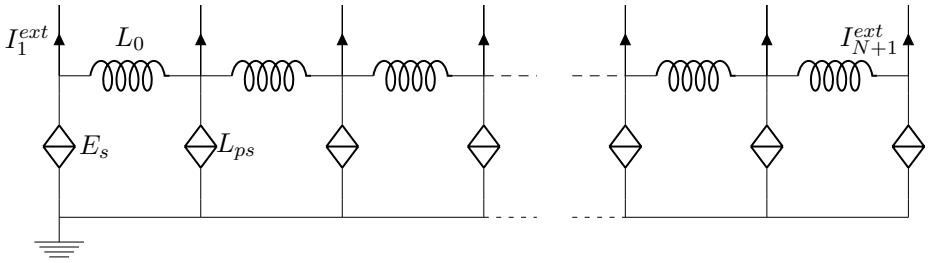

Figure 2.13: A sketch of the quantum phase slip ladder. Each loop of the ladder contains the horizontal inductance L_0 and two vertical connections, the quantum phase slip elements. The quantum phase slip elements are characterized by an inductance L_{ps} and the phase slip energy E_s.

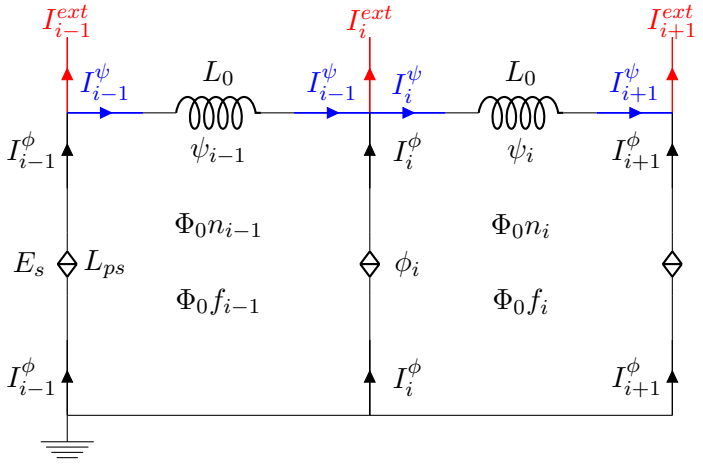

Figure 2.14: A segment of the QPS-ladder in Fig.2.13. In each loop the sum over the phases dropping over the QPS-elements ϕ_i and $-\phi_{i+1}$ and the phase ψ_i over the inductance L_0 is equal to the total magnetic flux in the loop given by the number of flux quanta n_i and the external frustration f_i. The sum over the external bias current $-I_i^{ext}$, the horizontal currents I_{i-1}^{ψ} and $-I_i^{\psi}$ and the current through the QPS-element I_i^{ϕ} is zero according to Kirchoff's circuit laws.

where n_i is the number of magnetic flux quanta Φ_0 in the i-th loop of the array, as seen in Fig.2.14. Together with the magnetic frustration f_i it gives the total magnetic flux through the loop. The flux quanta in the loops play the same role as the excess Cooper pairs on the superconducting islands of the Josephson junction array. A quantum phase slip through the i-th QPS-element is a tunnelling event of one flux quantum from loop $i-1$ to loop i.

Contrary to the disordered background charges in Josephson junction arrays we do not expect a large number of disordered sources of magnetic flux in the background of the QPS-arrays. The frustration f_i can be assumed to be zero if no further external sources of magnetic frustration are present. It is however very simple to produce a homogeneous frustration by applying a magnetic field. The f_i are simply given by the external magnetic flux per loop divided by the flux quantum Φ_0. The homogeneous frustration corresponds to the offset voltage U in the Josephson junction array model. Both set a chemical potential or preferred filling factor for the Cooper pairs or flux quanta in the respective systems. We will further discuss some consequences of externally controlled frustration at the end of this chapter in Sec.2.5.

The second set of equations that reduces the number of independent degrees of freedom in the quantum phase slip ladder is derived from the sum rule for the electric currents at each intersection of superconducting wires. As the intersections can not be net sources of charge the net current has to be zero,

$$\sum_i I_i = 0 \ . \tag{2.114}$$

Considering the currents of the upper intersection between two loops in the bulk of the array in Fig.2.14, the sum of the two currents I_i^{ψ} through the inductances L_0 and the current through the QPS-element I_i^{ϕ} has to be equal to the current I_i^{ext} leaving the array,

$$-I_i^{phi} + I_{i-1}^{\psi} - I_i^{\psi} = I_i^{ext} \ , \tag{2.115}$$

$$-q_i^{\phi} + q_{i-1}^{\psi} - q_i^{\psi} = Q_i^{ext} \ , \tag{2.116}$$

where q_i^{ψ} and q_i^{ϕ} are the total charges that have passed through the i-th inductances L_0 and L_{ps} and Q_i^{ext} is the total charge that has left the array at intersection i,

$$I_i^{\psi} = \dot{q}_i^{\psi} \ , \quad I_i^{\phi} = \dot{q}_i^{\phi} \ , \tag{2.117}$$

$$I_i^{ext} = \dot{Q}_i^{ext} \ . \tag{2.118}$$

The Q_i^{ext} provide the biasing of the QPS-array. The analogue to the boundary biasing in the Josephson junction array is a situation where only Q_1^{ext} and Q_{N+1}^{ext} are nonzero.

Using Faraday's law of induction,

$$\dot{I}_i^{\phi} = \frac{1}{L_{ps}} \dot{\phi}_i \ , \tag{2.119}$$

$$\dot{I}_i^{\psi} = \frac{1}{L_0} \dot{\psi}_i \ , \tag{2.120}$$

we can express Kirchhoff's law Eq.2.113 in terms of the flown charges,

$$L_{ps} \dot{q}_i^{\phi} + L_0 \dot{q}_i^{\psi} - L_{ps} \dot{q}_{i+1}^{\phi} = \Phi_0 \left(n_i + f_i \right) \ . \tag{2.121}$$

The conditions connecting the flown charges to the discrete number of flux quanta are dual to Kirchoff's law and the charge neutrality condition Eq.2.41, Eq.2.43 and Eq.2.40 in Josephson junction arrays.

The Lagrangian for a bulk loop of the quantum phase slip ladder contains the inductive energy of the phase differences over L_{ps} and L_0 and the cosine of the charge flown through the QPS-element in the potential. It is given by,

$$\mathcal{L}_i^{ps} = \frac{1}{2} L_{ps} \left(\dot{q}_i^{\phi} \right)^2 + \frac{1}{2} L_0 \left(\dot{q}_i^{\psi} \right)^2 + E_s \cos \left(\frac{\pi}{e} q_i^{\phi} \right) \ . \tag{2.122}$$

Just as for the Josephson junction array, the Lagrangian of the right terminating loop and the current sum rule Eq.2.116 for both terminating loops have to be adjusted,

$$\begin{aligned} q_1^{\phi} + q_1^{\psi} &= Q_1^{ext} \ , \\ q_{N+1}^{\phi} - q_N^{\psi} &= Q_{N+1}^{ext} \ . \end{aligned} \tag{2.123}$$

This time the inductive term of the horizontal superconducting connections is missing from the last Lagrangian as there are only N horizontal connections,

$$\mathcal{L}_{N+1}^{ps} = \frac{1}{2} L_{ps} \left(\dot{q}_{N+1}^{\phi} \right)^2 + E_s \cos \left(\frac{\pi}{e} q_{N+1}^{\phi} \right) \ , \tag{2.124}$$

so that the total Lagrangian of the ladder is the sum,

$$\mathcal{L}^{ps} = \sum_{i=1}^{N} \mathcal{L}_i^{ps} + \mathcal{L}_{N+1}^{ps} \ . \tag{2.125}$$

From now on we can follow the same mathematical derivation as for the Josephson junction arrays. We quickly present the results, all explanations and discussion from the Josephson array derivation apply analogously under the exchange of the role of charge and phase as well as capacitance and inductance. The quantum phase slip ladder Hamiltonian, H_{ps}, is given by,

$$H_{ps} = \sum_i \frac{1}{2L_{ps}}\phi_i^2 + \frac{1}{2L_0}\left(\psi_i\right)^2 - E_s \cos\left(\frac{\pi}{e}q_i^{\phi}\right) + \frac{1}{2L_{ps}}\phi_{N+1}^2 \ . \tag{2.126}$$

As a function of the discrete numbers n_i of flux quanta Φ_0 in the loops, the Hamiltonian takes the form,

$$H_{ps} = \sum_{i\ j} \frac{1}{2}\left(\Phi_0\left(n_i + f_i\right) + Q_i^{ext}\right)\left(L_m^{-1}\right)_{ij}\left(\Phi_0\left(n_j + f_j\right) + Q_j^{ext}\right) - \sum_i E_s \cos\left(\frac{\pi}{e}q_i^{\phi}\right) \ , \tag{2.127}$$

with,

$$\cos\left(\frac{\pi}{e}q_i^{\phi}\right) = \sum_i \left(|n_{i+1}+1, n_i - 1\rangle\langle n_{i+1}, n_i| + |n_{i+1}-1, n_i+1\rangle\langle n_{i+1}, n_i| + \text{h.c.}\right) \ , \tag{2.128}$$

where L_m is the inductance matrix that has the same function as the capacitance matrix C_m in the Josephson junction array,

$$\left(L_m\right)_{ij} = \left(2L_{ps} + L_0\right)\delta_{i,j} - L_{ps}\delta_{i,j-1} - L_{ps}\delta_{i,j+1} \ . \tag{2.129}$$

The relevant energy scale of the interaction between two flux quanta in different loops is determined by the magnetic energy E_L,

$$E_L = \frac{1}{2L_s}\Phi_0^2 \ . \tag{2.130}$$

The length scale Λ is now the square root of the ratio of the two inductances of the array,

$$\Lambda = \sqrt{\frac{L_{ps}}{L_0}} \ . \tag{2.131}$$

Instead of a quasi-charge Q_i we define a quasi-phase Φ_i, along with the fields m_i and the

quasi-frustration F_i,

$$m_i = -\sum_{j=1}^{i-1} n_j \quad i > 1 \ , \tag{2.132}$$

$$n_i = m_i - m_{i+1} \ , \tag{2.133}$$

$$F_i = \sum_{j=1}^{i-1} f_j \quad i > 0 \ , \tag{2.134}$$

$$\Phi_i = \sum_{j=1}^{i-1} (\psi_j) + \phi_1 \ , \tag{2.135}$$

$$\phi_i = \sum_{j=1}^{i-1} (\psi_j + \Phi_0 \ f_j) + \Phi_0 \sum_{j=1}^{i-1} n_i + \phi_1 \tag{2.136}$$

$$= \Phi_i + \Phi_0 \ F_i - \Phi_0 m_i \ , \tag{2.137}$$

$$\psi_i = \Phi_{i+1} - \Phi_i \ . \tag{2.138}$$

By using either a Hubbard-Stratonovich transformation or by including infinitesimal capacitances C_{inf} parallel to the QPS-element, the quasi-phases Φ_i are introduced into the QPS-ladder Hamiltonian and the m_i from different loops of the ladder are decoupled. As for the infinitesimal inductances L_{inf} in the Josephson junction array, we want to note that the presence of capacitances C_{inf} is realistic from a microscopic point of view. The horizontal superconducting connections in the upper and lower rail with inductance L_0 are superconducting wires with a finite length in real space. In principle a geometric capacitance exists between the upper and lower rail, it will however be small compared to the other parameters of the array.

Finally we arrive at the dual Hamiltonian to the quasi-charge Hamiltonian $H(\{Q\})$ Eq.2.67 of the Josephson junction array,

$$H_{ps}(\{\Phi\}) = \sum_{i=1}^{N} \frac{(\Phi_0 m_i - \Phi_0 F_i - \Phi_i)^2}{2L_{ps}} + \frac{(\Phi_i - \Phi_{i+1})^2}{2L_0} + \Phi_i Q_i^{ext} - E_s \cos\left(\frac{\pi}{e} q_i^{\phi}\right) \ . \tag{2.139}$$

2.3.1 The quasi-phase model

Due to the duality of the models we can map everything we did to obtain an effective model of the Josephson junction chain to the quantum phase slip ladder. An effective quasi-phase model for a single QPS-element in a superconducting ring was developed in Ref.[28]. As the ladder-model in the Born-Oppenheimer approximation separates into N independent Hamiltonians the derivation of the effective potential in Ref.[28] is also valid for a QPS-ladder. We will quickly give the most important steps in the derivation of the quasi-phase model of the ladder for later reference.

Taking the quasi-phases Φ_i to change adiabatically compared to the phase slip rate E_s, we can regard $\{\Phi_i\}$ as a set of classical parameters of the quantum phase slip ladder Hamiltonian $H_{ps}(\{\Phi\})$. Like the Josephson junction array Hamiltonian, it separates into $N+1$ single particle Hamiltonians,

$$H_i^{ps}(\Phi_i) = \frac{(\Phi_0 \hat{m}_i - \Phi_0 F_i - \Phi_i)^2}{2L_{ps}} - E_s \left(|m_i + 1\rangle \langle m_i| + \text{h.c.}\right) \ , \tag{2.140}$$

where the phase-slip inductance L_{ps} takes the place of the Josephson junction capacitance C_J and the phase slip energy E_s the place of the Josephson energy E_J. An effective potential for the quasi-phase is obtained from the ground-state energy of $H_i^{ps}(\Phi_i)$,

$$E_\Phi(\Phi) = \langle \text{g.s.}| \frac{(\Phi_0 \hat{m} - \Phi)^2}{2L_{ps}} - E_s \left(|m+1\rangle \langle m| + \text{h.c.} \right) |\text{g.s.}\rangle \ . \tag{2.141}$$

Again higher order corrections to the Born-Oppenheimer approximation in the finite velocity of the quasi-phase give an additional term in the Lagrangian. As inductance and capacitance are dual one obtains an effective capacitance $C_{eff}(\Phi)$ instead of a Bloch inductance,

$$\mathcal{L}_\Phi = \sum_i \frac{1}{2} C_{eff}(\Phi_i + \Phi_0 F_i) \left(\partial_t \Phi_i\right)^2 - \frac{(\Phi_i - \Phi_{i+1})^2}{2L_0} - E_\Phi \left(\Phi_i + \Phi_0 F_i\right) + I_i^{ext} \Phi_i \ , \tag{2.142}$$

$$H_\Phi = \sum_i \frac{1}{2C_{eff}(\Phi_i + \Phi_0 F_i)} \left(Q_i^\Phi\right)^2 + \frac{(\Phi_i - \Phi_{i+1})^2}{2L_0} + E_\Phi \left(\Phi_i + \Phi_0 F_i\right) - I_i^{ext} \Phi_i \ , \tag{2.143}$$

where Q^Φ is the canonical conjugate of the quasi-phase Φ_i. The equations of motion of the bulk are given by,

$$I_i^{dyn} + \frac{2\Phi_i - \Phi_{i-1} - \Phi_{i+1}}{L_0} + I_\Phi \left(\Phi_i + F_i^\Phi\right) = I_i^{ext} \ , \tag{2.144}$$

with the short-hand notation,

$$I_i^{dyn} = C_{eff} \left(\Phi_i + F_i^\Phi\right) \ddot{\Phi}_i + \frac{\partial}{\partial \Phi_i} C_{eff} \left(\Phi_i + F_i^\Phi\right) \dot{\Phi}_i^2 \ , \tag{2.145}$$

$$F_i^\Phi = \Phi_0 F_i \ . \tag{2.146}$$

For the left and right terminating loops one obtains,

$$C_{eff} \left(\Phi_1\right) \ddot{\Phi}_1 + \frac{\partial}{\partial \Phi_1} C_{eff} \left(\Phi_1\right) \left(\dot{\Phi}_1\right)^2 + \frac{\Phi_1 - \Phi_2}{L_0} + I_\Phi \left(\Phi_1\right) = I_1^{ext} \ , \tag{2.147}$$

and,

$$I_{N+1}^{dyn} + \frac{\Phi_N - \Phi_{N+1}}{L_0} + I_\Phi \left(Q_{N+1} + F_{N+1}^\Phi\right) = I_{N+1}^{ext} \ . \tag{2.148}$$

We defined the function I_Φ,

$$I_\Phi \left(\Phi + \Phi_0 \ F\right) = \frac{\partial}{\partial \Phi} E_\Phi(\Phi + \Phi_0 \ F) \tag{2.149}$$

$$= \langle \text{g.s.}| \frac{1}{L_{ps}} \left(\Phi_0 \ m - \Phi - \Phi_0 \ F\right) |\text{g.s.}\rangle$$

$$= \left\langle \frac{1}{L_{ps}} \phi_i \right\rangle_{\text{g.s.}} = \left\langle I_i^\phi \right\rangle_{\text{g.s.}} \ , \tag{2.150}$$

that gives the expectation value of the current I_i^ϕ flowing through the i-th QPS-element. Note that biasing terms I_i^{ext} appear in all equations. We have not restricted ourselves to a purely boundary biased situation as in the Josephson junction chain.

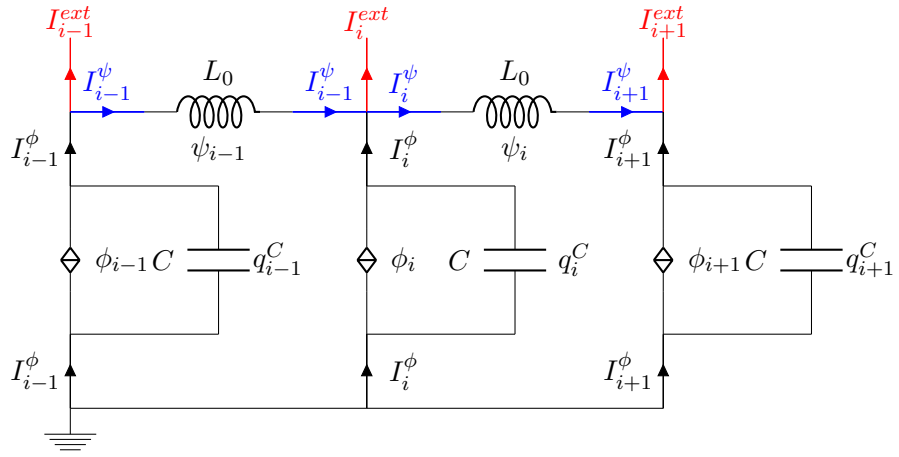

Figure 2.15: The sketch of a segment of a QPS-ladder in which the QPS-elements are shunted by large capacitances C. The model is dual to the Josephson junction array with large inductances (Fig.2.12). The capacitances introduce an additional degree of freedom, the charge q_i^C on the capacitance.

2.3.2 The quantum phase slip array with additional capacitances

In the duality between quantum phase slip circuits and Josephson junction circuits the role of inductance and capacitance is exchanged. The dual model to a Josephson junction array with large inductances in Sec.2.2.3 is a quantum phase slip ladder with a large capacitance C parallel to each quantum phase slip element. This model is shown in Fig.2.15.

In the QPS-ladder with large capacitances, the current sum rule is extended to include the charge q_i^C on the capacitance C,

$$-q_i^{\phi} + q_{i-1}^{\psi} - q_i^{\psi} + q_i^C = Q_i \ , \tag{2.151}$$

and all Lagrangians acquire a capacitative charging term,

$$\mathcal{L}_i^{ps} = \frac{1}{2} L_{ps} \left(\dot{q}_i^{\phi}\right)^2 + \frac{1}{2} L_0 \left(\dot{q}_i^{\psi}\right)^2 - \frac{1}{2C} \left(q_i^C\right)^2 + E_s \cos\left(\frac{\pi}{e} q_i^{\phi}\right) \ . \tag{2.152}$$

The derivation of the effective quasi-phase model is equivalent to the derivation of the effective quasi-charge model in the presence of large inductances in Sec.2.2.3. The quasi-phase Φ_i is not introduced as an additional degree of freedom by a Hubbard-Stratonovich transformation. It is the canonical conjugate of the independent degree of freedom q_i^C. The adiabaticity of the quasi-phase used in the Born-Oppenheimer approximation is guaranteed by the large capacitances C.

In the presence of capacitances much larger than the effective capacitance, $C \gg C_{eff}\left(\Phi\right)$, the time-evolution of the QPS-ladder is given by,

$$C\ddot{\Phi}_i + \frac{2\Phi_i - \Phi_{i-1} - \Phi_{i+1}}{L_0} + I_{\Phi}\left(\Phi_i + \Phi_0\ F_i\right) = I_i^{ext} \ , \tag{2.153}$$

$$C\ddot{\Phi}_1 + \frac{\Phi_1 - \Phi_2}{C_0} + I_{\Phi}\left(Q_1\right) = I_1^{ext} \ , \tag{2.154}$$

$$C\ddot{\Phi}_{N+1} + \frac{\Phi_N - \Phi_{N+1}}{C_0} + I_{\Phi}\left(Q_{N+1} + \Phi_0\ F_{N+1}\right) = I_{N+1}^{ext} \ . \tag{2.155}$$

The equations of motion are dual to those of a Josephson junction array with large inductances L under the exchange of charge and phase as well as capacitance and inductance.

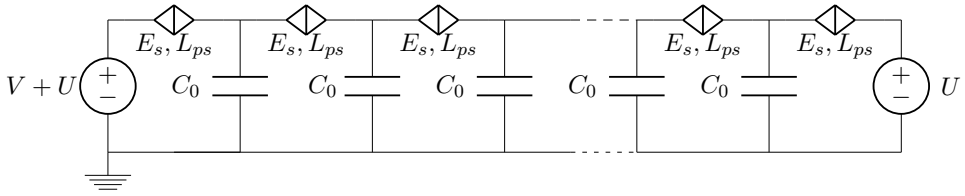

Figure 2.16: A sketch of the linear quantum phase slip chain. The quantum phase slip chain corresponds to a Josephson junction array (Fig. 2.6) where all Josephson junctions have been replaced by QPS-elements with phase slip energy E_s and inductance L_{ps}.

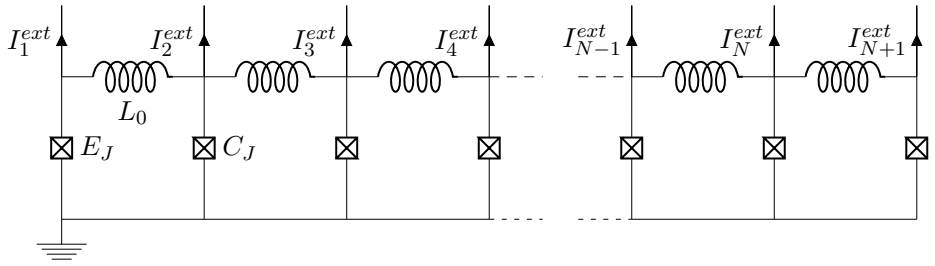

Figure 2.17: A sketch of the Josephson junction ladder. The Josephson junction ladder corresponds to a quantum phase slip ladder (Fig. 2.13) where all quantum phase slip elements have been replaced by Josephson junction with capacitance C_J and Josephson coupling energy E_J.

2.4 Additional array models

Due to the approximate equivalences between Josephson junctions and QPS-elements discussed in Sec.2.1 it can be possible to exchange Josephson junctions and QPS-elements in superconducting circuits without changing the low frequency behaviour. With this in mind we define two additional array models, the linear quantum phase slip chain (Fig.2.16) and the Josephson junction ladder (Fig.2.17). The linear QPS-chain is a linear chain of superconducting islands with capacitive coupling to the ground, just as in the Josephson junction array. Instead of Josephson junctions the islands are connected by QPS-elements with inductance L_{ps} and phase-slip energy E_{ps} . In the Josephson junction ladder the vertical QPS-elements from a quantum phase slip ladder (Fig.2.13) are replaced by Josephson junctions. The Josephson junction ladder is the discrete version of a long Josephson junction array. It has been studied theoretically and experimentally in great detail [10, 47, 48, 49, 50, 20, 51].

Using the definitions for quasi-charge Q_i, quasi-phase Φ_i and quasi-frustration from the Josephson junction array model Sec.2.2 and the QPS-ladder Sec.2.3 the two new arrays have the Hamiltonians of discrete sine-Gordon models. The Hamiltonian of the linear QPS-chain is given by,

$$H_{\text{ps-chain}} = \sum_i \frac{1}{2L_{ps}} (\phi_i)^2 + \frac{(Q_i - Q_{i+1})^2}{2C_0} + E_s \cos\left(\frac{\pi}{e} Q_i + 2\pi\ F_i\right) - (V+U)\, Q_1 + U Q_{N+1}, \tag{2.156}$$

where ϕ_i is the phase difference over the i-th QPS-element. The phase ϕ_i and the quasi-charge Q_i are canonical conjugates. The Hamiltonian of the Josephson junction ladder is

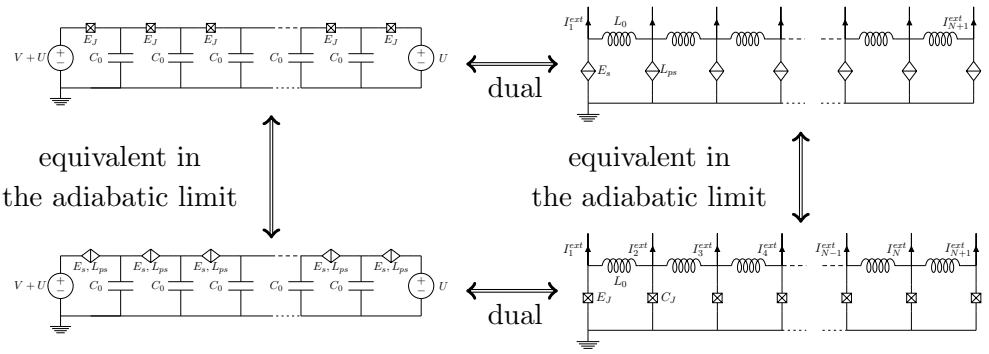

Figure 2.18: A schematic picture of the duality relation between Josephson junction array, QPS-ladder, QPS-chains and Josephson junction ladders. It follows from the duality of Josephson junctions and QPS-elements that in the upper and lower pair the ladder and the chain model are dual to each other. The effective quasi-phase model of a Josephson junction array in the adiabatic limit is approximately equivalent to the QPS-chain. The effective quasi-phase-model of the QPS-ladder in the adiabatic limit is equivalent to the Josephson junction ladder.

given by,

$$H_{\text{JJ-ladder}} = \sum_i \frac{1}{2C_J}\left(q_i^{\phi}\right)^2 + \frac{\left(\Phi_i - \Phi_{i+1}\right)^2}{2L_0} + E_J\cos\left(\Phi_i + \Phi_0 F_i\right) - I_i^{ext}\Phi_i \ , \qquad (2.157)$$

where q_i^{ϕ} is the charge on the Josephson junction capacitance C_J. Again the quasi-phase Φ_i and the charge q_i^{ϕ} are canonical conjugates. These sine-Gordon Hamiltonians are not effective models, they contain all original degrees of freedom and are valid at all frequencies.

The picture (Fig.2.18) describing the relation between the four types of arrays emerges. The Josephson junction array and the QPS-ladder form a dual pair of array models. The other dual pair of array models consists of the linear QPS-chain and the Josephson junction ladder. Furthermore, in parameter regimes where the Born-Oppenheimer approximation can be applied to the first pair of arrays, the resulting quasi-charge Eq.2.80 and quasi-phase Eq.2.143 models are approximately equivalent to the models of the second pair of arrays.

The main differences between the models are the quasi-charge dependence of the Bloch inductance $L_B(Q)$ and the quasi-phase dependence of the effective capacitance $C_{eff}(\Phi)$ and a different shape of the periodic effective potentials $E_Q(Q)$ and $E_\Phi(\Phi)$ from the exact cosine of $H_{\text{ps-chain}}$ and $H_{\text{JJ-ladder}}$.

The conceptual duality between the four arrays is not necessarily reflected in experimental implementations of the arrays. The discrete number of flux quanta per array loop in the QPS-ladder (or Josephson junction ladder) is the dual variable to the number of Cooper pairs in the Josephson junction array (or linear QPS-array). In principle each superconducting island of the linear chains has an additional discrete degree of freedom, the number of quasi-particles with charge e excited from the BCS-condensate. There is no flux-degree of freedom in the ladder-arrays that is dual to the quasi-particle number. The properties of ladder-arrays and linear chain arrays are only dual as long as the influence of quasi-particles in the chains can be neglected.

The expected distribution of the frustration f_i per array side is also different for arrays of superconducting islands and ladder arrays. On the superconducting islands background

charges are present [34] and the f_i have a stochastic distribution. It would be experimentally hard to gate every superconducting island in the array to control f_i by an externally applied voltage. We do not expect background fluxes in the loops of the ladder array. The bare frustration is zero $f_i = 0$. It is however easy to apply an external magnetic field to apply a uniform frustration to all array loops $f_i = f$. While this limits the use of duality in transferring theoretical and experimental results between dual arrays, it also means that one can explore a larger parameter space of the sine-Gordon-like models using both dual arrays.

There are certain types of experiments that could only be done in one of the four closely connected arrays as not all parameters of the superconducting elements can be controlled equally well. It is for example possible to externally control the Josephson coupling energy in the Josephson junction array by replacing the Josephson junctions with superconducting interference devices (SQUIDs). Each SQUID forms an effective Josephson junction with an E_J that is controlled by an external magnetic flux.

The quantum-phase slip energy E_s in the dual QPS-ladder on the other hand can not be controlled during the experiment but is set during device fabrication. The changing E_J results in changes in the amplitude and form of the effective quasi-charge potential.

In the linear QPS-chain the amplitude of the cosine is given by E_s and can not be controlled.

In the Josephson junction ladder the amplitude is the Josephson coupling energy and could be controlled by using a SQUID. However applying an external magnetic field to change E_J would also change the magnetic frustration in the loops of the ladder. In the Josephson junction ladder it is impossible to control E_J independently from the frustration.

2.5 The zero-dimensional limit

In this section we discuss the zero-dimensional limit of the Josephson junction and quantum phase-slip arrays. This limit $\Lambda \gg N$ reduces the complexity of the problem significantly. The zero-dimensional limit shows the most interesting features for specific configurations of frustration f_i other than a random distribution. In the Josephson junction arrays disordered background charges will be present [34] and a specific ordered distribution f_i can not be obtained. Therefore we will discuss the zero-dimensional limit of the quantum phase-slip ladder. In the QPS-ladder a homogeneous disorder configuration $f_i = f$ can be easily obtained in experiments by applying an external magnetic field. The situation is very similar to the well studied case of a Josephson junction ladder [10, 48, 49, 50, 20]. We mainly want to show the effect of the non-cosine-shaped effective potential.

We start from the effective quasi-phase model of the QPS-ladder Eq.2.142 derived in Sec.2.3.1,

$$\mathcal{L}_\Phi = \sum_i \frac{1}{2} C_{eff}(\Phi_i + \Phi_0 F_i) \left(\partial_t \Phi_i\right)^2 - \frac{\left(\Phi_i - \Phi_{i+1}\right)^2}{2L_0} - E_\Phi \left(\Phi_i + \Phi_0 F_i\right) + I_i^{ext} \Phi_i \ . \quad (2.158)$$

In the limit $\Lambda \gg N$ the inductive energy scale of the horizontal inductances L_0 in the QPS-ladder is much larger than the upper limit of the potential energy of the whole array,

$$E_{L0} := \frac{\Phi_0^2}{2L_0} = \Lambda^2 E_L \gg N^2 \max_\Phi \left(E_\Phi(\Phi)\right) \ . \quad (2.159)$$

The energy contribution of the inter-site coupling,

$$E_{\text{coupling}} = \frac{1}{2L_0} \left(\Phi_i - \Phi_{i+1}\right)^2 \ , \quad (2.160)$$

dominates the Lagrangian and is minimized by a flat quasi-phase distribution along the array $\Phi_i \approx \Phi_{i+1}$. In the limit of infinite Λ, the differences between quasi-phases vanish,

$$\frac{\Lambda}{N} \to \infty \quad \Rightarrow \quad \Phi_i - \Phi_j \to 0 \;\; \forall i,j \in \{1 \dots N\} \; . \tag{2.161}$$

We use this limit and substitute the quasi-phase distribution $\{\Phi_i\}$ with a single quasi-phase Φ. The quantum phase slip ladder looses all information about the spatial distribution of the quasi-phase and acts as a zero-dimensional system. This is also referred to as the lumped element approach. It has been used in Refs.[52, 4] as an approximate model of Josephson junction arrays. The zero-dimensional model is given by,

$$\mathcal{L}_\Phi = \frac{1}{2} C^t_{eff}(\Phi) \left(\dot{\Phi}\right)^2 - E^t_\Phi(\Phi) + I^{ext}\Phi \; , \tag{2.162}$$

$$C^t_\Phi(\Phi) = \sum_i C_{eff}(\Phi + \Phi_0 F_i) \; , \tag{2.163}$$

$$E^t_\Phi(\Phi) = \sum_i E_\Phi(\Phi + \Phi_0 F_i) \; , \tag{2.164}$$

$$I^{ext} = \sum_i I^{ext}_i \; , \tag{2.165}$$

where $C^t_\Phi(\Phi)$ is the total capacitance of the QPS-ladder, $E^t_\Phi(\Phi)$ is the total potential and I^{ext} is the total applied bias current. The equations of motion of the quasi-phase also reduce to a single equation,

$$C^t_{eff}(\Phi)\,\ddot{\Phi} + \frac{\partial}{\partial\Phi} C^t_{eff}(\Phi) \left(\dot{\Phi}\right)^2 + I^t_\Phi(\Phi) = I^{ext} \; , \tag{2.166}$$

with the total quasi-phase dependent current I^t_Φ through all QPS-elements of the ladder,

$$\begin{aligned} I^t_\Phi(\Phi) &= \frac{\partial}{\partial\Phi} E^t_\Phi(\Phi) \\ &= \sum_i I_\Phi(\Phi + \Phi_0 F_i) \; . \end{aligned} \tag{2.167}$$

We are now going to discuss the signature of a lumped QPS-ladder in an experimental setup where the ladder is biased by an DC-current and the voltage-response is measured.

Considering the DC case, we note that the equation of motion Eq.2.166 is very similar to the equation that describes the time-evolution of the phase-difference ϕ^q of a current-biased ideal Josephson junction in the quasi-classical limit [10],

$$C_J \ddot{\phi^q} + I_c \sin\left(\frac{2\pi}{\Phi_0}\phi^q\right) = I^{ext} \; , \tag{2.168}$$

with the critical current I_c. Here we have ignored all environmental couplings, including to the quasi-particles in the superconductors, that would lead to a dissipative term in the equation of motion. The equation of motion is only a valid description as long as the absolute value of I^{ext} is small enough that the phase ϕ^q is confined to one of the potential wells of the cosine potential. In the running regime, where ϕ^q can escape the minima of the potential due to external driving, the time-evolution of the phase is determined by the dissipation. The same is true for the QPS-ladder. We have not included dissipation in our model of quantum phase slip ladder.

The signature of a Josephson junction and a lumped QPS-ladder in the DC experiment is the same. Just as for the standard Josephson junction [10], the solution of the equations

of motion is static $\dot{\Phi} = \dot{\phi}^q = 0$ for a small current-bias,

$$\begin{aligned} I^t_\Phi(\Phi) &= I^{ext} \ , \\ I_c \sin\left(\frac{2\pi}{\Phi_0}\phi^q\right) &= I^{ext} \ . \end{aligned} \tag{2.169}$$

The system transitions to the running regime $\dot{\Phi} \neq 0$, when the static relations Eq.2.169 have no solution and the bias current I^{ext} exceeds the critical current I_c^{QPS},

$$I_c^{QPS} = \max_\Phi \left(I^t_\Phi(\Phi)\right) \ . \tag{2.170}$$

In an experiment the critical current is determined by the measured voltage response. In the static phase regime, the external current passes through the QPS-ladder without a voltage response and in the running phase a voltage-drop across the QPS-ladder develops [10].

One signature of the effective quasi-phase model that can be checked experimentally is the dependence of the critical current on the length of the ladder. When no external magnetic field is applied and the frustration is zero, $f_i = F_i = 0$, we call the system a clean QPS-ladder. In the clean case, the sum over the frustration configuration in the definition of the function I^t_Φ Eq.2.167 does not alter the functional form but gives an $(N+1)$-prefactor,

$$I^t_\Phi(\Phi) = N \ I_\Phi(\Phi) \ , \tag{2.171}$$

$$I_c^{QPS} = (N+1) \max_\Phi \left(I_\Phi(\Phi)\right) \ . \tag{2.172}$$

In the frustration-free case, one can expect the critical current to grow linearly with the size of the lumped QPS-ladder, as long as $N \ll \Lambda$. The linear scaling of I_c^{QPS} with the number of QPS-connections in the ladder may seem to be a trivial result but we will later see (Sec.3.3.1) that we do not find linear scaling in the clean case for $\Lambda < N$.

A better test of the quasi-phase model would be to experimentally check the predictions for the effective potential $E_\Phi(\Phi)$ or the current $I_\Phi(\Phi)$. By measuring the critical current in the clean case, one can determine the maximum of I_Φ. The quasi-phase model predicts that the amplitude of I_Φ decreases with increasing ratio of phase-slip energy and inductive energy, E_s/E_L. This could be measured with a set of experimental samples with different parameters.

With the help of the externally tunable frustration one can also obtain some information about the functional form of $I_\Phi(\Phi)$. The form of I_Φ changes smoothly from a saw-function in the limit $E_s/E_L \to 0$ to a cosine-shape in the case $E_s/E_L \gtrsim 1$. Applying an external magnetic field leads to a homogeneous frustration in every loop of the QPS-ladder, $f_i = f$ and the quasi-frustration grows linearly $F_i = \sum_{j=1}^{i-1} f_i \propto i$. In this case, taking the sum in the definition of the function I^t_Φ corresponds to averaging over N instances of a periodic function, each one shifted by the same amount $\Phi_0 f$ with respect to the previous one. The shift leads to a partial cancellation of maxima and minima of the single $I_\Phi(\Phi + \Phi_0 F_i)$ and a reduction in the amplitude of I^t_ϕ compared to the clean case. As the number of QPS-elements in the QPS-array is finite and $I_\Phi(\Phi)$ is Φ_0-periodic, the effect of the externally applied frustration is periodic,

$$I^t_\Phi(\Phi)\big|_{f_i=0} = I^t_\Phi(\Phi)\big|_{f_i=1} \ . \tag{2.173}$$

The effect of frustration is illustrated in Fig.2.19.

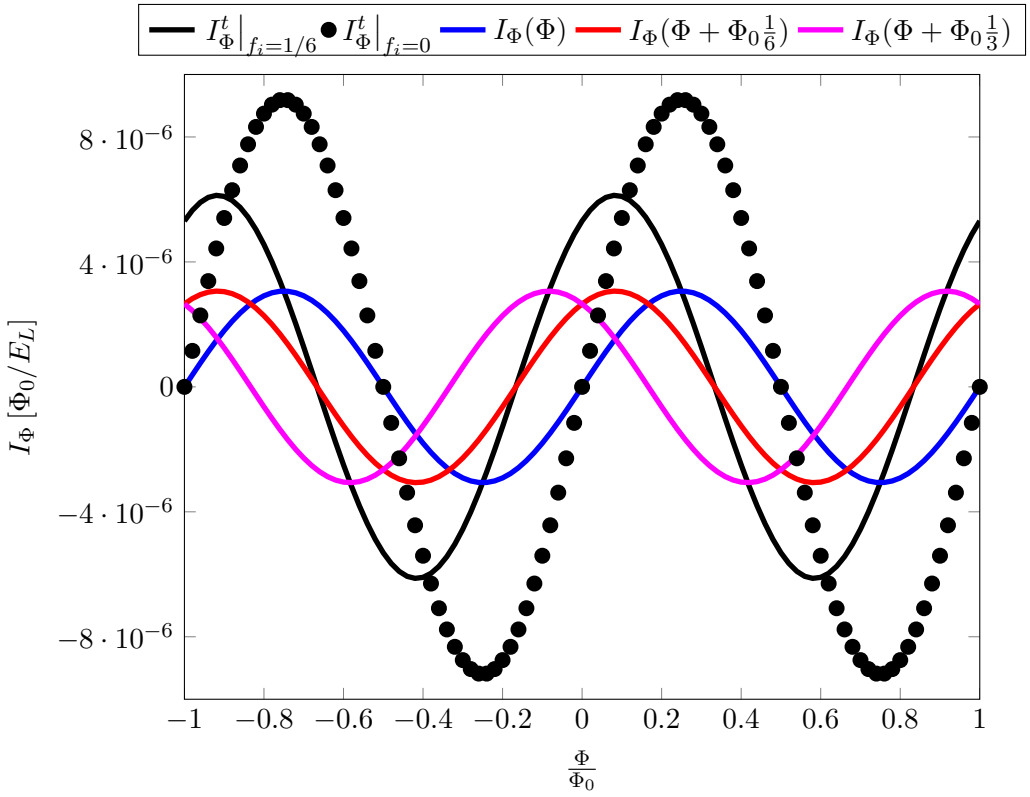

Figure 2.19: In a QPS-ladder with two loops $N = 2$ and a frustration of $f = \frac{1}{6}$, the function $I^t_\Phi\big|_{f=\frac{1}{6}}$ is a sum of the three shifted periodic functions $I_\Phi(\Phi)$, $I_\Phi(\Phi + \frac{1}{6}\Phi_0)$ and $I_\Phi(\Phi + \frac{1}{3}\Phi_0)$. Compared to the frustration free function $I^t_\Phi\big|_{f=0}$ the amplitude is reduced. The QPS-ladder is in the regime $E_s = 10E_L \gg E_L$ and the function $I_\Phi(\Phi)$ is approximately sinusoidal.

We first take the large E_s limit, where I_ϕ is sinusoidal. With the help of a sum rule for the sine we find for a homogeneous frustration,

$$I^t_\Phi(\Phi) = \sum_{j=0}^{N} I^m_c \sin\left(\frac{2\pi}{\Phi_0}\Phi + 2\pi\ j\ f\right) \tag{2.174}$$

$$= I^m_c \frac{\sin\left(2\pi\frac{N+1}{2}f\right)\sin\left(\frac{2\pi}{\Phi_0}\Phi + N\ \pi\ f\right)}{\sin\pi f}\ , \tag{2.175}$$

where I^m_c is the critical current of the effective quasi-phase potential of one QPS-element. This behaviour is known from Josephson junction ladders [10, 48]. At the special values of the frustration,

$$f_{min} = \frac{1}{(N+1)}n \qquad n \in \{1, 2, \ldots, N\}\ , \tag{2.176}$$

the function $I^t_\Phi(\Phi)$ is exactly zero for all quasi-phases. In this case the critical current of the QPS-ladder is zero $I^{QPS}_c = 0$ and no super-current can flow across the quantum phase slip ladder (see also Fig.2.20 for the case of $N = 1$). The mechanism is completely analogous the suppression of super-current through a SQUID.

In the opposite limit $E_s \ll E_L$, due to the saw-form of $I_\Phi(\Phi)$ a finite number of shifted functions, $I_\Phi(\Phi + \Phi_0 F_i)$, can never average to a constant $I^t_\Phi(\Phi)$ and the critical current at the special values of the external frustration is not exactly zero but strongly suppressed.

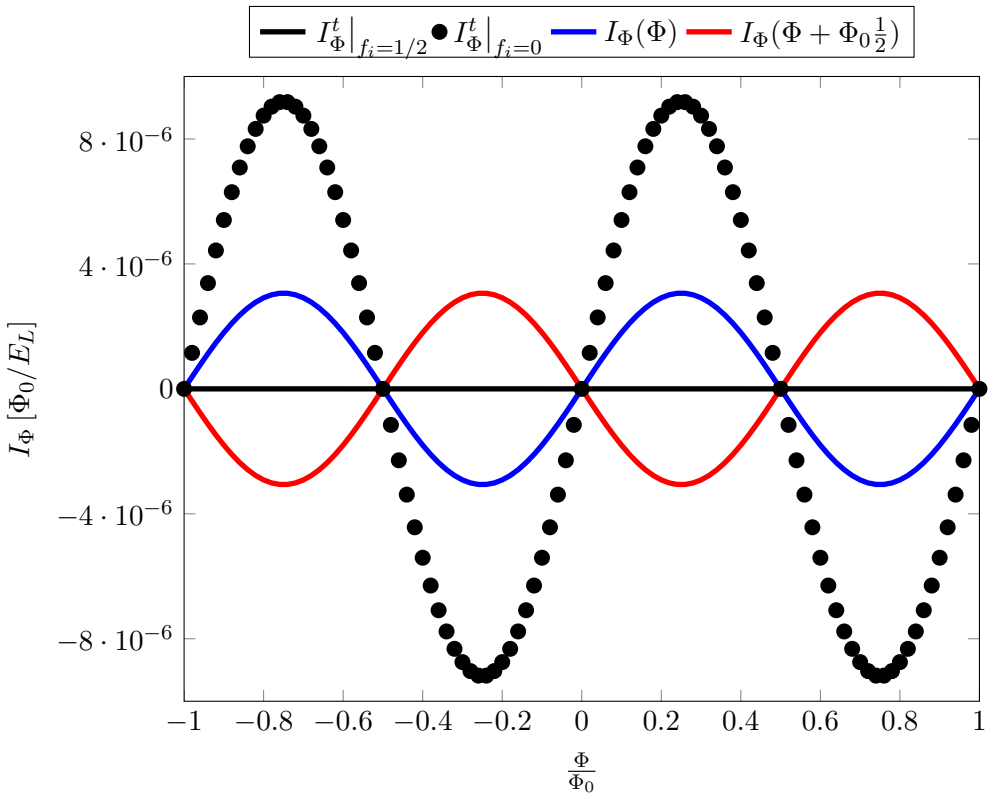

Figure 2.20: We plot the quasi-phase dependent functions I^t_Φ of a QPS-ladder with one loop $N = 1$ in the regime $E_s = 10E_L \gg E_L$. For a frustration of $f = \frac{1}{2}$ the two shifted periodic functions $I_\Phi(\Phi)$ and $I_\Phi(\Phi + \frac{1}{2}\Phi_0)$ compensate each other and the function $I^t_\Phi\big|_{f_i=\frac{1}{2}}$ is zero for all quasi-phases. A magnetic flux of half a flux-quantum Φ_0 in the loop reduces the critical current to zero. The situation is analogue to the suppression of the super-current in a SQUID. The total current-function with no frustration $I^t_\Phi\big|_{f_i=0}$ is plotted for comparison.

This is shown for $N + 1 = 2$ in Fig.2.21. The value of the critical current in the local minima increases with decreasing E_s/E_L as the function $I_\Phi(\Phi)$ becomes more saw-like.

Away from the special frustration f_{min}, the critical current is never completely suppressed in a finite ladder for arbitrary ratios E_s/E_L. The critical current as a function of the frustration is shown in Fig.2.22a and Fig.2.22b for the limiting cases of $E_s \gtrsim E_L$ and $E_s \ll E_L$. With growing N the critical current develops more and deeper local minima. The more periodic functions are summed over, the more the amplitude of the total function in the frustrated case is suppressed compared to the amplitude in the frustration free case.

The special frustration values f_{min} correspond to the minima in the Fraunhofer pattern that is found in the critical current of a Josephson junction in a magnetic field [53]. The Josephson junction corresponds to the continuum limit of the QPS-ladder array $1 \ll N \ll \Lambda$. The sum in the definition of the function I^t_Φ becomes an integral over the length of the Josephson junction perpendicular to the magnetic field that provides the external frustration[53],

$$I^t_\Phi(\Phi) = \int_0^L dx\ I^m_c \sin(\Phi + \Phi_0 f(x)) \ , \tag{2.177}$$

where $f(x)$ is a frustration density. The integral vanishes for all Φ when the total flux

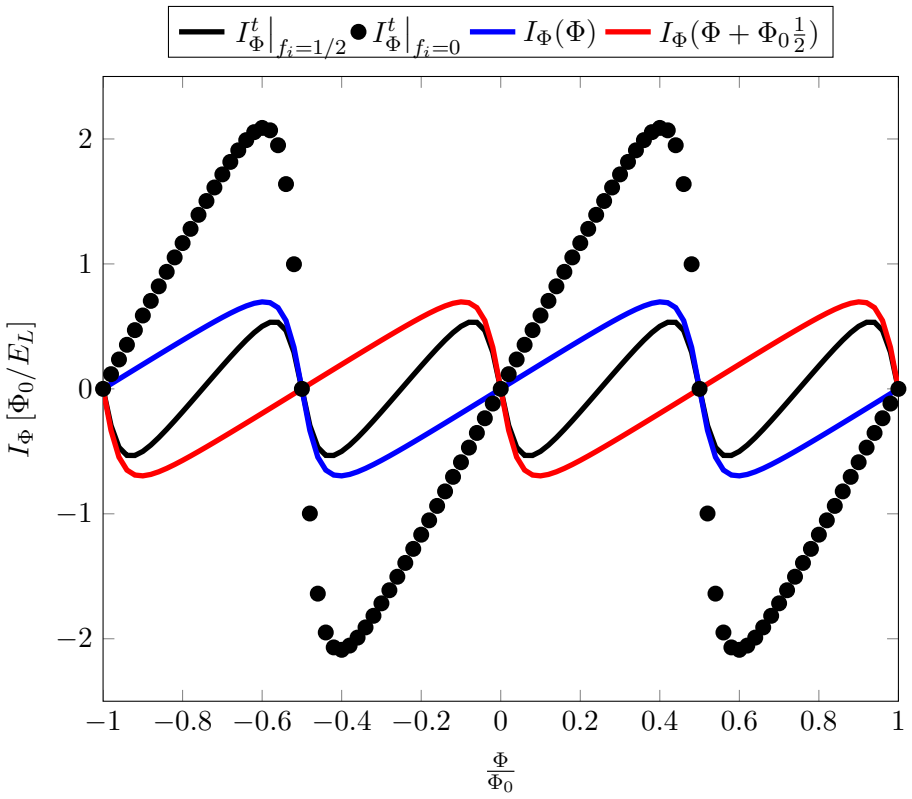

Figure 2.21: We plot the quasi-phase dependent functions I^t_Φ of a QPS-ladder with one loop $N = 1$ in the regime $E_s = 0.1\ E_L \ll E_L$ are plotted. As the shifted functions $I_\Phi(\Phi)$ and $I_\Phi(\Phi+\Phi_0\frac{1}{2})$ are approximately saw-shaped, the function $I^t_\Phi\big|_{f_i=\frac{1}{2}}$ for a frustration of $f = \frac{1}{2}$ is not exactly zero.

through the Josephson junction area is equal to half a flux-quantum,

$$f_t = \int_0^L dx f(x) = \frac{1}{2}\ . \tag{2.178}$$

The integral over the frustration density leads to a Fraunhofer pattern in the dependence of the critical current on the total frustration f_t [53].

In realistic models one has to include variations in the phase-slip energy of the QPS-elements. In Fig.2.23 we show the influence of the variation in E_S for the formation of the pseudo Fraunhofer pattern. The disorder inhibits destructive interference between the single functions $I_\Phi(\Phi)$ and increases I^t_ϕ at the minima. In the case of constructive interference the values of the maxima of I^t_Φ are also increased. The disorder includes deviations to smaller E_S for which the maxima of the individual functions $I_\Phi(\Phi)$ are larger. The disorder shifts the whole pattern upwards, but the main minima and maxima can still be distinguished. The same effect of disorder has been found in Josephson junction ladders with non-uniform Josephson junctions [48].

Experimental evidence for the validity of the effective quasi-phase model of the quantum phase slip ladder could be provided by finding pseudo Fraunhofer patterns (Fig.2.22a and Fig.2.22b) for different array lengths N in the experimentally measured dependence of the critical current on an external magnetic field.

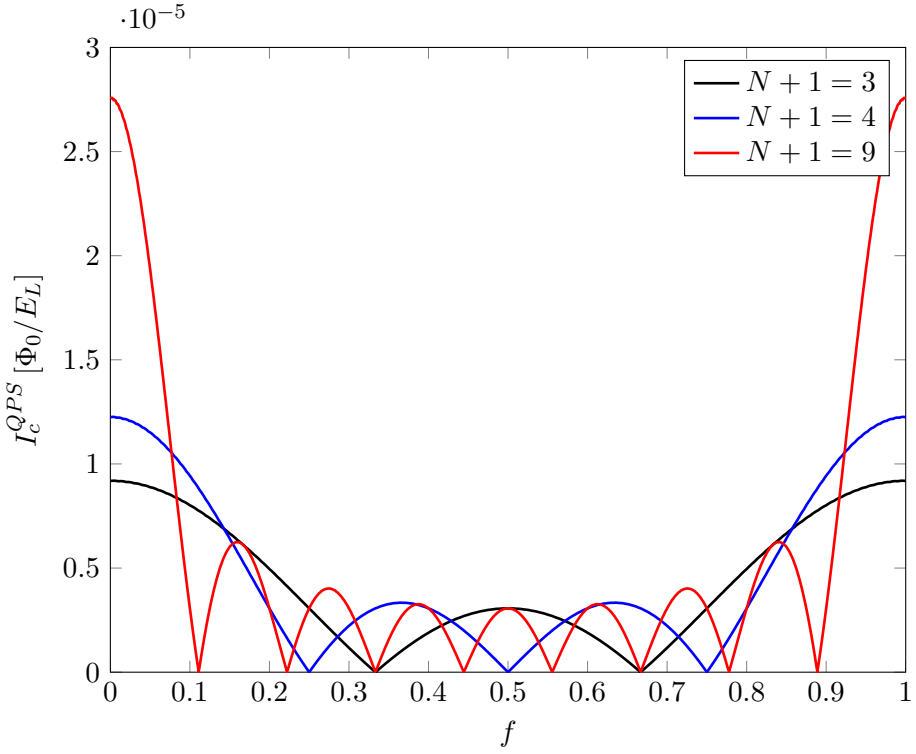

(a) The critical current I_c^{QPS} in the limit of large E_s, $E_s = 10\ E_L \gg E_L$, where the function I_Φ has a cosine shape. The critical current follows the discrete version of a Fraunhofer pattern. The critical current is zero when the frustration is an integer multiple of $\frac{1}{N+1}$.

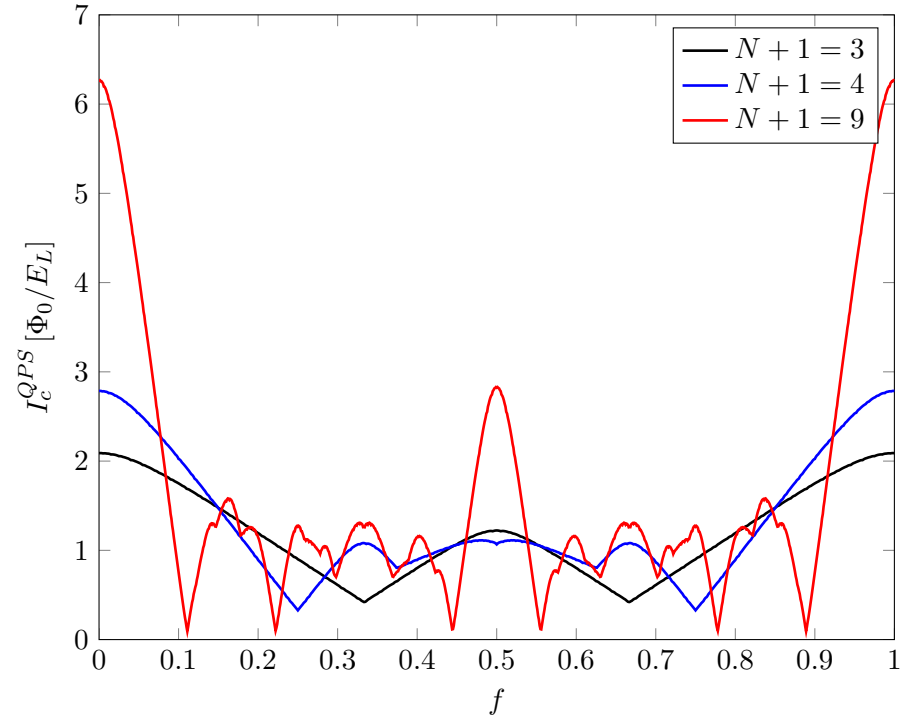

(b) The critical current in the limit of small E_s, $E_s = 0.1\ E_L \ll E_L$, where the function I_Φ has a saw-shape. The critical current follows a pseudo Fraunhofer pattern. Contrary to the sinusoidal case $E_s \gg E_L$ (Fig.2.22a) the critical current is not exactly zero at integer multiples of $\frac{1}{N+1}$, but has local minima at these points. The depth of the local minima increases with array-length N.

Figure 2.22: The critical current I_c^{QPS} over the homogeneous frustration $f_i = f$ provided by an external magnetic field. The function is plotted for the array lengths: $N = 2$ (black), $N = 3$ (blue) and $N = 8$ (red).

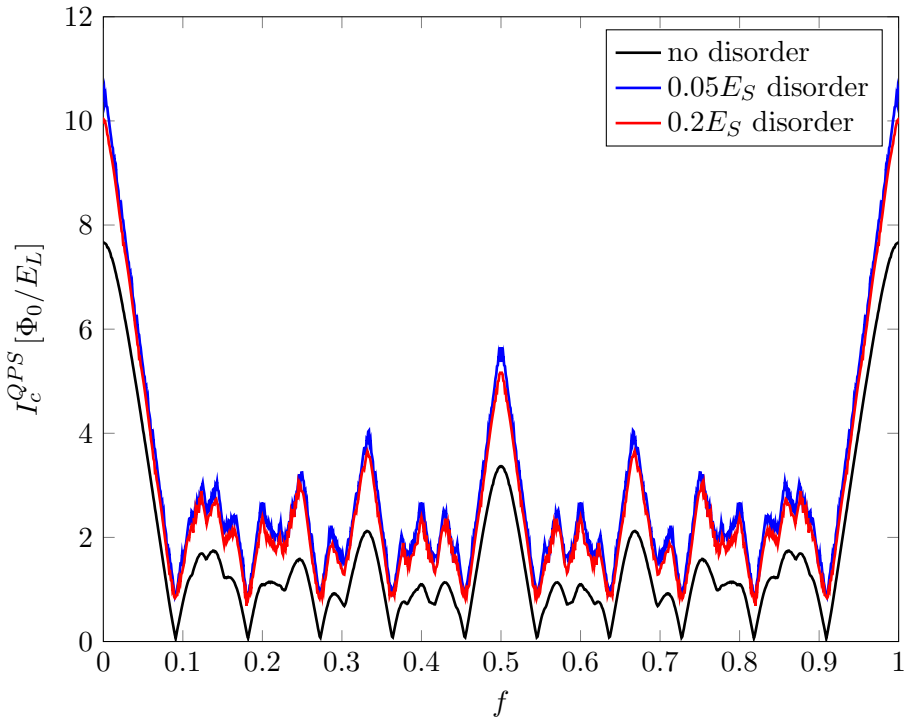

Figure 2.23: The pseudo-Fraunhofer pattern for different disorder strengths in the phase slip energy E_S (no disorder: black line, 5% disorder: blue line, 20% disorder: red line), for a $N = 10$ site array with average phase slip energy $E_S = \frac{1}{10}E_L$. The main effect of disorder is to shift the pseudo-Fraunhofer pattern upwards.

3. Charge pinning and the switching voltage

In this chapter we study the transition of Josephson junction arrays from the insulating to the transport regime driven by an applied bias voltage. We do not consider the transition in the opposite direction and the hysteresis in the IV curves that has been observed in experiments [52]. It will be shown that the dependence of the switching voltage of the transition can be obtained from depinning theory. In the broadest sense, depinning theory describes the onset of transport of elastic objects that are pinned by a random potential. It applies to many different physical systems, for example flux line lattices in type II superconductors [54, 55] and charge density waves [56]. The connection between the onset of transport in Josephson junction arrays and pinning of charge density waves (CDW) was first pointed out by Gurarie and Tsvelik in Ref.[17].

We start with a short introduction to basic depinning theory and its connection to the effective quasi-charge model of Josephson junction arrays. We then present numerical simulations of the switching voltage in the sine-Gordon-like model for three different disorder models. In the end we show that the experimentally observed dependence of the switching voltage on the Josephson energy can be obtained from the sine-Gordon-like model together with depinning theory. Parts of the results of the first section and the results of the last section have been published in Ref.[39].

3.1 Basics of depinning theory

In this section we introduce the aspects of depinning theory required to understand the depinning of the quasi-charge in Josephson junction arrays. A detailed discussion of depinning theory in general would by far exceed the scope of this work. The interested reader can find a detailed review of depinning theory in Ref.[16]. The general Hamiltonian of a pinned one-dimensional system is given by,

$$H_{dep} = \int dx \frac{1}{2C_{el}} (\partial_x Q(x))^2 + u\left[Q(x), x\right] + f_{dr} Q(x) \ , \tag{3.1}$$

where $Q(x)$ is the pinned field. Here Q is a dimensionless quantity. The elastic energy of the field $Q(x)$ is determined by the elastic constant $\frac{1}{C_{el}}$. The elastic field is pinned by the random pinning potential $u\left[Q(x), x\right]$ and driven by the homogeneous driving force f_{dr}.

In the pinned regime the applied force f_{dr} is not strong enough to overcome the potential barrier imposed on the elastic object $Q(x)$ by the random pinning potential $u\left[Q(x), x\right]$.

The pinned regime

We first consider the case where no driving is applied, $f_{dr} = 0$. The form of the elastic object is determined by a competition between the elastic term and the pinning term in H_{dep}. In the limit of vanishing stiffness the elastic field $Q(x)$ settles in one of the local minima of the pinning potential,

$$\frac{1}{C_{el}} \to 0 \ , \tag{3.2}$$

$$Q(x) \to Q_{min}(x) \ , \tag{3.3}$$

$$\partial_Q u\left[Q(x), x\right]|_{Q(x)=Q_{min}(x)} = 0 \ . \tag{3.4}$$

The opposite limit is the limit of vanishing pinning potential, $u\left[Q(x), x\right] \to 0$. In this limit only the elastic energy term remains. In a static state where we have no vibrational excitations, all deformations of the elastic object go to zero,

$$Q(x) \to Q \ . \tag{3.5}$$

Between the two limits one finds a crossover in the behaviour of Q. On small length-scales, where the elastic energy term dominates, $Q(x)$ is approximately constant. The field $Q(x)$ changes on large length-scales where the pinning potential dominates. The two regimes are separated by the length L_p. It was first determined by Larkin for a flux line lattice in type II superconductors [55]. The length L_p goes by many names depending on the physical systems that are pinned. In type II superconductors it is called Larkin length, in ferromagnets with domain boundaries Imry-Ma length [57] and for charge density waves it is called Fukuyama-Lee length [56]. In this work we use the term Larkin length. In type II superconductors Larkin found L_p by minimising the free energy of a volume $V_c = L_C R_C^2$ of the superconductor with a constant flux line lattice [55]. The spatial dimensions L_C and R_C for which the free energy of the volume is minimal give the length-scale of rigidity of the flux line lattice. The length-scale of the axis parallel to the flux line lattice is L_C and the length scale of the perpendicular axis is R_C.

In one-dimensional systems one can follow the derivation of Fukuyama and Lee [56]: One assumes that $Q(x)$ changes on the length-scale L_i and that the average value of $Q(x)$ over an interval of length L_i can be chosen to minimize the energy contribution of the pinning potential. The average energy gained by minimizing the potential energy is proportional to the square root of the length-scale L_i,

$$E_{pot}(L_i) = \left\langle \int_0^{L_i} \mathrm{d}x \, u[Q(x), x] \right\rangle_{dis} = -\alpha_{pot}\sqrt{L_i} \ , \tag{3.6}$$

where $\langle . \rangle_{dis}$ means averaging over the disorder and α_{pot} is a prefactor that depends on the exact form of $u[Q, x]$. On the other hand, the average elastic energy E_{el} of a field $Q(x)$ that changes smoothly on L_i is inversely proportional to the length L_i,

$$E_{el}(L_i) = \frac{1}{2C_{el}} \left\langle \int_0^{L_i} \mathrm{d}x \left(\partial_x Q(x)\right)^2 \right\rangle_{dis} = \alpha_{el} \frac{1}{2C_{el}} \frac{1}{L_i} \ , \tag{3.7}$$

where α_{el} is another L_i-independent prefactor. The total energy per unit length,

$$E_{tot}(L_i) = \frac{1}{L_i} \left(E_{pot}(L_i) + E_{el}(L_i)\right) \ , \tag{3.8}$$

is minimized with respect to the length L_i when the potential energy per unit length and the elastic energy per unit length have the same absolute value. This length defines the

crossover from length scales dominated by the elastic energy to length scales dominated by the pinning potential. The total energy $E_{tot}(L)$ is minimized by the Larkin length L_p.

A detailed calculation [16] shows that the prefactor in the potential energy is a function of the correlation function $R(Q)$ of the random pinning potential,

$$\langle u\left[Q_1, x_1\right] u\left[Q_2, x_2\right]\rangle_{dis} = R(Q_2 - Q_1)\delta(x_2 - x_1) \ . \tag{3.9}$$

Here it is assumed that the random pinning potential u is nearly delta-correlated in space. The delta-function is broadened on a length-scale l, shorter than the other length-scales of the problem.

The approximate value of the Larkin length in one-dimensional systems as a function of $R(Q)$, l and C_{el} is given by [16],

$$L_p \approx \left(\frac{3l^2}{C_{el}^2\left|R_{QQ}(0)\right|}\right)^{\frac{1}{3}} \ , \tag{3.10}$$

$$R_{QQ}(0) = \left.\frac{d^2}{dQ^2}R(Q)\right|_{Q=0} \ . \tag{3.11}$$

The depinning transition

Once the driving force f_{dr} exceeds a critical force f_{dp}, the pinning potential is overcome and the elastic object starts to move through the disordered medium. An intuitive argument to find the value of the critical driving force can be found by comparing the driving force to the pinning force at the Larkin length. The distribution of Q is rigid on length-scales up to the Larkin length. The elastic object can only start to move when the driving force exceeds the collective pinning force on a segment with length $L = L_p$,

$$L_p f_{dr} \geq F_{pot}(L_p) = \left\langle \int_0^{L_p} \mathrm{d}x\, \partial_Q u[Q(x), x] \right\rangle_{dis} \ . \tag{3.12}$$

At the same time, the Larkin length is just defined as the length scale at which the average pinning force and the average elastic force balance each other,

$$F_{pot}(L_p) \approx -F_{el}(L_p) \ , \tag{3.13}$$

$$F_{el}(L_p) = \frac{1}{C_{el}}\left\langle \int_0^{L_p} \mathrm{d}x\, \partial_x^2 Q(x) \right\rangle_{dis} \propto \frac{1}{C_{el}}\frac{1}{L_p} \ . \tag{3.14}$$

One can find the approximate value of the critical depinning force f_{dp} by replacing the average pinning force with the average elastic force at the Larkin length L_p,

$$f_{dp} \approx \frac{1}{C_{el}} l \frac{1}{L_p^2} \ . \tag{3.15}$$

Corrections to this intuitive approach have been obtained from renormalization-group-theory [16, 58, 59]. In this work we use the approximate value of the depinning force Eq.3.15.

3.2 Connection to Josephson junction arrays

We now consider the depinning of the quasi-charge in the effective sine-Gordon-like model (Eq.2.112) of the Josephson junction array,

$$H_Q = \sum_i \frac{1}{2} L \left(\dot{Q}_i\right)^2 + \frac{\left(Q_i - Q_{i+1}\right)^2}{2C_0} + E_Q\left(Q_i + 2e\ F_i\right) - \left(V + U\right) Q_1 + U Q_{N+1} \ . \tag{3.16}$$

We use the simplified model, where the quasi-charge dependent Bloch-inductance $L_B(Q)$ is replaced by a constant inductance L. We are interested in the transition from the insulating to the transport regime in the Josephson junction arrays. The point of the transition is determined by the breakdown of the static solution $\{Q_i\}$ of the equation of motion of the quasi-charge. In the static regime the terms proportional to the time-derivative of Q_i are zero, they have no influence on the value of the depinning voltage. The precise functional form of the Bloch-inductance can be neglected as long as $L_B(Q)$ is large enough to guarantee the adiabaticity of the quasi-charge.

We assume that the typical interaction length is large compared to the inter-site distance in the array,

$$\Lambda \gg 1 \ . \tag{3.17}$$

In this case the continuum limit of the quasi-charge model is justified and the depinning results obtained for a continuum model H_{dep} can be used,

$$Q_i \to Q(x) \ , \tag{3.18}$$
$$F_i \to F(x) \ , \tag{3.19}$$
$$Q_i - Q_{i+1} \to \partial_x Q(x) \ , \tag{3.20}$$
$$\sum_i \to \int \mathrm{dx} \ . \tag{3.21}$$

The Josephson junction array is boundary biased whereas the standard depinning model is driven by a homogeneous driving force f_{dr}. We can map the boundary biased Josephson junction array to a homogeneously driven system by shifting the quasicharge Q_i and quasi-disorder F_i by a parabolic function of the position in the array,

$$\tilde{Q}_i = Q_i - C_0 V \frac{(N+1-i)(N-i)}{2N} \ , \tag{3.22}$$
$$\tilde{F}_i = F_i + \frac{1}{2e} C_0 V \frac{(N+1-i)(N-i)}{2N} \ , \tag{3.23}$$

with the Hamiltonian,

$$H_Q = \sum_i \frac{1}{2} L \left(\dot{\tilde{Q}}_i\right)^2 + \frac{\left(\tilde{Q}_i - \tilde{Q}_{i+1}\right)^2}{2C_0} + E_Q\left(\tilde{Q}_i + 2e\ \tilde{F}_i\right) + E_{dr}\tilde{Q}_i \ . \tag{3.24}$$

The homogeneous electric field is then given by,

$$E_{dr} = \frac{V}{N} \ . \tag{3.25}$$

We can identify the parameters of the generic depinning model H_{dep} with the parameters of the Josephson junction array,

$$C_{el} = \frac{1}{(e)^2} C_0 \ , \tag{3.26}$$
$$f_{dr} = e\ E_{dr} \ . \tag{3.27}$$

The effective quasi-charge potential $E_Q(Q)$ together with the quasi-disorder F_i acts as the random pinning potential,

$$u\left[\tilde{Q}, i\right] = E_Q\left(\tilde{Q}_i + 2e\ \tilde{F}_i\right) \ . \tag{3.28}$$

To calculate the correlation function $R(Q)$ of the pinning potential we have to specify the disorder model of the bare charge-disorder f_i.

3.2.1 Maximal disorder

We first consider the maximally disordered model,

$$2e\ f_i \in [-e, e]\ , \tag{3.29}$$

$$p(f_i) = \Theta_H(\frac{1}{2} - |f_i|)\ , \tag{3.30}$$

where $p(f_i)$ is the probability distribution of the disorder f_i and Θ_H is the Heaviside Θ-function. This model corresponds to the strongest possible charge disorder in Josephson junction arrays. A disorder charge with an absolute value larger than the elementary charge e on an array island is compensated by placing an additional (anti)-Cooper pair on the island while lowering the charging energy at the same time. The disorder is bounded by $\pm e$ and a box-distribution of disorder-charges inside these boundaries is the maximal disorder. The shift of $2e\ f_i$ back into the $[-e, e]$-interval is also the physical model for the origin of the box-disorder. Assuming the distribution of charge-disorder $p(f_i)$ is originally Gaussian with a standard deviation much larger than $1/2$,

$$p(f_i) = \frac{1}{\sigma\sqrt{2\pi}} e^{-\frac{1}{2}\frac{f_i^2}{\sigma^2}}\ , \tag{3.31}$$

$$\sigma \gg \frac{1}{2}\ , \tag{3.32}$$

the disorder outside the $[-e, e]$-interval is shifted back into the interval creating an approximately equal probability to find the disorder charge $2e\ f_i$ anywhere in $[-e, e]$.

In the maximal disorder model the quasi-disorder $\tilde{F}_i$ itself is correlated between different array islands i and j,

$$\left\langle \tilde{F}_i \tilde{F}_j \right\rangle_{dis} \neq 0 \quad \text{for} \quad i \neq j\ . \tag{3.33}$$

The quasi-disorder $\tilde{F}_{i+1}$ can be decomposed into,

$$\tilde{F}_{i+1} = f_i + F_{i-1} + \frac{1}{2e} C_0 V \frac{(N-i)(N-i-1)}{2N} = f_i + f_i^0\ , \tag{3.34}$$

with an offset f_i^0 to the box-distributed disorder f_i. All information about the correlation with the disorder $\tilde{F}_j$ on other array sites is contained in f_i^0. The quasi-charge potential on the other hand is a function of the quasi-charge with a periodicity of $2e$. Since the disorder f_i is box distributed in an interval that corresponds to the periodicity of the potential, the offset can be absorbed into another uncorrelated box-distributed disorder term,

$$E_Q\left(\tilde{Q} + 2e\ \tilde{f}_i + 2e\ f_i^0\right) = E_Q\left(\tilde{Q} + 2e\ \tilde{f}_i'\right)\ , \tag{3.35}$$

$$2e\ f_i' \in [-e, e]\ , \tag{3.36}$$

$$p(f_i') = \Theta_H(\frac{1}{2} - \left|f_i'\right|)\ . \tag{3.37}$$

From the point of view of the quasi-charge potential, the quasi-disorder $\tilde{F}_i$ in the maximally disordered model is uncorrelated. The correlation function of the pinning potential is δ-correlated,

$$\left\langle E_Q\left(\tilde{Q}_1 + 2e\ \tilde{F}_i\right) E_Q\left(\tilde{Q}_2 + 2e\ \tilde{F}_j\right)\right\rangle_{dis} = R(Q_2 - Q_1)\delta_{i,j}\ , \tag{3.38}$$

where the δ-function of the continuous model H_{dep} is replaced by a Kronecker δ. While the δ-function is understood to be broadened on a small length l, the minimal correlation

length of the disorder in the discrete model is the lattice constant. As we measure all distances in units of the lattice constant we find $l = 1$ in the quasi-charge model of the Josephson junction arrays.

The correlation function $R(Q)$ is given by,

$$R(Q) = \int_{-\frac{1}{2}}^{\frac{1}{2}} \mathrm{dF}\ E_Q(Q + 2e\ F) E_Q(2e\ F)\ . \tag{3.39}$$

For an arbitrary ratio of Josephson coupling energy E_J and charging energy the functional form of the potential $E_Q(Q)$ and the correlation function $R(Q)$ can be calculated numerically. In the limit $E_J \gg E_C$ one finds,

$$E_Q(Q) = E_Q^{max} \left[1 - \cos\left(\frac{\pi}{e} Q\right)\right]\ , \tag{3.40}$$

$$R(Q) = \left(E_Q^{max}\right)^2 \pi \cos\left(\frac{\pi}{e} Q\right)\ , \tag{3.41}$$

where E_Q^{max} is the amplitude of the quasi-charge potential.

The general expression for the switching voltage V_{sw} is obtained by inserting Eq.3.27, Eq.3.26 and Eq.3.15 in Eq.3.25,

$$V_{sw} = \frac{1}{e}\ N \frac{e^2}{C_0} \frac{1}{L_p^2}\ , \tag{3.42}$$

$$L_p = \left(\frac{3}{C_0^2 \left|\frac{1}{(e)^2} R_{QQ}(0)\right|}\right)^{\frac{1}{3}}\ . \tag{3.43}$$

In the maximal disordered model the switching voltage is proportional to the system length N. In the special case $E_J \gg E_C$ the expression for the Larkin length takes the simple form,

$$R_{QQ}(0) = \left(E_Q^{max}\right)^2 \frac{\pi^3}{e^2}\ , \tag{3.44}$$

$$L_p = \left(\frac{3e^4}{\pi^3 C_0^2 \left(E_Q^{max}\right)^2}\right)^{\frac{1}{3}}\ , \tag{3.45}$$

and the switching voltage is given by,

$$V_{sw} = N\ 3^{-\frac{2}{3}} \pi^2\ \frac{e}{C_0} \left(\frac{1}{e^4} \left(E_Q^{max}\right)^2\right)^{\frac{2}{3}}\ . \tag{3.46}$$

In Josephson junction arrays the experimentally relevant parameters of the array are the charging energy E_C, the Josephson coupling energy E_J, the array length N and the interaction length Λ. To express the switching voltage in terms of these parameters we define the function $\tilde{R}$,

$$\left.\frac{\partial^2}{\partial Q^2} R(Q)\right|_{Q=0} = \frac{E_C^2}{e^2} \tilde{R}\left(\frac{E_J}{E_C}\right)\ . \tag{3.47}$$

The dimensionless correlation function $\tilde{R}$ depends on only one free parameter of the system, the dimensionless ratio of the Josephson and charging energy. The function needs to be

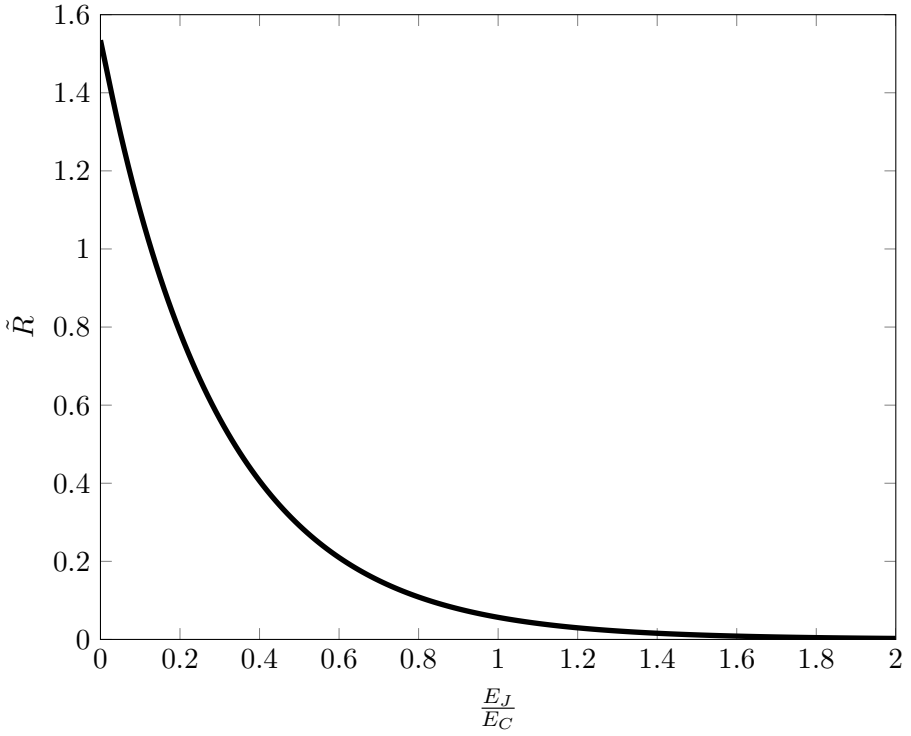

Figure 3.1: The numerically determined dimensionless correlation function $\tilde{R}$ as a function of E_J/E_C. (Figure and caption Ref.[39])

determined numerically only once (see Fig.3.1) for all possible values of array length and C_0. The switching voltage is given by,

$$V_{sw} = \frac{NE_C}{2e}\,\Lambda^{-\frac{2}{3}}\left(\frac{4}{3}\right)^{\frac{2}{3}}\left\{\tilde{R}\left(\frac{E_J}{E_C}\right)\right\}^{\frac{2}{3}} \quad . \tag{3.48}$$

The depinning of the whole elastic object given by the quasi-charge distribution $\{Q_i\}$ is remarkably different from the depinning of a single charge soliton in a disordered array. The latter case was analyzed within the disordered sine-Gordon model in Ref.[60]. It was shown that the depinning critical force grows with the soliton length Λ. In our case, however, the depinning transition is a collective phenomenon happening in the whole array. At the transition point the array contains, on average, one extra charge of $2e$ per Larkin length, $L_p \propto \Lambda^{4/3}\tilde{R}^{-1/3}$. With increasing Λ, the number of pinned charges decreases and it becomes easier to drive the system in the transport regime, $V_{sw} \propto \Lambda^{-\frac{2}{3}}\tilde{R}^{2/3}$.

The switching voltage decreases with increasing interaction length Λ. At the same time the Larkin length increases,

$$L_p \propto \Lambda^{\frac{4}{3}} \quad . \tag{3.49}$$

In finite arrays the Larkin length becomes equal to the system size N when the interaction length reaches the value,

$$\Lambda_N = N^{\frac{3}{4}}\left(\frac{4}{3}\right)^{\frac{1}{4}}\left\{\tilde{R}\left(\frac{E_J}{E_C}\right)\right\}^{\frac{1}{4}} \quad . \tag{3.50}$$

Increasing Λ further while keeping E_C constant only increases the coupling-strength $\frac{1}{C_0}$ between the quasi-charge on neighbouring islands. The Larkin length, the length-scale

on which the quasi-charge Q is approximately constant, should increase. The Larkin length however is equal to the system size. The quasi-charge is already approximately constant along the whole array. Increasing the coupling strength further has no effect. For $\Lambda \gg \Lambda_N$ the switching voltage is independent of the interaction length as long as E_C is kept constant. A lower boundary for the switching voltage is approximately given by,

$$V_{sw} \approx \sqrt{N}\frac{E_C}{2e}\frac{2}{3^{\frac{1}{2}}}\left\{\tilde{R}\left(\frac{E_J}{E_C}\right)\right\}^{\frac{1}{2}} \ . \tag{3.51}$$

This is the switching voltage V_{sw} one finds for $\Lambda = \Lambda_N$. In reality V_{sw} saturates for smaller Λ, when N is of the same order of magnitude as L_p (for comparison see the numerical simulations in Sec.3.3.2). This leaves the principal behaviour of Eq.3.51 unchanged and contributes a prefactor of order one in the expression for the switching voltage.

3.2.2 Self consistency

We can now show, that the adiabaticity assumption in the quasi-charge model is self-consistent for Josephson coupling energies E_J comparable to the charging energy E_C. We consider the characteristic oscillation frequency ω of an array segment of length L_p with rigid quasi-charge Q. We approximate the Bloch inductance by a constant value in the interval $Q \in [-e, e]$,

$$L_B(Q) \approx L_J \ , \tag{3.52}$$

$$L_J = \frac{\Phi_0^2}{4\pi^2 E_J} \ , \tag{3.53}$$

where L_J is the Josephson inductance. The energy of the array segment is approximately given by the energy of a harmonic oscillator,

$$E = L_p\ \frac{L_J}{2}\dot{Q}^2 + E_Q^{max}\sqrt{L_p}\frac{Q^2}{4e^2} \ . \tag{3.54}$$

The average potential energy due to the interaction with the disorder grows with the square of the length of the segment [55]. The frequency of the harmonic oscillator grows with the Josephson coupling energy and the amplitude of the quasi-charge potential E_Q^{max}. It decreases with the Larkin length,

$$\omega^2 \propto E_J E_Q^{max} L_p^{-\frac{1}{2}} \ . \tag{3.55}$$

The adiabaticity assumption is justified when oscillations of the quasi-charge of the array segment do not lead to Landau-Zener transitions. For $E_J \sim E_C$ this is at least the case when,

$$E_J \geq \omega \ , \tag{3.56}$$

$$E_J \geq \alpha\sqrt{E_J E_Q^{max}}L_p^{-\frac{1}{4}} \ , \tag{3.57}$$

with a numerical prefactor α of the order of one. Using the inequality,

$$E_Q^{max}\left(\frac{E_J^{min}}{E_C}\right) \leq \frac{E_C}{4} \ , \tag{3.58}$$

we see that the adiabaticity condition,

$$\frac{E_J}{E_C} \geq \beta L_p^{-\frac{1}{2}} \ , \tag{3.59}$$

can always be fulfilled for a constant numerical prefactor β, when the Larkin length L_p is sufficiently large.

3.2.3 Weak disorder

In the weak disorder case the bare disorder f_i is not evenly distributed in the $[-e, e]$-interval. We consider two models of weak disorder, the weak box disorder,

$$2e\ f_i \in [-\gamma\ e, \gamma\ e]\ , \tag{3.60}$$

$$p(f_i) = \frac{1}{\gamma}\Theta_H(\frac{\gamma}{2} - |f_i|)\ , \tag{3.61}$$

with the disorder strength $\gamma < 1$ and Gaussian disorder,

$$p(f_i) = \frac{1}{\sigma\sqrt{2\pi}} e^{-\frac{1}{2}\frac{f_i^2}{\sigma^2}}\ , \tag{3.62}$$

with a standard deviation $\sigma < 1/2$.

In the weak disorder models the spatial correlation in the quasi-disorder $\tilde{F}_{i+1}$ can not be neglected, even in the argument of the quasi-charge potential $E_Q(Q)$. The maximal value of the disorder $2e\ f_i$ is smaller than the periodicity of the potential and the offset f_i^0 can not be absorbed into an uncorrelated box-distributed disorder term f_i'. With the long range correlation in the quasi-disorder $\tilde{F}_i$, the correlation function of the pinning potential also acquires a long range correlation component. We decompose the correlation function into short and long-range components,

$$\left\langle E_Q\left(\tilde{Q}_1 + 2e\ \tilde{F}_i\right) E_Q\left(\tilde{Q}_2 + 2e\ \tilde{F}_j\right)\right\rangle_{dis} = R(Q_1 - Q_2)\delta_{i,j} + R_2(Q_1 - Q_2, i, j)\ , \tag{3.63}$$

with the δ-correlated component $R(Q)$ and the long range correlation function $R_2(Q, i, j)$. Due to the long range correlations the intuitive picture of the depinning-transition is not valid anymore. For a long range correlation function,

$$R_2(Q_1, Q_2, i, j) \propto |i - j|^{-a}\ , \tag{3.64}$$

that decays with a power law, the problem has been approached with the functional renormalization group method (FRG) in Ref.[61] and Ref.[62].

It was shown in Ref.[63] and Ref.[64] that the long-range correlations lead to the emergence of a new length-scale in the pinned system, the typical correlation length L_{corr}. The roughness function $w(x)$ of a pinned system shows a different behaviour, namely a different roughness exponent ζ_{rough}, depending on whether the system is probed at length-scales smaller or larger than the correlation length [64]. We derive a typical correlation lengths for the two weak disorder models under the assumption that E_Q can be approximated as a cosine-potential,

$$E_J \sim E_C\ , \tag{3.65}$$

$$E_Q(Q) \approx E_Q^{max}\left[1 - \cos\left(\frac{\pi}{e}Q\right)\right]\ . \tag{3.66}$$

In the next section (Sec.3.3.3) we compare the numerical results for the depinning-transition of the weak box-disorder model with the analytic estimate for the typical correlation length-scale.

To calculate the correlation function of the pinning-potential of two different array sites j and k we set, without the loss of generality, $j < k$. The correlation function in the weak

box-disorder model is given by an integral over the disorder,

$$R_2(Q,j,k) = \left(E_Q^{max}\right)^2 \int_{-\infty}^{\infty} \mathrm{d}F_j \tilde{p}(F_j) \left(\frac{1}{\gamma}\right)^{k-j} \int_{-\frac{\gamma}{2}}^{\frac{\gamma}{2}} \mathrm{d}f_j \ldots \int_{-\frac{\gamma}{2}}^{\frac{\gamma}{2}} \mathrm{d}f_{k-1} \cos\left(Y_1\right) \cos\left(Y_2\right) \ , \tag{3.67}$$

$$Y_1 = Q + 2e\ F_j + C_0 V \frac{(N+1-j)(N-j)}{2N} \ , \tag{3.68}$$

$$Y_2 = Q + 2e\ F_j + 2e \sum_{l=j}^{k-1} f_l + C_0 V \frac{(N+1-k)(N-k)}{2N} \ , \tag{3.69}$$

where $\tilde{p}(F_j)$ is the probability distribution of the quasi-disorder F_j. Expanding the cosine to exponentials one obtains,

$$R_2(Q,j,k) = \left(E_Q^{max}\right)^2 \int_{-\infty}^{\infty} \mathrm{d}F_j \tilde{p}(F_j) \left(\frac{\sin\left(\pi\gamma\right)}{\pi\gamma}\right)^{k-j} \ , \\ \frac{1}{2}\left(e^{2\pi i\ X_1} + (-1)^{k-j} e^{-2\pi i\ X_1} + (-1)^{k-j} e^{2\pi i\ X_2} + e^{-2\pi i\ X_2}\right) \ , \tag{3.70}$$

$$X_1 = \frac{1}{2e} Q + 2F_j + \frac{C_0 V}{2e} \frac{1}{2N} \left[(N+1-k)(N-k) + (N+1-j)(N-j)\right] \ , \tag{3.71}$$

$$X_1 = \frac{1}{2e} Q + \frac{C_0 V}{2e} \frac{1}{2N} \left[(N+1-k)(N-k) - (N+1-j)(N-j)\right] \ . \tag{3.72}$$

We find that the absolute value of the correlation function R_2 is bounded by an envelope function R_E,

$$|R_2(Q,j,k)| \leq R_E(Q,k-j) = 2\ \left(E_Q^{max}\right)^2 \left(\frac{\sin\left(\pi\gamma\right)}{\pi\gamma}\right)^{k-j} \ . \tag{3.73}$$

The long-range correlation function decays exponentially with the distance $k-j$. The correlation of the pinning-potential decays on the length-scale,

$$L_{corr} = -\frac{1}{\ln\left(\frac{\sin(\pi\gamma)}{\pi\gamma}\right)} \ . \tag{3.74}$$

As expected the correlation length goes to zero in the limit of the maximal disorder and diverges in the clean limit without disorder,

$$\gamma \to 1 \qquad \Rightarrow \qquad L_{corr} \to 0 \ , \tag{3.75}$$

$$\gamma \to 0 \qquad \Rightarrow \qquad L_{corr} \to \infty \ . \tag{3.76}$$

For a Gaussian distribution of the bare disorder f_i the correlation function is,

$$R_2(Q,j,k) = \left(E_Q^{max}\right)^2 \int_{-\infty}^{\infty} \mathrm{d}F_j \tilde{p}(F_j) \left(\frac{1}{\sqrt{2\pi}\sigma}\right)^{k-j} \int_{-\infty}^{\infty} \mathrm{d}f_j e^{-\frac{1}{2}\frac{f_j^2}{\sigma^2}} \ldots \\ \int_{-\frac{\gamma}{2}}^{\frac{\gamma}{2}} \mathrm{d}f_{k-1} e^{-\frac{1}{2}\frac{f_{k-1}^2}{\sigma^2}} \cos\left(Y_1\right) \cos\left(Y_2\right) \ . \tag{3.77}$$

The disorder integrals are solved by completing the square and we find the correlation function,

$$R_2(Q,j,k) = \left(E_Q^{max}\right)^2 \int_{-\infty}^{\infty} \mathrm{d}F_j \tilde{p}(F_j) \left(e^{-2\pi^2\sigma^2}\right)^{k-j} \left(\cos(X_1) + \cos(X_2)\right) \ . \tag{3.78}$$

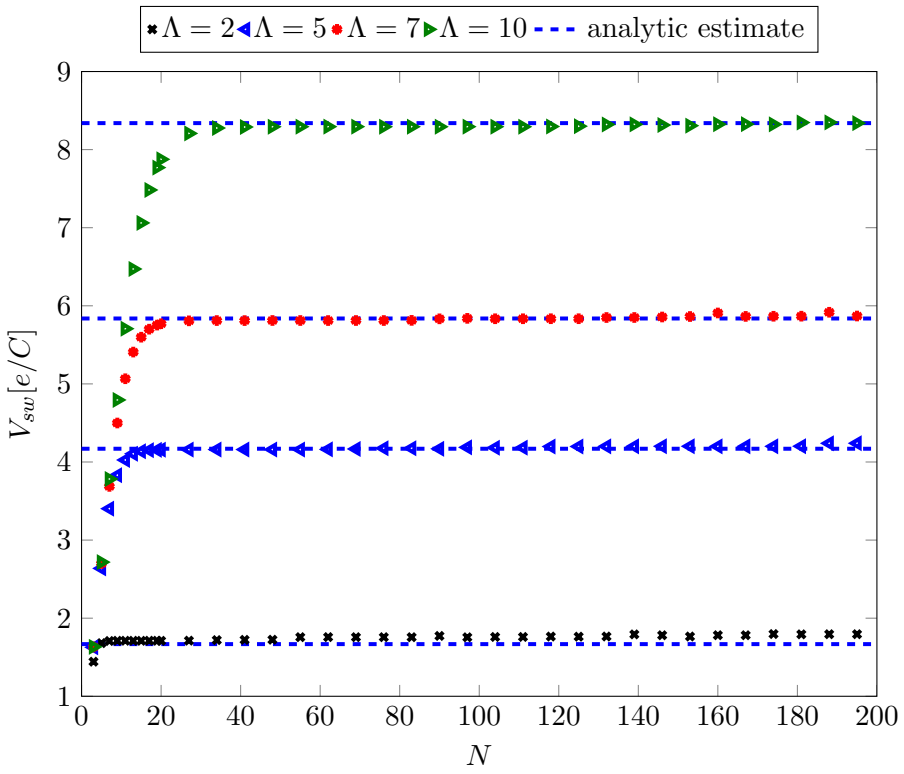

Figure 3.2: The switching-voltage of the clean array is plotted as a function of the array-length for several values of the interaction-length Λ. As long as the array is more than twice as long as Λ, the switching-voltage is independent of the length N and proportional to Λ. The switching-voltage has the value predicted by an analytic estimate by Haviland and Delsing[3]. In the region where the array is shorter than Λ the system is in the zero-dimensional limit discussed in Sec.2.5. The switching-voltage is proportional to N and does not depend on Λ.

The correlation length is determined by the standard deviation σ of the bare disorder,

$$L_{corr} = \frac{1}{2\pi^2\sigma^2} \ . \tag{3.79}$$

In the limit of an infinitely broad distribution, the system approaches the maximal box-disorder limit,

$$\sigma \to \infty \quad \Rightarrow \quad L_{corr} \to 0 \ , \tag{3.80}$$

$$\sigma \to 0 \quad \Rightarrow \quad L_{corr} \to \infty \ . \tag{3.81}$$

3.3 Numerical simulations

The switching voltage V_{sw} of the Josephson junction array can be obtained by numerically solving the equations of motion of the quasi-charge in a boundary biased array,

$$L\ddot{Q}_i + \frac{2Q_i - Q_{i-1} - Q_{i+1}}{C_0} + \alpha_R\dot{Q}_i + V_Q\left(Q_i + 2e\ F_i\right) = 0 \ , \tag{3.82}$$

$$L\ddot{Q}_1 + \frac{Q_1 - Q_2}{C_0} + \alpha_R\dot{Q}_2 + V_Q\left(Q_1\right) = V \ , \tag{3.83}$$

$$L\ddot{Q}_{N+1} + \frac{Q_{N+1} - Q_N}{C_0} + \alpha_R\dot{Q}_{N+1} + V_Q\left(Q_{N+1} + 2e\ F_{N+1}\right) = 0 \ . \tag{3.84}$$

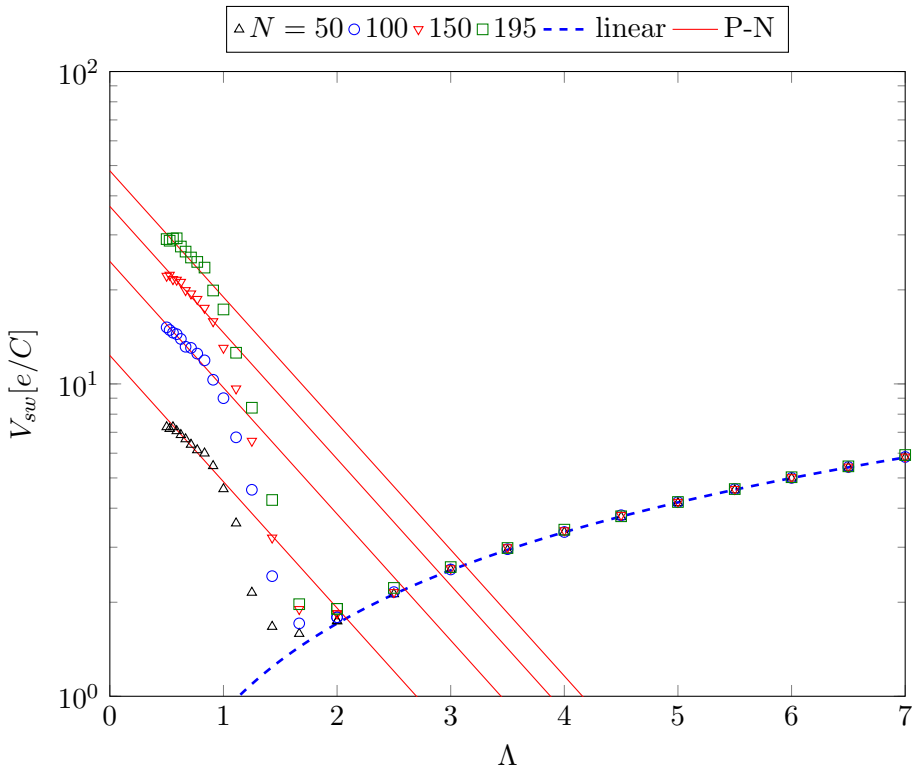

Figure 3.3: The switching-voltage V_{sw} as a function of the interaction length Λ for different array-lengths N in the clean array. As long as Λ is larger than 2 the analytic estimate Eq.3.90 is reproduced and it is $V_{sw} \propto \Lambda$, as it is shown by the linear fit (dashed line) in the plot. For smaller Λ non-propagating $2e$-charge-excitations can be created in the array by the adiabatic switch-on of the voltage. The number of the charge-excitations is proportional to the array-length and the switching-voltage is proportional to N-times the depinning-voltage of one charge-excitation. The depinning-voltage of the charge-excitations has been fitted (red lines) to an exponential function $V_{sol} = \beta e^{-\gamma\Lambda}$ as it arises from the Peierls-Nabarro-Potential[46, 60].

Here we set the offset voltage to zero $U = 0$ and apply the bias voltage V on the left of the array. We include a phenomenological Ohmic dissipation term with a resistance constant α_R. Similar numerically simulations of the switching voltage in arrays of normal tunnel contacts have been conducted a long time ago in Ref.[65].

The switching voltage is determined by adiabatically applying the bias voltage and determining whether a stable solution for the quasi-charge distribution Q_i can be found. Although the bias voltage is increased slowly, the switch-on time of the voltage V in the numerical simulation is finite. The phenomenological dissipative term has to be included to compensate the small current introduced by the switch-on of V. The introduction of a phenomenological term is also a standard tool in the derivation of the depinning force f_{dp} in renormalization-group-treatments of pinned systems [16]. The resistance constant α_R determines the strength of the electrical current in the running regime. It does not affect the switching voltage. The inductance L and the resistance α_R both affect the dynamical properties of the system, they have no influence on the breakdown of the static quasi-charge state.

In each simulation the Josephson array is initialised in an empty state $Q_i = 0$. For an equilibration time T_{eql} no voltage is applied and the array can equilibrate with the background charge disorder f_i. During an adiabatic switch-on time T_{ad} the applied voltage

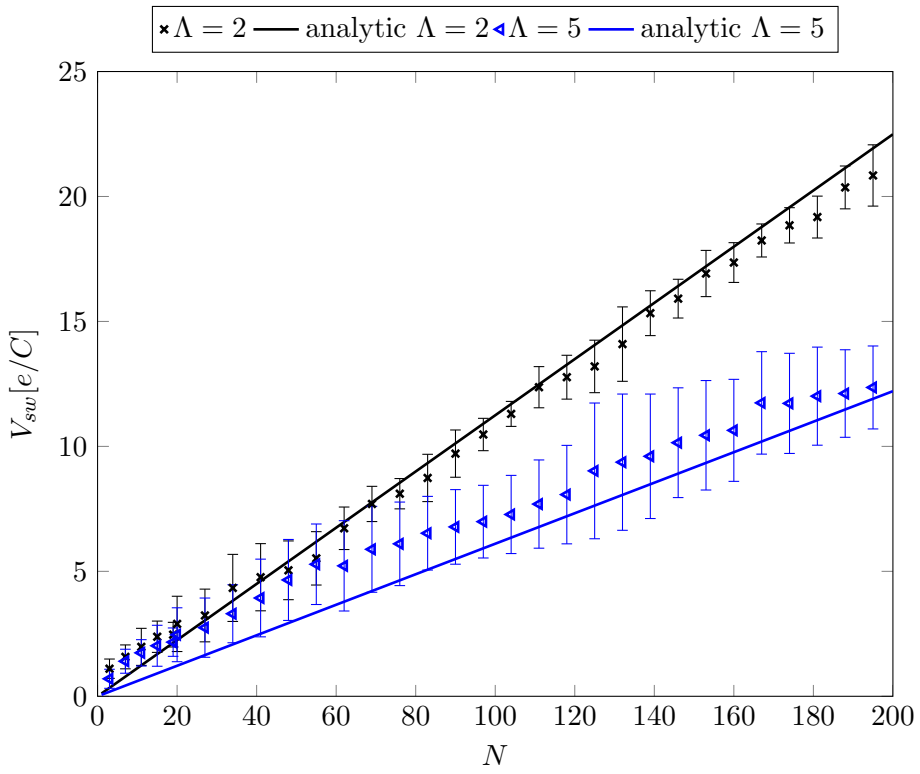

Figure 3.4: The switching-voltage V_{sw} as a function of the array-length in a disordered array. For $\Lambda = 2$ (black crosses) the switching-voltage grows linearly with the array-length N, fitting to the analytic estimate (black line). For $\Lambda = 5$ (blue triangles) the V_{sw} is proportional at higher array lengths when $N \approx 100 \approx 2.5L_p$ and fits the analytic estimate (blue solid line) from Eq.3.48. Due to the strong dependence on the random disorder-configuration the linear dependence is only realised on average. The error-bars give the standard-deviation of the switching-voltage in the sample of disorder-configurations.

V is increased linearly to the desired value. After a second waiting time T_{wait}, during which all diabatically induced currents can decay, the quasi-charge current $\dot{Q}_i$ is averaged over all array sites i and a short time Δt. To account for the finite numerical precision, the Josephson junction array is taken to be in the running regime when the averaged current exceeds a small threshold current I_t and in the insulating regime otherwise. To determine the switching voltage for a single set of parameters and one disorder realisation a series of simulations of the time-evolution with converging bias voltages V is calculated. The series is stopped when the switching voltage has been determined within a numerical uncertainty of,

$$\Delta V_{sw} = 0.001 \frac{e}{C} \,. \tag{3.85}$$

In all simulations we choose the charging and Josephson energies to be equal, $E_J = E_C$. The length of the array N and the interaction length Λ are varied.

3.3.1 The clean array

The clean case of Josephson junction arrays was used as the default model in a number of experimental papers on Josephson junction arrays [3, 13, 4]. The model might be more relevant for QPS-arrays than Josephson junction arrays as the former lack the strong charge disorder that can be found in the latter. In the continuum limit ($\Lambda \gg 1$) for long

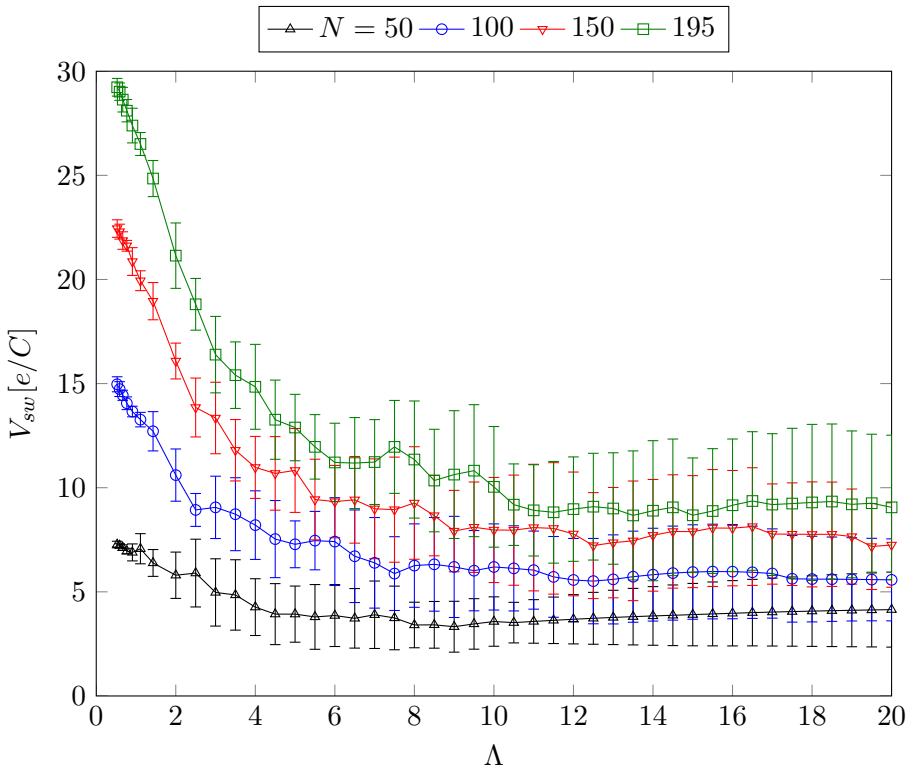

Figure 3.5: The switching-voltage as a function of the interaction-length Λ in disordered arrays for a wide range of Λ. For $\Lambda < 2$ the depinning-theory for the continuum limit is not applicable. For large Λ the Larkin length L_p is comparable to the array length. V_{sw} is independent of Λ. See also Eq.3.51.

arrays ($\Lambda \ll N$) the effective quasi-charge model of the clean array is equal to the sine-Gordon model with a modified potential model. The solutions of the standard sine-Gordon equation of motion are the well known quasi-charge solitons [12, 60],

$$Q(x) = \frac{4e}{\pi} \arctan\left(e^{\gamma_{sol}\frac{x-vt}{\Lambda}}\right) , \tag{3.86}$$

$$\gamma_{sol} = \frac{1}{\sqrt{1-\frac{v^2}{LC_0}}} , \tag{3.87}$$

with the soliton velocity v. The spatial derivative of a static soliton $v = 0$ has a maximal value of

$$\partial_x Q(x)|_{v=0} \leq \frac{2e}{\pi}\frac{1}{\Lambda} . \tag{3.88}$$

The voltage bias takes the form of a boundary condition on the spatial derivative at $x = 0$,

$$\partial_x Q(x)|_{x=0} = C_0 V . \tag{3.89}$$

This was used in Ref.[3] to estimate the maximal bias voltage for which a static soliton can exist at the array ends. This voltage is the switching voltage of the clean array,

$$V_{sw} = \frac{4}{\sqrt{\pi}}\sqrt{\frac{e}{C_0}V_Q^{max}} \propto \Lambda , \tag{3.90}$$

$$V_Q^{max} = \max_Q \left(\partial_Q E_Q(Q)\right) . \tag{3.91}$$

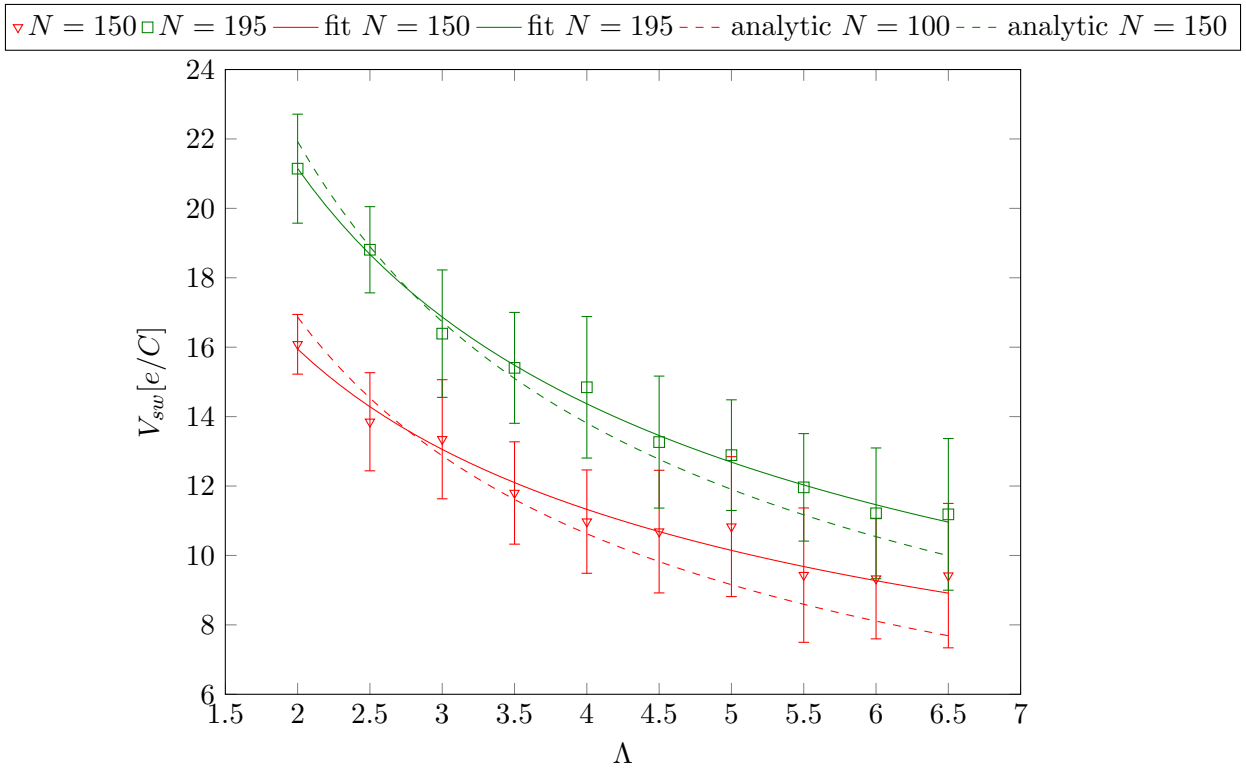

Figure 3.6: The switching-voltage as a function of the interaction-length Λ in disordered arrays. In the intermediate regime the switching voltage V_{sw} can be fitted to a power-law decay with Λ. From the fit (solid lines) we obtain an exponent of -0.49 ($N = 150$) and -0.56 ($N = 195$) instead of $-\frac{2}{3}$ as expected form the analytic estimate Eq.3.48 (dashed lines).

The switching voltage does not depend on the array length and is proportional to the interaction length Λ. Both features are confirmed by the numerical simulations in Fig.3.2 and Fig.3.3.

In the limit $\Lambda > N$ the clean array model reduces to the zero-dimensional case for zero frustration $f_i = 0$ that was discussed in Sec.2.5. As we expect form our previous discussion the switching voltage (corresponding to the total critical current in QPS-ladders) increases linearly with array size and is independent of Λ (Fig.3.2).

When the interaction length Λ is comparable to the inter-site distance we are no longer in the continuum limit and the analytic approximation Eq.3.90 is not valid. When decreasing Λ we find a transition region between $\Lambda = 2$ and $\Lambda = 1$. The system reaches a new regime at $\Lambda = 1$. The switching-voltage is proportional to the length N and the Λ-dependence can be fitted to an exponential behaviour,

$$V_{sw} = N\beta e^{-\gamma\Lambda} \ , \tag{3.92}$$

as seen in Fig.3.3. Only one set of fitting parameters β, γ is used for all four simulated array-lengths. The Λ-dependence arises from the Peierls-Nabarro-pinning-potential[46]. In the context of Josephson-junction-arrays this was discussed by Fedorov et al. for the depinning of a single $2e$-charge-excitation [60].

The change of the switching voltage behaviour can be understood in the following way. The interaction length Λ is a measure for the ratio of the elastic coupling between neighbouring islands and the depth of the pinning-potential. For small interaction lengths $\Lambda < 2$, $2e$-charge-excitations can be created at the biased end of the array without driving the array

in the conducting regime. During the adiabatic increase of the bias voltage the whole array is filled with non-propagating charge excitation. To drive the array in the transport regime, the applied voltage needs to overcome the pinning-force acting on all the charge-excitations in the array. Since the number of charge-excitations in the array scales with its length, the required switching-voltage is proportional to N-times the depinning voltage of one $2e$-charge-excitation obtained from the Peierls-Nabarro-potential.

3.3.2 The maximally disordered array

Here we present the switching voltage obtained from numerical simulations of the maximally disordered model.

In Fig.3.4 we compare the dependence of the switching voltage V_{sw} on the parameter N with analytic estimate Eq.3.48. At large N where the array is longer than the Larkin length $N > L_p$ we find that the numerical simulations fit to the expected linear dependence on the system length. For small system lengths the switching voltage does not increase linearly with N, as expected from Eq.3.51.

The numerically determined dependence of V_{sw} on Λ is shown in Fig.3.5 and Fig.3.6. For small Λ the inter-site distance is comparable to Λ and the continuum limit of the standard depinning-picture does not apply. For large Λ the Larkin-length is comparable to the array-length N and we observe a saturation of the switching voltage with Λ. The saturation sets in for,

$$N \approx \alpha_{sat} L_p \ , \tag{3.93}$$

where α_{sat} is of order of one. Comparing the the analytic estimate Eq.3.51 with the saturation points we expect α_{sat} in the range between $\alpha_{sat} \approx 2.5$ and $\alpha_{sat} \approx 3.5$.

In the intermediate regime we expect a power-law behaviour with an exponent of $-\frac{2}{3}$ (Eq.3.48). Fitting the numerical data to a power-law we obtain the exponents -0.49 ± 0.05 ($N = 150$) and -0.56 ± 0.03 ($N = 195$). Due to the limitations in numerically accessible array-lengths we can not obtain a robust confirmation of the value of the exponent of Λ from the numerical simulations.

In principle a numerical simulation includes all higher order corrections to the values of the switching voltage that were obtained from intuitive arguments in Sec.3.1. The numerical data we obtained for the maximally disordered model is not sufficient to draw definitive conclusions about the corrections to the approximate values of the switching voltage (Eq.3.51 and Eq.3.48). We will continue to use the approximate values for V_{sw} in the rest of this work.

3.3.3 Weak disorder and emergent correlation length

To validate our analytic model of the introduction of a new length-scale by weak disorder we have simulated the depinning-transition of the Josephson junction array with weak box-disorder. We chose the disorder strengths $\gamma = 0.25$ ($L_{corr}(\gamma = 0.25) \approx 10$) and $\gamma = 0.125$ ($L_{corr}(\gamma = 0.125) \approx 40$). In Fig.3.7 it is shown that the system undergoes a transition when the array-length becomes equal to the correlation length, $N = L_{corr}$. Below $N < L_{corr}$ the Josephson junction array is described by the clean array model ($\gamma = 0$). Above the transition the switching voltage increases linearly with N. The N-dependence of the switching voltage matches the maximally disordered model $\gamma = 1$. When the correlation length is significantly larger than the array size we can approximate all correlated disorder terms F_i by a single value $F_i \approx F$. The perfectly correlated disorder term F can be absorbed into the definition of the quasi-charge and the system is equivalent to the clean array without disorder $F_i = 0$.

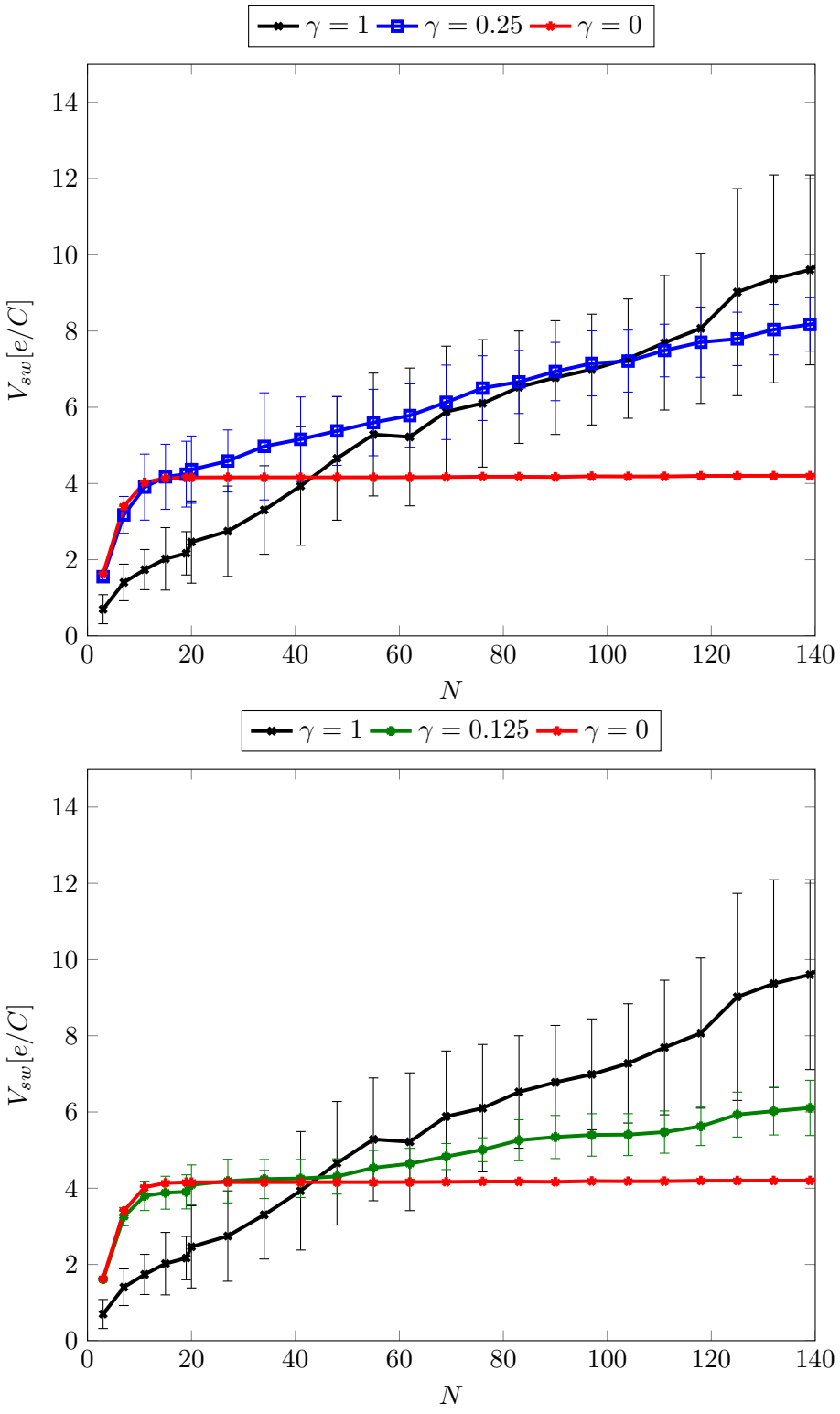

Figure 3.7: The switching-voltage V_{sw} as a function of the array-length in a weak box-disorder model of the Josephson array ($\gamma = 0.125$ green markers, lower plot, $\gamma = 0.25$ blue markers, upper plot). For comparison the switching voltages of the clean case ($\gamma = 0$, red markers) and the maximally disordered model ($\gamma = 1$, black markers) are included in the plots. When the array length becomes larger than the correlation length L_{corr} the behaviour of the weakly disordered models changes. Below $N = L_{corr}$, the switching voltage has approximately the same value as in the clean case. Above $N = L_{corr}$ it increases linearly with N as in the maximal disorder model ($L_{corr}(\gamma = 0.25) \approx 10$ and $L_{corr}(\gamma = 0.125) \approx 40$).

3.4 Fitting an experiment

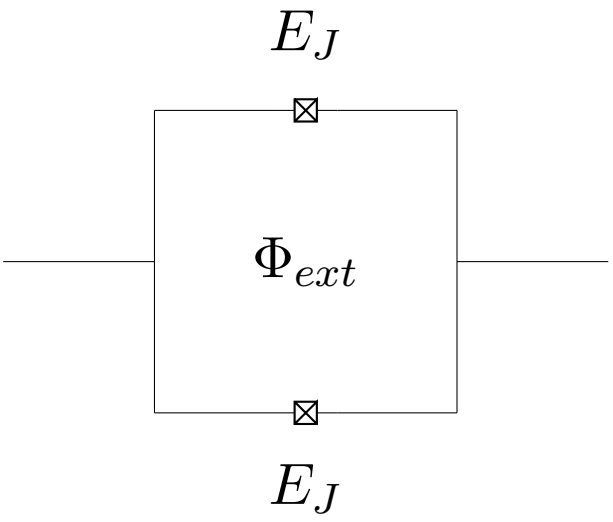

Figure 3.8: Sketch of a superconducting quantum interference device (SQUID). Both Josephson junctions have the same bare Josephson coupling energy. The SQUID-loop is threaded by an external magnetic flux Φ.

At the end of this chapter we compare the results for the switching voltage obtained from depinning theory with the experimental data on the switching behaviour of six different Josephson junction arrays. The experimental data was provided by R.Schäfer, H. Rotzinger, W. Cui, A. Fiebig and A.V. Ustinov (all Karlsruhe Institut of Technology, KIT, Germany). The results have been published in Ref.[39].

In the six arrays the Josephson junctions are replaced by superconducting quantum interference devices (SQUIDs) (see Fig.3.8). The SQUIDs consist of two equal Josephson junctions with Josephson junction energy $\frac{1}{2}E_J^m$. The junctions are placed symmetrically in a superconducting loop. The SQUID acts as an effective Josephson junction with tunable E_J. In the absence of additional fields Cooper pairs can tunnel through both Josephson junctions in the loop and the SQUID acts as a Josephson junction with Josephson energy E_J^m, twice the Josephson energy of the bare junctions. When an external magnetic field is applied the magnetic flux through the loop Φ causes interference between the tunneling through the upper and lower bare junction. As a function of the flux the Josephson energy of the SQUID is given by,

$$E_J = E_J^m \cos\left(\frac{\Phi}{\Phi_0}\right) \ , \tag{3.94}$$

where Φ_0 is the magnetic flux quantum. This dependence is used in experiments to control the effective Josephson coupling energy of the arrays by applying a magnetic field. The switching voltage is determined as a function of the magnetic flux through the SQUID loops. Due to the periodicity of the Josephson coupling energy, $V_{sw}(\Phi)$ is Φ_0-periodic in the magnetic flux.

The six experimental samples are divided into two sets. Samples A255, B255, C255 where fabricated with the same target values for C_0, C_J and E_J. All three samples consist of 255 SQUIDs. The samples D39, E59 and F255 where fabricated with different uniform target values for the system parameters. The array lengths of the samples are $N = 39$, $N = 59$ and $N = 255$. We assume that all samples are strongly disordered so that we can apply the maximal disorder model.

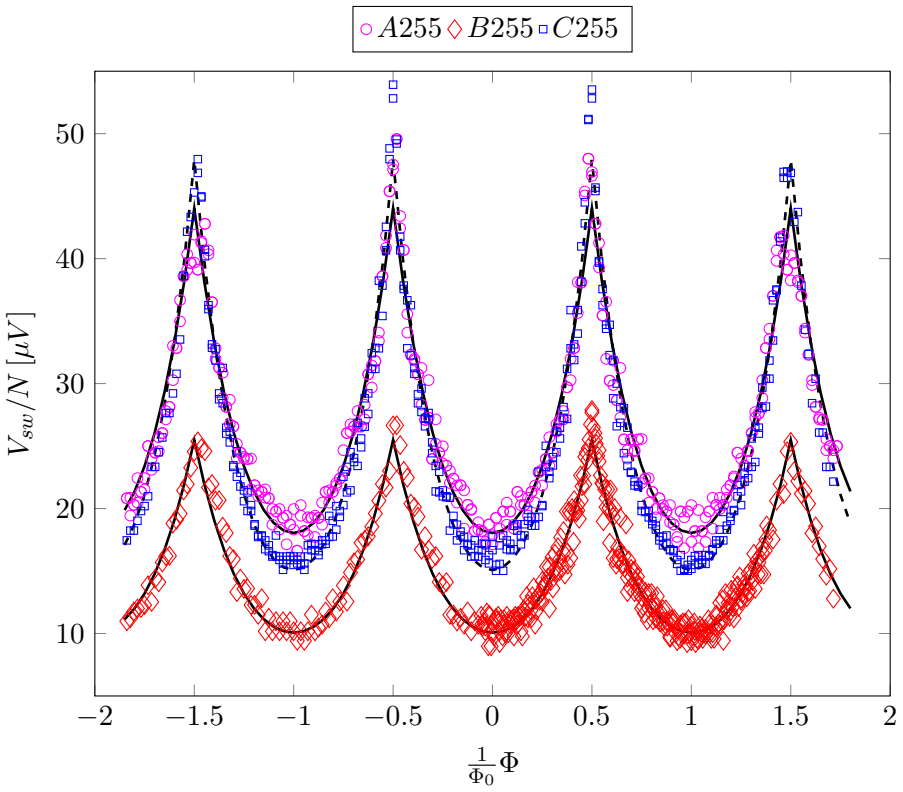

Figure 3.9: The switching voltage normalized to the array length N as a function of the magnetic flux Φ for three arrays of length 255. Solid lines are fitted functions, markers show experimental data. (Figure and Caption Ref.[39])

We obtain the analytic formula for V_{sw} as a function of magnetic flux by inserting the expression for the Josephson energy in Eq.3.48,

$$V_{sw} = \frac{NE_C}{2e}\Lambda^{-\frac{2}{3}}\left(\frac{4}{3}\right)^{\frac{2}{3}}\left\{\tilde{R}\left(\frac{E_J^m}{E_C}\cos\left(\frac{\Phi_{ext}}{\Phi_0}\right)\right)\right\}^{\frac{2}{3}} . \tag{3.95}$$

When fitting the experimental data to Eq.3.95 (see Fig.3.10) we determine two free fit parameters. The Josephson junction arrays have three so far undetermined parameters, the interaction length Λ, the charging energy E_C and the bare Josephson energy E_J^m. Values for E_J^m and E_C can be obtained experimentally from the conductance at high bias voltages. At high enough bias voltage the current is carried by quasi-particles and E_J^m is given by the normal resistance of the junctions. The expected value of the charging energy E_C^{exp} can be found from the offset in the IV-curve of the junctions with the help of P-of-E theory [38]. The experimental value obtained for E_J^m is more reliable and is used to determine E_C and Λ from the fitting parameters. The results of the fit of A255 and C255 to Eq.3.95 is given in Tab.3.1.

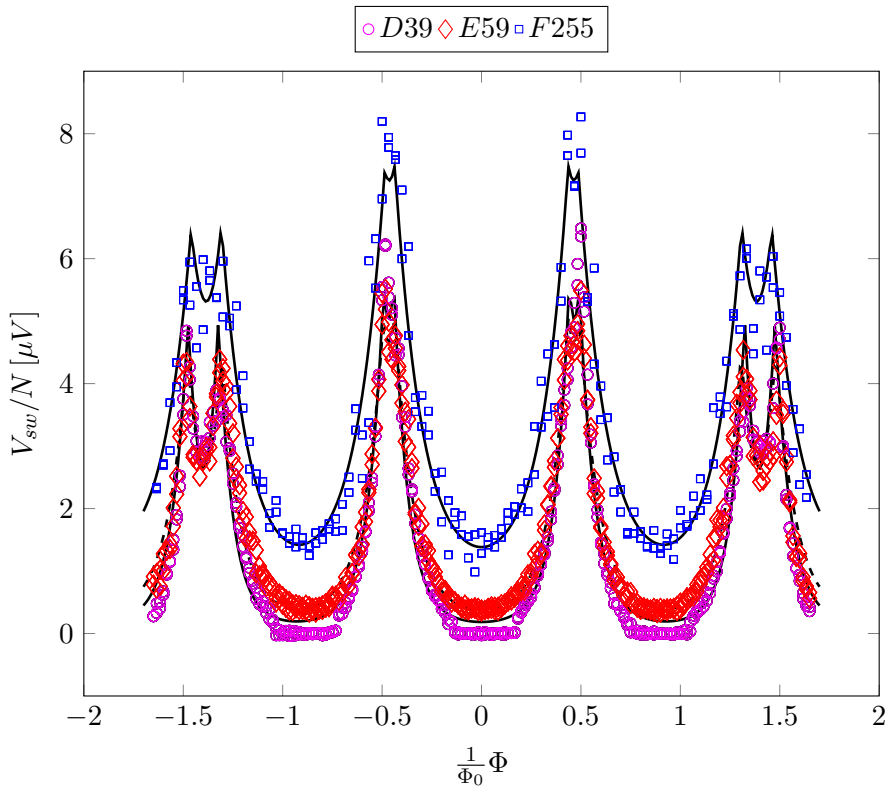

Figure 3.10: The switching voltage normalized to array length N as a function of the magnetic flux Φ for arrays of length 39, 59 and 255. Solid lines are fitted functions, markers show experimental data. Using Eq.(3.48) we can resolve the double-peak-structure for larger Φ caused by an $ABABAB\ldots$ pattern in the SQUID-loop areas. This pattern is also responsible for the deviation from the Φ_0-periodicity at higher Φ.(Figure and Caption Ref.[39])

array	N	E_C^{exp}	E_J^m	Λ	E_C
A255	255	380μeV	125μeV	13.6 ± 0.3	$310 \pm 4\mu$eV
B255	255	372μeV	113μeV	$\Lambda \gtrsim 17.5$	$209 \pm 4\mu$eV
C255	255	368μeV	125μeV	8.1 ± 0.1	$239 \pm 2\mu$eV
D39	39	88μeV	180μeV	$\Lambda \gtrsim 5.5$	$78 \pm 1.5\mu$eV
E59	59	116μeV	160μeV	$\Lambda \gtrsim 7.5$	$92 \pm 2\mu$eV
F255	255	148μeV	117μeV	$\Lambda \gtrsim 17.5$	$106 \pm 2\mu$eV

Table 3.1: The experimental estimates and fitted values for Josephson junction arrays A255 to F255. (Table and caption Ref.[39]).

The data from sample B255 should not be fitted to Eq.3.95. The Λ found in the fit to Eq.3.95 corresponds to a Larkin length that is comparable to a third of the array size $L_p \gtrsim \frac{1}{3}N$. As we found in Sec.3.1, the Λ-dependence of the switching voltage saturates for $L_p \approx \frac{1}{3}N$. We fit the numerical data to the analytic estimate for the switching voltage in the saturated regime Eq.3.51,

$$V_{sw} \propto \sqrt{N}\frac{E_C}{2e}\left\{\tilde{R}\left(\frac{E_J^m}{E_C}\cos\left(\frac{\Phi_{ext}}{\Phi_0}\right)\right)\right\}^{\frac{1}{2}} . \tag{3.96}$$

The right side of the expression for the switching voltage in short arrays contains an undetermined prefactor of the order of one. We only use the free fitting parameter E_J^m/E_C

to determine the charging energy. For the interaction length Λ we can only give an approximate lower boundary where we expect the saturation to set in. The lower boundary of Λ is determined by,

$$3L_p = N \ . \tag{3.97}$$

The result of the fitting is given in Tab3.1.

All samples from the second set D39 to F255 belong to the category of short arrays with a saturated Λ-dependence. In this set of samples the fabrication did not result in a homogeneous loop size of the SQUIDs but in an $ABABAB\ldots$ alternating pattern of SQUID areas. This is a known effect in the fabrication of SQUID-arrays [3]. In the maximally disordered model the disorder F_i is uncorrelated and we can double the size of the unit-cell to obtain a homogeneous model of AB-elements. The new expression for the switching voltage is,

$$V_{sw} \propto \sqrt{N}\frac{E_C}{2e}\left\{\frac{1}{2}\tilde{R}\left(\frac{E_J^m}{E_C}\cos\left(A\frac{\pi\Phi}{\Phi_0}\right)\right)+\frac{1}{2}\tilde{R}\left(\frac{E_J^m}{E_C}\cos\left(B\frac{\pi\Phi}{\Phi_0}\right)\right)\right\}^{\frac{1}{2}} \ , \tag{3.98}$$

where A and B are the alternating SQUID areas in units of the average area used to define Φ. The experimental data from D39 to F255 has been fitted to Eq.3.98 in Fig.3.10 and the results are given in Tab.3.1.

Overall the analytic expressions for the switching voltage in the short (Eq.3.51) and long (Eq.3.48) Josephson junction arrays show good agreement with numerical simulations and experimental data. We can regard this as evidence that the transition from insulating to transport behaviour in voltage biased Josephson junction is a depinning transition of an effective quasi-charge model.

4. Method development: The stochastic Bloch-Redfield algorithm

In this chapter we introduce the stochastic Bloch-Redfield algorithm that allows us to simulate the time-evolution of large solid state open quantum systems. The chapter is devoted to method development. The numerical approach introduced in this chapter is demonstrated on the example problem of a superconducting single electron transistor (SSET) in the next chapter (Ch.5) and used for transport simulations of Josephson junction arrays in Ch.4. The results presented in this chapter have partially been published in Ref.[66].

Most mesoscopic superconducting devices interact with an environment or reservoir, for example phonon baths or ensembles of two-level-fluctuators, leading to relaxation and dephasing of the quantum-system. Due to the environmental noise the system is no longer in a pure quantum state but in a classical mixture of quantum states. The full information about the state of the system is given by the density matrix ρ.

To correspond to a real physical system the density matrix at all times has to have a trace of one, meaning that the combined probability to find the system in one of the basis states is one. It also has to be positive semidefinite, which means there can be no negative probability to find the system in one quantum state. For time-independent problems, it was shown by Lindblad[67, 68] that the most general form of the equation of motion of a density matrix that guarantees these properties is the Lindblad-equation,

$$\dot{\rho} = i\left[\rho, H_S\right] + \sum_{\alpha} \Gamma_\alpha \left(-\frac{1}{2}\left\{ L_\alpha^\dagger L_\alpha, \rho \right\} + L_\alpha \rho L_\alpha^\dagger \right) , \tag{4.1}$$

where H_S is the Hamiltonian of the coherent time-evolution, Γ_α are the relaxation and dephasing rates and the L_α are the Lindblad operators. The rates are always larger or equal to zero, $\Gamma_\alpha > 0$.

In principle it is only necessary to solve this master equation to obtain the full time-evolution of the density matrix ρ. For a given system with a Hilbert or Fock-space of dimension N, the density matrix has N^2 elements and the master equation can be written as a differential vector-equation,

$$\dot{\vec{\rho}} \;=\; \mathcal{L}\vec{\rho}\,, \tag{4.2}$$

where the superoperator $\mathcal{L}$ is an $N^2 \times N^2$-matrix. As a consequence, the complexity rises very fast with the number of quantum-states of the system and it is impossible to solve the master equation numerically for problems with a large Hilbert space dimension N.

It is possible to deal with this problem to a certain extent by using stochastic Schrödinger equations (SSE). The stochastic Schrödinger equation is an equation for the time-evolution of a system-state $|\psi(t)\rangle$ that contains stochastic elements. The SSE is constructed in such a way that averaging over a sufficiently large number of stochastic solutions of the SSE reproduces the solution of the original master equation. There is no unique choice of stochastic Schrödinger equations corresponding to a certain master-equation. Two common choices or unravellings of stochastic Schrödinger equations are quantum state diffusion[69], which relies on continuous stochastic changes, and quantum-jumps which uses stochastically distributed jump events [70, 71, 72, 73, 74, 75, 76]. The interested reader can find extensive introductions to quantum state diffusion in a book by Ian Percival [69] and to quantum jumps in a book by Wiseman and Milburn [21].

In the Lindblad-form of the master-equation (Eq.4.1) the form of the decoherence-operators L_α and the decoherence rates Γ_α are often postulated. In this case it is a phenomenological theory with respect to decoherence. In many situations it is sufficient to use generic Lindblad-operators that correspond to relaxation and dephasing in the system and use the decoherence rates as parameters of the model, for example if we deal with a simple two-state-system where the bath is the quantised electromagnetic-field of a cavity and the radiation field couples to the system via the dipole-moments of the system-states.

Especially in solid-state physics, where the bath is responsible for decoherence and the coupling to this bath can be very complex it is often not sufficient to work on this phenomenological level. A method that derives the master-equation for an open quantum-system from the microscopic theory of the bath and the system-bath-coupling is the Bloch-Redfield-theory [77, 78]. It is often used in solid-state physics, especially in the context of quantum information [79, 80, 81, 82, 83].

In the rest of this chapter we will show how we can combine the microscopic approach of Bloch-Redfield-theory and the numerical efficiency of quantum-jumps. The standard quantum-jump-method is presented in Sec.4.1 and the Bloch-Redfield-theory is introduced in Sec.4.2. In Sec.4.3 we derive a stochastic version of the Bloch-Redfield approach and in Sec.4.4 we show the connection between the stochastic Bloch-Redfield-method and the kinetic Monte-Carlo-algorithm.

4.1 Quantum jumps

In this section we will give a short introduction to quantum-jumps following the logic of Dalibard et al. [72] for the reader unfamiliar with these topics and to introduce our notation.

The concept of the quantum-jump-approach can be most easily understood starting from the example of a system interacting with a quantised light-mode in the presence of a photon detector [75, 21]. Indeed some of the early applications of quantum-jumps considered exactly such systems[72]. In the simplest case the systems correspond to a two-state qubit with states $|\uparrow\rangle$ and $|\downarrow\rangle$. We assume that the qubit is in resonance with the radiation-field,

$$H_S = \omega\sigma_z \ , \tag{4.3}$$

$$H_B = \omega\left(a^\dagger a + \frac{1}{2}\right) \ . \tag{4.4}$$

We apply the rotating wave approximation (RWA) to the coupling with the radiation field so that the coupling Hamiltonian H_{SB}^{int} can be expressed with standard creation $a^\dagger$ and

annihilation a operators acting on the radiation field and Pauli-operators acting on the qubit,

$$H_{SB}^{int} = g\left(a^\dagger\sigma^- + a\sigma^+\right) \ . \tag{4.5}$$

We consider the system in the interaction picture so that the total Hamiltonian is reduced to the coupling operator in the interaction picture,

$$H \ = \ H_{SB}^{int} \ . \tag{4.6}$$

Let us assume that at time t the state of the qubit is given by,

$$|\psi(t)\rangle \ = \ \sin(\theta)|\uparrow\rangle + \cos(\theta)|\downarrow\rangle \ , \tag{4.7}$$

where θ is an arbitrary mixing angle between the two states $|\uparrow\rangle$ and $|\downarrow\rangle$, $0 \leq \theta < 2\pi$. The light-mode contains no photon,

$$|n(t)\rangle \ = \ |0\rangle \ . \tag{4.8}$$

We call the combined state $|\phi(t)\rangle = |\psi(t)\rangle|n(t)\rangle$.

The coupling between the qubit and the radiation field leads to photon-emissions of the qubit with rate Γ. The master-equation for the density matrix of the qubit can be easily found with standard methods[84],

$$\dot{\rho} = -\Gamma\left[\frac{1}{2}\left\{\sigma^+\sigma^-,\rho\right\} - \sigma^-\rho\sigma^+\right] \ . \tag{4.9}$$

Now assume that after a short time-interval the photon-detector will detect whether the light-mode is in the one-photon or the vacuum state. The time-interval Δt is taken to be short. We can expand the time-evolution of the system to first order in Δt [72]. The amount of population that has shifted from the $|\uparrow\rangle\otimes|0\rangle$ to the $|\downarrow\rangle\otimes|1\rangle$-state is proportional to the decay rate Γ times the time-interval Δt,

$$|\phi(t+\Delta t)\rangle = \left[(1-\frac{1}{2}\Gamma\Delta t)\sin(\theta)|\uparrow\rangle + \cos(\theta)|\downarrow\rangle\right]\otimes|0\rangle + \Gamma\Delta t\sin(\theta)|\downarrow\rangle\otimes|1\rangle \ .$$

Measuring the photon-number-state corresponds to measuring whether the qubit has interacted with the light-mode or not. The measurement projects the state $|\phi(t+\Delta t)\rangle$ into the $|n\rangle = |0\rangle$ or the $|n\rangle = |1\rangle$ sub-space. The probability of each measurement outcome is given by,

$$\begin{aligned} p_0 = |\langle 0|\phi(t+\Delta t)\rangle|^2 &= \left|(1-\frac{1}{2}\Gamma\sin(\theta)\Delta t)\,|\uparrow\rangle + \cos(\theta)\,|\downarrow\rangle\right|^2 \\ &= 1-\Gamma\sin(\theta)^2\Delta t + \mathcal{O}(\Delta t^2) \ , \qquad (4.10) \\ p_1 = 1-p_0 &= \Gamma\sin(\theta)^2\Delta t + \mathcal{O}(\Delta t^2) \ . \qquad (4.11) \end{aligned}$$

Note that the normalization can be a difficult point in the unraveling of master equations into stochastic-Schrödinger-equations in general. To obtain the SSE the time-evolution is often considered for an infinitesimal time-step dt and the full time-evolution is expanded into a series which is truncated at a certain finite order η. The new state obtained by applying the truncated series expansion is usually only normalized up to $dt^{\eta+1}$. This can lead to a probability-mismatch for the different measurement-outcomes. Take for

example the expression for the probability p_1 we found above (Eq.4.11), if we had used the probability,

$$p_1 = |\langle 1|\phi(t+\Delta)\rangle|^2 \tag{4.12}$$
$$= 0 + \mathcal{O}\left(\Delta t^2\right) \ , \tag{4.13}$$

the probability of a quantum jump would be zero according to our truncation scheme. The probabilities of the jumps obtained by measuring the bath-state do not sum up to one. The probability p_1 has to be obtained from p_0 where the correction to leading order in Δt can be calculated.

If a photon is detected, the state of the qubit changes drastically, the system state after the measurement $|\phi'\rangle$ is given by,

$$\begin{aligned} |\phi'\rangle &= \frac{1}{|\langle 1|\phi(t+\Delta t)\rangle|}\langle 1|\phi(t+\Delta t)\rangle \otimes |0\rangle \\ &= |\downarrow\rangle \otimes |0\rangle = |\psi'\rangle \otimes |0\rangle \ , \end{aligned} \tag{4.14}$$

where the photon number-state is returned to $|0\rangle$ since the photon is absorbed in the measurement process. The measurement projects the qubit into the $|\downarrow\rangle$-state, a quantum-jump has occurred.

If no photon is detected the qubit-state changes only gradually,

$$\begin{aligned} |\phi''\rangle =& \frac{1}{\sqrt{p_0}}\langle 0|\phi(t+\Delta t)\rangle \otimes |0\rangle \\ =& \left[\left\{1 - \frac{1}{2}\Gamma\Delta t + \frac{1}{2}\Gamma\sin(\theta)^2\Delta t + \mathcal{O}(\Delta t^2)\right\}\sin(\theta)|\uparrow\rangle \right. \\ &\left. + \left\{1 + \frac{1}{2}\Gamma\sin(\theta)^2\Delta t + \mathcal{O}(\Delta t^2)\right\}\cos(\theta)|\downarrow\rangle\right] \otimes |0\rangle \\ =& |\psi''\rangle \otimes |0\rangle \ . \end{aligned} \tag{4.15}$$

The information that no photon was emitted in the time-span Δt does not correspond to a full measurement of the qubit-state. The distribution between the $|\uparrow\rangle$ and $|\downarrow\rangle$-states in the qubit is shifted in favour of the $|\downarrow\rangle$-state. The failure to detect a photon increases the probability that the qubit is in the state that can not emit a photon. Repeating this kind of time-evolution over Δt, the state of the qubit decays steadily from the mixed-state to the $|\downarrow\rangle$-state until it either jumps from the mixed state to the pure state $|\uparrow\rangle$ or it reaches $|\downarrow\rangle$ purely by decay. A detailed discussion of the coexistence of a continuous change in the state of a quantum system with sudden quantum-jumps can be found in a paper on quantum trajectories by Brun [75].

To confirm that we regain the original master-equation we now construct the average change in the density-matrix of the qubit from the two possible measurement outcomes. We reduce the finite time-step Δt to the infinitesimal dt. The density matrices corresponding to the pure states $|\psi'\rangle$ and $|\psi''\rangle$ are given by $|\psi'\rangle\langle\psi'|$ and $|\psi''\rangle\langle\psi''|$. The time derivative is given by the weighted sum over the pure density matrices. The weights are the probabilities of the state $|\phi(t)\rangle$ evolving to state $|\phi'\rangle$ or $|\phi''\rangle$. These are the probabilities p_0 and p_1 of the measurement of the photon-number resulting in $|0\rangle$ or $|1\rangle$ and the qubit-state collapsing to $|\psi'\rangle$ or $|\psi''\rangle$ respectively,

$$\frac{d\rho(t)}{dt} = \frac{1}{dt}\left[\rho(t+dt) - \rho(t)\right] \tag{4.16}$$
$$= \frac{1}{dt}\left[p_0|\psi''\rangle\langle\psi''| + p_1|\psi'\rangle\langle\psi'| - |\psi(t)\rangle\langle\psi(t)|\right] \tag{4.17}$$
$$= -\frac{1}{2}\Gamma\left[\sigma^+\sigma^-\rho + \rho\sigma^+\sigma^- - 2\sigma^-\rho(t)\sigma^+\right] \ . \tag{4.18}$$

The master equation obtained by the averaging over the stochastic distribution of the pure states $|\psi'\rangle$ and $|\psi''\rangle$ is the same master-equation that describes the radiative decay of the qubit Eq.4.9. The correct time-evolution of ρ can be obtained by numerically calculating many realisations of the stochastic trajectories given by Eq.4.14 and Eq.4.15. The average over the density matrices obtained from the trajectory states at each time is the density-matrix of the mixed state of the qubit.

The approach above is not limited to the simple case of one qubit in contact with one laser-mode. Every Lindblad master-equation Eq.4.1 can be unravelled into a stochastic-Schrödinger-equation with this quantum-jump-approach. Looking at the Lindblad-equation,

$$\dot{\rho} = i\left[\rho, H\right] + \sum_{\alpha}\left(\Gamma_{\alpha} - \frac{1}{2}\left\{L_{\alpha}^{\dagger}L_{\alpha}, \rho\right\} + L_{\alpha}\rho L_{\alpha}^{\dagger}\right) \ , \tag{4.19}$$

we can identify the Lindblad-operators L_α and $L_\alpha^\dagger$ with the σ^+ and σ^- operators of the special qubit case. To unravel the master-equation into a stochastic-Schrödinger-equation we allow for the state of the system $|\psi(t)\rangle$ to evolve into one of $N_\alpha + 1$ possible states $|\psi(t+dt)\rangle^{\alpha/0}$ in the infinitesimal time-interval dt, where N_α is the number of Lindblad-operators.

The states the system-state $|\psi(t)\rangle$ can evolve to are given by,

$$|\psi(t+dt)\rangle^{0} = \frac{1}{\sqrt{p_0}}(\mathbb{1} - iH_{co}dt)|\psi(t)\rangle \ , \tag{4.20}$$

$$H_{co} = H + i\frac{1}{2}\sum_{\alpha}\Gamma_{\alpha}L_{\alpha}^{\dagger}L_{\alpha} \ , \tag{4.21}$$

$$p_0 = \langle\psi(t)|(\mathbb{1} - iH_{co}dt)|\psi(t)\rangle \ , \tag{4.22}$$

$$|\psi(t+dt)\rangle^{\alpha} = \frac{1}{\sqrt{p_\alpha}}\sqrt{\Gamma_\alpha dt}L_\alpha|\psi(t)\rangle \tag{4.23}$$

$$= \frac{1}{|L_\alpha|\psi(t)\rangle|}L_\alpha|\psi(t)\rangle \ , \tag{4.24}$$

$$p_\alpha = \langle\psi(t)|\Gamma_\alpha L_\alpha^\dagger L_\alpha|\psi(t)\rangle dt \ . \tag{4.25}$$

The states $|\psi(t+dt)\rangle^\alpha$ are jump-states, they correspond to a quantum-jump of the system due to the Lindblad-operator (or jump-operator) L_α. The probability of each quantum-jump p_α is determined by the rate Γ_α the time dt and the norm of the state after the jump $|L_\alpha|\psi(t)\rangle|$.

The dependence of the jump-probability on the norm of the jumped state may seem surprising at first. After all the jump-probability should correspond to the rate Γ_α of the $L_\alpha\rho L_\alpha^\dagger$-term in the master-equation Eq.4.1. Contrary to the density-matrix the pure system-states used in stochastic-Schrödinger-equations can not capture the classical statistical mixture of quantum-states. The system-state after a jump needs to be normalized. In the Lindblad-equation the norm of $L_\alpha\rho L_\alpha^\dagger$ can be small compared to the norm of the density matrix $\rho(t)$ so that the Lindblad operator L_α leads to a slow change of the density-matrix even if the rate Γ_α is large. To reproduce this behaviour in the stochastic-Schrödinger-equation the probability of a quantum-jump needs to be suppressed by the norm of the jumped state $L_\alpha|\psi(t)\rangle$.

The $\sqrt{dt}$-factor is fundamentally connected to the ability of the Lindblad-master-equation to turn the density-matrix of a pure quantum-state $|\phi\rangle$ into the density matrix of a statistical-mixture of quantum-states. If a density-matrix could always be expressed as the product of a pure quantum-state and its hermitian conjugate $\rho = |\phi\rangle\langle\phi|$, its differential would simply be given by,

$$d\rho = d(|\phi\rangle\langle\phi|) = |d\phi\rangle\langle\phi| + |\phi\rangle\langle d\phi| \ . \tag{4.26}$$

In the infinitesimal time dt either the left ket-state or the conjugated right bra-state changes, not both states simultaneously. The term $L_\alpha \rho L_\alpha^\dagger$ in the master-equation Eq.4.1 acts on the density matrix from both sides. If one would unravel this operator product into an infinitesimal change of the state $|\phi\rangle$ linear in the infinitesimal time-step dt,

$$|d\phi(t)\rangle^\alpha \propto L_\alpha |\phi(t)\rangle dt \ , \tag{4.27}$$

the corresponding infinitesimal change of the density-matrix,

$$d\rho(t)^\alpha \propto |d\phi(t)\rangle^\alpha \langle d\phi(t)|^\alpha = L_\alpha |\phi(t)\rangle\langle\phi(t)| L_\alpha^\dagger dt^2 \ , \tag{4.28}$$

would be quadratic in the infinitesimal time-step dt. This term could not contribute to the time-derivative of the density matrix at first order and thus the $L_\alpha \rho L_\alpha^\dagger$-part of the master-equation could not be reconstructed in this formulation.

The Lindblad-operators acting on both sides of the density matrix in Eq.4.1 take the density matrix out of the subspace where it is given by the product of the ket $|\phi\rangle$ and bra $\langle\phi|$ of the same state. This part of the master-equation can not be mapped to a standard differential equation for the time-evolution of a quantum-state. It can be mapped to a stochastic equation of motion for a quantum-state. In averaging over the many possible realisations of the stochastic time-evolution we regain a density-matrix that corresponds to a statistical mixture of pure quantum-states even though for each realisation of the time evolution the state $|\phi(t)\rangle$ is a pure state at all times t.

In the stochastic-Schrödinger-equation, the occurrence of dt^2 can be compensated by introducing the infinitesimal time-element $\sqrt{dt}$ so that $(\sqrt{dt})^2$ is of the same order as the standard infinitesimal dt and $\sqrt{dt}dt$ is of higher order and can be disregarded. The same ansatz is central to the Itô-calculus used in quantum state diffusion[69].

The infinitesimal element $|d\phi(t)\rangle$ is composed of two elements linear in dt and $\sqrt{dt}$ respectively,

$$|d\phi(t)\rangle = p_0 |d\phi\rangle^0 + \sum_\alpha p_\alpha |d\phi\rangle^\alpha \ , \tag{4.29}$$

$$|d\phi\rangle^0 \propto dt \ , \tag{4.30}$$

$$p_\alpha |d\phi\rangle^\alpha \propto \sqrt{dt} \ . \tag{4.31}$$

The time-evolution linear in dt and $\sqrt{dt}$ is orthogonal. Averaged over many realisations the contribution linear in $\sqrt{dt}$ gives a contribution to the time evolution of the density-matrix that is linear in dt,

$$p_\alpha^2 |d\phi\rangle^\alpha \langle d\phi|^\alpha = \Gamma_\alpha L_\alpha \rho L_\alpha^\dagger dt \ . \tag{4.32}$$

While p_α gives the probability of ρ turning from the density-matrix of a pure-state into a statistical mixture of quantum states, p_0 is the probability of ρ staying a pure-state density-matrix during the time-evolution $t \to t + dt$. The time-evolution-operator H_{co} combines the coherent time-evolution of the Hamiltonian H with the combinations of the Lindblad operators $-i\frac{1}{2}\sum_\alpha L_\alpha^\dagger L_\alpha$ that only act on one side of ρ in Eq.4.1 and do not take ρ out of the pure-state-subspace.

The complex combined Hamiltonian H_{co} is not Hermitian and reduces the norm of the state $|\phi(t)\rangle$ it acts on. The combined effect of the imaginary part of H_{co} and the renormalization with $\frac{1}{\sqrt{p_0}}$ is to change the amplitudes in the linear combination of basis states that forms $|\phi(t)\rangle$. It reduces the amplitudes of the states from which a quantum-jump L_α can occur

and increases the amplitudes of the states which are stable with respect to the jump operator L_α.

Constructing density-matrices from the states $|\phi(t+dt)\rangle^0$ and $|\phi(t+dt)\rangle^\alpha$ and averaging weighted by the probabilities p_0 and p_α we obtain,

$$\dot{\rho} = [\rho, H] + \sum_\alpha \Gamma_\alpha - \left(\frac{1}{2} \left\{ L_\alpha^\dagger L_\alpha, \rho \right\} + L_\alpha \rho L_\alpha^\dagger \right) \ , \tag{4.33}$$

the original Lindblad-equation. A more in-depth discussion of the relation of different unravellings can be found by the interested reader in Ref.[69].

In this work we always use the quantum-jump unravelling [85, 86, 87, 88, 89, 90, 91, 92, 93]. If one wants to connect the quantum-jump-unravelling to a physical picture one could think of additional degrees of freedom $|\chi_\alpha\rangle$ which are decoupled from the system. The state $|\chi_\alpha\rangle$ is only affected by the jump-operator L_α so that,

$$\begin{aligned} L_\alpha |\chi_\alpha\rangle &= |\chi_\alpha + 1\rangle \ , \\ L_\alpha^\dagger L_\alpha |\chi_\alpha\rangle &= |\chi_\alpha\rangle \ . \end{aligned} \tag{4.34}$$

The additional degrees of freedom count how often the Lindblad-operators act on the system. If we assume that we can constantly measure the state $|\chi_\alpha\rangle$ the measurement-outcome will project the system into a state where no jump occurred with probability p_0 and into a jumped state with p_α.

In an intuitive algorithm for a numerical implementation the probabilities of no-jump p_0 and the jumps p_α are calculated at each numerical time-step and it is decided by a random-number-generator whether and which quantum-jump occurs.

In real numerical simulations the implementation is usually slightly modified from the intuitive algorithm [21]. The probability p_0 of no jump occurring is quadratic in $|\phi(t)\rangle$. Due to the renormalization, the no-jump time-evolution is no longer linear in $|\phi(t)\rangle$. This makes numerical simulations of the time-evolution much more time-consuming. It is common[21] to not renormalise the state $|\phi(t+dt)\rangle^0$ as long as no jump occurs. In this algorithm first a random number r_1 is generated, then the time-evolution of the state $|\phi_{u.n.}(t)\rangle$ is calculated using the Schrödinger-equation and the combined Hamiltonian H_{co} without renormalizing the state at every time-step. The time-evolution is stopped once the square of the norm of the state is smaller than the random number. The renormalization of the state $\frac{1}{\sqrt{p_0}}$ and the probability of no-jump p_0 are connected so that the combined probability $P_0(0,t)$ of no-jump occurring in the time-interval $[0,t]$ and the squared norm have the same exponential time-dependence,

$$P_0(0,t) \propto \exp\left[\ln(p_0) \frac{t}{\Delta t} \right] \ , \tag{4.35}$$

$$||\phi_{u.n.}(t)\rangle|^2 \propto \exp\left[-2\ln\left(\frac{1}{\sqrt{p_0}} \right) + \ln\left(\frac{t}{\Delta t} \right) \right] = \exp\left[\ln(p_0) \frac{t}{\Delta t} \right] \ . \tag{4.36}$$

Waiting until the norm of the state has decayed to r_1 is on average equivalent to deciding at each timestep if a jump occurs with probability $1 - p_0$ or not. Once it is determined that a jump occurs at time t, the state is renormalized and a second random-number r_2 is used to choose the quantum-jump-operator Γ_α.

4.2 The Bloch-Redfield equation

In this section we show the derivation of the Bloch-Redfield-master-equation from the microscopic model of the bath and system-bath-coupling that leads to decoherence. Detailed

introductions to Bloch-Redfield-theory can be found in many textbooks and review-articles for example by Carmichael [84] or Weiss [94]. Nevertheless we want to present a short derivation since we refer to certain steps in the derivation later on. The reader familiar with the Bloch-Redfield approach can continue with section Sec.4.3.

Before we begin with the derivation we want to note that the Bloch-Redfield-equation unlike the Lindblad-equation can produce density-matrices that are not physical at all times. Due to the imperfect nature of the approximations in the derivation of the Bloch-Redfield-equation the density-matrix obtained from the Bloch-Redfield-master-equation is not guaranteed to have a trace of one or to be positive semidefinite at all times. Both are necessary conditions if the density-matrix is to correspond to a physical system. However these problems typically only arise on short timescales after initialising the system with the density-matrix of a pure state which can be very different from the equilibrium density-matrix. If the secular approximation is applied, the Bloch-Redfield-equation can be mapped to the Lindblad-form[82] and the density-matrix is guaranteed to have a physical form at all times. We will discuss the secular approximation later on.

The Bloch-Redfield-approach assumes that the considered system defined by the system-Hamiltonian H_S is in contact with a bath. In principle there can be several independent baths and the derivation of the master equation will hold in the same way. We limit ourselves to one bath for simplicity.

The bath is defined by its Hamiltonian H_B and its equilibrium density-matrix ρ_B. We refer to the combination of system and bath as the world-system or just the "world". The world-system is given by,

$$H_W = H_S + H_B + H_{SB} \ , \tag{4.37}$$

$$H_{SB} = \sum_i g_i X_i z_i \ , \tag{4.38}$$

with the coupling Hamiltonian H_{SB}, a linear combination of products of system (z_i) and bath (X_i) coupling-operators with coupling-strength g_i. It should be noted that the X_i and z_i do not need to be Hermitian individually as long as H_{SB} is.

The von Neumann-equation for the time-evolution of the world-density-matrix ρ_W is given by,

$$\dot{\rho}_W(t) = i\left[\rho_W(t), H_W\right] \ . \tag{4.39}$$

The standard derivation[84, 77, 78] of the Bloch-Redfield-equation is to change into the interaction picture with respect to H_S and H_B,

$$\dot{\rho}^I_W(t) = i\left[\rho^I_W(t), H_I(t)\right] \ , \tag{4.40}$$

$$\rho^I_W(t) = e^{i(H_S+H_B)(t-t_0)}\rho_W(t)e^{-i(H_S+H_B)(t-t_0)} \ , \tag{4.41}$$

$$H_I(t) = e^{-i(H_S+H_B)(t-t_0)}H_{SB}e^{i(H_S+H_B)(t-t_0)} \ , \tag{4.42}$$

and to insert the integral form of the von Neumann-equation Eq.4.40,

$$\rho^I_W(t) = \rho^I_W(t_0) + \int_{t_0}^{t} dt' i\left[\rho^I_W(t'), H_I(t')\right] \ , \tag{4.43}$$

into itself,

$$\dot{\rho}^I_W(t) = i\left[\rho^I_W(t_0), H_I(t)\right] - \int_{t_0}^{t} dt' \left[\left[\rho^I_W(t'), H_I(t')\right], H_I(t)\right] \ . \tag{4.44}$$

The Bloch-Redfield-approach is based on the assumption of weak coupling between system and bath. Since the coupling-strength g_i is small compared to the other parameters of the problem the equation of motion can be truncated at the second order in g_i.

It is assumed that at time t_0 the world-density-matrix $\rho_W(t_0)$ is a direct product between the system-density-matrix ρ_S and the bath-density-matrix ρ_B,

$$\rho_W^I(t_0) = \rho_S^I(t_0) \otimes \rho_B^I(t_0) \ . \tag{4.45}$$

The system and the bath are not entangled at t_0. The entanglement created between system and bath is at least linear in the interaction-Hamiltonian and so of first order of the coupling g_i,

$$\rho_W^I(t) = \rho_S^I(t) \otimes \rho_B^I(t) + \mathcal{O}(H_I) \ . \tag{4.46}$$

Since we truncate Eq.4.44 at the second order of g_i the contribution of the entanglement-correction to $\rho_W^I(t)$ is neglected on the right side of Eq.4.44.

Assuming ρ_W is always a direct product allows us to trace out the degrees of freedom of the bath to obtain the time-evolution of the density-matrix of the system. In taking the trace of Eq.4.44 one essentially reduces the equation of motion of the world to the equation of motion of the system under the influence of the bath.

We assume that the trace of the term linear in the bath-operator X_i is zero. If the expectation value $\langle X_i \rangle = Tr\,(X_i \rho_B)$ was not zero, the linear contribution of the system-bath-coupling-operator H_{SB} would correspond to a Lamb-shift in the original system-Hamiltonian,

$$H_S \to H_S' = H_S + \sum_i g_i \langle X_i \rangle z_i \ . \tag{4.47}$$

The Lamb-shift could be absorbed into the original Hamiltonian H_S.

The bath is assumed to be large enough so that the density-matrix of the bath ρ_B is always in the thermal equilibrium and time-independent. The time-evolution of the system is given by,

$$\begin{aligned}\dot{\rho}_S^I(t) = -\int_{t_0}^{t} \mathrm{dt'} \sum_{i,j} & Tr\left(\rho_B X_i(t') X_j(t)\right)\left(\rho_S^I(t') z_i(t') z_j(t) - z_i(t') \rho_S^I(t') z_j(t)\right) \\ & - Tr\left(\rho_B X_j(t) X_i(t')\right)\left(z_j(t) \rho_S^I(t') z_i(t') - z_j(t) z_i(t') \rho_S^I(t')\right) \ .\end{aligned} \tag{4.48}$$

The bath-properties enter the equation via the correlation functions of the bath-coupling-operators X_i and X_j,

$$\tilde{C}_{ij}(t,t') = \tilde{C_{ij}}(t-t') = \left\langle X_i(t-t') X_j(0) \right\rangle_B \ . \tag{4.49}$$

The correlation function $\tilde{C}_{ij}(\tau)$ depends only on the time difference $\tau = t - t'$, not on the absolute times, unless the density-matrix of the bath ρ_B is time-dependent.

The separation between system and bath is only justified as long as the correlation function $\tilde{C}_{ij}$ decays on a timescale τ_{corr} that is short compared to the timescale set by the interaction between system and bath. When the correlation time is long compared to the inverse interaction-strength $\frac{1}{g_i}$ we can not trace out the degrees of freedom of the bath. The bath has to be treated as a coherent part of the system.

If we can separate system and bath, the t'-integral in Eq.4.48 can be shifted to an integral over the time-difference τ and the integration can be extended to the interval $[0, \infty)$ as $\tilde{C}_{ij}(\tau)$ is approximately zero for $|\tau| \geq t - t_0$,

$$\dot{\rho}_S^I(t) = -\int_0^\infty \mathrm{d}\tau \sum_{i,j} \tilde{C}_{ij}(-\tau) \left(\rho_S^I(t-\tau) z_i(t-\tau) z_j(t) - z_i(t-\tau)\rho_S^I(t-\tau) z_j(t)\right) \\ -\tilde{C}_{ji}(\tau) \left(z_j(t)\rho_S^I(t-\tau) z_i(t-\tau) - z_j(t) z_i(t-\tau)\rho_S^I(t\tau)\right) \tag{4.50}$$

In this form the time-evolution of $\rho_S^I(t)$ is not strictly Markovian, the time-derivative of $\rho_S^I(t)$ does not only depend on the state of ρ_S^I at time t but also at earlier time t' via the τ-integral on the right hand side of Eq.4.50.

In the final step of the derivation of the Bloch-Redfield-equation we apply the Markov approximation to the system-density-matrix ρ_S^I. We replace $\rho_S^I(t-\tau)$ with $\rho_S^I(t)$ on the right-hand-side of Eq.4.50. The time-derivative of the system-density-matrix at time t now depends solely on the state of ρ_S^I at time t.

Using the Markov approximation and returning to the Schrödinger picture we obtain the final form of the Bloch-Redfield-equation in the time-integral formulation,

$$\dot{\rho}_S(t) = i\left[\rho_S(t), H_S\right] - \int_0^\infty d\tau \sum_{ij} \tilde{C}_{ij}(-\tau) \left[\rho_S(t) z_i e^{iH_S\tau} z_j e^{-iH_S\tau} - z_i \rho_S(t) e^{iH_S\tau} z_j e^{-iH_S\tau}\right] \\ -C_{ji}(\tau) \left[e^{iH_S\tau} z_j e^{-iH_S\tau} \rho_S(t) z_i - e^{iH_S\tau} z_j e^{-iH_S\tau} z_i \rho_S(t)\right] . \tag{4.51}$$

This approximation is valid as long as the time-evolution of $\rho_S(t)$ is completely dominated by the bare system-Hamiltonian H_S on the timescale τ_{corr}.The interaction with the bath does not cause dephasing or relaxation in $\rho_S(t)$ on this timescale. The time-evolution due to the system-Hamiltonian H_S is shifted from the density-matrix to the operators.

Physically in the Markov approximation, the state of the bath changed by the interaction with the system at time t_0 returns to equilibrium long before the changed bath-state can have an effect at later times $t + t_0 + \tau$. Information can only flow from the system to the bath. Interaction-strengths g_i that allow the system to regain information about its state at earlier times via the bath break Markovianity.

In essence the Bloch-Redfield equation describes the time-evolution of a system weakly coupled to a large bath so that the complex bath can be reduced to the correlation function $\tilde{C}_{ij}(\tau)$ with respect to its influence on the bath.

The time-integral-formulation of Eq.4.51 is not very useful to find numerical or analytical solutions to the Bloch-Redfield-equation. The integral can be evaluated by introducing an infinitesimal convergence factor $e^{-\epsilon\tau}$ for $\tau \to \infty$ and using the Fourier-transform of the correlation function, the spectral function,

$$C_{ij}(\omega) = \int_{-\infty}^{\infty} \tilde{C}_{ij}(\tau) e^{-i\omega\tau} d\tau \ . \tag{4.52}$$

This is most easily done in the eigenbasis of the system-Hamiltonian. We denote the basis states of H_S with greek letters ($|\beta\rangle$, $|\gamma\rangle$, $|\delta\rangle$, $|\eta\rangle$). The unitary transformation matrix V diagonalises the system Hamiltonian. The system-coupling-operators in the eigenbasis are denoted as $\xi_i = V^\dagger z_i V$. The Bloch-Redfield-equation can be written as,

$$\dot{\rho}_S(t) = i\left[\rho_S(t), H_S\right] - P\left(\rho_S(t)\right) \tag{4.53}$$

with the superoperator $P(\rho)$ leading to dephasing and relaxation,

$$P(\rho) = -\frac{1}{2\pi}\lim_{\epsilon\to 0}\int_{-\infty}^{\infty} d\omega \int_0^{\infty} d\tau \sum_{i,j}\sum_{\beta,\gamma,\delta,\eta} \xi_j^{\beta,\gamma}\xi_i^{\eta,\delta}\Big\{\tilde{C}_{ij}(-\tau)e^{i\omega\tau}e^{-i\omega_{\beta\gamma}\tau}e^{-\epsilon\tau}Z^1_{\beta,\gamma,\delta,\eta}(\rho(t)) \\ -\tilde{C}_{ji}(\tau)e^{i\omega\tau}e^{-i\omega_{\beta\gamma}\tau}e^{-\epsilon\tau}Z^2_{\beta,\gamma,\delta,\eta}(\rho(t))\Big\} \ , \tag{4.54}$$

where we used,

$$Z^1_{\beta,\gamma,\delta,\eta}(\rho(t)) = [\rho_S(t)|\eta\rangle\langle\delta||\beta\rangle\langle\gamma| - |\eta\rangle\langle\delta|\rho_S(t)|\beta\rangle\langle\gamma|] \ , \tag{4.55}$$

$$Z^2_{\beta,\gamma,\delta,\eta}(\rho(t)) = [|\beta\rangle\langle\gamma|\rho_S(t)|\eta\rangle\langle\delta| - |\beta\rangle\langle\gamma||\eta\rangle\langle\delta|\rho_S(t)] \ . \tag{4.56}$$

We defined the energy-difference between eigenstates $\omega_{\beta\gamma}$ as,

$$\omega_{\beta\gamma} = E_\gamma - E_\beta \ , \tag{4.57}$$

$$\xi_i^{\beta\gamma} = \langle\beta|\xi_i|\gamma\rangle \ . \tag{4.58}$$

We use an integral-identity to convert the time-integral into a δ-function and a Cauchy principal value,

$$\lim_{\epsilon\to 0}\int_0^{\infty} e^{i\omega\tau}e^{-i\omega_{\beta\gamma}\tau}e^{-\epsilon\tau} = 2\pi\delta(\omega-\omega_{\beta\gamma}) - i\ \text{P.V.}\frac{1}{\omega-\omega_{\beta\gamma}} \tag{4.59}$$

The Cauchy principal value, P.V.$\frac{1}{\omega-\omega_{\beta\gamma}}$, contributes an imaginary correction to the omega-integral in Eq.4.54. This contribution modifies the energy-levels of the system like the Lamb-shift (in the case where the bath is given by the quantized electro-magnetic field it is the Lamb-shift). When using the Bloch-Redfield-equation it is commonly assumed that the principal-value-contribution is already included in H_S and the imaginary part of the ω-integral is ignored[84].

The spectral-function-form of the Bloch-Redfield-equation contains all time integrals in $C_{ji}(\omega)$,

$$\dot{\rho}_S(t) = i\,[\rho_S(t), H_S] - \frac{1}{2}\sum_{i,j}\sum_{\beta,\gamma,\delta,\eta}\xi_j^{\beta,\gamma}\xi_i^{\eta,\delta}\{C_{ij}(-\omega_{\beta\gamma})\,[\rho_S(t)|\eta\rangle\langle\delta||\beta\rangle\langle\gamma| - |\eta\rangle\langle\delta|\rho_S(t)|\beta\rangle\langle\gamma|] \\ -C_{ji}(\omega_{\beta\gamma})\,[|\beta\rangle\langle\gamma|\rho_S(t)|\eta\rangle\langle\delta| - |\beta\rangle\langle\gamma||\eta\rangle\langle\delta|\rho_S(t)]\}\,, \tag{4.60}$$

The strength of dephasing and relaxation is determined by the spectral function evaluated at the energy-differences of the system. The spectral function $C_{ij}(\omega)$ is a measure of the weight of an energy-transfer of ω between the system and the bath by the bath coupling-operators X_i and X_j. The system coupling-operators z_i and z_j can correspond to a combination of several transitions between system-energy-eigenstates. Each of these transitions $|\beta\rangle\langle\gamma|$ is weighted with the value of the spectral-function at the transition frequency $\omega_{\beta\gamma}$. For later reference we introduce a shorthand notation for the Bloch-Redfield-equation in the eigenbasis,

$$\rho_V(t) = V\rho_S(t)V^\dagger \ , \\ \dot{\rho}_V(t) = i\left[\rho_V(t), V^\dagger H_S V\right] - \frac{1}{2}\sum_{i,j}\left[\rho_S(t)\zeta_{ij}^-\xi_i - \xi_i\rho_S(t)\zeta_{ij}^- - \zeta_{ji}^+\rho_S(t)\xi_i + \xi_i\zeta_{ji}^+\rho_S(t)\right] \ , \tag{4.61}$$

with the spectral-weighted coupling-operators,

$$\langle\beta|\zeta_{ij}^{\pm}|\gamma\rangle = \langle\beta|\xi_j|\gamma\rangle C_{ij}(\pm\omega_{\beta\gamma}) \ . \tag{4.62}$$

It is often possible to further simplify the Bloch-Redfield-equation with the secular approximation. In the interaction picture the coupling operators in Eq.4.60 acquire an oscillating time-dependence,

$$\dot{\rho}_S^I(t) = -\frac{1}{2}\sum_{i,j}\sum_{\beta,\gamma,\delta,\eta} e^{-i(\omega_{\beta\gamma}-\omega_{\delta\eta})t}\xi_j^{\beta,\gamma}\xi_i^{\eta,\delta}\left\{C_{ij}(-\omega_{\beta\gamma})\left[\rho_S^I(t)|\eta\rangle\langle\delta||\beta\rangle\langle\gamma| - |\eta\rangle\langle\delta|\rho_S^I(t)|\beta\rangle\langle\gamma|\right]\right.$$
$$\left. -C_{ji}(\omega_{\beta\gamma})\left[|\beta\rangle\langle\gamma|\rho_S^I(t)|\eta\rangle\langle\delta| - |\beta\rangle\langle\gamma||\eta\rangle\langle\delta|\rho_S^I(t)\right]\right\}, \tag{4.63}$$

The exponential function $e^{-i(\omega_{\beta\gamma}-\omega_{\delta\eta})t}$ oscillates on the time-scale of the coherent time-evolution of the system. In the interaction picture the density matrix $\rho_S^I(t)$ changes on the time-scale of the dephasing-time T_2 and relaxation-time T_1 of the system.

The average contribution of the terms with,

$$|\omega_{\beta\gamma} - \omega_{\delta\eta}| \gg \max\left(\left\{\frac{1}{T_1}, \frac{1}{T_2}\right\}\right) \tag{4.64}$$

to the Bloch-Redfield master equation Eq.4.63 vanishes due to the fast oscillations. The strict secular approximation postulates that each combination of transition frequencies is either exactly zero,

$$\omega_{\beta\gamma} - \omega_{\delta\eta} = 0 \ , \tag{4.65}$$

or large compared to T_1 and T_2 (Eq.4.64). The sum over the eigenbasis in Eq.4.63 is modified by introducing a Kronecker delta,

$$\sum_{\beta,\gamma,\delta,\eta} \rightarrow \sum_{\beta,\gamma,\delta,\eta} \delta(\omega_{\beta\gamma} - \omega_{\delta\eta}) \ . \tag{4.66}$$

Only pairs of transitions with the same transition frequency contribute to the incoherent time-evolution. The strict secular approximation is not a good approximation when the problem contains pairs of transitions so that $\omega_{\beta\gamma}$ and $\omega_{\delta\eta}$ are not equal but the difference is comparable to $1/T_1$ and $1/T_2$. In small systems the strict secular approximation can be relaxed by hand for specific combinations of transitions. In this work we always understand the secular approximation to be the strict secular approximation defined by Eq.4.66.

4.3 Stochastic Bloch-Redfield-theory

In this section we unravel the full Bloch-Redfield-master-equation into a stochastic differential equation to obtain the stochastic Bloch-Redfield algorithm (also published in Ref.[66]). In this way we combine the microscopic foundations of the Bloch-Redfield-theory with the gains in numerical efficiency of the quantum-jump approach. The presented algorithm is general in the sense that it makes no specific assumptions about the model of the system except that the standard Bloch-Redfield approach is applicable.

So far to our knowledge all stochastic unravellings that take into account the microscopic model of the environment, as it has to be done in a solid state environment [80, 66], have to be adapted to the specific model. Often a master equation in Lindblad form has been derived by hand for the microscopic model of the bath [85, 86, 87, 88, 89, 90, 91, 92, 93]. Other works have extended stochastic unravellings to non-Markovian problems [95, 96].

As a specific Markovian correlation function $\tilde{C}(t)$ in the Bloch-Redfield equation is just a special case of a general non-Markovian memory kernel one can in principle use one of the non-Markovian unravellings for a specific bath model with a known spectral function.

In one case additional fictitious oscillator modes were added to the system [95]. The fictitious oscillator modes are chosen in such a way that by tracing out their degrees of freedom one obtains a non-Markovian master equation of the form Eq.4.51 with the original non-Markovian memory kernel $\tilde{C}_{ij}(\tau)$. The full system with the fictitious oscillator modes is then simulated with the quantum-jump-method. In another case the non-Markovian unravelling was based on the quantum-state-diffusion unravelling[97, 96]. In this method the size of the Hilbert space is not expanded. However, one has to find a suitable analytic ansatz for each type of system and noise environment and one has to evaluate a time-integral over the memory-kernel at each simulation-step. Both these methods are numerically much more expensive as they can also deal with non-Markovian problems. The advantage of our method is that it provides a closed algorithm that does not have to be adapted separately to each microscopic bath model.

At a first glance the main obstacle to rewrite the Bloch-Redfield-equation Eq.4.61 into a stochastic-Schrödinger-equation is the imbalance of the operators acting on the density-matrix ρ from left and right. Unlike the Lindblad-operators L_α and $L_\alpha^\dagger$ th operators ξ_i and ζ_{ij}^- are not Hermitian conjugates. This imbalance is a manifestation of a fundamental difference between the Bloch-Redfield-equation and the Lindblad-equation. Density matrices obtained from the Lindblad equation always have physical form, those obtained for Bloch-Redfield can contain unphysical negative probabilities to find the system in certain states.

Density matrices ρ obtained from a stochastic unravelling are always physical. They are an average over pure-state density matrices $|\phi\rangle\langle\phi|$. Each pure state density matrix has a trace of one $\mathrm{Tr}(|\phi\rangle\langle\phi|)$ and is positive semidefinite. Averaging over many pure state matrices,

$$\rho = \sum_{i=1}^{m} \frac{1}{m} |\phi_i\rangle\langle\phi_i| \ , \tag{4.67}$$

preserves the physical properties. As the Lindblad equation is the most general master equation that produces such density matrices, a time-independent master equation can only be stochastically unravelled if it is mappable to Lindblad form.

Unravelling the Bloch-Redfield-equation into a stochastic-Schrödinger-equation requires additional approximations. In the strict secular approximation the Bloch-Redfield-equation can be rewritten in Lindblad-form [82]. We will use a notation that is especially suited to turn the Lindblad-form into a stochastic-Schrödinger-equation. Later on we will discuss which part of the secular-approximation are essential to obtain the stochastic form of Bloch-Redfield and introduce the piecewise flat spectral-function (PWFS) approximation.

We start with the Bloch-Redfield equation Eq.4.60 in the secular approximation,

$$\dot{\rho}_S(t) = i\,[\rho_S(t), H_S] - \frac{1}{2}\sum_{i,j}\sum_{\beta,\gamma,\delta,\eta} \delta(\omega_{\beta\gamma}-\omega_{\delta\eta})\xi_j^{\beta,\gamma}\xi_i^{\eta,\delta}\left\{C_{ij}(-\omega_{\beta\gamma})Z^1_{\beta,\gamma,\delta,\eta}(\rho(t)) - C_{ji}(\omega_{\beta\gamma})Z^2_{\beta,\gamma,\delta,\eta}(\rho(t))\right\} \ . \tag{4.68}$$

The energy differences $\omega_{\beta\gamma}$ of system eigenstates $|\beta\rangle$ and $|\gamma\rangle$ can be written as an antisymmetric $N\times N$-matrix of the same dimension as the coupling operators ξ_i. For each unique value of the eigenenergy-differences ω we define a subset $\mathcal{M}(\omega)$ of the $N\times N$ complex vector-space so that,

$$\mathcal{M}(\omega) = \left\{M \in \mathbb{C}^{N\times N} \mid \forall\ \beta,\gamma\ \ \omega_{\beta\gamma}\neq\omega \ \Rightarrow\ M_{\beta\gamma}=0\right\} \ . \tag{4.69}$$

For each subset we define $\mathcal{P}(\omega)$ as the projector into that subset. Let m_E be the number of unique eigenenergy-differences ω and m_C the number of coupling operators ξ_i. The maximal value of m_E for a completely non-degenerate system is $m_E = N^2 - N + 1$. We now decompose the m_C coupling-operators ξ_i into $m_C \times m_E$ new coupling operators ξ_k^J,

$$\xi_k^J = \xi^J_{(m_E(i-1)+n)} = \mathcal{P}(\omega_n)\xi_i \ . \tag{4.70}$$

If we take, for example, the following ω-matrix and coupling operator,

$$\omega = \begin{pmatrix} 0 & \omega_1 & \omega_2 \\ -\omega_1 & 0 & \omega_1 \\ \vdots & \vdots & 0 \end{pmatrix} \ , \qquad \xi_1 = \begin{pmatrix} \xi_1^{11} & \xi_1^{12} & \xi_1^{13} \\ \vdots & \xi_1^{22} & \xi_1^{23} \\ & \vdots & \xi_1^{33} \end{pmatrix} \ , \tag{4.71}$$

the decomposed coupling operators are given by,

$$\xi_1^J = \begin{pmatrix} \xi_1^{11} & 0 & 0 \\ 0 & \xi_1^{22} & 0 \\ 0 & 0 & \xi_1^{33} \end{pmatrix} \ , \qquad \xi_2^J = \begin{pmatrix} 0 & \xi_1^{12} & 0 \\ 0 & 0 & \xi_1^{23} \\ 0 & 0 & 0 \end{pmatrix} \ , \qquad \xi_3^J = \begin{pmatrix} 0 & 0 & \xi_1^{13} \\ 0 & 0 & 0 \\ 0 & 0 & 0 \end{pmatrix} \quad \dots \tag{4.72}$$

Each of the new coupling-operators ξ_k^J corresponds to exactly one eigenenergy-difference ω_k and the spectral-function $C_{ij}(\pm\omega)$ is substituted by two rate-matrices $\Gamma^{\pm}$,

$$\Gamma^{\pm}_{kl} = C_{i(k,l)j(k,l)}\left(\pm\omega(k)\right) \ . \tag{4.73}$$

We make the additional assumption that all pairs of original coupling operators ξ_i and ξ_j with a non-zero spectral-function $C_{ij}(\omega)$ are Hermitian conjugates,

$$C_{ij}(\omega) \neq 0 \quad \Rightarrow \quad \xi_j = \xi_i^\dagger \ . \tag{4.74}$$

In most practical cases this is no restriction of the form of the system-bath-coupling. Typically microscopic coupling operators correspond either to observables that are Hermitian by themselves or to creation and annihilation-operators as in the Jaynes-Cummings-model. This restriction is not valid when the noise sources are spatially correlated [82, 66].

In general this assumption does not carry over to the new coupling operators ξ_k^J and ξ_l^J and rate matrices $\Gamma^{\pm}_{kl}$. Take for example the simple three-dimensional case Eq.4.72, assuming a non-zero spectral-function $C_{11}(\omega)$ of the original coupling operator ξ_1, the rate matrix elements $\Gamma^{\pm}_{23}$ are not zero even though ξ_2^J and ξ_3^J are not Hermitian conjugates. This is precisely where we make use of the strict specular approximation. Up to this point the construction of the new coupling operators is completely general for all Bloch-Redfield-equations. In the strict secular approximation only the combination of ξ_k^J and ξ_l^J with $\omega(k) = -\omega(l)$ contributes to the time-evolution. Since the ω-matrix is real and antisymmetric,

$$\omega_{\gamma\beta} = E_\beta - E_\gamma = -\left(E_\gamma - E_\beta\right) = -\omega_{\beta\gamma} \ , \tag{4.75}$$

it follows that,

$$\xi_k^J = \mathcal{P}(\omega)\xi_i = \left(\mathcal{P}(-\omega)\xi_i^\dagger\right)^\dagger = \left(\mathcal{P}(-\omega)\xi_j\right)^\dagger = \left(\xi_l^J\right)^\dagger \ . \tag{4.76}$$

Therefore we can absorb the Kronecker-delta of the secular approximation in Eq.4.68 into the rate-matrices $\Gamma^{\pm}_{kl}$ so that the matrix element is zero except for $\xi_k^J = \left(\xi_l^J\right)^\dagger$. We can now write the Bloch-Redfield-equation as,

$$\dot{\rho}_S(t) = i\left[\rho_S(t), H_S\right] - \frac{1}{2}\sum_{k,l}\sum_{\beta,\gamma,\delta,\eta} \langle|\beta|\xi_l^J|\gamma\rangle\langle\delta|\xi_k^J|\eta\rangle \left\{\Gamma^-_{kl} Z^1_{\beta,\gamma,\delta,\eta}(\rho(t)) - \Gamma^+_{lk} Z^2_{\beta,\gamma,\delta,\eta}(\rho(t))\right\} \ . \tag{4.77}$$

Or in the shorthand notation of Eq.4.61,

$$\dot{\rho}_S(t) = i\left[\rho_S(t)H_S\right] - \frac{1}{2}\sum_{k,l}\left\{\Gamma^-_{kl}\left[\rho_S(t)\xi^J_l\xi^J_k - \xi^J_k\rho_S(t)\xi^J_l\right] - \Gamma^+_{lk}\left[\xi^J_l\rho_S(t)\xi^J_k - \xi^J_l\xi^J_k\rho_S(t)\right]\right\} \ , \tag{4.78}$$

In the second part of the decoherence-contribution we can exchange the names of the indices k and l in the sum over all coupling-operators and use $\Gamma^+_{lk} = \Gamma^-_{kl}$ to eliminate all occurrences of Γ^+_{kl}. Using,

$$\Gamma^-_{kl} = \Gamma_k\delta_{sec}(k,l) \ , \tag{4.79}$$

$$\delta_{sec}(k,l) = \begin{cases} 0 & \text{for} \quad \left(\xi^J_l\right)^\dagger \neq \xi^J_k \\ 1 & \text{for} \quad \left(\xi^J_l\right)^\dagger = \xi^J_k \end{cases} \ , \tag{4.80}$$

we finally arrive at,

$$\dot{\rho}_S(t) = i\left[\rho_S(t)H_S\right] + \frac{1}{2}\sum_k \Gamma_k\left[2\xi^J_k\rho_S(t)(\xi^J_k)^\dagger - \rho_S(t)(\xi^J_k)^\dagger\xi^J_k - \xi^J_k(\xi^J_k)^\dagger\rho_S(t)\right] \ . \tag{4.81}$$

The equation of motion has taken the Lindblad-form and can be turned into a stochastic-Schrödinger-equation as in Eq.4.20. The coupling-operators have become the jump-operators ξ^J_k.

Rewriting the Bloch-Redfield-equation in Lindblad form and applying the known quantum-jump approach is conceptionally straightforward. It is important to note that the stochastic Bloch-Redfield approach is of practical interest for physical systems whose number of states is much larger than in most situations where the Bloch-Redfield-equation is normally applied. We obtain a new jump-operator for each combination of an original coupling-operator and a unique transition frequency. The number of jump-operators can be very large compared to the number of coupling operators in standard Bloch-Redfield-equations and the number of phenomenological jump-operators used in a standard Lindblad quantum-jump-approach. In a system with just two original jump-operators ξ_i and 200 states we could obtain over seventy thousand jump-operators ξ^J_k.

So far we have used the strict secular approximation to derive the stochastic Bloch-Redfield approach. As explained in more detail in section Sec.4.2 the strict secular approximation assumes that the frequency corresponding to the difference of two eigenenergy-differences $\Delta_{\beta\gamma\delta\eta} = \omega_{\beta\gamma} - \omega_{\delta\eta}$ is either zero or oscillates fast on the timescales set by relaxation T_1 and dephasing T_2 of the system. This is not generally the case. It is always possible that the system has an intermediate frequency $\Delta_{\beta\delta\gamma\eta}$ which is nonzero but of the same order as relaxation and dephasing rates Γ_1 and Γ_2. The contribution of coupling-operators corresponding to such an intermediate frequency can neither be neglected due to fast oscillations nor can $\Delta_{\beta\delta\gamma\eta}$ be approximated by zero since it changes the phase of a system state significantly on the timescale of decoherence.

The occurrence of such an intermediate frequency $\Delta_{\beta\gamma\delta\eta}$ is even more likely in the large systems suited for the stochastic Bloch-Redfield-algorithm as the number of eigenenergy-differences $\omega_{\beta\gamma}$ scales with system-size squared $\mathcal{O}(N^2)$. In small systems intermediate frequencies can be dealt with by excluding the corresponding coupling terms from the secular approximation.

In large systems where a stochastic unravelling approach is of interest we follow a different approach. Since the bath-operator-correlation-function $\tilde{C}_{ij}(\tau)$ decays on timescales much shorter than T_1 and T_2, the Fourier-transformed spectral function $C_{ij}(\omega)$ varies only slowly

on frequency-scales smaller than the decoherence rates Γ_1 and Γ_2. We now approximate the spectral function $C_{ij}(\omega)$ by a series of bins,

$$C_{ij}(\omega) \approx C_{ij}^{pwf}(\omega) = \sum_n C_{ij}^n \Theta(\omega - \omega_n)\Theta(\omega_{n+1} - \omega) \ , \tag{4.82}$$

where $\Theta(\omega)$ is the Heaviside Θ-function and the bin-amplitudes C_{ij}^n and intervals $[\omega_n, \omega_{n+1}]$ are chosen such that,

$$\forall n : \quad \omega \in [\omega_n, \omega_{n+1}] \Rightarrow \left| C_{ij}(\omega) - C_{ij}^n \right| \leq \delta C \ , \tag{4.83}$$

with the cut-off-parameter of the approximation δC. We refer to the approximated spectral function $C^{pwf}(\omega)$ as the piecewise flat spectral function. We now assume that the original correlation function C_{ij} is smooth enough so that the bin-size of the approximated correlation-function C_{ij}^{pwf} is much larger than the dephasing and relaxation rates of the system,

$$\forall n : \quad \omega_{n+1} - \omega_n \gg \Gamma_1, \Gamma_2 \ . \tag{4.84}$$

We also assume that, for two transition frequencies $\omega_{\beta\gamma}$ and $\omega_{\delta\eta}$ differing by an intermediate frequency $\Delta_{\beta\gamma\delta\eta}$, we can either choose C_{ij}^a so that $\omega_{\beta\gamma}$ and $\omega_{\delta\eta}$ belong to the same bin, or the weight of the matrix-elements $\langle\beta|\xi_i|\gamma\rangle$ and $\langle\delta|\xi_j|\eta\rangle$ can be neglected compared to the sum of all other transitions in the Bloch-Redfield-equation Eq.4.60.

This approximation is justified for most systems in practice. If a large number of transition frequencies $\omega_{\beta\gamma}$ in a dense distribution correspond to nonzero matrix elements $\langle\beta|\xi_i|\gamma\rangle$, the weight of one pair of transitions $\langle\beta|\xi_i|\gamma\rangle$ and $\langle\eta|\xi_j|\delta\rangle$ is very small. If the distribution of transition frequencies is not dense and has gaps, we can choose the bins to avoid intermediate frequencies at the bin boundaries.

We neglect all combinations of transitions $|\beta\rangle\langle\gamma|$ and $|\eta\rangle\langle\delta|$ in Eq.4.60 where $\omega_{\beta\gamma}$ and $\omega_{\delta\eta}$ do not belong to the same bin in C_{ij}^{pwf}. They are either negligible compared to all other contributions or their contribution to the Bloch-Redfield-equation oscillates so fast that we discard them as we did in the secular approximation in Eq.4.63. We refer to this as the piecewise flat spectral function (PWFS) approximation.

The values of the piecewise flat spectral function $C_{ij}^{pwf}(\omega)$ at the transition frequencies $\omega_{\beta\gamma}$ can be written in the same matrix-form as the transition frequencies themselves,

$$\langle\beta|\mathcal{C}_{ij}|\gamma\rangle \equiv C_{ij}^{pwf}(\omega_{\beta\gamma}) \ . \tag{4.85}$$

We use the same kind of decomposition as in Eq.4.69 and Eq.4.70 but instead of the matrix-elements with the same transition frequencies we are grouping the identical weights of the transtions $\langle\beta|\mathcal{C}_{ij}|\gamma\rangle$ together. With the unique entries Γ_m of $\mathcal{C}_{ij}$ we define new subsets of the $N \times N$-matrix-space,

$$\mathcal{M}(\Gamma_m) = \left\{ M \in \mathbb{C}^{N\times N} \mid \langle\beta|\mathcal{C}_{ij}|\gamma\rangle \neq \Gamma_m \Rightarrow M_{\beta\gamma} = 0 \right\} \ , \tag{4.86}$$

with the corresponding projector $\mathcal{P}(\Gamma)$ and the jump-operators,

$$\xi_k^J = \mathcal{P}(\Gamma_m)\xi_{i(k)} \ . \tag{4.87}$$

Each coupling-operator ξ_i is decomposed into a different number of jump-operators. The number of unique rates Γ_m depends on the exact distributions of bins in C_{ij}^{pwf} and the number of non-zero matrix-elements in the coupling-operators.

In the PWFS approximation all contributions of transitions from different bins in C_{ij}^{pwf} are neglected. The bins determine the unique rates Γ_m. All contributions of products $\xi_k^J(\xi_l^J)^\dagger$ of jump-operators corresponding to different rates Γ_k and Γ_l are neglected. The double sum over pairs of jump-operators is reduced to a single sum over all jump-operators,

$$\sum_{kl} \xi_k^J(\xi_l^J)^\dagger \to \sum_k \xi_k^J(\xi_k^J)^\dagger \ . \tag{4.88}$$

The Bloch-Redfield-equation (Eq.4.60) in the PWFS approximation can again be mapped to Lindblad-form as we did in the strict secular approximation. The only difference is the definition of the jump-operators (Eq.4.87) and the jump rates (Eq.4.85).

Note that the number of jump-operators in the PWFS approximation is typically much smaller than the number of operators in the complete secular approximation. A large number of eigenenergy-differences $\omega_{\beta\gamma}$ can correspond to one bin in C_{ij}^{pwf} so that the corresponding transitions $|\beta\rangle\langle\gamma|$ all belong to one jump-operator instead of requiring one jump-operator for each transition.

The PWFS approximation does not only deal with intermediate frequencies $\Delta_{\beta\gamma\delta\eta}$ for which the secular approximation is not applicable, it also solves a scaling problem. In numerical calculations the time consumed by the construction of the jump-operators is non-negligible. Each jump-operator is an $N\times N$-matrix and the construction of jump-operators scales as $\mathcal{O}(N^2)$ with system-size N. In the complete secular approximation the number of jump-operators also scales as $\mathcal{O}(N^2)$ so that the combined numerical complexity of the jump-operator-construction is $\mathcal{O}(N^4)$, the same complexity as the numerical solution of the full Bloch-Redfield-master-equation for the density-matrix ρ. The stochastic-Schrödinger-equation approach looses its scaling-advantage in the strict secular approximation.

In the PWFS approximation the number of jump-operators does not scale as $\mathcal{O}(N^2)$. The transition frequencies $\omega_{\beta\gamma}$ of many transitions belong to the same bin in C_{ij}^{pwf}. The construction of the jump-operators scales as $\mathcal{O}(N^2)$ the same as the calculation of one stochastic trajectory of a state $|\psi(t)\rangle$. The stochastic Bloch-Redfield-algorithm in the PWFS approximation has the same scaling behaviour as the quantum-jump-algorithm for a Lindblad-equation.

So far we have considered stochastic-Schrödinger-equations simply as a way to obtain the time-evolution of the density matrix more efficiently than by solving the non-stochastic master-equation for the density matrix. It has been pointed out in Ref.[98] that one trajectory of the quantum-state $|\phi(t)\rangle$ corresponds to the physical time-evolution of the system in contact with a bath that is constantly measured as long as the time-evolution of the density-matrix is given by a completely Markovian Lindblad-equation. This corresponds to the physical interpretation of the quantum-jump-procedure at the end of Sec.4.1.

The premise from Ref.[98] is not given in the stochastic Bloch-Redfield approach. In a completely Markovian master equation the time differential of the density matrix at time t only depends on the density matrix at the same time. The memory kernel in the Bloch-Redfield equation in time-integral form is a δ-function,

$$\tilde{C}_{ij}(t) \propto \delta(t) \ . \tag{4.89}$$

In typical solid-state environments this condition only holds for times larger than a time-scale set by the bath. The time-scale can be so small that it is irrelevant for the time-evolution of the system. This is the case when the spectral function $C_{ij}(\omega)$ is constant for all relevant eigenenergies of the system. When we however conceptually consider continuous measurements, Eq.4.89 has to hold on all time-scales. In a complex solid-state environment a single trajectory has no straightforward physical interpretation. It is merely a tool to obtain the full time-evolution of the density matrix.

4.4 From stochastic Bloch-Redfield to kinetic Monte-Carlo

In this section we show under which conditions the stochastic Bloch-Redfield-algorithm corresponds to the kinetic Monte-Carlo (KMC) algorithm [99, 100, 101, 102]. Kinetic Monte-Carlo is one of the most widely used simulation-methods based on Monte-Carlo-algorithms. The main feature of the kinetic Monte-Carlo-algorithm is its ability to simulate the incoherent time-evolution of the system under consideration, whereas many other Monte-Carlo methods simply converge to the equilibrium state of the simulated system. This makes the kinetic Monte-Carlo-algorithm a very important tool in the study of equilibration and externally driven transport processes in chemistry and physics [101, 102]. In solid-state physics the KMC algorithm has also been used to simulate transport processes in linear and bilinear Josephson junction chains [103, 15]. For a detailed discussion of kinetic Monte-Carlo see for example Ref.[101]. Kinetic Monte-Carlo does not take into account the coherent quantum-mechanical evolution of the system. It only simulates the incoherent transitions between the states of the system.

In the KMC-procedure a set of N system-states $\{j\}$ and transition rates between them Γ_{jk} are given. For a system in state j at time t_1 the vector s with the elements s_k,

$$s_k = \sum_{l=1}^{k} \Gamma_{jl} \ , \tag{4.90}$$

is defined. A random number $r_1 \in (0,1)$ is chosen and the k-th system-state is selected so that,

$$s_k \leq s_N \cdot r_1 < s_{k+1} \ . \tag{4.91}$$

State k is the new state after the stochastic Monte-Carlo-step. The time is incremented by the escape time Δt. The time increment of the KMC-step is obtained from the probability distribution for the time Δt after which a system escapes from state j to any other state for an exponential decay $p_j(t) = \exp(-s_N t)$. The probability distribution is given by [101],

$$p_{esc}(\Delta t) = s_N e^{-s_N \Delta t} \ . \tag{4.92}$$

Drawing from an exponential distribution Eq.4.92 is equivalent to drawing a number r_2 from an even distribution in the interval $(0,1)$ and using,

$$\Delta t = -s_N \cdot \ln(r_2) \ . \tag{4.93}$$

The escape time is proportional to the logarithm of the random number r_2.

In the stochastic Bloch-Redfield algorithm the calculation of a single trajectory between the quantum jumps can be drastically simplified if the jump operators ξ_k^J project the state $|\psi(t)\rangle$ to an eigenstate of the system-Hamiltonian H_S with each quantum jump . Assume that at time t_i a quantum jump takes the system-state from the eigenstate $|\beta_{i-1}\rangle$ to the eigenstate $|\beta_i\rangle$ and the trajectory-state $|\psi(t_i)\rangle$ has a phase of ϕ_i at t_i. The system state $|\psi(t)\rangle$ in the interval $[t_i, t_{i+1}]$ is given by,

$$\begin{aligned} &\forall\ t \in [t_i, t_{i+1}] : \\ &\qquad |\psi(t)\rangle = e^{i\phi_i} e^{-E_{\beta_i}(t-t_i)} |\beta_i\rangle \ . \end{aligned} \tag{4.94}$$

The time of the next quantum jump can be determined by the decay of the state-norm of the unnormalized trajectory-state. The jump occurs once the squared norm of the unnormalized state $|\psi_{u.n.}(t)\rangle$ is smaller than a random number $r_1 \in (0,1)$. Under the

assumption that the jump operators act as projectors, the state $|\psi_{u.n.}(t)\rangle$ is guaranteed to be proportional to an eigenstate and one finds,

$$\frac{d}{dt}|\psi_{u.n.}(t)\rangle = -iE_i - \frac{1}{2}\sum_k \Gamma_k \left(\xi_k^J\right)^\dagger \xi_k^J |\psi_{u.n.}(t)\rangle \ , \tag{4.95}$$

$$\langle\psi_{u.n.}(t)|\psi_{u.n.}(t)\rangle = \exp\left(-\sum_k \Gamma_k \langle\beta_i| \left(\xi_k^J\right)^\dagger \xi_k^J |\beta_i\rangle (t-t_i)\right) \ , \tag{4.96}$$

$$t_{i+1} = t_i + \ln(\frac{1}{r_i})\left(\sum_k \Gamma_k \langle\beta_i| \left(\xi_k^J\right)^\dagger \xi_k^J |\beta_i\rangle\right)^{-1} \ , \tag{4.97}$$

$$\phi_{i+1} = \phi_i - E_{\beta_i}(t_{i+1} - t_i) \ . \tag{4.98}$$

The expression Eq.4.97 determines the time between jumps $\Delta t = t_{i+1} - t_i$ in the stochastic Bloch-Redfield algorithm. Comparing Eq.4.97 and Eq.4.93 we see that the only difference between the classic KMC algorithm and the stochastic Bloch-Redfield-algorithm for pure eigenstates is the order of stochastically choosing the transition and the transition time which is purely a matter of convention.

Given that the system state $|\psi(t)\rangle$ between quantum jumps is an energy eigenstate the stochastic Bloch-Redfield algorithm maps directly to the established kinetic Monte-Carlo method. For the moment we assume that the system state is already proportional to an energy eigenstate at the beginning of the time-evolution.

All possible quantum jumps will correspond to transitions between energy eigenstates of the system if and only if all jump-operators meet the condition,

$$\begin{aligned} &\forall |\beta\rangle, |\gamma\rangle, |\delta\rangle \ \text{ eigenstates of } H_S \ , \ \forall \ \xi_k^J : \\ &\qquad \langle\beta|\xi_k^J|\gamma\rangle = \langle\delta|\xi_k^J|\gamma\rangle \Rightarrow |\beta\rangle = |\delta\rangle \ . \end{aligned} \tag{4.99}$$

Jump operators have to correspond to exactly one transition between eigenstates,

$$\xi_k^J \propto |\beta\rangle\langle\gamma| \ . \tag{4.100}$$

The only exception is the jump operator that corresponds to transition frequencies of zero $\omega_{\beta\beta} = 0$ and therefore pure dephasing,

$$\xi_{\text{deph}}^J = \sum_\beta c_\beta \, |\beta\rangle \, \langle\beta| \ , \tag{4.101}$$

where the c_β are arbitrary coefficients.

Condition Eq.4.99 contains the strict secular approximation. Each jump operator corresponds to exactly one transition and therefore to exactly one transition frequency. The condition corresponds to the strict secular approximation in a system where all transition frequencies are different,

$$\forall \ |\beta\rangle, |\gamma\rangle, |\delta\rangle, |\eta\rangle \qquad \text{eigenstates of } H_S \tag{4.102}$$

$$\omega_{\beta\gamma} = \omega_{\delta\eta} \quad \Rightarrow |\beta\rangle = |\delta\rangle, \quad |\gamma\rangle = |\eta\rangle \ . \tag{4.103}$$

In general the initial state of a stochastic Bloch-Redfield simulation will not be an energy eigenstate of the system Hamiltonian. When the condition for the mapping to KMC is met, the time evolution can be simulated with the stochastic Bloch-Redfield algorithm until the first off-diagonal quantum jump with a jump operator Eq.4.100 occurs. The off-diagonal quantum-jump projects the system-state to an energy eigenstate. Once the

system is in an energy eigenstate the stochastic Bloch-Redfield algorithm is equivalent to the KMC algorithm.

At the end of this section we want to note two important points. First, given that all approximations are valid, we can reconstruct the full time-evolution of the density-matrix although we only simulate the incoherent processes in the KMC-inspired algorithm. Usually the KMC algorithm is used to obtain only the populations of a certain basis-set of the system, the diagonal elements of the density-matrix. We can reconstruct the full density matrix since we already diagonalized the system. The system-state with the full phase-information can be obtained for any time from our knowledge of the eigenenergies E_β and eigenstates $|\beta\rangle$.

As a second point, we want to stress that the shown connection between the stochastic Bloch-Redfield and kinetic Monte-Carlo algorithms in no way means that we can simply substitute the stochastic Bloch-Redfield algorithm with the KMC algorithm nor can we simply expand normal KMC-simulations to obtain the full density-matrix. The reformulation of the stochastic Bloch-Redfield algorithm in KMC-form only works in the eigenbasis of the system-Hamiltonian. In the Bloch-Redfield approach it is always necessary to diagonalize the system-Hamiltonian to calculate the dephasing and relaxation-rates from the spectral function $C_{ij}(\omega)$. In the typical KMC-simulation, where the incoherent transition-rates are obtained by other means, the original basis is used as an approximation of the eigenbasis, e.g. the occupation basis in a lattice with very small tunnelling-matrix-elements. A diagonalization of the system-Hamiltonian is neither necessary nor feasible for the typical system-sizes.

Take for example the transport of interacting Cooper-pairs and anti-Cooper-pairs in a one-dimensional Josephson-junction-array, a lattice of length N. A complete state-basis of this system has dimension 3^N, if we restrict ourselves to the case where each site can be occupied by a Cooper-pair, anti-Cooper-pair or be empty. It is not possible to find the eigensystem of the corresponding system-Hamiltonian for an array of 50 sites with computational resources typically available today. With a KMC algorithm the current transport in such and larger systems can be simulated on a standard personal computer [103, 15].

5. Applying the stochastic Bloch-Redfield algorithm to an SSET

In this chapter we will demonstrate the practical application of the stochastic Bloch-Redfield-method. The superconducting single electron transistor (SSET) is used as an exemplary system. The SSET has been studied in great detail theoretically [104, 1, 2, 105] and experimentally [106]. Depending on the number of tunnelled-charge states one chooses to include the energetically accessible Hilbert space of an SSET can be arbitrarily large. It is an ideal test case to compare the results of the stochastic Bloch-Redfield-algorithm with established techniques. The numerical results presented in this chapter have also been published by the author in Ref.[66].

An SSET consists of a superconducting island connected to two superconducting leads by insulating Josephson-junctions (see Fig.5.1). The superconducting island is capacitively coupled to the ground with a capacitance C_g. Each Josephson-junction can be characterised with the Josephson coupling energy E_J and the capacitance of the junction C_J. The total capacitance of the island with respect to the ground is,

$$C = 2C_J + C_g \ , \tag{5.1}$$

An offset voltage V_g is applied between the superconducting island and the ground and the left and right Josephson-junctions are biased by the voltages V_1 and V_2 with the total bias voltage $V_{\text{bias}} = V_2 - V_1$.

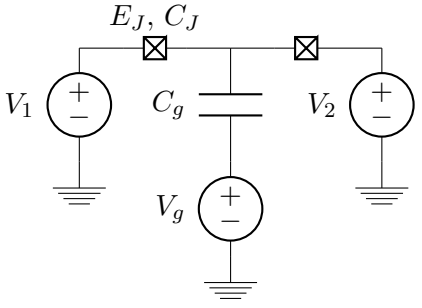

Figure 5.1: Circuit diagram of the SSET with capacitance to the ground C_g, the bias voltages V_1,V_2, the voltage to the ground V_g and the Josephson junctions with the Josephson energy E_J and the capacitance C_J. (As published in Ref.[66])

The superconducting island is small enough so that the number of Cooper-pairs and quasi-particles on the island is a good quantum-number. The state of the island is given by the number N of elementary charges on the island compared to a neutral equilibrium. We assume that the charging energy E_C^{is} of the island,

$$E_C^{is} = \frac{e^2}{2C} \ . \tag{5.2}$$

is large enough that it is sufficient to consider the states with $N \in -2 \ldots 2$. At each point in time the island can be empty or be occupied by an anti-Cooper pair, an anti-quasi-particle, a quasi-particle or a Cooper pair. We do not include quasi-particle double-occupancies. It is assumed that two quasi-particles on the superconducting islands relax to a Cooper pair occupation state on a time-scale much shorter than all other time-scales of the problem.

While the state of the superconducting island alone is given by N, the state of the SSET can be characterized by the number of charges on the island N and the number of charges $\bar{N}$ that have tunnelled through the right Josephson junction. Normally the variable $\bar{N}$ is not considered as a degree of freedom of the system. The transport properties of the SSET can be obtained from a master equation for the density matrix of the N-states alone (see for example Ref.[2]). We are however free to consider an arbitrarily large basis $\left|N, \bar{N}\right\rangle$ with $\bar{N}$ bounded by $m_{\bar{N}}$, $0 \leq \bar{N} < m_{\bar{N}}$. The corresponding Hilbert space has dimension $5m_{\bar{N}}$. We can therefore test the stochastic Bloch-Redfield algorithm introduced in the previous chapter (Chap.4) with a system that has a large Hilbert space. At the same time we can compare the behaviour we obtain from the stochastic Bloch-Redfield approach with established results.

The Hamiltonian of the system in the variables N and $\bar{N}$ is given by [66],

$$H_S = H_C + H_V + H_t \ , \tag{5.3}$$

$$H_C = \frac{1}{2C}\left(e\hat{N} - n_g\right)^2 \ , \tag{5.4}$$

$$H_V = V_2 e\hat{\bar{N}} - V_1\left(e\hat{\bar{N}} - e\hat{N}\right) \ , \tag{5.5}$$

$$H_t = \sum_{N,\bar{N}} \left(E_J \left|N+2, \bar{N}-2\right\rangle \left\langle N, \bar{N}\right| + E_J \left|N+2, \bar{N}\right\rangle \left\langle N, \bar{N}\right| + \text{h.c.}\right) \ , \tag{5.6}$$

$$n_g = C_g V_g + C_J(V_2 - V_1) \ , \tag{5.7}$$

and consists of the charging Hamiltonian H_C with the offset charge n_g, the voltage Hamiltonian H_V and the Josephson tunneling Hamiltonian H_t. The bias part of the Hamiltonian H_V gives the energy gained by a charge carrier tunnelling through the Josephson-junctions connecting the dot with the leads. The tunneling Hamiltonian H_t consists of two parts. The first term changes $\bar{N}$ and is responsible for the Cooper pair tunnelling through the right junction. The second part leaves $\bar{N}$ unchanged and corresponds to the coherent tunnelling through the left junction.

As every mesoscopic solid-state system the SSET can couple to many different sources of environmental decoherence, for example the bath of thermally activated quasi-particles in the superconducting leads [2], fluctuations in the applied voltages due to external impedances $Z(\omega)$ [104, 105], the phonon-bath in the substrate on which the SSET is fabricated or two level fluctuators in the Josephson junctions as they are found in many qubits. Here we consider system bath models,

$$H = H_S + H_{SB} + H_B \ , \tag{5.8}$$

that are governed by the Bloch-Redfield equation Eq.4.61.

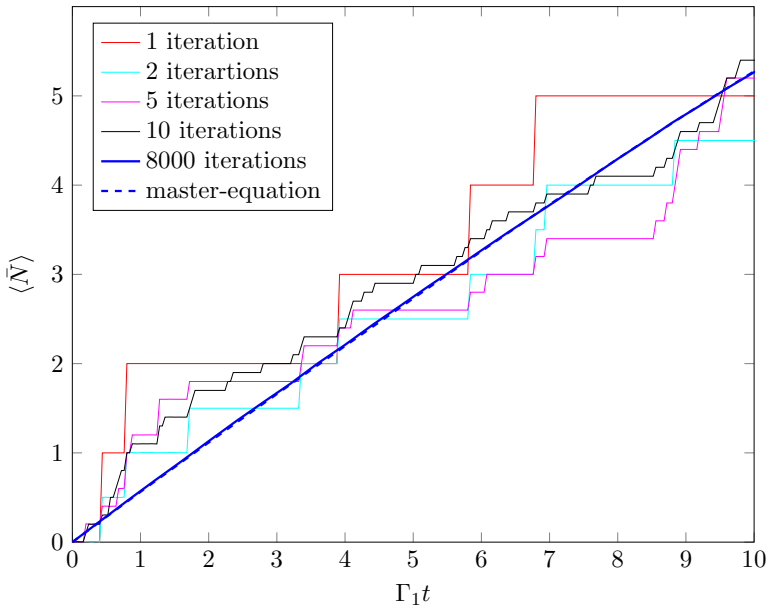

Figure 5.2: A plot of the convergence of the expectation value of the time-evolution of the tunnelled charges $\langle \bar{N} \rangle$ in the JQP cycle when averaged over an increasing number of iterations of the stochastic Bloch-Redfield algorithm in the PWFS approximation. After 8000 iterations the result is almost indistinguishable from the solution of the master-equation (dashed blue line). The expectation value $\langle \bar{N} \rangle$, which corresponds to the transported charge, increase linearly over time. (Figure and caption Ref.[66])

5.1 The Josephson Quasi Particle Cycle

A characteristic process in SSETs is the Josephson quasi particle cycle (JQP cycle) [104, 106]. In this section we discuss the physics behind the JQP cycle and show how the JQP cycle can be simulated with standard density matrix master-equations and the stochastic Bloch-Redfield method in the secular approximation and in the piecewise flat spectral function approximation (PWFS approximation).

The DC-transport in an SSET under small voltage bias $V_b = V_2 - V_1$ is constricted by a Coulomb blockade depending on the equilibrium offset charge n_g. As in every normal SET for $-0.5e \leq n_g \leq 0.5e$ the states with no Cooper pairs or quasi-particles on the island $\left|N = 0, \bar{N}\right\rangle$ have the lowest energy with respect to the charging Hamiltonian H_C. An additional Cooper pair on the island requires an additional energy of $\Delta E_C = \frac{1}{2C}(2e - n_g)^2$, whereas an additional quasi-particle requires $\Delta E_{qp} = \frac{1}{2C}(e - n_g)^2$. In a normal conducting SET with no Cooper pairs this leads to a n_g-dependent Coulomb blockade threshold voltage for DC-transport,

$$V_t^{normal}(n_g) \quad = \quad \frac{1}{2C}\frac{(e - n_g)^2}{e} \ . \tag{5.9}$$

In the SSET it is not sufficient for the bias voltage V_b to overcome the Coulomb blockade to have quasi-particle transport, at low temperatures all electrons are in the superconducting condensate and the number of occupied quasi-particle states in the leads is negligible. For a quasi-particle excitation of charge e to incoherently tunnel into the island or from the

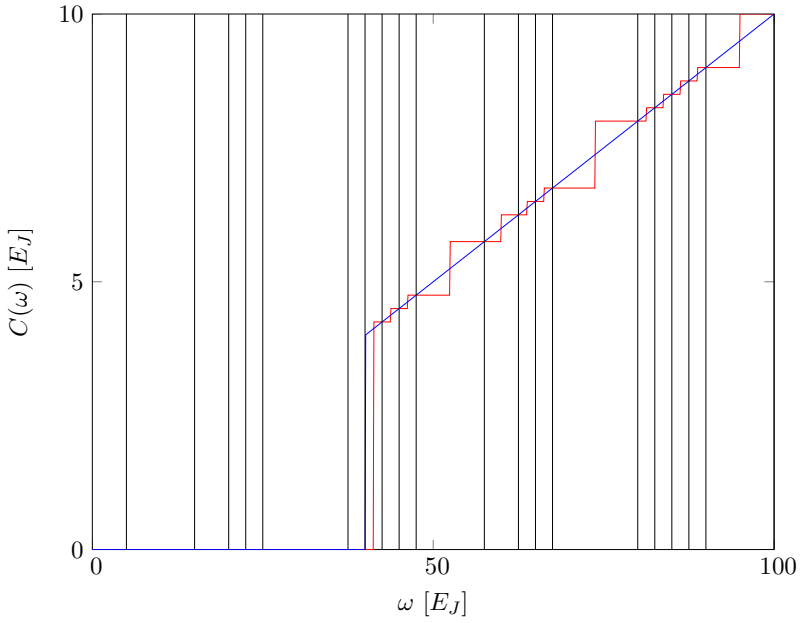

Figure 5.3: The piecewise flat spectral function approximation: The spectral function $C(\omega)$ (blue) is approximated by the piecewise-flat function $C^{pwf}(\omega)$ (red) defined by the values of $C(\omega)$ at the transition frequencies $\omega_{\beta\gamma}$ of the system (black lines). The transition frequencies in the JQPC-example are spaced so far apart that each transition frequency corresponds to another bin in $C^{pwf}(\omega)$. In the intervals between the transition frequencies $C^{pwf}(\omega)$ can take very different values from $C(\omega)$, however this is not important as the value of the spectral function at these energies does not enter the Bloch-Redfield equation. (Figure and caption Ref.[66])

island a Cooper pair has to be broken at an energy cost of 2Δ. Overall one obtains the threshold voltage for quasi-particle transport in the SSET,

$$V_t = \frac{1}{E}\left(\frac{(e-n_g)^2}{2C} + 4\Delta\right) . \tag{5.10}$$

Depending on the parameter regime the transport behaviour can be modified by the parity effect. In the state with one additional quasi-particle on the superconducting island the quasi-particle is forced to occupy a state with at least energy Δ since the quasi-particle density of states is zero below the superconducting gap Δ. This one quasi-particle can incoherently tunnel from the island into one of the leads without breaking a Cooper pair with the assorted energy cost 2Δ. The tunnelling rate of the quasi-particle is however suppressed by a small prefactor since the number of exited quasi-particles on the island has to be compared with the number of electrons in the condensate. A detailed discussion of the parity effect in SSETs can be found in Ref.[1]. We assume that the parity effect can be neglected for the system we consider.

Usually pure Cooper pair transport does not contribute to the DC-transport through a voltage biased SSET. Coherent Cooper pair tunnelling under a dc bias voltage can only lead to an AC-current response as the energy gained by the charge carriers from the bias voltage is not dissipated. Incoherent Cooper pair tunnelling as obtained from P-of-E theory can in principle contribute to DC-conductance but the tunnelling rates are proportional

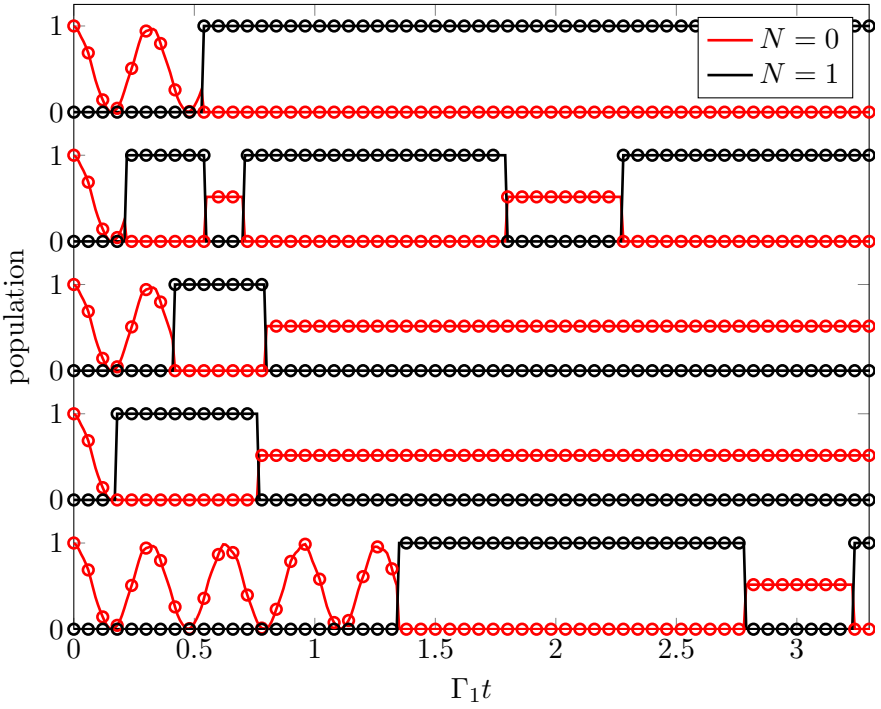

Figure 5.4: The population in the states $N = 0$ and $N = 1$ of the SSET for several single trajectories of the stochastic Bloch-Redfield algorithm. The population is plotted with an offset for each trajectory. For the chosen parameter of the JQP cycle the PWFS (solid lines) and the secular approximation (circles) are equivalent as explained in Fig.5.3. The PWFS-approximation and the secular trajectories were initialized with the same seed for the random number generator. As the system was not initialized in an eigenstate the quantum jump trajectories show coherent oscillations of the system state before the system is projected into an eigenstate by the first quantum jump. (Figure and caption Ref.[66])

to E_J^2 [38] and the contribution can be neglected for small Josephson energies E_J.

The Josephson quasi-particle cycle lowers the transport threshold voltage due to a combination of coherent Cooper pair and incoherent quasi-particle tunnelling. We assume that the dissipative environment of the SSET is given by the quasi-particle bath of the superconducting leads. The system bath Hamiltonian H_{SB} is given by the quasi-particle tunnelling operators,

$$H_{SB} = \sum_{N,\bar{N}} \left(\left| N-1, \bar{N} \right\rangle \left\langle N, \bar{N} \right| X_{\text{left}} + \left| N+1, \bar{N}-1 \right\rangle \left\langle N, \bar{N} \right| X_{\text{right}} + \text{h.c.} \right) \ , \qquad (5.11)$$

where $X_{\text{left/right}}$ are the bath coupling operators for the left and right lead. The spectral function of the bath coupling operators can be expressed as an energy integral [1],

$$C(\omega) = \frac{1}{e^2 R_t} \int_{-\infty}^{\infty} d\epsilon \int_{-\infty}^{\infty} d\epsilon' \mathcal{N}(\epsilon) \mathcal{N}(\epsilon') f(\epsilon) \left[1 - f(\epsilon') \right] \delta(\epsilon - \epsilon' - \omega) \ . \qquad (5.12)$$

The population of the states on both sides of the Josephson junction is given by the Fermi function $f(\epsilon)$, $\mathcal{N}(\epsilon)$ gives the density of states of the quasi-particle states and R_t is the normal tunnelling resistance of the Josephson junction. The exact value of the spectral function can be calculated numerically. We limit ourselves to the low temperature limit

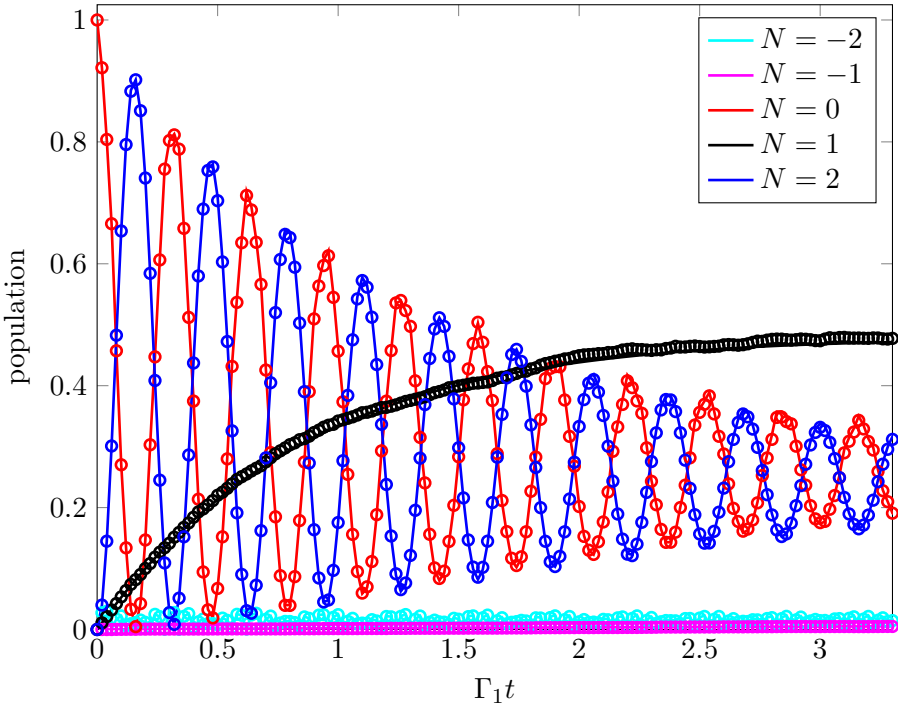

Figure 5.5: The time-evolution of the population of the charge-states of the SSET-island $N = -2$ to $N = 2$ in the JQP cycle over a short time obtained by averaging over 8000 of the trajectories seen in Fig.5.4 (circles). The master-equation gives the same result (solid line) as the stochastic Bloch-Redfield algorithm in the PFS-approximation . Population oscillates coherently between states $|N = 0\rangle$ and $|N = 2\rangle$. The amplitude of the oscillation decays as dephasing destroys the coherent quantum-oscillations. Population relaxes from states $|N = 0\rangle$ and $|N = 2\rangle$ to state $|N = 1\rangle$ via dissipative quasi-particle tunnelling. (Figure and caption Ref.[66])

where the spectral function can be approximated as,

$$C(\omega) = \frac{1}{e^2 R_t} \Theta(\omega - 2\Delta)\omega \ , \tag{5.13}$$

with the superconducting energy gap Δ. In the low temperature limit, the spectral function is zero for transition energies ω smaller than twice the superconducting energy gap. Incoherent quasi-particle tunnelling only occurs when the charging energy difference ΔE is large enough to split a Cooper pair in two quasi-particles. We characterise the strength of incoherent quasi-particle tunnelling by introducing the rate Γ_1,

$$\Gamma_1 = \frac{2\Delta}{e^2 R_t} \ . \tag{5.14}$$

To achieve a Josephson quasi-particle cycle in the SSET, the gate charge is set to one $n_g = 1$. The states with one quasi-particle on the superconducting island are energetically favourable. The states with one Cooper pair and the states with no charge on the island have degenerate charging energies,

$$\left\langle N = 1, \bar{N} \right| H_C \left| N = 1, \bar{N} \right\rangle = 0 \ , \tag{5.15}$$

$$\left\langle N = 0, \bar{N} \right| H_C \left| N = 0, \bar{N} \right\rangle = \left\langle N = 2, \bar{N} \right| H_C \left| N = 2, \bar{N} \right\rangle = E_C^{is} \ . \tag{5.16}$$

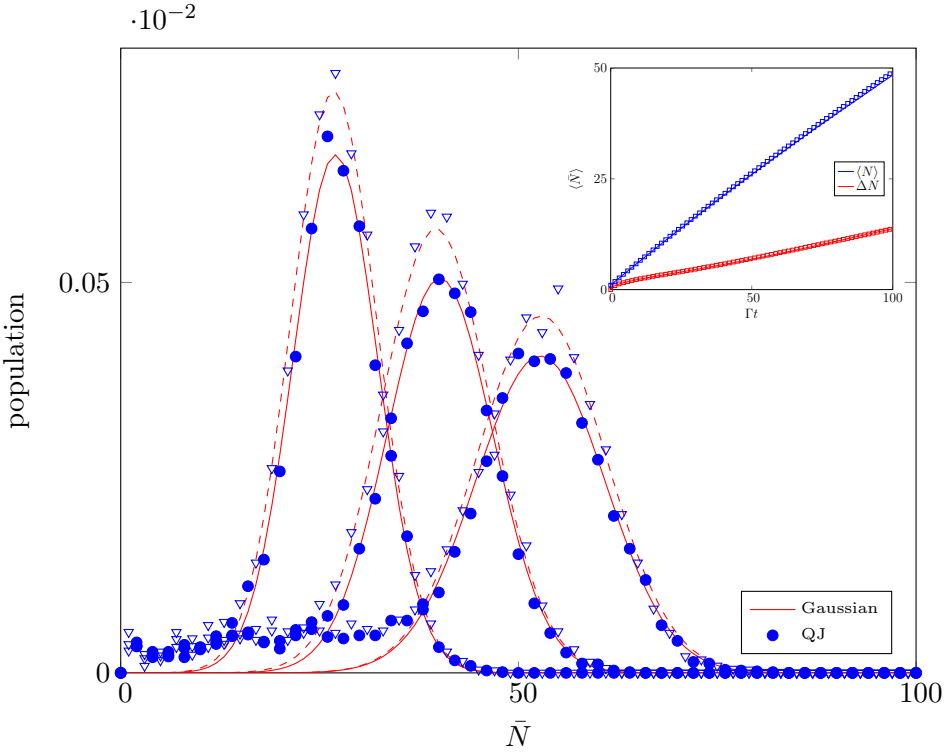

Figure 5.6: The distribution of the population at $\Gamma t = 50$, $\Gamma t = 75$ and $\Gamma t = 100$ of the $\left|\bar{N}\right\rangle$-states. The distribution has a peak that moves to larger $\bar{N}$ and broadens over time as charge is transported. The form of the peak can be fitted to the sum of two Gaussians with the same width and peak position but different amplitudes for odd (dots and solid line) and even (triangles and dashed line) $\bar{N}$-states.
Inlay: Plot of the expectation value $\left\langle \bar{N} \right\rangle$ (blue/light) and the standard deviation $\Delta\bar{N}$ (red/dark) for a large system ($\bar{N}_{max} = 100$) and long simulation time, $\Gamma t_{max} = 100$, not accessible with numerical solution to the full density matrix master equation. Results of the stochastic Bloch-Redfield algorithm in the secular (squares) and PFS (circles) approximation after 8000 iterations are shown. The expectation value $\left\langle \bar{N} \right\rangle$ and $\Delta\bar{N}$ increase linearly for the whole simulation as expected [2]. (Figure and caption Ref.[66])

The bias voltages are set to,

$$V_1 = 0 \ , \tag{5.17}$$

$$V_2 = E_C + 2\Delta \ . \tag{5.18}$$

The Josephson quasi-particle cycle consists of three tunneling events. Starting from a state with an empty island $\left|N = 0, \bar{N}\right\rangle$, a Cooper pair can tunnel coherently trough the left junction without dissipating energy. The energy difference between the new state $\left|N = 2, \bar{N}\right\rangle$ and the state $\left|N = 1, \bar{N} + 1\right\rangle$ is large enough to break up the Cooper pair and lead to the incoherent tunnelling of a quasi-particle through the right Josephson junction. A second incoherent tunnelling event brings the system back to a state with an empty island $\left|N = 0, \bar{N} + 2\right\rangle$ and the cycle can start again.

We have simulated the transport through the SSET in the Josephson quasi-particle cycle

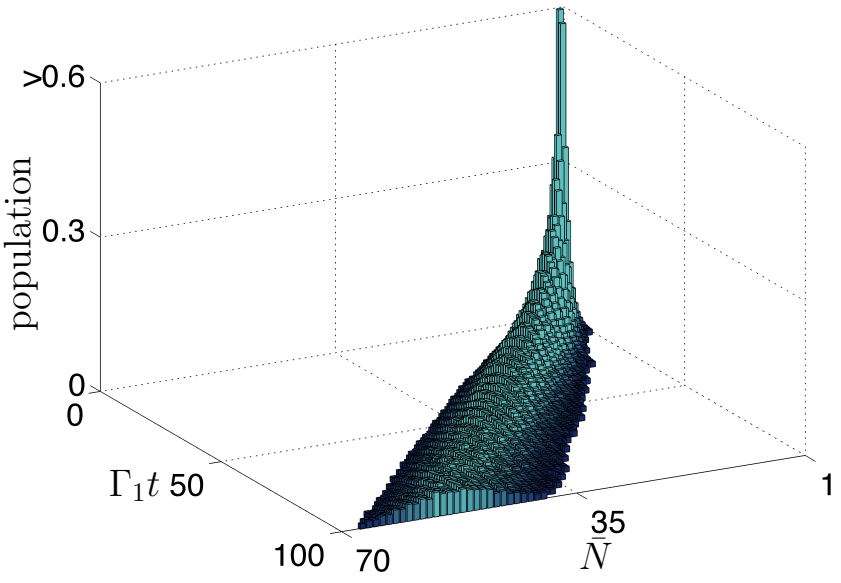

Figure 5.7: Three-dimensional representation of the spreading of the population (height) over the $|\bar{N}\rangle$-states (x-axis) and time (y-axis) in the stochastic Bloch-Redfield JQPC-simulation of the large system. States with population < 0.01 have been truncated for clarity. Starting in a single peak at $\Gamma t = 0$ the population spreads out over several $|\bar{N}\rangle$-states over time while the center of the distribution moves to higher $\bar{N}$. (Figure and caption Ref.[66])

with the stochastic Bloch-Redfield method for the parameters,

$$\Delta = 20\ E_J\ , \tag{5.19}$$

$$E_C^{is} = 2.5\ E_J\ , \tag{5.20}$$

$$\Gamma_1 = 0.2\ E_J\ . \tag{5.21}$$

The number m_{stoch} of independent stochastic trajectories in the stochastic Bloch-Redfield algorithm was set to $m_{stoch} = 8000$. Two different system sizes $m_{\bar{N}}$ where simulated. Simulations for $m_{\bar{N}} = 11$ and 55-dimensional Hilbert space were compared to solutions obtained from solving the standard Bloch-Redfield equation with a numerical Runge-Kutta algorithm. The comparison of the master-equation method and the stochastic Bloch-Redfield method is shown in Fig.5.2. Both methods yield the same result. The figure also shows the convergence of the results when averaging over increasing numbers of stochastic trajectories.

In the model of the Josephson quasi-particle cycle the strict secular approximation and the piecewise flat spectral function (PWFS) approximation (see Chap.4) are equivalent. The differences between the transition frequencies of the JQP-cycle-Hamiltonian is large compared to the slope of the spectral function Eq.5.13. Each transition between states $|N, \bar{N}\rangle \langle N', \bar{N}'|$ corresponds to a different bin in the PWFS approximation (Fig.5.3). Mixed terms of transitions with different transition frequencies are neglected from the Bloch-Redfield master equation.

Since all jump operators correspond to exactly one transition between eigenstates the system is projected into an energy eigenstate after each quantum jump. After the first

quantum jump no coherent oscillations occur in the populations of the $|N\rangle$-states of a single trajectory. The coherent oscillations are only recovered after averaging over many trajectories, as shown in Fig.5.4 and Fig.5.5.

The numerical advantage of the stochastic unravelling is demonstrated by a simulation with a larger system size $m_{barN} = 101$. Here the Hilbert space has dimension 505. The system is much to large to be solved by the usual master-equation approach. Using the stochastic Bloch-Redfield approach we can not only simulate the time evolution of the system (Fig.5.6) we can also go to much longer simulation times. It takes longer until the SSET reaches the maximal value of $\bar{N}$. In the larger systems we can observe how the probability distribution for the number of charges $\bar{N}$ transported by the JQP cycle is established. As shown in Fig.5.6, the distribution of $\bar{N}$ takes the form of two Gaussians for even and odd $\bar{N}$. The mean of the Gaussian increases linearly in time corresponding to the charge transport in the JQP-cycle. The mean deviation of the charge distribution $\bar{N}$ also increases linearly in time. A similar behaviour has been predicted in Ref.[2] for the number of charges tunnelling over a certain time interval τ in a JQP cycle. In Fig.5.7 we show the spread and shift in the population of the $\bar{N}$-states over time.

5.2 Incoherent Cooper pair tunnelling

To demonstrate the difference between the strict secular and the piecewise flat spectral function approximation we consider pure incoherent Cooper pair transport in the SSET in this section. We neglect the coupling of the SSET to the quasi-particle bath. The system-bath coupling is strictly longitudinal,

$$H_{SB} = \hat{N} X_{\text{long}} \ , \tag{5.22}$$

where X_{long} is the longitudinal bath coupling operator. We assume that the spectral function of the bath coupling operator in the relevant energy range is given by an Ohmic function for positive frequencies and by the detailed balance relation for negative frequencies. For $\omega > 0$ one can write,

$$C(\omega) = \Gamma_2 \ , \tag{5.23}$$

$$C(-\omega) = e^{-\beta\omega} C(\omega) \ , \tag{5.24}$$

$$\beta = \frac{1}{k_B T} \ . \tag{5.25}$$

Due to the coherent tunnelling amplitude of Cooper pairs E_J the purely longitudinal system coupling operator has off-diagonal matrix elements in the energy-eigenbasis of the system. The off-diagonal terms lead to dissipative transitions in the energy-eigenbasis. In the original charge-basis the dissipative transitions correspond to incoherent Cooper pair tunnelling. The emergence of dissipative tunnelling rates due to longitudinal noise and coherent tunnelling terms is a standard feature of P-of-E theory [38]. We will discuss P-of-E theory in greater detail in the next chapter Chap.6.

The SSET parameters are unchanged from the JQP simulations, it is biased similarly to the JQP cycle simulations,

$$\Delta = 20 \ E_J \ , \tag{5.26}$$

$$E_c = 2.5 \ E_J \ , \tag{5.27}$$

and we choose a similar voltage biasing,

$$n_g = 1 \ , \tag{5.28}$$

$$V_1 = 0 \ , \tag{5.29}$$

$$V_2 = 12.5 \ E_j \ . \tag{5.30}$$

The parameters of the environmental noise are set to,

$$\beta = 100\frac{1}{E_J} \ , \tag{5.31}$$

$$\Gamma_2 = 0.2 \ E_j \ . \tag{5.32}$$

In Fig.5.8 we compare the time-evolution of the population of the charge states of the island of single trajectories in the strict secular and PWFS approximation. In the strict secular approximation the population only changes when a quantum jump occurs, in the PWFS approximation the population shows coherent oscillations between quantum jumps. As in the JQP cycle the jump operators in the strict secular approximation project the system to energy eigenstates. Due to the flat spectral function of the longitudinal coupling operators, the piecewise flat spectral function has only one bin for positive frequencies. In this case it is the opposite of the strict secular approximation. Instead of one jump operator for each possible transition between energy eigenstates there is only one jump operator containing all possible dissipative transitions in the PWFS approximation. A quantum jump does not project the system into an energy-eigenstate and we find coherent oscillations between the eigenstates in a single stochastic trajectory. After averaging over many trajectories the strict secular and the PWFS approximation still yield the same result that agrees with a standard master equation treatment. The strict secular approximation is valid in the chosen parameter regime.

The long time behaviour of the probability distribution of tunneled charges $\bar{N}$ is shown in Fig.5.9. As in the JQP cycle the distribution broadens over time and the center shifts to larger $\bar{N}$. The transport behaviour is linear. The model we consider here does not include quasi-particle tunneling. The number of transported charges can only change by two elementary charges in each tunnelling event. Only even $\bar{N}$ states can be populated.

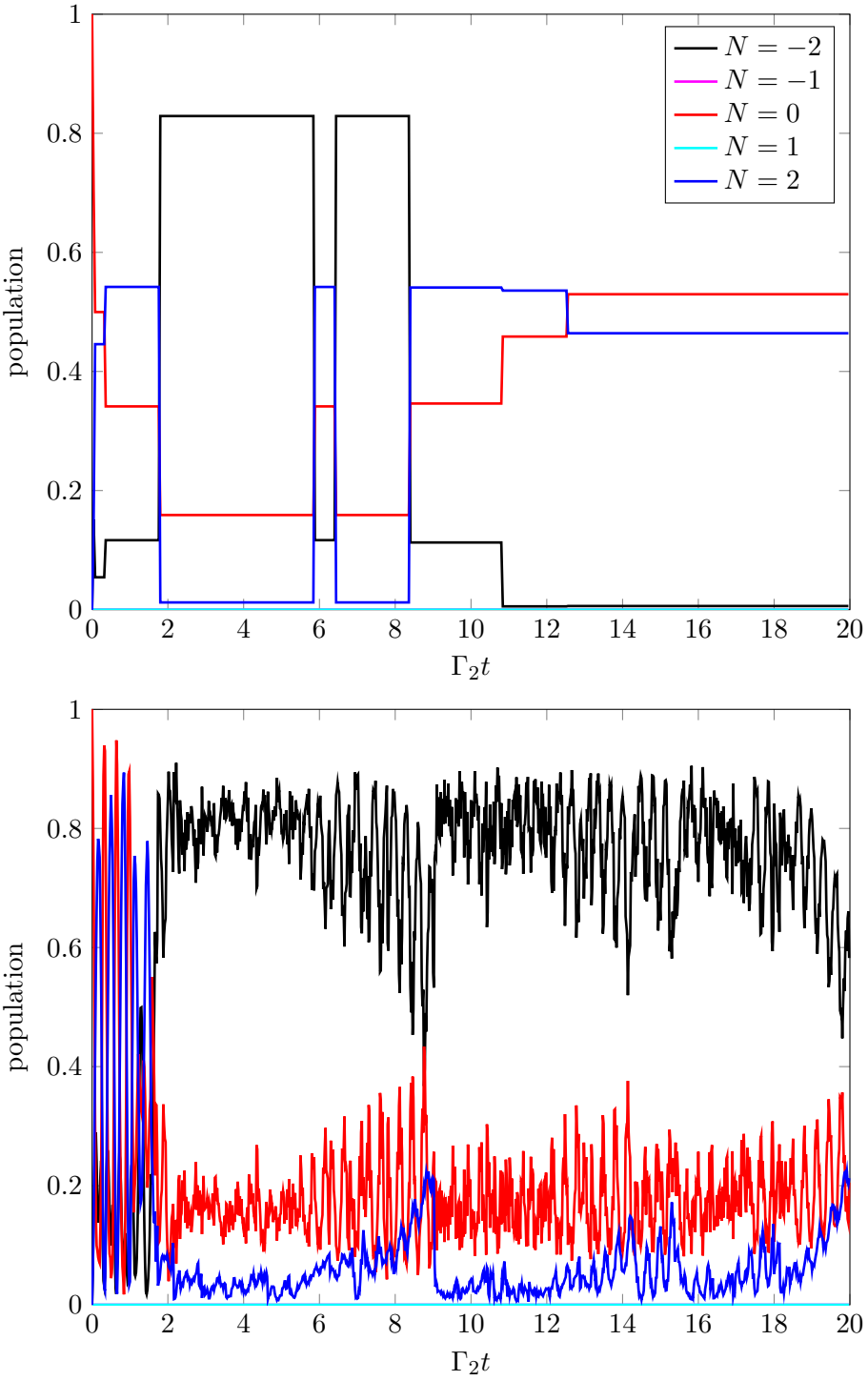

Figure 5.8: The stochastic trajectories of the ICPT-system in the secular (upper plot) and in the PWFS (lower plot) approximation. (Figure and caption Ref.[66]). Both plots use the same color code for the population: $N = -2$ black, $N = -1$ magenta, $N = 0$ red, $N = 1$ cyan and $N = 2$ blue.

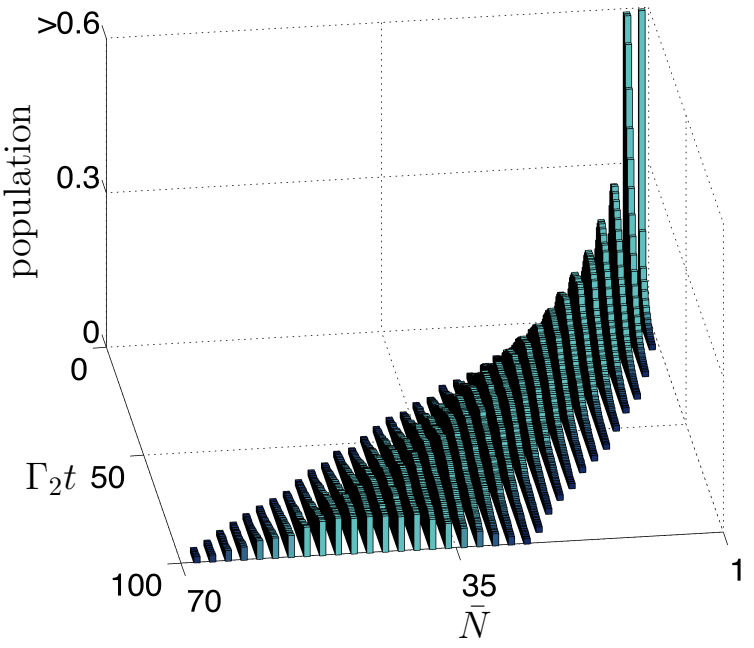

Figure 5.9: The three-dimensional representation of the population for a long simulation $\Gamma t_{max} = 500$ of a large ICPT-system $\bar{N}_{max} = 100$. The main difference between the ICPT-case and the JQPC-case (Fig.5.7) is that incoherent Cooper-pair tunnelling only connects states which differ by $\bar{N} = 2$ and therefore only odd $|\bar{N}\rangle$-states are occupied in this case. (Figure and caption Ref.[66])

6. Charge transport: Simulating coherent Cooper pair tunnelling

In this chapter we consider Josephson junction arrays in the transport regime. We employ numerical simulations of coherent and incoherent transport processes of Cooper pairs to obtain the transport properties of a Josephson junction array. In the model we present in Sec.6.2.1 we limit ourselves to a short inner section of a Josephson junction array and limit the number of Cooper pairs and anti-Cooper pairs in this section. The model we consider describes more closely a single excess Cooper-pair in a homogeneously biased Josephson junction ring (as discussed in Ref.[35]) than an open boundary-biased Josephson junction array. Even in the limited model the Hilbert space of the system is very large. We use the stochastic Bloch-Redfield algorithm developed in Ch.4 to simulate the full time-evolution of the density matrix according to Bloch-Redfield theory.

In Sec.6.1 we present the $P(E)$-theory [38] that is used in literature together with kinetic Monte-Carlo simulations to model the transport of Cooper pairs and quasi-particles through Josephson junction arrays [15]. By comparing the results of the $P(E)$ approach and the Bloch-Redfield simulations we gain information on the parameter regimes where it is appropriate to use $P(E)$-theory to obtain the incoherent tunnelling rates of the Cooper pairs.

Since the first experimental realisations of Josephson junction arrays [3, 4] it has been known that the current through the array increases linearly with the applied voltage V once it exceeds the switching voltage V_{sw}. The current as a function of the applied voltage has a nonzero offset so that Ohms law, $V = RI$, is not exactly met. The differential conductance of the IV-curve is proportional to the square of the Josephson coupling energy. At much higher voltages than the switching voltage a transition to a second conduction regime with higher differential conductance occurs [14]. An experimental IV-curve including the high voltage regime is shown in Fig.6.1. In the second conductance regime, the bias voltage is large enough to create quasi-particles by breaking Cooper pairs along the array and the resistance is determined by the normal resistance of the array. The current at the transition from first to second conductance regime is of the same order of magnitude as the Zener current. The Zener current is the current at which the velocity of the quasi-charge from Sec.2.2.2 is so large that one can assume that Landau-Zener transitions from lower to higher Bloch-bands occur at every degeneracy-point of the effective quasi-charge model (see Ch.2).

When the Josephson junction array is described with the help of a sine-Gordon-like model,

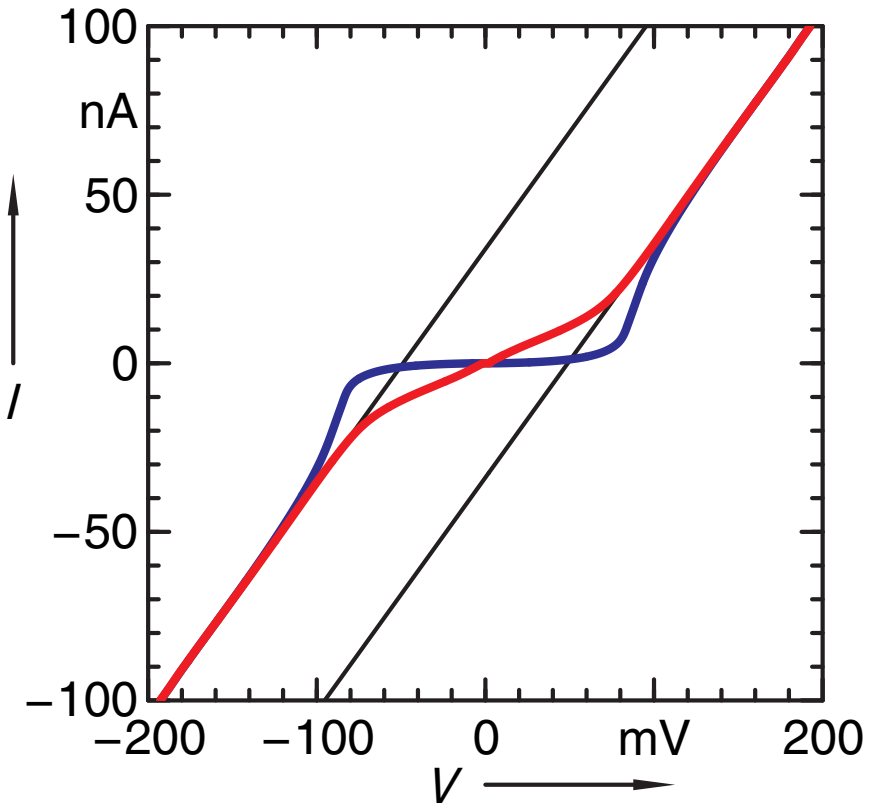

Figure 6.1: A plot of experimental IV-curves of a Josephson junction array recorded over a large voltage range from Ref.[14]. The effective Josephson energy E_J can be suppressed with an external magnetic field (compare Sec.3.4). In the red curve E_J is not suppressed, in the blue curve E_J is maximally suppressed with a half flux quantum per SQUID.

the finite differential conductance in the transport regime is often accounted for by including a phenomenological resistive term in the equation of motion Eq.2.91 [13, 52],

$$L\ddot{Q}_i + \frac{2Q_i - Q_{i-1} - Q_{i+1}}{C_0} + \alpha_R(\dot{Q}_i)\dot{Q}_i + V_Q\left(Q_i + 2e\ F_i\right) = 0\ , \tag{6.1}$$

where $\alpha_R(\dot{Q}_i)$ is the friction coefficient of the quasi-charge. In the simplest case of a purely Ohmic phenomenological resistance R we have $\alpha_R(\dot{Q}_i) = \frac{1}{R}$. In Refs.[13] and [52] a nonlinear resistance is used,

$$\alpha_R(\dot{Q}_i) = \begin{cases} 0 & \text{for} \quad \dot{Q}_i \leq I_{tr} \\ \frac{1}{R} & \text{for} \quad \dot{Q}_i > I_{tr} \end{cases}\ . \tag{6.2}$$

Dissipation only sets in once the current exceeds a threshold current I_{tr}.

Including a phenomenological resistance does not explain on a microscopic level why the differential conductance is proportional to the squared Josephson coupling energy. In the literature the dependence on the Josephson coupling energy is commonly explained by deriving the incoherent Cooper pair tunnelling rates from $P(E)$-theory [15, 14].

6.1 $P(E)$-theory and kinetic Monte Carlo

In this section we give a short recap of the well known $P(E)$-theory in the context of tunnelling through Josephson junctions. A detailed discussion can be found in Ref.[38].

We then quickly review how $P(E)$-theory has been used in literature together with kinetic Monte Carlo simulations [15] to obtain the transport properties of a Josephson junction array.

The purpose of $P(E)$-theory is to obtain the incoherent tunnelling rates of the charge carriers through the Josephson junction. Let us consider an island connected to a lead with a Josephson junction that is biased with a fluctuating voltage. The system Hamiltonian is given by the charging energy of the states of the island H_{charge}, the Cooper pair tunnelling term and the energy of Cooper pairs on the island due to the externally applied voltage,

$$\tilde{H} = H_{\text{charge}} + \tilde{H}_{\text{tun}} + 2eV\hat{m} \ , \tag{6.3}$$

$$\tilde{H}_{\text{tun}} = E_J \sum_m |m+1\rangle \langle m| + \text{h.c.} \ . \tag{6.4}$$

The voltage difference over the Josephson junction can be absorbed into the tunnelling Hamiltonian by a unitary transformation. The transformation corresponds to changing into a rotating frame of reference. A description of the transformation procedure is given in Ref.[38]. In the rotating frame the system is given by,

$$H = H_{\text{charge}} + H_{\text{tun}} \ , \tag{6.5}$$

$$H_{\text{tun}} = E_J \sum_m e^{-i\phi} |m+1\rangle \langle m| + \text{h.c.} \ . \tag{6.6}$$

The voltage difference is included in the phase ϕ in the tunnelling term. A Cooper pair tunnelling through the Josephson junction picks up a phase of ϕ. The phase ϕ also couples the system to the environmental bath. The bath in this case is given by the environmental impedance of the circuit.

If incoherent tunnelling of quasi-particles is considered instead of the incoherent Cooper pair tunnelling, the sum over Cooper pair numbers m has to be replaced by a sum over quasi-particle states $|k\rangle$. The Josephson coupling energy E_J is replaced by the quasi-particle tunnelling rates $T_{kk'}$.

$P(E)$-theory uses Fermi's golden rule to obtain the tunnelling probability of the charge carriers. Given an initial state $|i\rangle$ and a final state $|f\rangle$ connected by the tunnelling Hamiltonian the transition rate is [38],

$$\Gamma_{i\to f} = 2\pi \left|\langle f| H_{\text{tun}} |i\rangle\right|^2 \delta\left(E_i - E_f\right) \ , \tag{6.7}$$

where we have omitted a factor of $1/\hbar$ as we set $\hbar = 1$. The initial and final states are states of the whole system-bath combination, including the degrees of freedom of the bath. To obtain the transition rate $\Gamma^c_{i\to f}$ between two charge-states of the system, $|i^c\rangle$ and $|f^c\rangle$, we have to trace out the degrees of freedom of the bath, $\left|i^B\right\rangle$ and $\left|f^B\right\rangle$, just as in the derivation of the Bloch-Redfield equation(Sec.4.2),

$$\Gamma^c_{i\to f} = 2\pi \sum_{i^B, f^B} \left\langle i^B\right| \rho_B \left|i^B\right\rangle \left|\left\langle f^B\right| e^{-i\phi} \left|i^B\right\rangle\right|^2 \sum_m 2E_J^2 \left|\langle f^c \left|m+1\right\rangle \langle m \left|i^c\right\rangle\right|^2 \delta\left(\Delta E_{i,f}\right) \ , \tag{6.8}$$

$$\Delta E_{i,f} = E^c_i - E^c_f + E^B_i - E^B_f \ . \tag{6.9}$$

The matrix element $\left\langle i^B\right| \rho_B \left|i^B\right\rangle$ of the density matrix of the bath ρ_B gives the probability to find the bath in the initial state $\left|i^B\right\rangle$. Only the phase difference ϕ couples to the bath degrees of freedom and only operators containing ϕ have to be averaged over the bath

states. It can be shown [38] that, by expanding the δ-function into an integral over time, the system-bath coupling takes the form of a correlator of exponential coupling operators,

$$\Gamma^c_{i\to f} = \int_{-\infty}^{\infty} \mathrm{dt}\ 2\pi \left\langle e^{i\phi(t)} e^{-i\phi(0)} \right\rangle_B \sum_m 2E_J^2 \left| \langle f^c \left| m+1 \right\rangle \langle m \left| i^c \right\rangle \right|^2 e^{i\left(E_i^c - E_f^c\right)t} \ , \tag{6.10}$$

where $\phi(t)$ is the phase-operator in the interaction picture with respect to the bath Hamiltonian. In the case of a Gaussian bath where Wick's theorem holds, the correlator of exponentials can be written as an exponential of a correlator [38],

$$\left\langle e^{i\phi(t)} e^{-i\phi(0)} \right\rangle_B = e^{\langle [\phi(t)-\phi(0)]\phi(0)\rangle_B} \ . \tag{6.11}$$

The Fourier transform of the correlation function is called the $P(E)$-function,

$$P(E) = \frac{1}{2\pi} \int_{-\infty}^{\infty} \mathrm{dt} e^{\langle [\phi(t)-\phi(0)]\phi(0)\rangle_B} e^{iEt} \ . \tag{6.12}$$

The tunnelling rate from an occupied charge state $|i^c\rangle$ to an unoccupied state $|f^c\rangle$ is given by the $P(E)$ function evaluated at the energy difference times the tunnelling matrix element squared,

$$\Gamma^c_{i\to f} = \sum_m 2E_J^2 \left| \langle f^c \left| m+1 \right\rangle \langle m \left| i^c \right\rangle \right|^2 P\left(E_i^c - E_f^c\right) \ . \tag{6.13}$$

In the case of quasi-particle tunnelling one has to consider that the number of occupied quasi-particle states on one side of the junction and the unoccupied states on the other side of the junction are determined by the Fermi distribution $f(E)$ [38],

$$\Gamma^c_{i\to f} = \frac{1}{e^2 R_T} \int \mathrm{dE_1 dE_2}\ \nu(E_1)\nu(E_2)\ f(E_1)\left[1 - f(E_2 + E_i^c - E_f^c)\right] P\left(E_1 - E_2\right) \ , \tag{6.14}$$

where $\nu(E)$ is the density of states of the quasi-particles and the tunnelling matrix elements $E_J^2 \langle f^c \left| m+1 \right\rangle \langle m \left| i^c \right\rangle$ are contained in the normal tunnelling resistance R_T of the junction.

The proportionality to the squared tunnelling matrix element highlights the crucial difference between $P(E)$-theory as it is used to model Josephson junction arrays [15] and Bloch-Redfield theory as presented in Sec.4.2. The $P(E)$-theory is perturbative in the tunnelling term of the system Hamiltonian. The Bloch-Redfield theory is perturbative in the system-bath-coupling strength. $P(E)$-theory assumes that the charge states connected by the tunnelling terms are a good approximation of the eigenbasis. In that sense $P(E)$-theory is always a local theory that describes the tunnelling of charge carriers through certain Josephson junctions in the array. Bloch-Redfield theory connects the eigenstates of the Josephson junction array. A Cooper pair is delocalised over several array sites and relaxation corresponds to the incoherent transition from one delocalised state to another. The relaxation can not be interpreted as a charge carrier tunnelling through a distinct Josephson junction in the array. We will come back to the difference between $P(E)$ and Bloch-Redfield in the next section.

As $P(E)$-theory explicitly connects charge states its use is always warranted in a situation where corrections due to coherent tunnelling are excluded in the first place. In the kinetic Monte Carlo simulation of Ref.[15] this is exactly the case. We will now give a short summary of the simulations and results of Ref.[15], these results constitute the motivation of the study of the corrections due to coherent Cooper pair tunnelling in the following section.

In the simulations of a 50-site Josephson junction array in Ref.[15] no coherent superpositions between states is allowed. The Josephson junction array is not treated as a quantum

system, but as a classical system or rather a quantum system completely dominated by the incoherent time-evolution. In Ref.[15] it was observed that each island is in one of five possible states, unoccupied, occupied by a quasi-particle, occupied by a Cooper pair, occupied by an anti-quasi-particle and occupied by an anti-Cooper pair. These states are also the states with the lowest charging energies.

The system state only changes by incoherent tunnelling of Cooper pairs or quasi-particles. Coherent Cooper-pair tunnelling is omitted from the time-evolution in the model of Ref.[15]. In the numerical simulations of Ref.[15] the system state is propagated according to the kinetic Monte Carlo algorithm by randomly choosing an incoherent charge tunnelling event and a tunnelling time. The probability distribution of the stochastic processes is derived from the incoherent charge tunnelling rates. The details of the algorithm can be found in Ref.[101] or Ch.4.

The incoherent tunnelling rates of the Cooper pairs and quasi-particles used in Ref.[15] are derived from $P(E)$-theory under the assumption that the environmental bath for each Josephson junction is given by the impedance of the rest of the array. As seen in Fig.6.2 each Josephson junction in the array is taken to be shunted by the normal state resistance of the junction R_T. In Ref.[15] it is then assumed that the relevant environment in the $P(E)$ derivation of the tunnelling rates can be approximated by the total impedance $Z_t(\omega)$, the combination of the impedance of the Josephson junction impedance $Z_J(\omega)$ and the impedance of half the Josephson junction array $Z(\omega)$ (compare Fig.6.3),

$$Z_t(\omega) = \left(Z_J^{-1}(\omega) + \frac{1}{2} Z^{-1}(\omega) \right)^{-1} , \tag{6.15}$$

$$Z_J^{-1}(\omega) = i\omega C_J , \tag{6.16}$$

$$Z(\omega) = \left(i\omega C_{HA} + \frac{2}{N R_T} \right)^{-1} , \tag{6.17}$$

$$C_{HA} = \frac{1}{2} \left(C_0 + \sqrt{C_0 \left(4C_J + C_0 \right)} \right) . \tag{6.18}$$

The impedance $Z(\omega)$ of the half array is determined by the total capacitance C_{HA} of the half Josephson junction array and the resistance of half the array, $N/2$ times the normal state resistance R_T.

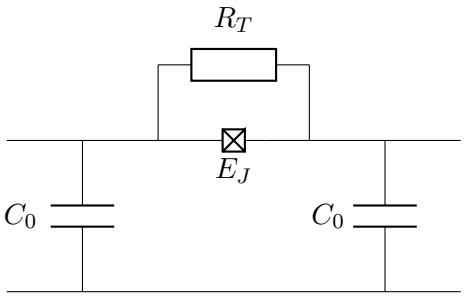

Figure 6.2: A sketch of one Josephson junction in the Josephson junction array. In the model of Ref.[15] the dissipative environment is given by the normal Resistance R_T that shunts every Josephson junction, a widely used model in the theory of incoherent quasi-particle tunnelling [38].

The noise model of Ref.[15] works well with $P(E)$-theory as it assumes that dissipative processes are a local phenomenon at the individual Josephson junctions in the array. The rest of the array is treated as the noise environment. This assumption is not valid when the Cooper pairs are delocalised over large parts of the Josephson junction array.

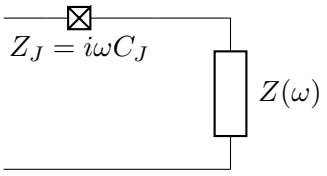

Figure 6.3: In Ref.[15] the collective effect of all resistive shunts and capacitances in the Josephson junction array on a single junction is approximated by assuming that each single Josephson junction in the array sees an effective impedance environment that corresponds to the impedance of the half array $Z(\omega)$.

Following the well known procedure to obtain the $P(E)$-function from an impedance environment [38], the $P(E)$-function is Gaussian shaped for quasi-particle and Cooper pair tunnelling in the parameter regime of Ref.[15],

$$P(E) = \sqrt{\frac{\beta}{\pi k E_C}} e^{-\beta \frac{\left(E - \frac{1}{4} k E_C\right)^2}{k E_C}} \ , \tag{6.19}$$

$$k = \begin{cases} 1 & \text{for quasi-particle tunnelling} \\ 4 & \text{for Cooper pair tunnelling} \end{cases} \ . \tag{6.20}$$

Using the standard relation between Josephson coupling energy and normal resistance [107],

$$E_J = \frac{\hbar}{2eR_T} \frac{\pi\Delta}{2e} \tanh\left(\Delta\beta\right) \ , \tag{6.21}$$

the simulations in Ref.[15] could reproduce several characteristic features of the transport regime of Josephson junction arrays.

At low applied bias voltages the simulations in Ref.[15] show insulating behaviour. With increasing bias voltage the Josephson junction array starts to conduct current above a certain threshold voltage and after a transition region the current increases linearly with the applied voltage. Although the model of Ref.[15] includes incoherent Cooper pair and quasi-particle tunnelling and only the incoherent Cooper pair tunnelling rate is proportional to E_J^2, the initial transport regime is controlled by Cooper pair tunnelling and the current is also proportional to the squared Josephson coupling energy.

The simulations that show good qualitative agreement with experimentally known behaviour [14] rely on the applicability of $P(E)$-theory. Especially the E_J^2-dependence is a direct consequence of the perturbative nature of the tunnelling matrix element in $P(E)$-theory. On the other hand it is known that the qualitative transport behaviour of Josephson junction arrays holds up to values of the Josephson coupling energy that are comparable to the Josephson charging energy $E_J \approx E_C$ [14]. This concludes the summary of the results of the numerical simulations from Ref.[15]. The success of these simulations in reproducing experimentally observed features of the transport regime serves as our motivation to investigate the validity of the $P(E)$ approach in a simplified model by comparing it to Bloch-Redfield theory in the next section.

6.2 Coherent transport

In this section we are using Bloch-Redfield theory to simulate the coherent and incoherent charge transport through a simplified model of a Josephson junction array and compare it to the purely incoherent transport obtained from $P(E)$-theory.

To see the importance of the coherent processes that are omitted in $P(E)$-theory let us first consider the simplest possible example, a two level system, for example two charging sites, that is longitudinally coupled to a bath,

$$H = H_S + H_{SB} + H_B \tag{6.22}$$

$$= \begin{pmatrix} \frac{1}{2}E_C & E_J \\ E_J & -\frac{1}{2}E_C \end{pmatrix} \otimes \mathbb{1} + g \begin{pmatrix} 1 & 0 \\ 0 & -1 \end{pmatrix} \otimes X + \begin{pmatrix} 1 & 0 \\ 0 & 1 \end{pmatrix} \otimes H_B \ , \tag{6.23}$$

where X is the bath coupling operator and H_B is the bath Hamiltonian. As usual in Bloch-Redfield theory all relevant information about the environment is contained in the spectral function of the bath coupling operator $C_{XX}(\omega)$.

The rate of charge tunnelling is determined by the relaxation rate of the system which can be obtained from the Bloch-Redfield equation as discussed in Ch.4. The dephasing and decoherence rates in the Bloch-Redfield equation are determined by the system coupling operator σ_z rotated into the energy eigenbasis. We call this operator in the eigenbasis ξ. To obtain ξ we first diagonalize the system Hamiltonian,

$$U^\dagger \begin{pmatrix} \frac{1}{2}E_C & E_J \\ E_J & -\frac{1}{2}E_C \end{pmatrix} U = \sqrt{\frac{E_C^2}{4} + E_J^2} \begin{pmatrix} 1 & 0 \\ 0 & -1 \end{pmatrix} \ , \tag{6.24}$$

$$U = \begin{pmatrix} \cos(\frac{1}{2}\theta) & \sin(\frac{1}{2}\theta) \\ -\sin(\frac{1}{2}\theta) & \cos(\frac{1}{2}\theta) \end{pmatrix} \ , \tag{6.25}$$

$$\tan(\theta) = 2\frac{E_J}{E_C} \ , \tag{6.26}$$

and then rotate the original system coupling operator,

$$\xi = U^\dagger \begin{pmatrix} 1 & 0 \\ 0 & -1 \end{pmatrix} U = \begin{pmatrix} \cos(\theta) & \sin(\theta) \\ \sin(\theta) & \cos(\theta) \end{pmatrix} \ . \tag{6.27}$$

The relaxation rate $\Gamma_{\rm rel}$ of the system is proportional to the square of the off-diagonal matrix element of ξ times the spectral function evaluated at the transition frequency ΔE. The transition frequency corresponds to the energy difference between the two energy eigenstates,

$$\Gamma_{\rm rel} \propto \sin^2(\theta) C_{XX}(\Delta E) \ , \tag{6.28}$$

$$\Delta E = \sqrt{\frac{E_C^2}{4} + E_J^2} \ . \tag{6.29}$$

For the detailed discussion see Ch.4.

Of course the two-dimensional matrix H_S can be diagonalized directly. Here however we deliberately use time-independent perturbation theory to compare the problem with the perturbative $P(E)$-theory. In the case that the charging energy is much larger than the coupling energy $E_J \ll E_C$, the unitary matrix U is approximately given by the identity matrix with corrections of the order of E_J/E_C,

$$U = \mathbb{1} + \mathcal{O}\left(\frac{E_J}{E_C}\right) \ , \tag{6.30}$$

$$\sin(\frac{1}{2}\theta) = 0 + \mathcal{O}\left(\frac{E_J}{E_C}\right) \ . \tag{6.31}$$

The eigenstates are approximately given by the original charge states and the eigenenergies by,

$$E_{1/2} = \pm\frac{1}{2}E_C + \mathcal{O}\left(\frac{E_J}{E_C}\right) , \tag{6.32}$$

$$C_{XX}(\Delta E) \approx C_{XX}(E_C) . \tag{6.33}$$

The physical process of energy relaxation can be approximated by incoherent tunnelling processes between the two original charge states. The weight given by the spectral function at the transition frequencies is independent from E_J. The coupling energy E_J enters the relaxation rate Γ_{rel} only via the off-diagonal elements of ξ. The relaxation rate is in leading order proportional to E_J^2,

$$\Gamma_{\text{rel}} \propto \sin^2(\theta) \propto \left(\frac{E_J}{E_C}\right)^2 + \mathcal{O}\left(\frac{E_J^3}{E_C^3}\right) . \tag{6.34}$$

In the small E_J-regime Bloch-Redfield theory gives us the same picture and the same result as $P(E)$-theory.

Considering the other extreme case of vanishing charging energy,

$$E_C = 0 , \tag{6.35}$$

$$H = \begin{pmatrix} 0 & E_J \\ E_J & 0 \end{pmatrix} \otimes \mathbb{1} + g \begin{pmatrix} 1 & 0 \\ 0 & -1 \end{pmatrix} \otimes X + \begin{pmatrix} 1 & 0 \\ 0 & 1 \end{pmatrix} \otimes H_B , \tag{6.36}$$

one can immediately see that the picture of tunnelling charges in the original basis is not applicable. The eigenbasis of the system is given by the symmetric and antisymmetric delocalised states,

$$U = \frac{1}{\sqrt{2}} \begin{pmatrix} 1 & 1 \\ 1 & -1 \end{pmatrix} , \tag{6.37}$$

and relaxation can not be regarded as a charge hopping from the first to the second site or back. In this extreme case the off-diagonal matrix elements of ξ are independent from E_J and the coupling energy enters the relaxation rate solely via the spectral function

$$\Gamma_{\text{rel}} \propto C_{XX}(2E_J) . \tag{6.38}$$

For an Ohmic spectral function one would for example expect the dissipation to be proportional to E_J and not E_J^2.

The same trade-off between the Josephson coupling energy and the energy differences between neighbouring islands determines the range of validity of $P(E)$-theory in Josephson junction arrays. To investigate further we study the behaviour of a simplified model of an inner section of a Josephson junction array.

6.2.1 The model

In the simplified model we consider an inner section of the Josephson junction array. The section has $N = 20$ sites. As we are mostly interested in the relative importance of coherent and incoherent Cooper pair tunnelling we neglect the contribution of quasi-particles and only take Cooper pairs and anti-Cooper pairs into account.

In this chapter we do not want to consider the problem of charge injection from the leads into the array, as it was done in Ch.3 and Ref.[3]. We always take the initial state to correspond to one excess Cooper pair at the left end of the simulated section of the array.

Furthermore we assume that no additional net charges enter the simulated section of the array from the surrounding parts of the Josephson junction array.

The only way to create additional charge carriers in the simulated section of the array is the creation of Cooper pair/anti-Cooper pair dipoles. We will only include the dipole excitations around a single Cooper pair in the array that are energetically closest to the bare Cooper pair state. In the eigenbasis of the Josephson junction array the mixing between charging states due to the coherent Cooper pair tunnelling amplitude E_J increases with decreasing energy difference. The energetically closest dipole states contribute the leading corrections to the transport properties of a Cooper pair. The dipoles dress the bare Cooper pair. To take into account the relevant dipole excitations we use a model introduced in Ref.[12]. The dipole excitations around a Cooper pair in the Josephson junction array are mapped to states of a spin-chain.

The charging energy of any Cooper pair configuration in a Josephson junction array is determined by the inverse capacitance matrix of the array, C_m^{-1}. For the purpose of estimating the relevant excitations, the charging energy of a configuration $\{n_i\}$ of Cooper pairs can be approximately obtained from an exponentially decaying interaction,

$$E^c(\{n_i\}) = \sum_{ij} \frac{(2e)^2}{2} n_i \left(C_m^{-1}\right)_{ij} n_j \approx \sum_{ij} \frac{1}{2} \Lambda E_C n_i n_j e^{-\frac{|i-j|}{\Lambda}} \ , \tag{6.39}$$

where it was assumed that all charges are far enough from the ends of the array so that all boundary effects can be neglected. The approximate charging energies of a single Cooper pair E^c_{cp} and a single dipole on neighbouring islands E^c_{dp} are given by,

$$E^c_{cp} \approx \frac{1}{2} \Lambda E_C \ , \tag{6.40}$$

$$E^c_{dp} = E^c(\{\dots n_i = \pm 1, n_{i+1} = \mp 1, \dots\}) \approx \Lambda E_C \left(1 - e^{-\frac{1}{\Lambda}}\right) \approx E_C \ . \tag{6.41}$$

When placing an additional dipole in the array far away from the single Cooper pair the exponentially decaying interaction can be neglected and the energy difference to the bare Cooper pair state is simply given by E^c_{dp}. If we on the other hand place a dipole next to a single Cooper pair in the array, so that positive and negative charges alternate, the energy difference between bare and dressed state is given by,

$$\begin{aligned} \Delta E_{dp} &= E^c(\{\dots n_i = 1, n_{i+1} = -1, n_{i+2} = 1 \dots\}) - E^c_{cp} \\ &\approx \Lambda E_C \left(1 - 2e^{-\frac{1}{\Lambda}} + e^{-\frac{2}{\Lambda}}\right) \\ &\approx \frac{2}{\Lambda} E_C \ , \end{aligned} \tag{6.42}$$

and inverting the orientation of the dipole leads to an energy difference of

$$E^c(\{\dots n_i = 1, n_{i+1} = 1, n_{i+2} = -1 \dots\}) - E^c_{cp} \approx \Lambda E_C \left(1 - e^{-\frac{2}{\Lambda}}\right) \tag{6.43}$$

$$\approx 2E_C \ . \tag{6.44}$$

In the most relevant dressed states the dipoles are located in the vicinity of the bare Cooper pair, where the exponentially decaying interaction is relevant. The length-scale of this environment is given by Λ. The dipoles are oriented so that Cooper pairs and anti-Cooper pairs alternate when going along the Josephson junction array.

The alternating charge states of an N-site section of an array can be mapped to the states of a $N+1$-site spin chain [12]. The empty section is either mapped to the state with

all spins up or to the state with all spins down. A spin flip from $|\downarrow\rangle_i$ to $|\uparrow\rangle_{i+1}$ between neighbouring sites is mapped to a Cooper pair on site i, $|n_i = +1\rangle$, the opposite flip from $|\uparrow\rangle_i$ to $|\downarrow\rangle_{i+1}$ is mapped to an anti-Cooper pair $|n_i = -1\rangle$. As a positive charge in the alternating states is always followed by a negative charge an up-flip in the spin-chain is always followed by a down-flip. In the mapping the Hilbert-space of a spin-chain is never left by two or more consecutive up-flips. An example of the mapping is shown in Fig.6.4.

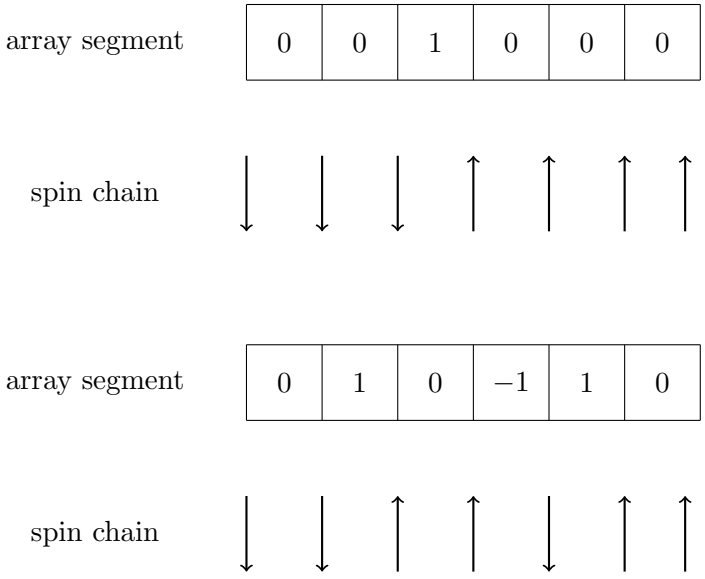

Figure 6.4: Two examples of the mapping from dressed Cooper pair states in a section of an array to states of a spin chain [12]. A positive charge is mapped to an upwards spin-flip between neighbouring sites, a negative charge is mapped to a downwards spin-flip. In alternating charge configurations an upwards spin-flip is always followed by a downwards spin-flip.

In our simplified model we use the spin-chain representation to take all dipole excitations into account that are within L_{dip} sites of the bare Cooper pair. In the numerical simulations we use different dipole lengths L_{dip} to investigate how the transport behaviour changes when including dressed states with higher charging energy. The case $L_{dip} = 0$ corresponds to a single bare Cooper pair propagating through the 20-site Josephson junction array. We also consider $L_{dip} = \Lambda - 1$, $L_{dip} = \Lambda$ and $L_{dip} = \Lambda + 1$ for an interaction length of $\Lambda = 3$.

To avoid complications from the interactions with the finite array boundaries, we assume that the simulated section is in the middle of the array, far away from the boundaries. Numerically this is achieved by calculating all charging energies from the inverse capacitance matrix of C_m^{-1} of an array with $N + 8\Lambda$ sites,

$$E^c(\{n_i\}) = \sum_{ij} \frac{(2e)^2}{2} \bar{n}_i \left(C_m^{-1}\right)_{ij} \bar{n}_j \ , \tag{6.45}$$

$$\bar{n}_i = \begin{cases} 0 & i \leq 4\Lambda \\ n_i & 4\Lambda < i \leq 4\Lambda + N \\ 0 & 4\Lambda + N < i \end{cases} \ . \tag{6.46}$$

Empty charge arrays with length 4Λ are amended on both sites of the charge configuration $\{n_i\}$ of the section of the array we are simulating. Due to the large distance, the interaction of charges in the inner section with the boundaries is negligible.

The voltage is applied homogeneously along the array with a voltage V_h across each Josephson junction. The applied voltage can be included as a shift of the energy in the charge

basis,

$$E^V(\{n_i\}) = \sum_j (2e) V_h \cdot j \cdot n_j \ . \tag{6.47}$$

The simplified model is a good approximation for a section of a ring-shaped Josephson junction array. A Josephson junction ring is not connected to external leads. The net charge in the array does not change with time, allowing for exactly one excess Cooper pair in the ring. In such a ring the voltage would be applied inductively by a constantly changing magnetic flux through the ring (as proposed in [35]). The voltage drops homogeneously over the whole array. In an open Josephson junction array the applied voltage can not be separated from the interaction with the boundaries and the injection of charge carriers. A boundary-applied voltage injects charge carriers into the first array site. The additional charge at the end of the array repels charge carriers further inside the array. The charge carriers are pushed further and further inside the array effectively spreading the applied voltage along the array.

In the kinetic Monte Carlo simulations [15] the distribution of charge carriers in the transport regime leads to a redistribution of the applied voltage along the array. The effective voltage drops approximately linearly over the Josephson junction array. One can therefore argue that in the transport regime the average effect of the interaction of one dressed Cooper pair with the other charges can be approximated by a homogeneous voltage drop.

We assume that the superconducting islands in the Josephson junction array couple to Ohmic noise baths via coupling operators that are diagonal in the charge basis. Each capacitance C_0 in the Josephson junction array is connected to the ground via a resistance R. The resistance is a source of Ohmic voltage noise δV. For a sketch see Fig.6.5. Considering a single island of the Josephson junction array, this noise model is the same as introduced in Ref.[108] for the voltage noise in a Josephson charge qubit.

In the system bath model, the system Hamiltonian H_S contains all charging energy and coherent tunnelling terms. The system bath coupling operator is diagonal in the charge basis,

$$H = H_S + \sum_i n_i X_i + H_B \ . \tag{6.48}$$

All superconducting islands are coupled to independent baths that are not correlated. The spectral function of two bath coupling operators from the same island i has the standard Ohmic form,

$$C_{ii}(\omega) = 4\alpha \ \omega \ \Theta(\omega_c - \omega) \ \frac{1}{e^{-\beta\omega} + 1} \ , \tag{6.49}$$

where α is the Ohmic bath coupling strength . We assume that the cut off frequency ω_c of the spectral function is large enough, so that all relevant energies of the system are smaller and it does not affect the time evolution of the system. We consider a low temperature limit where the spectral function is approximately zero for negative energies and linear for positive frequencies,

$$C_{ii}(\omega) \approx \begin{cases} 4\alpha \ \omega \ \Theta(\omega_c - \omega) & \omega \geq 0 \\ 0 & \omega < 0 \end{cases} \tag{6.50}$$

Our model, as shown in Fig.6.5, corresponds to a junction shunted by an impedance dominated by the large resistance R. The $P(E)$-function for such a model can be found in the Literature, for example in Ref.[38] At small positive energies E the $P(E)$-function

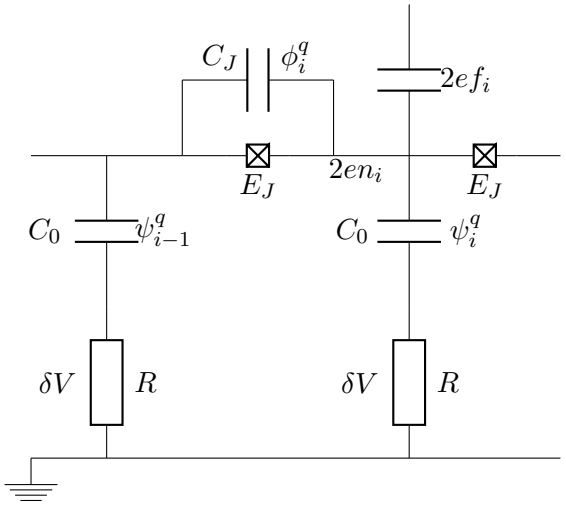

Figure 6.5: A sketch of a section of an array with the noise sources of the simplified model. The resistances R that connect the capacitances C_0 to the ground introduce voltage noise δV into the Josephson junction array. The noise couples via the charging energy of the capacitances C_0 longitudinally to the Cooper pair occupation of each superconducting island. The spectral function of the resistive noise source is assumed to be determined by the standard Ohmic spectral density $J(\omega)$ (Eq.6.49).

follows a power law with an exponent that is determined by the system-bath coupling strength α,

$$P(E) \propto E^{2\alpha-1} \ . \tag{6.51}$$

More precisely for positive energies we use the expression from Ref.[38],

$$P(E) = \frac{e^{-2\gamma\alpha}}{\Gamma(2\alpha)} \frac{1}{E} \left[\pi\alpha \frac{E}{E_c}\right]^{2\alpha} \ , \tag{6.52}$$

where γ is Euler's constant and Γ is the gamma-function. The $P(E)$-function for negative frequencies is obtained from detailed balance,

$$P(-E) = e^{-\beta E} P(E) \ . \tag{6.53}$$

With this $P(E)$-function the time evolution of the system density matrix ρ in the charge basis is given by,

$$\rho_{ij} = 0 \qquad \text{for } i \neq j \ , \tag{6.54}$$

$$\dot{\rho}_{ii}(t) = \sum_j -E_J^2 P(E_i^c - E_j^c)\rho_{ii}(t) + E_J^2 P(E_j^c - E_i^c)\rho_{jj}(t) \ . \tag{6.55}$$

The off-diagonal elements of the density matrix are zero since we only consider the incoherent time-evolution in the $P(E)$ simulation.

6.2.2 Numerical simulations

The time-evolution of the density matrix of the section of the array is simulated in the Bloch-Redfield approach and the $P(E)$-theory. We use different basis sets that include increasing numbers of dipole dressed Cooper pair states. The dressed states we consider

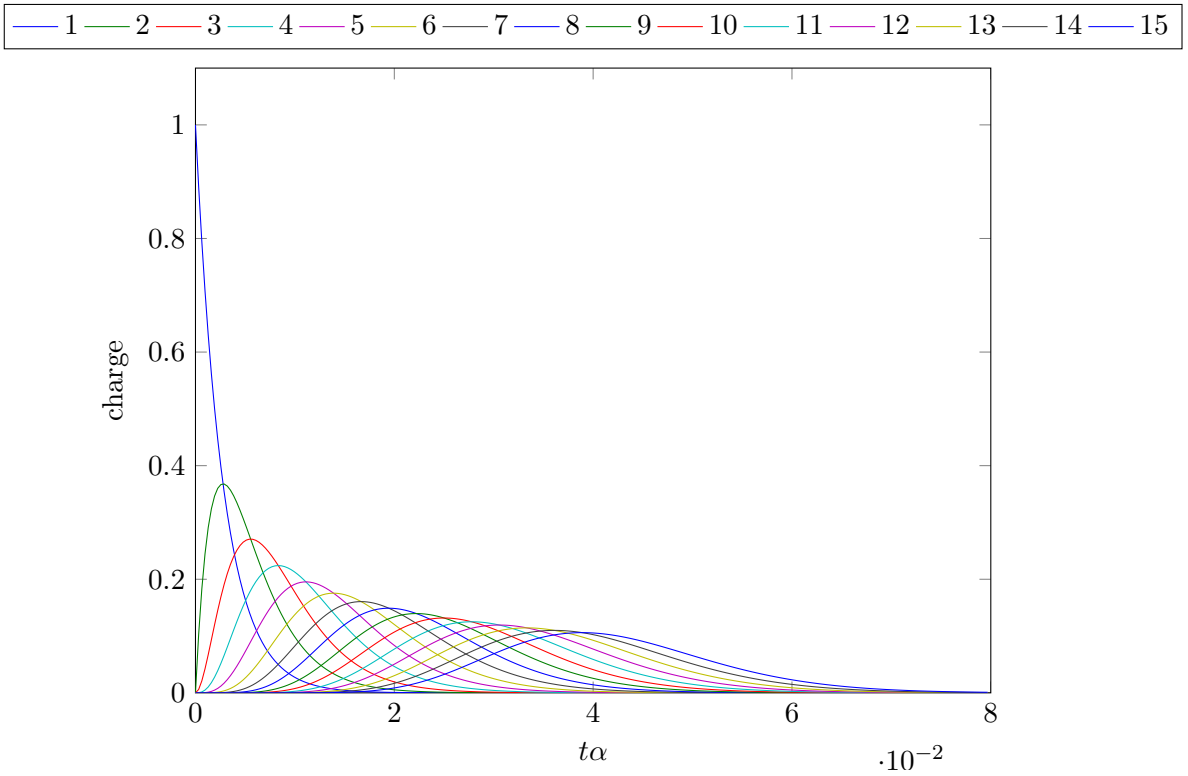

Figure 6.6: The expectation value of the charge on the array sites in a $P(E)$ simulation plotted against simulation time t times the system-bath coupling strength α. For better visibility only the charge on the first 10 sites is plotted. The simulation includes charge states with dipoles on the $L_{dip} = \Lambda$ sites around the excess Cooper pair. The applied voltage is $V_h = \frac{1}{8}\frac{E_C}{e}$. The positive charge located on the first site at $t = 0$ spreads over several neighbouring sites. At the same time the center of the broadening charge distribution propagates slowly along the array.

contain dipoles on the $L_{dip} \in \{0, \Lambda - 1, \Lambda, \Lambda + 1\}$ sites around the bare Cooper pairs. In all simulations we set the interaction length Λ and the system-bath coupling strength to,

$$\Lambda = 3 \ , \tag{6.56}$$

$$\alpha = 0.025 E_C \ , \tag{6.57}$$

$$E_C = 32\mu\text{eV} \ . \tag{6.58}$$

We are in the low temperature limit,

$$\beta = \frac{1}{k_B T} = 100\,(\mu\text{eV})^{-1} \ , \tag{6.59}$$

$$e^{-\beta E_c} \approx 0 \ . \tag{6.60}$$

From the numerical simulations we obtain the expectation value $2en_i$ of the charge on the i-th island of the array,

$$n_i(t) = \langle \hat{n}_i(t) \rangle = \text{Tr}\left(2e\hat{n}_i \rho(t)\right) \ , \tag{6.61}$$

where $\rho(t)$ is the time-dependent density matrix obtained from solving the Bloch-Redfield equation or from the rate equation of the $P(E)$ approach (Eq.6.55). An example of the charge distribution $\{2en_i\}$ is given in Fig.6.6. The $2e$-charge is located on the first site at $t = 0$ and is propagated along the array over time while spreading over several sites.

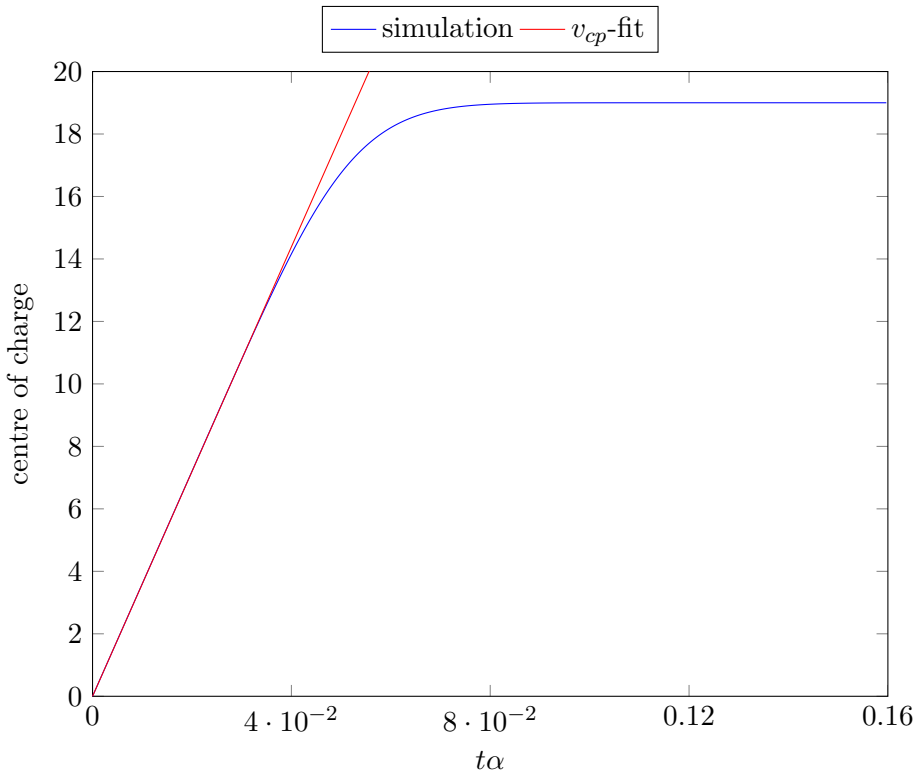

Figure 6.7: Averaging over the charge distribution (compare Fig.6.6) we obtain the centre of charge, the mean location of the excess Cooper pair in the array. The same simulation parameters as in Fig.6.6 were used. The centre of charge increases linearly with time and saturates once the dressed Cooper pair reaches the end of the finite array. We define the Cooper pair transport velocity v_{cp} as the slope of the linear increase of the center of charge.

To characterize the transport of the excess Cooper pair we define the center of charge x_{cc},

$$x_{cc}(t) = \sum_j j \; n_j(t) \; . \tag{6.62}$$

An example of the time-evolution of the center of charge is plotted in Fig.6.7. The center of charge increases linearly with time until it reaches the end of the finite array. Depending on the parameter regime and whether we use a Bloch-Redfield simulation or a $P(E)$ simulation the region of linear increase can be preceded by coherent oscillations of the centre of charge.

We use the region of linear transport to define the Cooper pair velocity v_{cp}, a measure of the transport properties of the system,

$$x_{cc}(t) = v_{cp} t + \eta \; , \tag{6.63}$$

where η is an offset due to nonlinear behaviour at the beginning of the time-evolution. For each transport simulation v_{cp} is obtained by fitting a linear function to the region of linear increase. We now look at the E_J and V_h-dependence of v_{cp} to compare the different array models with $L_{dip} \in \{0, \Lambda - 1, \Lambda, \Lambda + 1\}$ and the Bloch-Redfield and $P(E)$ approaches.

Low Voltages

First we consider low applied voltages, $2eV_h < E_C$. For the $P(E)$ simulations the Josephson energy dependence of v_{cp} at fixed voltages (as shown in Fig.6.8, Fig.6.9 and Fig.6.10)

can be directly obtained from Eq.6.55. All tunnelling rates are proportional to the squared Josephson energy. Changing the Josephson energy speeds up all processes in the $P(E)$ simulation by a factor of E_J^2. The Cooper pair velocity is proportional to E_J^2.

The effect of including additional dipole states ($L_{dip} = \Lambda - 1$, $L_{dip} = \Lambda$, $L_{dip} = \Lambda + 1$) in the simulations compared to the bare Cooper pair states $L_{dip} = 0$ depends on the relative strength of homogeneous voltage V_h and the energy required to create a dipole next to the bare Cooper pair ΔE_{cp}. When the additional dipole energy exceeds the energy gained by a Cooper pair tunnelling to an island with lower potential,

$$\Delta E_{dp} > 2eV_h \ , \tag{6.64}$$

the creation of dipoles in the array is thermally suppressed. Since we are in the zero temperature limit, no dipole states can be created by incoherent tunnelling. Including additional dipole dressed states in the simulation has no effect on the transport properties as these states are never populated. The Cooper pair velocity of all simulations including dressed states ($L_{dip} > 0$) is the same as for $L_{dip} = 0$. This can be seen in Fig.6.8 for $L_{dip} = \Lambda - 1$ and $L_{dip} = \Lambda$ and in Fig.6.12 for $L_{dip} = \Lambda + 1$. Due to the large number of basis states (512) all simulations for $L_{dip} = \Lambda + 1$ were calculated with the stochastic Bloch-Redfield algorithm (Ch.4).

In the other case,

$$\Delta E_{dp} < 2eV_h \ , \tag{6.65}$$

the applied voltage is large enough to create dipoles next to the bare Cooper pair. Increasing the number of allowed dipole states with L_{dip} also increases the phase space available for incoherent tunnelling. The Cooper pair velocity v_{cp} increases with increasing L_{dip}. This situation is shown in Fig.6.10.
Calculating the Cooper pair velocity as a function of the applied voltage V_h with fixed E_J (see Fig.6.13) one can see the transition from the first to the second regime at $V_h = 0.25\frac{E_C}{e}$.

The power law of the voltage dependence of the Cooper pair velocity for the bare Cooper pair states ($L_{dip} = 0$) can be directly obtained from the power law of the $P(E)$-function, Eq.6.51. In the absence of dipole dressed states all basis states have the same charging energy. The energy difference between the charge states is simply given by the homogeneously applied voltage. The incoherent tunnelling rates between neighbouring islands i and $i + 1$ are,

$$\Gamma_{i \to i+1} = E_J^2 P(2eV_h) \ , \tag{6.66}$$

$$\Gamma_{i+1 \to i} = E_J^2 P(-2eV_h) = 0 \ . \tag{6.67}$$

The Cooper pair velocity is proportional to the incoherent tunnelling rates. At fixed E_J v_{cp} has the same functional form as the $P(E)$ function.

To determine whether the use of $P(E)$-theory is a valid approach we compare the results with the Bloch-Redfield simulations in Fig.6.8, Fig.6.9, Fig.6.11 and Fig.6.12. At small voltages the results of the two methods do not agree. If we take for example the E_J-dependence of the Bloch-Redfield simulations for $L_{dip} = 0$, v_{cp} increases linearly with the Josephson coupling energy and not quadratically as in the $P(E)$-theory.

The reason behind the discrepancy is simple. We are considering an inner section of the array far away from all boundaries. The charging energy of a bare excess Cooper pair is the same for each island of the array. In the considered $N = 20$-site section of the array, we find a twentyfold degeneracy of the charging energy of the bare Cooper pair states. The energy difference between the bare Cooper pair states is completely determined by the

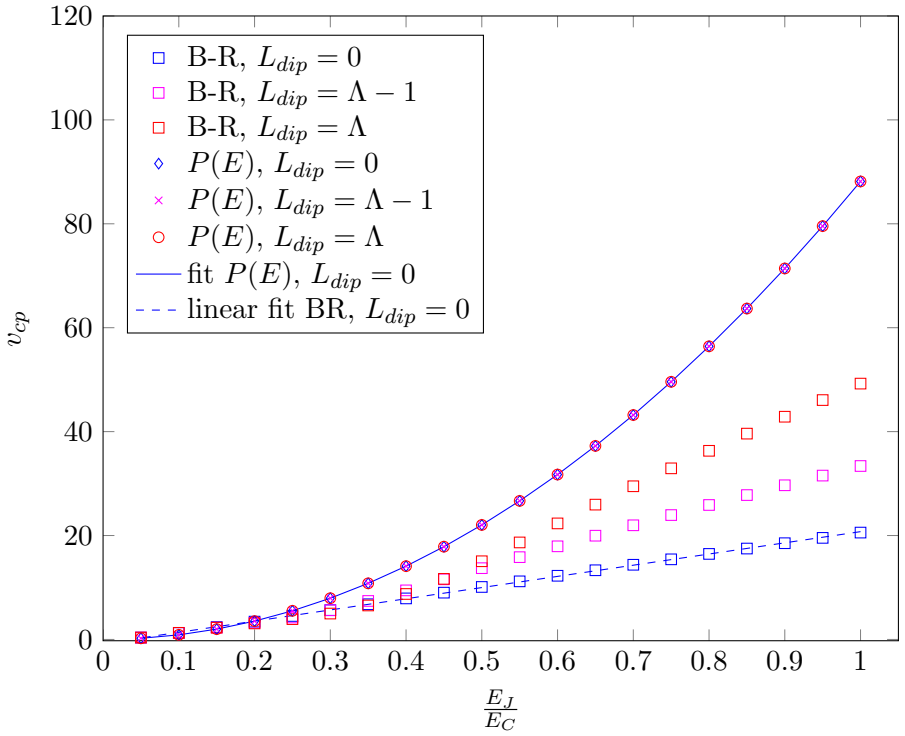

Figure 6.8: The Cooper pair velocity v_{cp} as a function of the Josephson energy E_J for a homogeneous voltage $V_h = \frac{1}{32}\frac{E_C}{e}$. The Cooper pair transport was simulated with $P(E)$ and Bloch-Redfield theory for a charge basis that included dressed Cooper pair states with dipoles on the L_{dip} sites surrounding the Cooper pair. The solid blue line labeled as "fit $P(E)$, $L_{dip} = 0$ " is obtained from fitting the $P(E)$ result for the undressed Cooper pair basis to the expected $v_{cp} \propto E_J^2$-behaviour. The results of the $P(E)$ simulations of all L_{dip} lie on the same curve.
The Cooper pair velocity obtained from Bloch Redfield theory with $L_{dip} = 0$ increases linearly with the Josephson energy E_J. At E_J smaller than the additional energy of a dipole ΔE_{dp} the results for all simulations with $L_{dip} = 0$, $L_{dip} = \Lambda - 1$ and $L_{dip} = \Lambda$ agree. At larger Josephson energies the Cooper pair velocity v_{cp} does not converge with increasing L_{dip}.

applied voltage V_h. The degeneracy of the N bare Cooper pair states is also present when additionally including dressed Cooper pair states ($L_{dip} \in \{\Lambda - 1, \Lambda, \Lambda + 1\}$). At small voltages, where the electrostatic energy difference is small compared to the Josephson coupling energy,

$$2eV_h < E_J \ , \tag{6.68}$$

the coherent Cooper pair tunnelling can not be regarded as a small perturbation to the eigenenergies of charge states $|\{n_i\}\rangle$. $P(E)$-theory does not give a valid description of the physical system. At higher fixed voltages ($V_h = \frac{1}{8}\frac{E_C}{e}$ Fig.6.9 and $V_h = \frac{1}{4}\frac{E_C}{e}$ Fig.6.11), the Cooper pair velocity v_{cp} obtained from Bloch-Redfield simulations is proportional to E_J^2 at small E_J and approximately agrees with the $P(E)$ result. Only at larger E_J we find a transition to linear E_J dependence and a breakdown of the perturbation theory in E_J.

The same effect can be seen in Fig.6.14 when comparing the voltage dependence of v_{cp} obtained from $P(E)$ and Bloch-Redfield theory. At low applied voltages the perturbation theory in the Josephson coupling energy is not valid and Bloch-Redfield theory and $P(E)$-

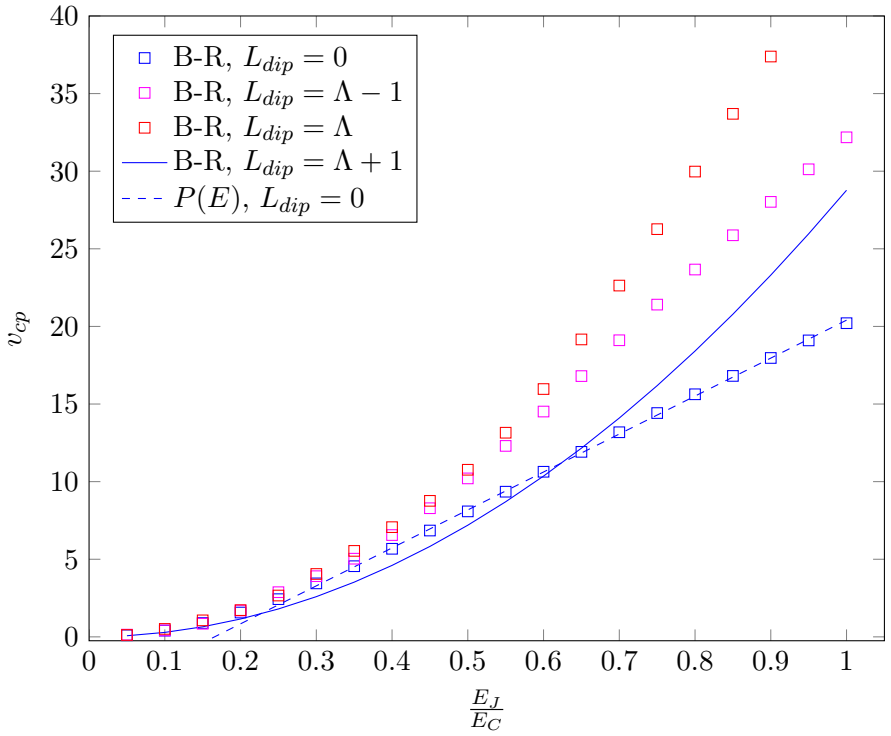

Figure 6.9: The Cooper pair velocity v_{cp} as a function of the Josephson energy E_J for a homogeneous voltage $V_h = \frac{1}{8}\frac{E_C}{e}$. The $P(E)$ results for all $L_{dip} \in \{0, \Lambda - 1, \Lambda\}$ lie on the same curve. For simplicity we only plot the fit of the $P(E)$ results to the expected E_J^2 behaviour. At small E_J the energy difference between states connected by coherent tunnelling is larger than the Josephson coupling energy $\Delta E = 2eV_h > E_J$. The coherent tunnelling can be treated perturbatively and the $P(E)$ and Bloch-Redfield result agree. At larger Josephson energy the coherent tunnelling can not be treated perturbatively and the velocity v_{cp} as a function of E_J changes from a quadratic to a linear dependence.

theory give completely different v_{cp}. With increasing V_h, approaching the limit,

$$2eV_h = E_J \ , \tag{6.69}$$

the Bloch-Redfield results converge towards the $P(E)$ results. The two curves for $L_{dip} = \Lambda + 1$ have not yet converged in this limit but converge at higher voltages as shown in Fig.6.16.

When the Josephson coupling energy is considerably smaller than the additional energy of a dipole,

$$E_J < \Delta E_{dp} \ , \tag{6.70}$$

the coherent tunnelling amplitude is too small to cause significant mixing between the initial bare state and the dipole dressed states that are included for $L_{dip} \in \{\Lambda-1, \Lambda, \Lambda+1\}$. The results of all Bloch-Redfield simulations with different dipole lengths L_{dip} agree. At Josephson energies larger that ΔE_{dp} the mixing with the dressed states leads to a faster conductance and higher v_{cp} for $L_{dip} \geq \Lambda - 1$. This can be nicely seen in Fig.6.8 and Fig.6.9 where the results of the three Bloch-Redfield simulations start to deviate at $E_J = 0.3E_C$.

The last point we want to make considering the Bloch-Redfield simulations at low applied voltages V_h concerns the validity of the reduced basis sets we choose for our simplified

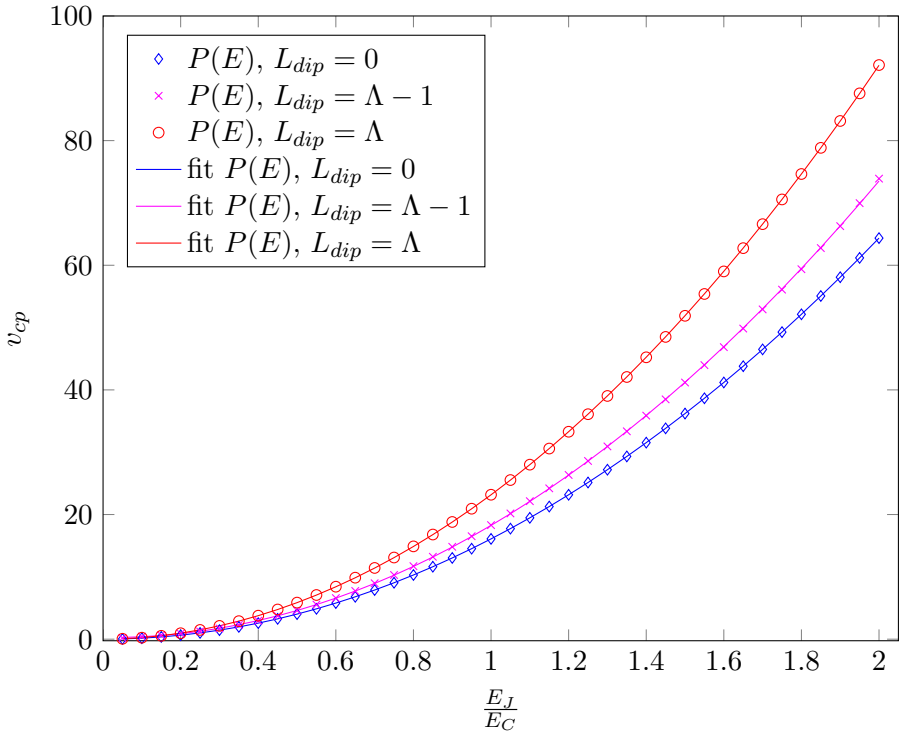

Figure 6.10: The Cooper pair velocity v_{cp} as a function of the Josephson energy E_J for a homogeneous voltage $V_h = \frac{1}{4}\frac{E_C}{e}$ obtained solely from $P(E)$ simulations. The applied homogeneous voltage is high enough to allow for the creation of dipoles by incoherent tunnelling. We obtain different transport velocities for $L_{dip} = 0$, $L_{dip} = \Lambda - 1$ and $L_{dip} = \Lambda$ in the $P(E)$ simulations. For each of the three basis sets, the Josephson energy dependence of the velocity fits the behaviour $v_{cp} \propto E_j^2$ expected from the E_J dependence of the $P(E)$ tunnelling rates (Eq.6.13).

model. In the limit $E_J \to E_C$ the Josephson energy approaches the charging energy of an isolated dipole E_{dp}^c. The coherent tunnelling amplitude is large enough to create dipoles at arbitrary distances from the bare Cooper pair in the array. Using a basis with finite L_{dip} is not justified for $E_J \geq E_C$. This is also the reason why v_{cp} does not converge with increasing number of included dipole states (increasing L_{dip}) at $E_J = E_C$.

High Voltages

Let us now consider high applied voltages,

$$2eV_h > E_C \ . \tag{6.71}$$

Here we face the same problem as for Josephson coupling energies that exceed the charging energy E_C. The applied voltage V_h is high enough to create dipoles at arbitrary distances from the bare Cooper pairs by incoherent tunnelling. A basis with finite L_{dip}, where charge dipoles are only allowed in a certain distance from the bare Cooper pair, can not describe the full transport behaviour of the Josephson junction array.

On the other hand we can regard the simulations as a first approximation of the propagation of one of the many dressed charge carriers in a strongly biased Josephson junction array. This approximation disregards the precise interaction of the simulated dressed Cooper pair with all other Cooper pairs in the array and replaces it with a homogeneously applied voltage.

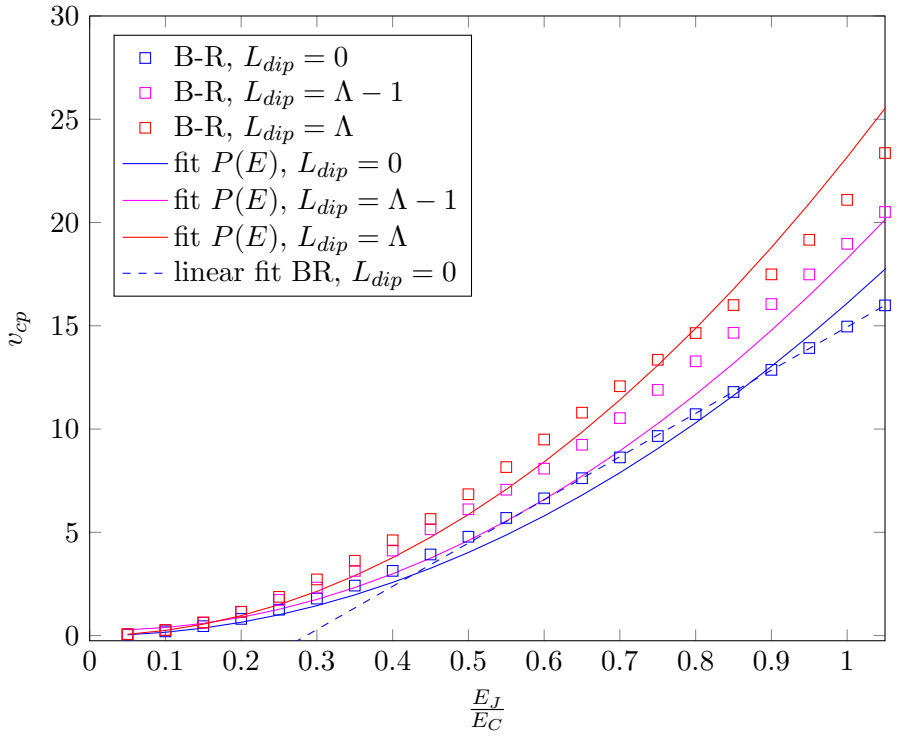

Figure 6.11: The Cooper pair velocity v_{cp} as a function of the Josephson energy E_J for a homogeneous voltage $V_h = \frac{1}{4}\frac{E_C}{e}$, including the results from the Bloch-Redfield simulations. As in Fig.6.9 the Bloch-Redfield results show a E_J^2 behaviour for small E_J and transition to a linear dependence on E_J for larger E_J. Compared to Fig.6.9 the transition happens as higher E_J.

In the high voltage regime the eigenenergies of the charge states are large compared to the typical Josephson coupling energy E_J. The coherent tunnelling can be considered as a small perturbation. The perturbative expansion in the derivation of the $P(E)$-theory is valid. We obtain the Cooper pair velocity obtained from $P(E)$-theory and Bloch-Redfield theory up to large Josephson energies $E_J > E_C$ as is shown in Fig.6.15. Calculating v_{cp} as a function of applied voltage (Fig.6.16) we see that Bloch-Redfield and $P(E)$ results converge with increasing voltage for all dipole lengths L_{dip}. The small deviation between the two methods for $L_{dip} = 0$ and $L_{dip} = \Lambda - 1$ at very high voltages is due to the fact that the expression for $P(E)$, Eq.6.52, only holds for small energy differences.

Conclusion

In conclusion we can state that at low homogeneous voltages it is not sufficient to determine the transport properties from $P(E)$-theory. A full Bloch-Redfield treatment including the coherent tunnelling is necessary. This parameter regime is only relevant for a ring-shaped Josephson junction array. In open Josephson junction arrays the low applied voltages would not be sufficient to overcome the charge injection threshold and bring the system in the conducting regime.

At high applied voltages the dressed Cooper pair basis with finite dipole length L_{dip} is not a good basis of the biased array as the high voltage can create dipole states at every site in the array. When the collective effect of the other charge carriers in the array on a dressed Cooper pair can be approximated as a homogeneous voltage, the $P(E)$-theory gives a valid description of the propagation of the dressed Cooper pair in the high voltage regime. This is the valid regime for the transport in open Josephson junction arrays, as the applied

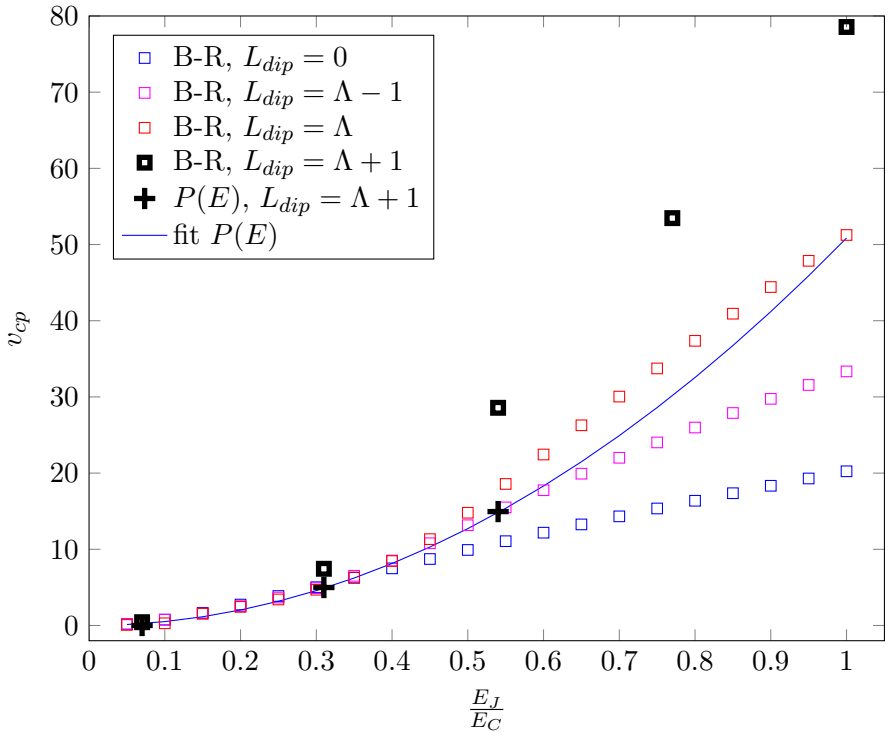

Figure 6.12: The Cooper pair velocity v_{cp} as a function of the Josephson energy E_J for a homogeneous voltage $V_h = \frac{1}{16}\frac{E_C}{e}$. Here we show simulations with the larger basis set that includes dressed states with dipoles on $L_{dip} = \Lambda+1$ sites around the bare Cooper pair. The time evolution of the system with the large charge basis was simulated with the stochastic Bloch Redfield algorithm (Ch.4). As for $L_{dip} = \Lambda - 1$ and $L_{dip} = \Lambda$ the $P(E)$ result for $L_{dip} = \Lambda + 1$ is the same as for bare Cooper pairs ($L_{dip} = 0$), since the creation of Cooper pairs by incoherent tunnelling is energetically impossible.

bias voltages are of order of $N\frac{E_C}{e}$ or larger. A full simulation of the transport properties can then be obtained with the help of the kinetic Monte Carlo algorithm that includes all possible charge states. The KMC method is self consistent when the dissipated energy ΔE at all incoherent tunnelling events is larger than the Josephson coupling energy.

Finally we can see that the E_J^2 dependence of the transport current seen in experiments is not an universal feature but emerges in certain parameter regimes. The same is true for the nearly Ohmic IV-behaviour seen in experiments on open Josephson junction arrays. Although we explicitly assume an Ohmic noise source the transport velocity of a single dressed Cooper pair decreases with applied voltage. The linear increase in current with voltage is a many body effect.

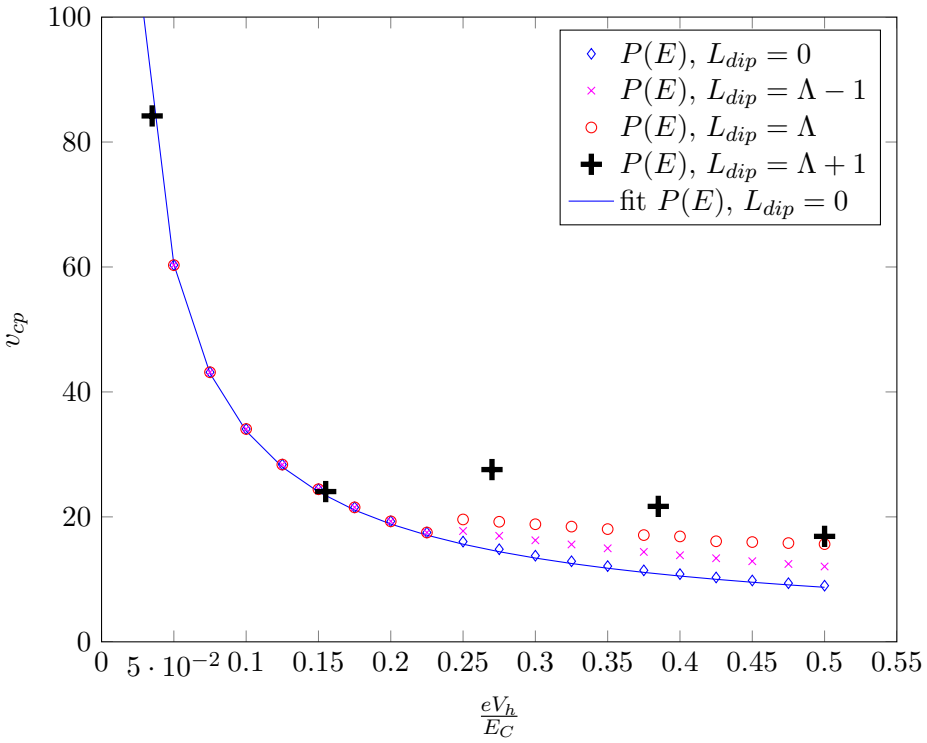

Figure 6.13: The Cooper pair velocity v_{cp} as a function of applied voltage in the low voltage regime. The Josephson coupling energy is equal to the charging energy $E_J = E_C$. For better visibility only the results of the $P(E)$ simulations are shown. The voltage dependence in the case that only bare Cooper pair states are considered $L_{dip} = 0$ follows the power law expected for the $P(E)$ function (Eq.6.51), $v_{cp} \propto V^{-1+2\alpha}$. For homogeneous voltages below the threshold of the creation of dipoles $\frac{1}{e}\Delta E_{dp}$ the $P(E)$ results for $L_{dip} = 0$, $L_{dip} = \Lambda - 1$, $L_{dip} = \Lambda$ and $L_{dip} = \Lambda + 1$ all follow the same power law. Once the creation of dipoles is energetically possible the phase space available for tunnelling increases and the Cooper pair velocity v_{cp} increases with L_{dip}.

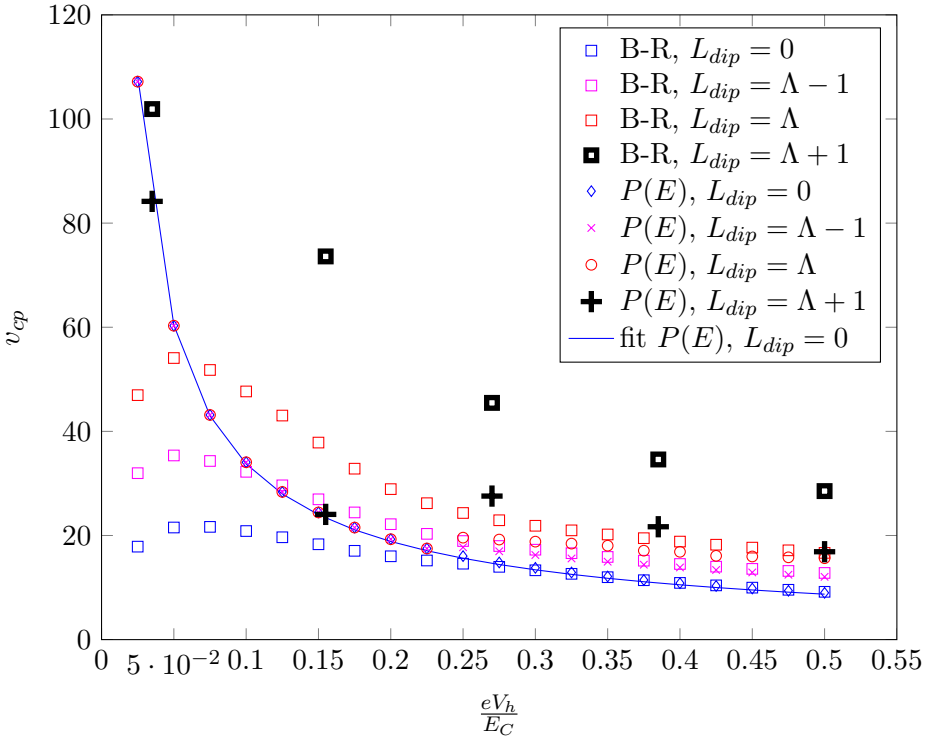

Figure 6.14: The Cooper pair velocity v_{cp} as a function of applied voltage in the low voltage regime. The Josephson coupling energy is equal to the charging energy $E_J = E_C$. Compared to Fig.6.13 we now include the results from the Bloch-Redfield simulations. As expected from Fig.6.8 and Fig.6.9 at low voltages the coherent tunnelling can not be treated as a perturbation and the Bloch-Redfield result deviates significantly from the $P(E)$ result. As V_h approaches $\frac{1}{2}\frac{E_C}{e}$ the energy differences between neighbouring sites $2eV_h$ becomes comparable to the Josephson energy E_J. The velocity v_{cp} obtained from the Bloch-Redfield simulations approaches the result obtained from the perturbative treatment of the coherent tunnelling term in $P(E)$-theory. In the shown voltage range we do not yet see convergence of $P(E)$ and Bloch-Redfield theory for $L_{dip} = \Lambda + 1$. The two results converge at higher voltages shown in Fig.6.16.

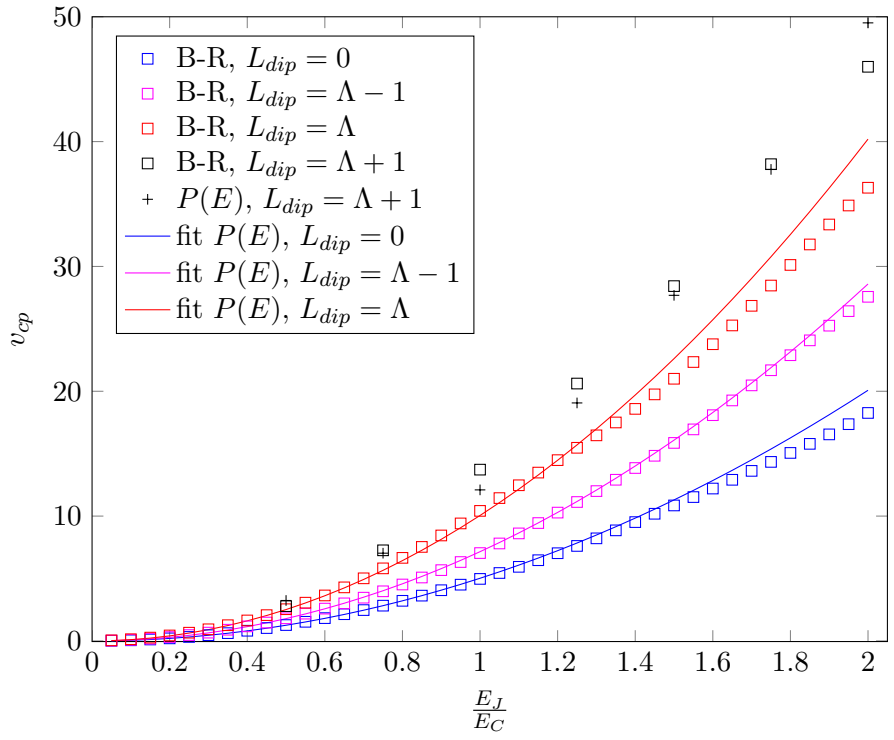

Figure 6.15: The Cooper pair velocity v_{cp} as a function of the Josephson energy E_J for a homogeneous voltage $V_h = \frac{E_C}{e}$. The applied homogeneous voltage V_h is so high that it is energetically possible to create dipole excitations at arbitrary distances from the bare Cooper pair. The dressed Cooper pair basis is not the correct basis to treat transport as it omits charge configurations that can be reached easily by coherent tunnelling. The Cooper pair velocity will not converge for a finite L_{dip}. If we nevertheless restrict ourselves to the dressed state basis the energy differences between charge states are dominated by the energy contribution of the homogeneous voltage V_h. As long as $2eV_h > E_J$, which is the case here, the perturbative treatment of coherent tunnelling in $P(E)$-theory is a good approximation and the Bloch-Redfield and $P(E)$ results approximately agree.

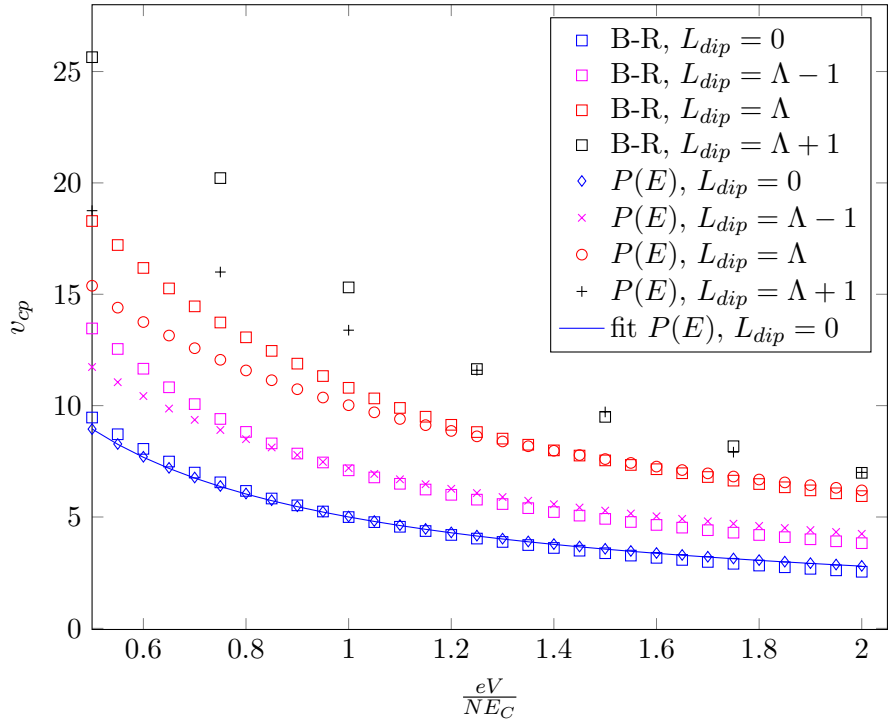

Figure 6.16: The Cooper pair velocity v_{cp} as a function of applied voltage in the high voltage regime. the Josephson coupling energy is equal to the charging energy $E_J = E_C$.

7. Conclusion

The conductance properties of one-dimensional Josephson junction arrays are a current and not yet completely understood problem at the intersection of traditional condensed matter theory and superconducting quantum information systems. This thesis provides three main results concerning the conductance properties of Josephson junction arrays in the insulator phase.

First it shows the connection of Josephson junction arrays with other one dimensional arrays of superconducting circuit elements, quantum phase slip ladders, linear chains of quantum phase slip elements and Josephson junction ladders. The Josephson junction array is dual to the quantum phase slip ladder under the exchange of charge and phase as well as capacitance and inductance. In the low frequency limit the Josephson junction array is approximately equivalent to a linear quantum phase slip chain. The quantum phase slip ladder in the low frequency limit is on the other hand approximately equivalent to a Josephson junction ladder. Finally we find that the Josephson junction ladder and the quantum phase slip chain are again dual systems. The duality and approximate equivalence of the one-dimensional superconducting arrays can in principle be used to study complementing regions of parameter space to achieve a better understanding of the underlying model. One could, for example, study the strongly disordered limit in Josephson junction arrays, which suffer from charge disorder, and the clean case in quantum phase slip ladders.

The second result is the explanation of the onset of transport in boundary biased arrays with the help of depinning theory. We provided analytic estimates of the switching voltage V_{sw} for the two cases of long and short Josephson junction arrays. Numerical simulations showed good overall agreement between the analytic estimate and the numerical data. The biggest deviation was found in the power-law of the switching voltage as a function of the interaction length Λ. The analytic estimate predicts an exponent of $-\frac{2}{3}$ and fitting the numerical data resulted in exponents of approximately -0.5 ± 0.05. The deviation in the exponent might be the result of neglecting corrections to the analytic estimate that are usually included in the depinning-theory by employing a renormalization group treatment [16].

It could also be shown that weak disorder in the Josephson junction array leads to a new correlation length in the model. Arrays that are shorter than the correlation length behave like clean arrays, arrays longer than the correlation length show the same behaviour as strongly disordered arrays. Numerical simulations found the transition at the correlation length that was obtained analytically from the disorder model.

The analytic estimates of the switching voltage were used to fit experimental data on the switching voltage provided by R. Schäfer, H. Rotzinger, W. Cui, A. Fiebig and A.V. Ustinov (all Karlsruhe Institut of Technology, KIT, Germany). The parameters obtained from the fit are in good agreement with experimental expectations, thereby providing confirmation for the presented model of the onset of transport in Josephson junction arrays.

The third result is a check of the validity of the incoherent tunnelling model used in literature [15] to simulate the transport in Josephson junction arrays. We numerically simulated a simplified model, a homogeneously biased Josephson junction array segment that contains only one excess Cooper pair that is dressed by surrounding Cooper pair dipoles. The model is more closely related to a Josephson junction array that forms a closed ring than to an open array set-up as it is used in experiments.

To be able to perform the simulations of the large open quantum systems we extended the numerical method of quantum jumps. The quantum jump method is an established numerical tool to use an efficient stochastic unravelling to obtain the solution of a Lindblad master equation. The developed stochastic Bloch-Redfield algorithm is capable of finding a stochastic unravelling directly from a Bloch-Redfield master equation.

At small applied voltages we find large corrections when including coherent Cooper pair tunnelling compared to a simulation that only takes incoherent tunnelling into account. At large applied voltages the simplified model is not a valid description of the whole array anymore. It does not take into account additional free charge carriers created by the dissolution of Cooper pair dipoles. In the simulations that use purely incoherent tunnelling processes [15] a large numbers of free charge carriers are present in the array at each time. It was found that the net effect of the free charge carriers on one screened Cooper pair can be approximated by a large homogeneous voltage drop over each Josephson junction. In this case both models, the incoherent tunnelling model and the model including coherent tunnelling, yield the same results. We have shown that the incoherent tunnelling model used in literature is a good approach to obtain the transport properties even when the Josephson coupling energy is comparable to the Josephson junction charging energy.

The work presented in this thesis has many possible extensions. Conceptually it would be desirable to describe the insulating and the conducting regime of the IV-curve in the same theoretical framework. A full description of the transport regime in the quasi-charge model requires a derivation of the dissipative term in the quasi-charge equation of motion from a microscopic model of the dissipative environment. Another possible direction of investigation is the temperature dependence of the switching voltage. The model used in this work assumed the zero temperature limit. The last open question we want to mention is the retrapping voltage. Whether the hysteresis in the IV-curve of Josephson junction arrays is due to the large effective inductances or overheating, understanding how the quasi-charge returns to the pinned configuration will be important to find a theoretical prediction of V_{re}.

This work has contributed to the understanding of some open questions of the physics of Josephson junction arrays, however there remains much to learn about these systems. Josephson junction arrays will stay an interesting theoretical and experimental research object for some time to come.

Bibliography

[1] Schön, G., Siewert, J., and Zaikin, A. D. December 1994 *Physica B: Condensed Matter* **203(3-4)**, 340–346.

[2] Choi, M.-S., Plastina, F., and Fazio, R. January 2003 *Physical Review B* **67(4)**, 045105.

[3] Haviland, D. B. and Delsing, P. September 1996 *Physical Review B* **54(10)**, R6857–R6860.

[4] Ågren, K., Peter, A., and Haviland, D. B. (2001) *Journal of low temperature physics* **124(1-2)**, 291–304.

[5] Bylander, J., Duty, T., and Delsing, P. March 2005 *Nature* **434(7031)**, 361–4.

[6] Bylander, J., Duty, T., Johansson, G., and Delsing, P. July 2007 *Physical Review B* **76(2)**, 020506.

[7] Ergül, A., Schaeffer, D., Lindblom, M., Haviland, D. B., Lidmar, J., and Johansson, J. September 2013 *Physical Review B* **88(10)**, 104501.

[8] Ergül, A., Lidmar, J., Johansson, J., Azizoğlu, Y., Schaeffer, D., and Haviland, D. B. September 2013 *New Journal of Physics* **15(9)**, 095014.

[9] Zimmer, J., Vogt, N., Fiebig, A., Syzranov, S. V., Lukashenko, A., Schäfer, R., Rotzinger, H., Shnirman, A., Marthaler, M., and Ustinov, a. V. October 2013 *Physical Review B* **88(14)**, 144506.

[10] Likharev, K. K. (1986) Dynamics of Josephson junctions and circuits, Gordon and Breach science publishers, New York.

[11] Lobos, A. M. and Giamarchi, T. March 2011 *Physical Review B* **84(2)**, 10.

[12] Homfeld, J., Protopopov, I., Rachel, S., and Shnirman, A. February 2011 *Physical Review B* **83(6)**, 064517.

[13] Haviland, D. B., Andersson, K., and Å gren, P. (2000) *Journal of Low Temperature Physics* **118**, 733–749.

[14] Schäfer, R., Cui, W., Grube, K., Rotzinger, H., and Ustinov, A. V. October 2013 *arxiv* **1310.4295**

[15] Cole, J. H., Leppäkangas, J., and Marthaler, M. June 2014 *New Journal of Physics* **16(6)**, 063019.

[16] Brazovskii, S. and Nattermann, T. March 2004 *Advances in Physics* **53(2)**, 177–252.

[17] Gurarie, V. and Tsvelik, A. M. May 2004 *Journal of Low Temperature Physics* **135(3/4)**, 245–255.

[18] Mooij, J. E. and Nazarov, Y. V. February 2006 *Nature Physics* **2(3)**, 169–172.

[19] Guichard, W. and Hekking, F. W. J. February 2010 *Physical Review B* **81(6)**, 064508.

[20] Ustinov, A., Cirillo, M., Larsen, B., Oboznov, V., Carelli, P., and Rotoli, G. February 1995 *Physical Review B* **51(5)**, 3081–3091.

[21] Wiseman, H. M. and Milburn, G. J. (2009) Quantum Measurement and Control, Cambridge University Press, Cambridge.

[22] Ben-Jacob, E., Mullen, K., and Amman, M. (1989) *Physics Letters A* **135(6)**, 390–396.

[23] Hermon, Z., Ben-Jacob, E., and Schön, G. July 1996 *Physical Review B* **54(2)**, 1234–1245.

[24] Gurarie, V. and Chalker, J. September 2002 *Physical Review Letters* **89(13)**, 1–4.

[25] Schön, G. and Zaikin, A. D. December 1990 *Physics Reports* **198(5-6)**, 237–412.

[26] Mooij, J. E. and Harmans, C. J. P. M. October 2005 *New Journal of Physics* **7**, 219–219.

[27] Bezryadin, A., Lau, C., and Tinkham, M. April 2000 *Nature* **404(6781)**, 971–4.

[28] Arutyunov, K., Golubev, D., and Zaikin, A. D. July 2008 *Physics Reports* **464(1-2)**, 1–70.

[29] Demtröder, W. (2000) Experimentalphysik 3: Atome, Moleküle und Festkörper, Springer Verlag, .

[30] Likharev, K. K. and Zorin, A. B. May 1985 *Journal of Low Temperature Physics* **59(3-4)**, 347–382.

[31] Koch, J., Manucharyan, V., Devoret, M. H., and Glazman, L. I. November 2009 *Physical Review Letters* **103(21)**, 217004.

[32] Hriscu, A. M. and Nazarov, Y. May 2011 *Physical Review B* **83(17)**, 174511–174527.

[33] Hriscu, A. M. and Nazarov, Y. V. February 2011 *Physical Review Letters* **106(7)**, 077004.

[34] Zorin, A. B. June 1996 *Physical Review Letters* **76(23)**, 4408–4411.

[35] Homfeld, J. Ladungssolitonen in eindimensionalen Anordnungen von Josephsonkontakten PhD thesis Karlsruhe Institut of Technology (2010).

[36] Hu, G. and O'Connell, R. June 1994 *Physical Review B* **49(23)**, 16773–16776.

[37] Lynch, R. May 1995 *Physics Reports* **256(6)**, 367–436.

[38] Ingold, G.-L. and Nazarov, Y. V. August 1992 Charge Tunneling Rates in Ultrasmall Junctions volume **294**, of NATO Science Series: B chapter Chapter 2, pp. 21–107 Plenum Press New York 1 edition.

[39] Vogt, N., Schäfer, R., Rotzinger, H., Cui, W., Fiebig, A., Shnirman, A., and Ustinov, A. V. July 2014 *arxiv* **1407.3353**.

[40] Ryder, L. H. (1985) Quantum Field Theory, Cambridge University Press, .

[41] Altland, A. and Simons, B. (2010) Condensed Matter Field Theory, Cambridge University Press, second edition.

[42] Zener, C. (1934) *Proceedings of the Royal Society of London. Series A* **145(855)**, 523–529.

[43] Landau, L. (1932) *Physics of the Soviet Union* **2**, 46–51.

[44] Stueckelberg, E. C. G. (1932) *Helvetica Physica Acta* **5**, 369.

[45] Majorana, E. February 1932 *Il Nuovo Cimento* **9(2)**, 43–50.

[46] Braun, O. M. and Kivshar, Y. S. December 1998 *Physics Reports* **306(1-2)**, 1–108.

[47] Hontsu, S. and Ishii, J. (1988) *Journal of Applied Physics* **63(6)**, 2021.

[48] Miller, J. H., Gunaratne, G. H., Huang, J., and Golding, T. D. (1991) *Applied Physics Letters* **59(25)**, 3330.

[49] Ustinov, A., Cirillo, M., and Malomed, B. April 1993 *Physical Review B* **47(13)**, 8357–8360.

[50] Bock, R., Phillips, J., van derZant, H., and Orlando, T. April 1994 *Physical Review B* **49(14)**, 10009–10012.

[51] Pfeiffer, J., Schuster, M., Abdumalikov, A. A., and Ustinov, A. January 2006 *Physical Review Letters* **96(3)**, 1–4.

[52] Agren, P., Johansson, J., Andersson, K., and Haviland, D. B. May 2000 *Physica B: Condensed Matter* **280(1-4)**, 414–415.

[53] Dynes, R. and Fulton, T. May 1971 *Physical Review B* **3(9)**, 3015–3023.

[54] Larkin, A. I. and Ovchinnikov, Y. N. (1973) *Sov Phys JETP* **38(4)**, 854–858.

[55] Larkin, A. I. and Ovchinnikov, Y. N. February 1979 *Journal of Low Temperature Physics* **34(3-4)**, 409–428.

[56] Fukuyama, H. and Lee, P. January 1978 *Physical Review B* **17(2)**, 535–541.

[57] Imry, Y. and Ma, S. k. November 1975 *Physical Review Letters* **35(21)**, 1399–1401.

[58] Chauve, P., Giamarchi, T., and Le Doussal, P. September 2000 *Physical Review B* **62(10)**, 6241–6267.

[59] Chauve, P., Le Doussal, P., and Wiese, K. J. February 2001 *Physical Review Letters* **86(9)**, 1785–1788.

[60] Fedorov, K. G., Fistul, M. V., and Ustinov, A. V. July 2011 *Physical Review B* **84(1)**, 014526.

[61] Fedorenko, A. A., Le Doussal, P., and Wiese, K. J. December 2006 *Physical Review E* **74(6)**, 061109.

[62] Fedorenko, A. March 2008 *Physical Review B* **77(9)**, 094203.

[63] Santucci, S., Grob, M., Toussaint, R., Schmittbuhl, J., Hansen, A., and Malø y, K. J. November 2010 *EPL (Europhysics Letters)* **92(4)**, 44001.

[64] Laurson, L. and Zapperi, S. November 2010 *Journal of Statistical Mechanics: Theory and Experiment* **2010(11)**, P11014.

[65] Middleton, A. A. and Wingreen, N. S. November 1993 *Physical Review Letters* **71(19)**, 3198–3201.

[66] Vogt, N., Jeske, J., and Cole, J. H. November 2013 *Physical Review B* **88(17)**, 174514.

[67] Lindblad, G. June 1976 *Commun. Math. Phys.* **48(2)**, 119–130.

[68] Gorini, V. (1976) *Journal of Mathematical Physics* **17(5)**, 821.

[69] Percival, I. (1998) Quantum state diffusion, Cambridge University Press, .

[70] Diósi, L. (1985) *Physics Letters A* **112(6)**, 288–292.

[71] Diósi, L. (1986) *Physics Letters A* **114(8)**, 451–454.

[72] Dalibard, J., Castin, Y., and Mø lmer, K. February 1992 *Physical Review Letters* **68(5)**, 580–583.

[73] Teich, W. G. and Mahler, G. March 1992 *Physical Review A* **45(5)**, 3300–3318.

[74] Wiseman, H. M. and Milburn, G. J. March 1993 *Physical Review A* **47(3)**, 1652–1666.

[75] Brun, T. A. August 2001 *American Journal of Physics* **70(7)**, 42.

[76] Gambetta, J. and Wiseman, H. M. October 2005 *Journal of Optics B: Quantum and Semiclassical Optics* **7(10)**, S250–S264.

[77] Bloch, F. February 1957 *Physical Review* **105(4)**, 1206–1222.

[78] Redfield, A. G. (1957) *IBM Journal of Research and Development* **1(1)**, 19.

[79] Makhlin, Y., Schön, G., and Shnirman, A. January 2004 *Chemical Physics* **296(2-3)**, 315–324.

[80] Shnirman, A., Schön, G., Martin, I., and Makhlin, Y. April 2005 *Physical Review Letters* **94(12)**, 127002.

[81] Cole, J. H., Müller, C., Bushev, P., Grabovskij, G. J., Lisenfeld, J., Lukashenko, A., Ustinov, A. V., and Shnirman, A. (2010) *Applied Physics Letters* **97(25)**, 252501.

[82] Jeske, J. and Cole, J. H. May 2013 *Physical Review A* **87(5)**, 052138.

[83] Jeske, J., Vogt, N., and Cole, J. H. December 2013 *Physical Review A* **88(6)**, 062333.

[84] Carmichael Howard, J. (1999) Statistical Methods in Quantum Optics 1, Springer, .

[85] Korotkov, A. N. August 1999 *Physical Review B* **60(8)**, 5737–5742.

[86] Goan, H. S., Milburn, G. J., Wiseman, H. M., and Sun, H. B. March 2001 *Physical Review B* **63(12)**, 125326.

[87] Korotkov, A. N. February 2001 *Physical Review B* **63(11)**, 115403.

[88] Korotkov, A. N. October 2001 *Physical Review B* **64(19)**, 193407.

[89] Oxtoby, N. P., Sun, H. B., and Wiseman, H. M. November 2003 *Journal of Physics: Condensed Matter* **15(46)**, 8055–8064.

[90] Korotkov, A. N. June 2003 *Physical Review B* **67(23)**, 235408.

[91] Oxtoby, N. P., Warszawski, P., Wiseman, H. M., Sun, H. B., and Polkinghorne, R. E. S. April 2005 *Physical Review B* **71(16)**, 165317.

[92] Oxtoby, N. P., Wiseman, H. M., and Sun, H. B. July 2006 *Physical Review B* **74(4)**, 045328.

[93] Oxtoby, N. P., Gambetta, J., and Wiseman, H. M. March 2008 *Physical Review B* **77(12)**, 125304.

[94] Weiss, U. (1999) Quantum dissipative systems, World Scientific, .

[95] Imamoglu, A. November 1994 *Physical Review A* **50(5)**, 3650–3653.

[96] Diósi, L., Gisin, N., and Strunz, W. T. September 1998 *Physical Review A* **58(3)**, 1699–1712.

[97] Diósi, L. and Strunz, W. T. November 1997 *Physics Letters A* **235(6)**, 569–573.

[98] Gambetta, J. and Wiseman, H. M. July 2002 *Physical Review A* **66(1)**, 012108.

[99] Bakhvalov, N. S. and Kazacha, G. S. (1989) *Zh. Eksp. Teor. Fiz* **1021(August 1988)**, 581–587.

[100] Wasshuber, C. (2001) Computational Single-Electronics, Computational Microelectronicsspringer, .

[101] Voter, A. (2005) *Radiation Effects in Solids* **237**, 1–23.

[102] Reuter, K. (2011) First-Principles Kinetic Monte Carlo Simulations for Heterogeneous Catalysis: Concepts, Status, and Frontiers In Olaf Deutschmann, (ed.), Modeling and Simulation of Heterogeneous Catalytic Reactions: From the Molecular Process to the Technical System, pp. 71–111 Wiley-VCH Verlag GmbH & Co. KGaA.

[103] Walker, K. and Cole, J. December 2013 *Physical Review B* **88(24)**, 245101.

[104] Brink, A. M., Odintsov, A. A., Bobbert, P. A., and Schön, G. October 1991 *Zeitschrift für Physik B Condensed Matter* **85(3)**, 459–467.

[105] Marthaler, M. Study of Quantum Electrodynamics in Superconducting Devices PhD thesis Karlsruhe Institute of Technology June 2009.

[106] Nakamura, Y., Korotkov, A. N., Chen, C. D., and Tsai, J. S. September 1997 *Physical Review B* **56(9)**, 5116–5119.

[107] Tinkham, M. (1975) Introduction to superconductivity, McGraw-Hill, .

[108] Shnirman, A., Makhlin, Y., and Schön, G. (2002) *Physica Scripta* **T102(1)**, 147.

Publikationsliste Nicolas Vogt

1. **Influence of two-level fluctuators on adiabatic passage techniques**,
   N. Vogt, J. H. Cole, M. Marthaler and G. Schön
   May 2012, *Physical Review B* **85(17)**, 174515.

2. **Thermally activated conductance in arrays of small Josephson junctions**,
   J. Zimmer, N. Vogt, A. Fiebig, S.V. Syzranov, A. Lukashenko, R. Schäfer, H. Rotzinger, A. Shnirman, M. Marthaler and A. V Ustinov
   October 2013, *Physical Review B* **88(14)**, 144506.

3. **Stochastic Bloch-Redfield theory: Quantum jumps in a solid-state environment**,
   N. Vogt, J. Jeske and J. H. Cole
   November 2013, *Physical Review B* **88(17)**, 174514.

4. **Excitation and state transfer through spin chains in the presence of spatially correlated noise**,
   J. Jeske, N. Vogt and J. H. Cole
   December 2013, *Physical Review A* **88(6)**, 062333.

5. **One-dimensional Josephson junction arrays: Lifting the Coulomb blockade by depining**,
   N. Vogt, R. Schäfer, H. Rotzinger, W. Cui, A. Fiebig, A. Shnirman and A. V Ustinov
   July 2014, *arxiv* **1407.3353**,
   Submitted to Physical Review Letters

Danksagung

Für die Unterstützung während der Anfertigung dieser Arbeit möchte ich vielen Menschen danken. Zuvorderst Professor Alexander Shnirman, der immer bereit war, meine Ideen zu unterstützen und mir dabei geholfen hat, eigene Lösungsansätze zu verfolgen. Professor Alexey Ustinov danke ich darür, dass er sich als Koreferent zur Verfügung gestellt hat und vor allem dafür, dass er es mir ermöglicht hat meine theoretische Arbeit mit experimentellen Ergebnissen in Verbindung zu setzen.

Mein besonderer Dank gilt Jared Cole. Nicht nur hat er, als er mich während meiner Diplomarbeit betreute , mein Interesse an Josephson junction arrays geweckt, er hat es mir auch ermöglicht, während meiner Promotion zehn wunderbare Monate an der RMIT University in Melbourne zu verbringen. Ich möchte mich außerdem bei Michael Marthaler für die Anleitung und Unterstützung bei meiner ersten Zusammenarbeit mit der Gruppe von Professor Ustinov bedanken.

Während der letzten Jahre habe ich sehr von der hervorragenden Arbeitsumgebung, sowohl am Institut für Theorie der Kondensierten Materie in Karlsruhe, als auch am RMIT in Melbourne, profitiert. Dafür möchte ich mich bei den vielen Institutsmitgliedern bedanken die mir die Zeit so angenehm gemacht haben. Insbesondere möchte ich diejenigen erwähnen, die mir duch wissenschaftliche Diskussionen und Zusammenarbeit weitergeholfen haben: Jan Jeske, Sergey Syzranov, Jochen Zimmer, Sebastian Skacel, Hannes Rotzinger, Roland Schäfer und Philip Wollfarth.

Ohne die Unterstützung durch Familie und Freunde wäre es mir nicht möglich gewesen, diese Arbeit anzufertigen. Dafür danke ich vor allem meinen Eltern, die immer hinter mir standen und mich in meiner Entscheidung zur Promotion bestärkt haben, aber auch Sebastian S., Stefan, Sahra, David, Sebastian L. und Matthias.